Protein-surfactant interactions

The interplay between structure, stability and kinetics

Andersen, Kell kleiner

Publication date:
2009

Document Version
Publisher's PDF, also known as Version of record

Protein-surfactant interactions

- The interplay between structure, stability and kinetics

Ph.D. Thesis

by

Kell Kleiner Andersen

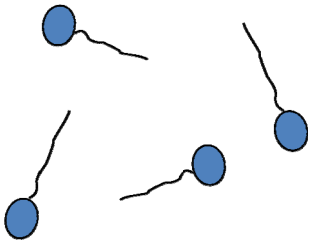

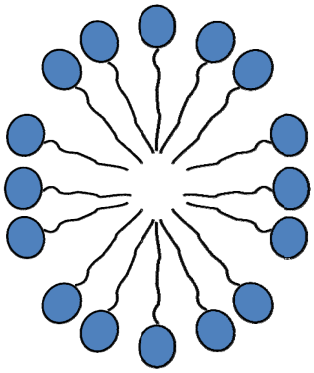

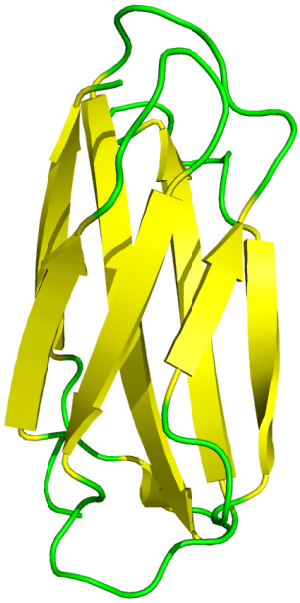

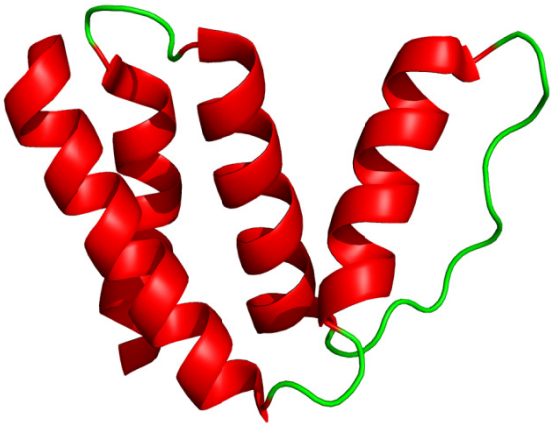

Department of Life Sciences

June, 2009

Aalborg University

Department of Life Sciences

Sohngaardsholmsvej 49

DK-9000 Aalborg

Title of Ph.D. thesis:
Protein-surfactant interactions –
The interplay between structure, stability and kinetics

Author:
Kell Kleiner Andersen
(+45) 51 90 25 50, kell@bio.aau.dk (kellandersen@yahoo.dk)
Aalborg University, Department of Life Sciences, Sohngårdsholmsvej 49, DK-9000 Aalborg

Supervisor:
Professor Daniel Erik Otzen
(+45) 20 72 52 38, dao@inano.dk
Interdisciplinary Nanoscience Center (iNANO) Department of Molecular Biology University of Aarhus Gustav Wieds Vej 10C, DK-8000 Aarhus

Thesis period:
September 1st 2005 to December 7th 2008

Ph.D. school:
The International Doctoral school of Technology and Science

Ph.D programme:
Biotechnology, Chemistry and Environmental Engineering

Issues printed:
10

Preface and acknowledgments

This thesis highlights the work done from September 1st, 2005 to December 7th, 2008 by undersigned in order to obtain the Ph.D. degree. The work was done under The International Doctoral School of Technology and Science, and funded by the innovation consortium BIOPRO.

The theme of this thesis is protein-surfactant interactions. The thesis will focus on these interactions from a laundry detergent point of view, where surfactants interact with both soil of protein origin as well as with enzymes added to detergents in order to enhance product performance.

The thesis is divided into three parts. Part one is an introduction composed of four chapters which provide a general description of how proteins and surfactants interact. Part two (chapter V) is the paper section where a total of six papers are presented. In part three (chapter VI) key results from the papers are summarized and discussed.
The first three chapters in the introduction will focus on: detergents in general, surfactant properties and protein-surfactants interactions, respectively. Chapter IV describes the most important techniques used in this thesis. Of the six papers presented in chapter V, the first three have been published in scientific journals. Paper IV has been resubmitted to journal of molecular biology and Paper V is a manuscript in preparation. Paper VI summarizes of the work carried out so far on the enzyme *Thermomyces lanuginosus* lipase. Although this material is not ready for publication, the important observations made so far validates a presentation of the data in this thesis. Important results are summarized and discussed in chapter IV. Finally references are presented in chapter VII.

This thesis does not include the published paper concerning S6 aggregation in the presence of surfactants (see paper section). Although this was a very nice collaboration the focus of this thesis is not protein aggregation and fibrillation. Furthermore the thesis does not include studies on the folding mechanism of the outer membrane protein A (OmpA) in surfactants. Although the interactions of surfactants with membrane proteins is very interesting and much time has been devoted to this project, thorough interpretation of the data is still required before it can be presented.

I would like to thank Professor Daniel Otzen for his excellent supervision not only during my Ph.D. period but also during my master thesis and before that three semester projects. Daniel has been an inspiration from the very beginning, and his enthusiasm for protein science has without a doubt stimulated my own interest for the many aspects within this field.

The work has been distributed equally at the Department of Life Sciences, Aalborg University and the Interdisciplinary Nanoscience Center (iNANO) Department of Molecular Biology, University of Aarhus. I would like to thank friends and colleagues, past and present, at both departments for a wonderful time during my time as a PhD student.

Professor Peter Westh, Roskilde University, has been an invaluable and infectiously enthusiastic mentor within the fascinating field of calorimetry. My 3-week visit to his lab provided a secure platform that I could build all my subsequent ITC studies on. Peter is also a major actor in the informal but very inspiring Protein Stability Network (PSN), which in addition includes Kim Borch and Claus Crone Fuglsang from Novozymes. Our regular PSN meetings have provided a wonderful forum to present and discuss countless ideas within protein-surfactant interactions and many other biophysical topics and I am sure that it will continue for years to come due to the highly complementary interests and energies in the network.

I am very grateful to Professor Jan Skov Pedersen and Dr. Cristiano Oliveira at the Department of Chemistry for devoting so much time to experimental and analytical Small Angle X-ray Scattering studies on ACBP and other protein-surfactant complexes. Their work constitutes a very important structural backbone in what has otherwise mainly been a thermodynamic and spectroscopic piece of work, and I firmly believe that SAXS will play a very large role in future work on protein-surfactant complexes.

Dr. Kim Lambertsen Larsen, Aalborg University, has been very helpful in the use of Capillary Electrophoresis. Dr. Reinhard Wimmer provided expert help with calculation of protein electrostatic potential. Professor Flemming Poulsen, University of Copenhagen, kindly sent a large number of ACBP mutants which shed new light on ACBP denaturation.

Dr. Thomas Callisen provided clear insight into the world of enzymes from an industrial point of view and has provided important feedback on many aspects of my work. Dr. Torben Madsen is acknowledged for his leadership of the BIOPRO consortium that has funded my Ph.D. and for continual interest in this project.

Lastly I would like to thank friends and family, who has stood by me during the ups and downs as a Ph.D. student. This support has not gone unnoticed. Loving thanks goes out to Ulla Ellegaard Hansen who gave birth to our daughter Isabell Ellgaard Andersen on 29th of December, 2007. This was truly a blessing making the time as a Ph.D. student even more exciting.

Kell Kleiner Andersen

Table of Contents

Resumè (Danish summary)

Emnet for denne Ph.D. afhandling er protein-surfaktant interaktioner. Proteiner, herunder enzymer anvendes bl.a. i vaskemidler til at fjerne vanskeligt snavs fra tøj. F.eks. kan enzymer fjerne mælk-, blod-, græs-, æg- og kødpletter, som ellers er vanskelige at rengøre. Enzymerne arbejder i synergi med surfaktanterne, som opløser snavs og transporterer det væk fra vasketøjet.

Både enzymer og surfaktanter har gavnlige effekter i vaskeprocessen. Surfaktanter interagerer dog ikke kun med vasketøj og snavs under vaskeprocessen men også med enzymer. Disse interaktioner kan være favorable men bestemt også ufavorable. Ladede surfaktanter denaturerer langt størstedelen af alle proteiner ved meget lave koncentrationer (mM eller mindre). Enzymerne, som bruges i vaskemidler, skal derfor til en vis grad være modstandsdygtige overfor denne denaturering således at de bibeholder aktivitet under vaskeprocessen.

For at kunne optimere enzymernes såvel som surfaktanternes præstation under vask er det vigtigt at vide hvordan disse to komponenter interagerer. Interaktionerne mellem proteiner og surfaktanter har været studeret i over 60 år, men til dags dato er der ingen generel model som beskriver disse interaktioner fyldestgørende. Denne afhandling forsøger at bidrage forståelsen af protein-surfaktant interaktioner ud fra følgende indgangsvinkel:

Der udvælges en række model-proteiner og interaktionerne mellem disse proteiner og surfaktanter, herunder både ladede og uladede, studeres med en række biofysiske metoder. Modelproteinerne er udvalgt på baggrund af deres sekundær struktur for at belyse betydningen af denne parameter. Model-proteinerne har derfor stor andel af hhv. α-, β- samt blandet α/β-struktur. Desuden inddrages der et industrielt anvendt enzym som interagerer med surfaktanter, men som er modstandsdygtig overfor surfaktant denaturering.

Vigtige resultater udledt i denne afhandling kan kort opsummeres:

1) Denatureringsstudier med anion surfaktanten sodium dodecyl sulfate (SDS) viser at proteiner med stor andel α-struktur generelt denaturerer lettere end proteiner med stor andel β-struktur. Dette afspejles i den koncentration af SDS som er nødvendig for at denaturere proteiner samt den hastighed hvorved denatureringen finder sted. Denne forskel mellem proteiner med stor andel af hhv. α- og β-struktur kan tilskrives flere langtrækkende interaktioner i β-struktur i modsætning til de mange lokale interaktioner der stabiliserer α-struktur.
2) Proteinet Acyl-coenzyme A binding protein (ACBP), som har stor andel α-struktur, denatureres af SDS i fire veldefinerede trin. Trin A) ACBP binder 1-3 SDS molekyler uden at miste nativ struktur. Trin B) yderlig SDS binding (i alt 16 SDS pr ACBP) resulterer i denaturering. I dette stadium dannes der et kompleks indeholdende en central (decorated) micelle som binder to ACBP polypeptid-kæder. Trin C) De to ACBP

molekyler dissocierer og binder hver især 42 SDS molekyler. Dette kompleks er organiseret således at SDS molekylerne danner en "skal" som omfavner ACBP. Trin D) I det sidste trin dannes der frie miceller i opløsning, hvilket sandsynligvis medfører et kompleks der kan beskrives som en udfoldet proteinkæde der omsvøber en række miceller. Den model kaldes i litteraturen også "necklace and bead" modellen.

3) Co-faktorer kan have indflydelse på hvordan surfaktanter denaturerer proteiner. Proteinet ACBP, som har stor andel af α-stuktur og ingen co-faktor, denatureres af SDS i få veldefinerede trin (se ovenfor). Myoglobin som også har stor andel α-struktur, men som desuden binder co-faktoren heme, denatureres af SDS i flere trin end ACBP. Denatureringsmekanismen for dette co-faktor bindende protein kan derfor beskrives som mere komplekst.
4) Langkædede alkyl-sulfater er mere potente denaturanter end kortkædede alkyl-sulfater. Koncentrationen af alkyl-sulfat som er nødvendig for at denaturere ACBP falder i takt med længere kædelængde. Den øgede potenthed afspejles også i udfoldningshastigheden, hvilken øges som funktion af længere kædelængde.
5) Micellestrukturen har betydning for hvordan surfaktanter interagerer med proteiner. F.eks. ses en nedgang i udfoldningshastigheden når SDS miceller går fra at have en sfærisk struktur til at have en elongeret ("rod-like") struktur.
6) Blandede miceller med både ladede og neutrale surfaktanter, er mindst lige så denaturerings-potente som monomer SDS. Hastigheden hvorved ACBP udfolder reduceres dog i takt med lavere molfraktionen SDS.
7) *Thermomyces lanuginosus* lipase (TlL), som er et industrielt anvendt enzym, udfolder meget langsomt og kan derfor beskrives som et kinetisk stabilt protein (halveringstid = 84 dage i fravær af denaturant ved pH 8). I praksis betyder dette at TlL er "fanget" i den native tilstand og derfor ikke undergår global udfoldning. Da surfaktanter denaturerer proteiner ved at binde til udfoldede/fleksible dele bliver TlL ikke denatureret i tilstedeværelse af SDS.

Summary

The theme of this PhD thesis is protein-surfactant interactions. Proteins, here among enzymes are used in detergents to remove difficult stains and soil from laundry items. E.g. enzymes can remove milk-, blood-, grass-, egg- and meat- stains which are otherwise difficult to clean. Enzymes work in synergy with surfactants, which dissolve soil and transport it away from laundry items.

Both enzymes and surfactants have properties that are beneficial in the washing process. However, surfactants do not only interact with soil and laundry items during the washing process but also with enzymes. These interactions can be favorable as well as unfavorable. Ionic surfactants denature most proteins at low concentrations (mM or less). Hence, enzymes used in detergents must to some degree withstand surfactant denaturation such that activity is maintained during the washing process.

In order to optimize enzyme as well as surfactant performance during the washing process it is important to know how these two components interact. Protein-surfactant interactions have been studied for over 60 years, however today there is no model that fully describes the mechanism of interaction. This thesis attempts to contribute to the knowledge of protein-surfactant interactions using the following approach:

A number of model proteins are selected and the interactions between these proteins and surfactants, here among both ionic and nonionic, are studied using a series of biophysical techniques. The model proteins are selected on behalf of their secondary structure in order to shed light on the importance of this parameter. The model proteins have high content of α-, β- and mixed α/β-secondary structure, respectively. In addition a commercial available enzyme is also studied, which is known to interact with surfactants but is resistant to surfactant denaturation.

Important results deducted from this thesis can be summarized in short:

1) Denaturation studies with the anion surfactant sodium dodecyl sulfate (SDS) show that proteins with high content of α-structure denature easily compared to proteins with a high content of β-structure. This is reflected in the concentration of SDS required to denature the proteins as well the rate of denaturation. The difference between proteins with large content of α- and β-structure can be assigned to the many long distance interactions in β-structure as compared to the many short distance interactions which stabilize α-structure.
2) Acyl-coenzyme A binding protein (ACBP), which has a high content of α-structure is denatured by SDS in four well-defined steps. Step A) ACBP binds 1-3 SDS molecules without losing native structure. Step B) Further SDS binding (total of 16) results in denaturation. The complex between protein and surfactant contains a central (decorated) micelle that binds two ACBP polypeptide chains. Step C) The two ACBP molecules dissociate and separately bind 42 SDS molecules. This complex is organized in such a

way that the SDS molecules form a “shell” that surrounds ACBP. Step D) Bulk micelles are formed and the unfolded ACBP polypeptide chain probably wraps around the bulk micelles. In the literature this complex is called the “necklace and bead” model.

3) Co-factors can influence how surfactants denature proteins. The protein ACBP, which has a high content of α-structure and no co-factor, is denatured by SDS in four well-defined steps (see above). Myoglobin, which also has a high degree of α-structure, but in addition binds the co-factor heme, is denatured is several more steps and the denaturing mechanism can thus be considered as more complex.
4) Long chain alkyl-sulfates are more potent denaturants as compared to short chain alkyl-sulfates. The concentration of alkyl-sulfate required to denature ACBP decreases with increasing length of the alkyl chain. The increased potency is also reflected in the rate of unfolding which increases with increasing length of the alkyl-chain.
5) Micelle structure is important for the interactions between proteins and surfactants. E.g. a decrease in the unfolding rate is observed upon the transition from spherical to elongated (“rod-like”) micelles.
6) Mixed micelles consisting of both ionic and nonionic surfactant are at least as potent as monomeric SDS. Unfolding kinetics however decrease with decreasing mole fractions of SDS.
7) *Thermomyces lanuginosus* lipase (TlL) which is a commercial available enzyme unfolds very slowly in water and can be classified as a kinetic stable enzyme (half rate = 84 days in the absence of denaturant at pH 8). In practical terms this means that TlL is “trapped” in the native state, and therefore does not undergo global unfolding. Because surfactants denature proteins by binding to unfolded/flexible regions TlL is not denatured by surfactants.

Abbreviations

ACBP	Acyl-coenzyme A-binding protein
αLA	α-lactalbumin
αLP	α-lytic protease
BSA	Bovine serum albumin
cmc	Critical micelle concentration
CE	Capillary electrophoresis
DDM	Dodecyl maltoside
DecM	Decyl maltoside
DSC	Differential scanning calorimetry
E.coli	*Escherichia coli*
EDTA	Ethylenediaminetetraacetic acid
EOF	Electroosmotic flow
FTIR	Fourier transform infrared spectroscopy
GdmCl	Guanidinium cloride
pI	Isoelectric point
ITC	Isothermal titration calorimetry
LAS	Linear alkyl benzene sulfonate
Mb	Myoglobin
MD	Molecular dynamics
MPD	2,4-methyl-2-pentanediol
NMR	Nuclear Magnetic Resonance
Phe	Phenylalanine
pI	Isoelectric point
SANS	Small angle neutron scattering
SAXS	Small angle x-ray scattering
SDS	Sodium dodecyl sulfate
SDS-PAGE	Sodium dodecyl sulfate - polyacrylamide gel electrophoresis
TII27	The 27th immunoglobulin domain from human cardiac titin
TlL	*Thermomyces lanuginosus* lipase
Tnfn3	The third fibronectin type III domainfrom human tenascin
Trp	Tryptophan
Tyr	Tyrosine

List of Papers

Papers included in the thesis

I) Unfolding of β-sheet proteins in SDS

Nielsen MM, Andersen KK, Westh P, Otzen DE.

Biophys J. 2007 May 15;92(10):3674-85.

II) Global study of myoglobin-surfactant interactions

Andersen KK, Westh P, Otzen DE.

Langmuir. 2008 Jan 15;24(2):399-407.

III) Stable intermediates determine proteins' primary unfolding sites in the presence of surfactants

Hansen JH, Petersen SV, Andersen KK, Enghild JJ, Damhus T, Otzen DE.

Biopolymers. 2009 Mar;91(3):221-31

IV) The role of decorated SDS micelles in sub-cmc protein denaturation and association

Andersen KK, Oliveira CLP, Larsen KL, Poulsen FM, Callisen TH, Westh P, Pedersen JS, Otzen DE.

Resubmitted to *Journal of Molecular Biology*

V) How chain length and charge affect surfactant denaturation of ACBP

Andersen KK, Otzen DE.

Manuscript in preparation

VI) *Thermomyces lanuginosus* Lipase is a kinetically stable enzyme

Andersen KK, Sehgal P, Callisen TH., Westh P, Otzen DE.

Work in progress

Papers not included in the thesis

Aggregation of S6 in a quasi-native state by sub-micellar SDS

Otzen DE, Nesgaard L, Andersen KK, Hansen JH, Christiansen G, Doe H, Sehgal P.

Biochim Biophys Acta. 2008 Feb;1784(2):400-14.

Folding mechanism of Outer membrane protein A (OmpA) in surfactant

Andersen KK, Otzen DE.

Manuscript in preparation

Chapter I: Introduction to Detergents

This chapter is devoted to detergents and will introduce the most important components present in modern formulations. The word detergent is derived from the latin word "*detergere*", which means to clean/remove. In today's meaning the word represents laundry, dish wash and industrial cleaning products. When referring to detergents throughout this thesis, this means laundry detergents unless otherwise stated.

Definition of surfactant, soap and detergent

Before we head out into the history of detergents I would like to clarify of what is meant when using the words surfactant, soap and detergent throughout this thesis. These phrases often overlap in the literature, and the papers presented in this thesis are no exception. To avoid to unnecessary confusion, the following should make it clear how the phrases intentionally should be used.

Detergents are the products that you normally buy in supermarkets and use for cleaning of clothes and other laundry items. A modern detergent contains ~20 or more components. Individual components will be described later however soaps and surfactants are typical components.

Surfactants and soaps have many properties in common, e.g. the molecular structure is composed of both hydrophilic and a hydrophobic parts (fig. 1). In addition, both surfactants and soaps can form supramolecular assemblies such as micelles. Soaps and surfactants also have some physiochemical properties which are different and these are important in respect to their use in detergents. The differences arise from the origin and the way surfactants and soaps are produced. Soaps are water-soluble sodium or potassium salts of fatty acids and are derived from either vegetable or animal fats (triglycerides). Due to their origin they are often referred to as natural soaps. Surfactants are manufactured from petroleum, and the molecular structure of surfactants is different compared to soaps. This difference in structure give rise to different physiochemical properties; a clear distinction between soaps and surfactants should thus be made. The molecular structures of surfactants are described in more detail in chapter II.

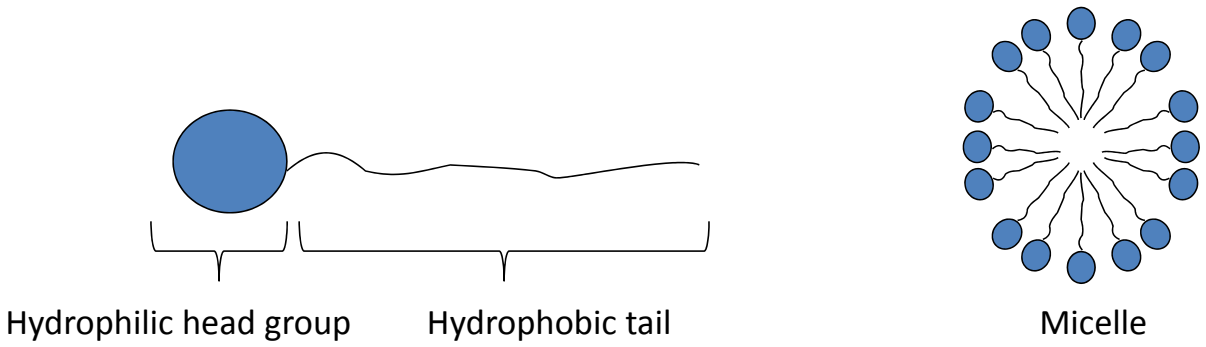

Figure 1. Schematic illustration of a single surfactant or soap molecule (left) and in the aggregated assembly of a micelle (right). Both surfactants and soaps are characterized by having a hydrophilic and hydrophobic groups.

History of Laundry Detergents in short

Detergents have been used for several thousands of years, continue to evolve and provide benefits for the end user. The first commercial household laundry detergent was introduced in 1907 by the German company Henkel under the product name Persil. This product was basically formulated with sodium and potassium salts of C12-C18 chain length fatty acids (soaps) [1, 2].

In 1913 Dr. Otto Röhm took the first patent [3] for the use of digestive enzymes from the pancreases for the removal of stains. The patent very precisely specifies the removal of fat and proteins and also points out the advantage on temperature: "*It appeared that the fabric could be cleaned in a shorter time with less exertion of strength and at a temperature far below the boiling point of water than without enzymes added. Further the fabric had a better appearance and much less soap was necessary*". The product *Burnus* produced by Rohm and Haas, contained crude trypsin (protease) and was used in laundry presoak [4]. The product did never really break through, simply because these enzymes from nature's point of view were not fit to work in detergent conditions (alkaline).

In the 1940s surfactants were produced from petroleum. Surfactants were in part developed in response to a shortage of animal fats and vegetable and oils during World War I and World War II [5]. They proved to be superior over the previously used soaps because they were much more effective for cleaning at cooler temperatures and in hard water [1]. Today surfactants are thus more widely used in detergents as compared to soaps.

In the 1950s enzymes from microorganisms were for the first time marketed. The fermentation of microorganisms provided new enzymes which were better suited for the chemical conditions in detergents. Furthermore fermentation provided a new and more cost beneficial way of producing enzymes [6].

The Danish company Novo began a research program in 1958 with enzymes for washing of clothes from the meat and fish industry [7]. The first product from Novo was Alcalase (*subtilisin* Carlsberg) a protease with alkaline pH optimum making it compatible with detergent conditions. Alcalase was introduces in *Biotex* in 1963, and the benefits of using enzymes became highly noticed [4].

Proteases prevailed for a long time as the only enzymes used in detergents but over the last couple of decades several other types of enzymes have been introduced here among amylases, cellulases, lipases and mannases [8, 9]. *Thermomyces lanuginosus* Lipase (TlL) studied in this thesis was the first commercially successful lipase and was launched in 1988 in the product *Hi Top* from the Japanese company Lion [4]. In addition TlL was the first successful industrial enzyme produced in a genetically modified organism [6].

In the 1980s with the breakthrough of recombinant gene technology, it became possible to improve the manufacturing process as well as commercialization of enzymes that previously could not be produced on an industrial scale. Enzyme improvement within the field of protein engineering and directed evolution [10] especially in the 1990s made it possible to produce "taylor-made" enzymes for specific tasks [8]. At the present time, development of

bioinformatics and the availability of sequence data has improved the efficiency of insolating genes of interest [8]. An overview of some the important landmarks in detergent history is presented in table 1.

Today, detergents are a billion dollar industry. The value of the world marked is around 70 billion dollars, including laundry-, dishwash- and industrial detergents. The volume of enzymes is around 1 % and accounts for ~5 % of the value (Thomas Callisen, senior manager, Novozymes, personal communication). The use of detergents is dependent on the geographic situation, e.g. in Spain and France the average use of detergents is 12-13 kg pr person pr year, while in China and Brazil the number is ~2.3 kg [11]. The penetration of enzymes into detergents is quite high; 95% in Western Europe, 70% in North America and Japan and 50 % in Latin America [7]. Today, three major companies manufacture enzymes for industrial purposes. These are Novozymes A/S, Genencor International Inc., recently acquired by Danisco and finally DSM NV [7].

Table 1. Selected landmarks in detergency history. Adapted from [5] and [1]

1907	*Persil* laundry detergent from Henkel is introduced. The product is based on soda, soap, perborate and silicate
1913	First patent on the use of enzymes (from the pancreas) in laundry detergent
1940s	Synthesis of surfactants from petroleum feed stocks
1950s	Enzymes from microorganisms are for the first time marketed
1960s	Environmental effects of non-biodegradable surfactants
1963	The protease Alcalase (*subtilisin* Carlsberg) is introduced in the product *Biotex*
1970s	Allergy problems associated to enzymes in dusty laundry detergent
1973	The first amylase is introduced (*Mustang* from Henkel) Washing temperatures are generally lowered due to the energy crisis
1980s	Gene technology is a breakthrough in enzyme production
1987	The first cellulace is introduced (*Attack* from Kao)
1988	The first microbial lipase is introduced (*Hi Top* from Lion)
1990s	Protein engineering improves enzymes

Detergents and Formulation

Typical laundry detergents are formulated to provide general cleaning; this includes removal of soil and stains as well as the ability to maintain whiteness and brightness [1]. Detergents contain a variety of different compounds, typically 20 or more and come in a variety of different shapes and sizes including: powder, liquid, tablet, gel and bar form. These components and their amount are referred to as the formulation.

The primary focus of this thesis is on protein-surfactant interactions. Surfactants and proteins will thus be described in more detail as compared to the other components in detergent formulations. From an industrial point of view, it is however important to keep in mind that not many applications involve only theses two components. For a more information about formulation reference [1] is highly recommended and is also used frequently in the following.

Water Hardness

Water hardness is a very important parameter when formulating detergents. Water hardness describes the concentration of metal ions in water, and especially Ca and Mg are important in relation to laundry detergents. Divalent ions can interact with anionic surfactants and cause precipitation; this leads to deposits on clothes making them look dirty. Furthermore precipitation also reduces the concentration of surfactant available for cleaning. To avoid precipitation builder and chelates (described below in more detail) are added in order to control the concentration of these divalent ions.

Detergent Components

The detergent formulator has a variety of ingredients that can optimize product performance. Since many of these components are not used in the studies presented in this thesis, they will only be described shortly. Detergent components can be categorized into the following groups [1]:

1) Surfactants
2) Dispersing polymers
3) Builders and Chelates
4) Bleaching systems
5) Co-solvents
6) Performance enhancers (includes enzymes)

Industrial Surfactants

As described above surfactants are more frequently used in detergents as compared to soaps. A list of common used surfactants and their structure is presented in table 2. Today, the linear alkyl benzene benzene sulfonates (LAS), alkyl sulfates, alkyl ethoxy sulfates and alkyl ether ethoxylates are the workhorse surfactants in most detergent formulations. Alkyl polyglucosides, alkyl glycosamides and methyl ester sulfonates are also widely used [1]. Typical hydrophobes for surfactants are alkyl chains between C10 and C20. Cationic surfactants are not commonly used because of their toxicity [12]. In addition, compared to anionic surfactants, cationic surfactants are generally less effective cleaning agents. Because most natural organic and mineral compounds carry a negative surface charge, cationic surfactants tend to adopt a “head-down” position on the surface (fig. 2). This position tends to neutralize the charge and provides a hydrophobic surface, which does not encourage cleaning [13].

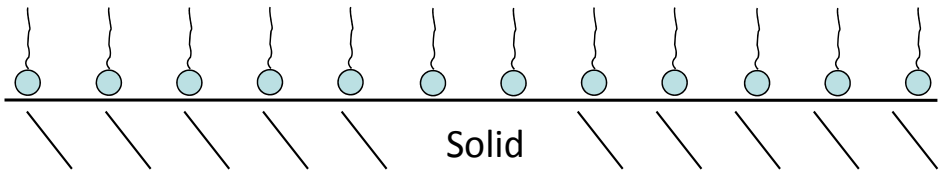

Figure 2. Example of how cationic surfactants adopt the “head-down” position on minerals and organic compounds with a negative surface charge. Adapted from [13]

Nonionic surfactants are increasing in importance because of their capacity to remove soil from synthetic fabrics. They exhibit good water solubility, are low foamers and are less sensitive to water hardness than ionic surfactants. Nonionic surfactants also show good biodegrability by proper choice of the hydrophobic moiety [14].
Surfactants are often used in combination. LAS is the most important surfactant due to low cost and excellent performance. As a standalone surfactant it however suffers due to its hardness sensitivity, poor surface activity and the difficulties associated with environmental degradation of aromatic hydrocarbons. LAS is thus mostly used in combination with lower concentrations of co-surfactants such as alcohol sulfates and alcohol ether sulfates [1].

Table 2. Common surfactants used in detergent formulations. Adapted from [1]

Class	Name	Structure
Anionic	Linear Alkyl Benzene Sulfonate	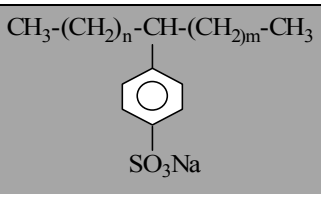
Anionic	Alcohol sulfate	CH_3-$(CH_2)_n$-O-SO_3Na
Anionic	Alcohol Ether Sulfate	CH_3-$(CH_2)_n$-O-$(CH_2$-CH_2-$O)_x$-SO_3Na
Anionic	Fatty acid (soap)	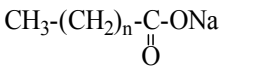
Anionic	Methyl ester sulfonate	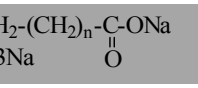
Nonionic	alcohol ethoxylate	CH_3-$(CH_2)_n$-O-$(CH_2$-$CH_2O)_n$H
Nonionic	Amine oxide	CH_3-$(CH_2)_n$-N-$(CH_3)_2H \rightarrow O$
Nonionic	Alkyl monoethanolamide	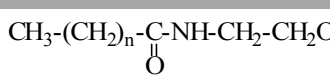
Nonionic	N-methylglycosamide	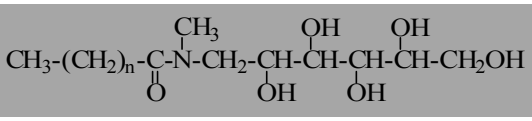
Zwitterionic	Amidopropyl betaine	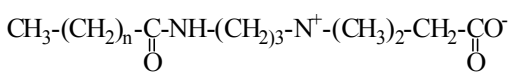
Zwitterionic	Alkyl sulfobetaine	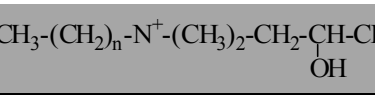

The surfactants used in this thesis are primarily the anionic alkyl-sulfates and the nonionic alkyl-maltosides. While LAS would be an obvious choice because it is the main anion surfactant used in detergents, SDS has traditionally been used as a model surfactant in protein-surfactant studies. Furthermore the LAS benzene group interferes with many spectroscopic techniques, and it was also found difficult to obtain LAS with well defined alkyl chain lengths. Alkyl-sulfates were thus chosen over LAS as a representative for anionic surfactants.

Alkyl-maltosides are often used as nonionic model surfactants. They have been extensively used within the field of membrane protein folding and stability, and can be obtained with very high purity and well defined chain lengths. Alkyl-maltosides were thus chosen as representatives for non-ionic surfactants. In addition, the use of alkyl-polyglucosides is gaining popularity within the detergent industry [2], which is due to environmental aspects such the manufacture from renewable source and biodegradability [15]. Another important reason for choosing alkyl-sulfates and alkyl-maltosides is that there is a much more extensive body of literature on protein interaction with alkyl-sulfates and alkyl-maltosides than with industrial surfactants, making it possible to do direct comparisons with these studies.

Enzymes

Enzymes are used in detergents to promote soil removal by the catalytic breakdown of specific soil components. The most typical enzymes used are proteases, lipases and amylases, but mannases and cellulases are gaining popularity [7, 9]. The actions of the most important enzymes are described below. During laundry wash enzymes are typically present in the mg range [7]. In general for enzymes to be effective in today's detergents they should have the following properties [16]:

- Alkaline pH optimum
- Efficacy at low wash temperatures of 20-40 ºC
- Stability at wash temperatures up to 60 ºC
- Stability in the presence of detergent ingredients
- Specificity broad enough to enable the degradation of a whole class of molecules

Enzymes also need to be stable such that activity is not lost during storage. In general enzymes (*in vivo* and *in vitro*) can be inactivated due to [12]:

- Protein unfolding and/or loss of a co-factor
- Misfolding and aggregation
- Covalent modification of amino acids needed for catalysis
- Binding of inhibitors at the active site
- Hydrolysis of peptide bonds.

Enzymes in detergents are primarily inactivated during storage because of the two first factors: protein unfolding and aggregation [12].

Proteases

Proteases were the first enzymes to be used in detergents and today they are still the most important class of enzymes for the detergent industry. They are present in about 75 % of detergents products worldwide [7]. The proteases used in detergents all originate from *Bacillus* species and have a size of approximately 27 kDa [17]. They are all serine-proteases [6], which catalytic triad composed of aspartic acid, histidine and serine. At the present time less than 15 proteases are used in detergents [17]. The proteases mainly differ in 1)

temperature and pH optima 2) dependence of Ca and Mg ion concentrations for stability and 3) compatibility with detergent components such as bleaching system and surfactants [7]. Auto-proteolysis is the main problem with proteases in liquid detergents. Reversible inhibitors like boric acid are therefore typically added to prevent proteolysis during storage [6].

Amylases

Next to proteases, amylases and lipases are the most popular enzymes in detergents. Amylases hydrolyze the glucosidic linkages in starch polymers. They were introduced in the 1970s and are gaining popularity because of the increasing number of stains containing starch. Modified starch is often used as thickeners in food products such as pudding, ketchup, spaghetti sauce, baby food and more. The amylases used in detergents are like the proteases mainly derived from the *Bacillus* family [7]. Removal of starch is important because starch can form film that that can pick up particulate soil after washing, which results in increasingly grey laundry items [18].

Lipases

Lipases are glycerol ester hydrolases and act on the carboxyl ester bonds of triglycerides [7, 19-21]. Upon hydrolysis of animal fat or plant oil free fatty acids and glycerol are released [6]. TlL studied in paper VI has a preference for medium chains (C10-C12), but is capable of degrading a wide variety of substrates [22, 23].

Lipases show low activity against monomeric substrate but are activated at the water-lipid interface of aggregated triglycerides. It has become increasingly difficult to remove triglycerides with decreasing washing temperatures because washing is performed under the melting temperature of various fatty substances [7]. Lipases are able to catalyze the hydrolysis of these substances and produce smaller units that have lower melting temperatures and are more readily dispersible at low washing temperatures. In addition lipases improve the odor and appearance of fabrics. An interesting feature related to the use of enzymes is that the full enzymatic effect is often only seen after several cycles of wash. New generation of lipases however provide strong benefits already noticeable in the first round of wash [7].

Cellulases

Besides removal of soil, enzymes can also provide fabric care benefits. This in an essential reason why cellulases are used in detergents. Cellulose fibers are composed of glucose polymers held together by β-1,4-glucosidic bonds. Cotton in clothes contain cellulose and wear and tear produces small fragment visible to the eye giving clothes a dull and used look. Cellulases remove theses fiber fragments thus providing anti-pilling, softness, whiteness and color clarification benefits. Cellulase benefit is not always noticeable after a single wash. This is related to the fact that several rounds of enzymatic digestion may be required to fully remove the small pieces of loose cotton [24].

New Enzymes

New types of enzymes are entering the detergent marked. These include mannases (introduced 2000) [9], pectate lyases (introduced 2003) and oxidoreductases. These new enzymes are more specialized than the enzymes previously introduced into the detergent market, are the use is thus not as widely spread as proteases, amylases and lipases.

Other Detergent Components

Besides surfactants and enzymes detergents contain of a variety of components. They will be described shortly in the following.

Dispersing Polymers

Dispersing polymers serve to suspend soil after removal from a surface. The suspension is important such as the soil is not redeposited. Usually two types of polymers are used in a formulation, one ionic and one nonionic. Polyethylene glycol and polyvinyl alcohol are examples of nonionic polymers. Ionic dispersing polymers usually compromise of homopolymers of acrylic or maleic acid [1].

Builders and Chelates

Builders and chelates act as both chemical and physical "backbone" in a formulation [25]. They serve to keep control of metal ions and adjust pH. The presence of builders and chelates serve as metal ion control agents, thus preventing precipitation of anionic surfactants. Builders and chelates include sodium triphosphate, sodium carbonates, noncrystalline sodium silicate, zeolites, layered silicates and citric acid. In 2001 the builders were dominated by sodium carbonate ($2.7 \cdot 10^6$ t), sodium triphosphate ($1.5 \cdot 10^6$ t) and zeolite ($1.25 \cdot 10^6$ t) [25]. Lately triphosphosphate, due to the effect on the environment (eutrophication of lakses and rivers) has been replaced by zeolites and polycarboxylate polymers [7]. The building system contributes significantly to the ionic strength and usually keeps the pH in the range 9-10.5 for solid detergents and between 7-8.5 in liquid detergent formulations [25].

Bleaching systems

Bleaches destroy chromophoric groups responsible for color in soils via oxidative attack. Bleach delivering approaches include: chloride-based bleaches, peroxide-based bleach, activated peroxide systems and metal catalysts. The most typical bleach component today is sodium percarbonate [7].

Co-solvents

Typical co-solvents are glycerol, ethanol and 1,2-propanediol and are primarily relevant for liquid detergents. They serve to stabilize enzymes and prevent phase separation.

Performance enhancers

Besides enzymes described above, performing enhancers include Brighteners/fabric whitening actives, foam boosters, antifoam agents, thickeners and soil release polymers.

Detergent Formulation and Washing Conditions

Today, the number of laundry detergent products is enormous. This is due to the many different washing conditions around the world. E.g. the total washing time in Europe is up till two hours while in North America the time is around a quarter of an hour. This difference in time is also reflected in the amount of water used during wash (see table 3). The trend in both Europe and North America during the last ~20 years has been towards lower wash temperatures such that energy costs are reduced. In contrast Latin America and Asia have always used low wash temperatures [7]. Wash temperatures as low as 2 ºC are sometimes used in Japan [1]. It has been possible to keep wash performance at the same level as that obtained at higher washing temperatures through the addition of small amounts of enzymes [7]. Both local and regional differences put the formulator in a position where the detergent product has to be formulated such that it is applicable to the local washing conditions.

Table 3. Average global machine wash conditions. Adapted from [1]

	Europe	**North America**	**Japan**
Water volume (L)	13	64	49
Washing time (min)	115	35	10
Temperature (ºC)	30-90	10-45	4-20
Water hardness (mM)	2.5	1.0	0.5
Detergent concentration (ppm)	5000-7500	1200-2000	600-1000

Representative formulations for liquid and solid detergent formulations are given in table 4 and 5. The formulations are presented in this chapter however important components such as surfactants will be discussed in chapter II. Notice the combination of ionic and nonionic surfactants as well as the use of enzymes. An important difference between liquid and solid detergents is co-solvents.

Table 4. Three representative liquid laundry detergent formulations by weight. Adapted from [1].

Ingredient/Product	A	B	C
C_{11}-C_{13} Linear alkyl benzene sulfonate	12	-	28
C_{12}-C_{15} Alkyl sulfate	-	18	-
C_{14}-C_{15} Alkyl sulfate	-	-	14
C_{14}-C_{15} Alkyl ethoxy sulfate	12	2	-
C_{12}-C_{13} Alcohol ethoxylate	3	4	-
C_{11}-C_{13} Alcohol ethoxylate	-	-	3
C_{16}-C_{18} Alkyl N-methyl glucamide	-	8	2
C_{12}-C_{14} Fatty acids	2	11	-
Oleic acid	-	-	3.4
Citric acid	3	5	5.4
Sodium cumene sulfonate	4	-	-
NaOH	6	-	0.4
Ethanol	-	3	7
1,2 propanediol	3	10	6
Monoethanolamine	3	9	17
Protease[a]	0.8	0.8	1
Amylase[a]	-	0.3	-
Lipase[a]	-	0.1	-
Cellulase[a]	-	0.1	-
Polyester-based soil release polymer	0.2	0.2	-
Water + minors	Balance	Balance	Balance

[a]Enzymes are added from liquid stocks where typical enzyme levels in the stock range from 1-8% by weight.

Table 5. Three representative granular laundry detergent formulations by weight. Adapted from [1].

Ingredient/Product	A	B	C
C_{11}-C_{13} Linear alkyl benzene sulfonate	8	10	-
C_{12}-C_{18} Alkyl ethoxy sulfate	-	-	5.3
C_{14}-C_{16} Secondary alkyl sulfate	2	-	-
C_{14}-C_{15} Alkyl sulfate	-	7	-
C_{16}-C_{18} Alkyl sulfate	2	-	-
C_{14}-C_{15} Alkyl ethoxy sulfate	-	1	-
C_{12}-C_{15} Alcohol ethoxylate	3.4	-	-
C_{14}-C_{15} Alcohol ethoxylate	-	1	3.3
Sodium tripolyphosphate (STPP)	-	-	10.7
Zeolite A	18	22	10.7
Carbonate	13	19	6
Silicate	1.4	1	7
Sodium sulfate	26	10	40
Na Perborate tetrahydrate	9	-	5
Na Perborate monohydrate	-	1	-
N`N``-tetraacetyl ethylene diamine (TAED)	1.5	-	0.5
Nonanoyloxybenzene sulfonate (NOBS)	-	4	-
1-hydroxyethane diphosphonic acid (HEDP)	0.3	-	-
DTPA	-	0.4	-
Protease[a]	0.8	0.3	0.3
Amylase[a]	0.8	0.1	0.1
Lipase[a]	0.2	-	0.2
Cellulase[a]	0.15	-	0.3
Acrylic/maleic copolymer	0.3	1	0.8
Carboxymethylcellulose (CMC)	0.2	-	0.2
Polyester-based soil release polymer	0.2	0.4	-
Minors	Balance	Balance	Balance

[a]Enzymes are added in granulated form where typical enzyme level in the granulate range from 1-8% by weight

Chapter II: Surfactants

Surfactants have a central role in this thesis and in this chapter the most important properties of surfactants in relation to interactions with proteins will be described. This includes classification of surfactants, mode of action and micelle structure.

Surfactant Classification

Surfactant usage in detergent mainly comes from their dual property of having both hydrophilic and hydrophobic groups (fig. 1). Surfactants are typically classified into the following four types based on their hydrophilic group:

- Anionic
- Cationic
- Zwitterionic (both positive and negative charge)
- Nonionic

Interfacial Properties and Mode of Action

Surfactants are as the name indicates surface active agents. In relation a wash process, an interface could be the water/soil or the water/air interface. The hydrophobic part of a surfactant, usually a hydrocarbon chain, will prefer contact with a hydrophobic medium e.g. air or oil, while the hydrophilic head group will prefer a polar medium e.g. water. Hence, when a surfactant is dissolved in water the surfactant will migrate to an interface where it will orient in such a way that as little as possible of the hydrophobic part is oriented towards the hydrophilic water. This property is called adsorption and changes the properties of the interface [26]. The attraction of surfactants to interfaces is illustrated in figure 3.

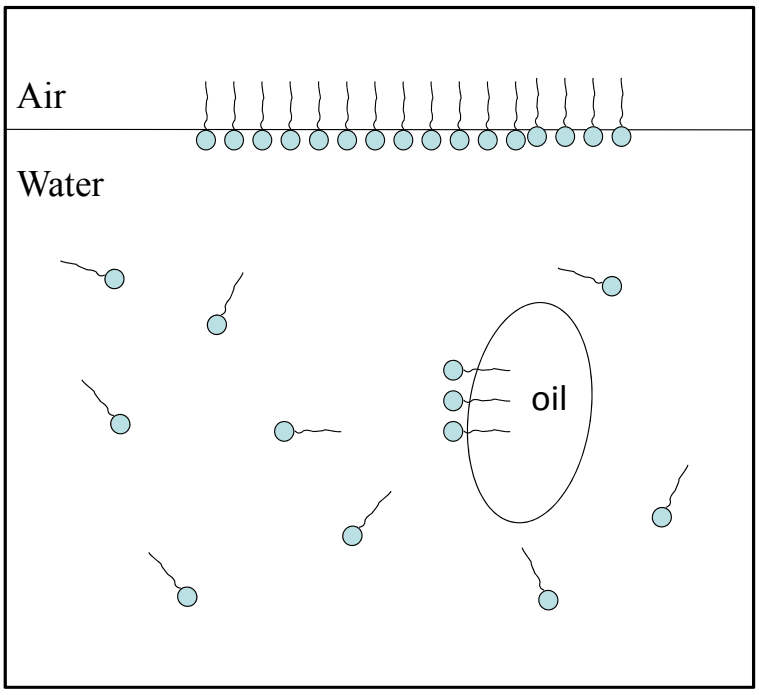

Figure 3. Surfactant behavior in water. The hydrophobic part of a surfactant will adsorb to hydrophobic surfaces, such as the air/water interface and water/oil interface.

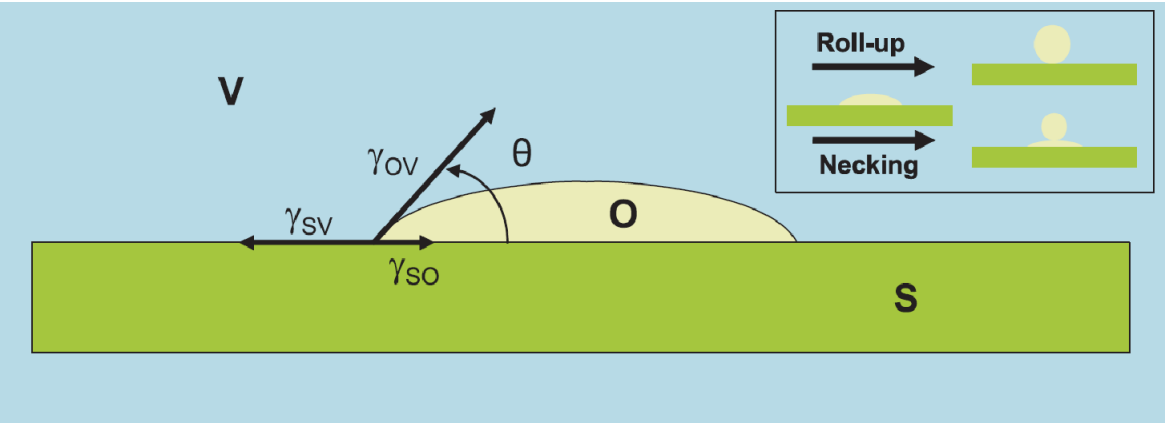

Figure 4. Surfactant cleaning of a fabric surface (S). The yellow color (O) illustrates an oil drop that is deposited on a solid surface (fabric) and surrounded by water (V). Θ is the angle of contact and γ_{sv}, γ_{so} and γ_{ov} are the interfacial tension between surface/water, surface/oil and oil/water, respectively. Surfactants can adsorb to the the oil drop or the fabric surface. This will change the tension between the interfaces, which in turn changes the angle of contact Θ. If γ_{sv} is primarily minimized, the angle of contact will increase and this will result in a "roll-up". If γ_{so} is primarily reduced this will lead to "necking". Illustration adapted from [2].

The primary purpose of surfactants is to wet surfaces and reduce the interfacial tension between oil and water such that soil is removed from the surface to be cleaned and dispersed in the aqueous phase [1]. The mode of action upon removal of soil, e.g. an oil drop, from a surface is illustrated in fig 4. The angle of contact (Θ) can be calculated using the Young equation:

$$cos\Theta = \frac{\gamma_{sv} - \gamma_{so}}{\gamma_{ov}}$$

Where, γ_{sv}, γ_{so} and γ_{ov} represent the surface tension between surface/water, surface/oil and oil/water, respectively.

The young equation can be used to explain how an oil droplet is removed from a surface. This equation will be included in the following which describes the events that take place when oil is removed from a surface. 1) Surfactants are transported to an interface. This can occur either as surfactant monomers or in the aggregated form of micelle. The transport of monomers is fairly rapid (10^{-5} cm^2/sec) while the transport of micelles is somewhat slower (10^{-7} cm^2/sec). 2) Surfactants adsorb to the oil/water, surface/oil, and oil/water interfaces, respectively. The adsorption of surfactants results in lowering of the interfacial energies at each of these interfaces. 3) A surfactant-soil complex is formed. The surfactants usually form a monolayer around the soil; however in some cases a bilayer is also formed. 4) The soil/surfactant complex is desorbed. Oily substances are typically desorbed either by "roll-up" or by "necking". "roll-up" occurs when the angle of contact (Θ) is increased, e.g. when γ_{sv} is primarily minimized. Such an effect is desirable because the entire oil drop is removed. "Necking" occurs when the angle of contact is unchanged, but γ_{ov} is decreased. Most of the oil drop is removed but a fraction will remain attached to the surface. 5) The soil-surfactant complex is transport of away from the surface and stabilized to prevent redeposition [1, 2, 27].

Aggregation of Surfactants

Surfactants have hydrophilic as well as hydrophobic properties. This amphiphilic nature highly influences how surfactants act in solution. Hydrophobic parts between individual surfactants can make favorable contacts thus avoiding unfavorable interactions with water. These hydrophobic interactions results in large supramolecular assemblies generally referred to as micelles. A highly simplified model of a micelle is presented in figure 1, but in reality micelles can adopt a variety of geometric described forms such as small spheres, disks, oblate or prolate ellipsoids or long cylinders [28, 29]. The size and shape of the supramolecular structures depends on many parameters such as: geometry of the surfactant, its charge, concentration, as well as physicochemical conditions such as temperature, ionic strength counter ion, shear rate, salt concentration and more [30-34]. A common feature of these aggregates is that the interior of the structure contains the hydrophobic part while the hydrophilic part is exposed to water. The formation of micelles is important as these supramolecular assemblies change the properties of the solution phase [26]. Figure 5 shows how some physical parameters change with the formation of micelles.

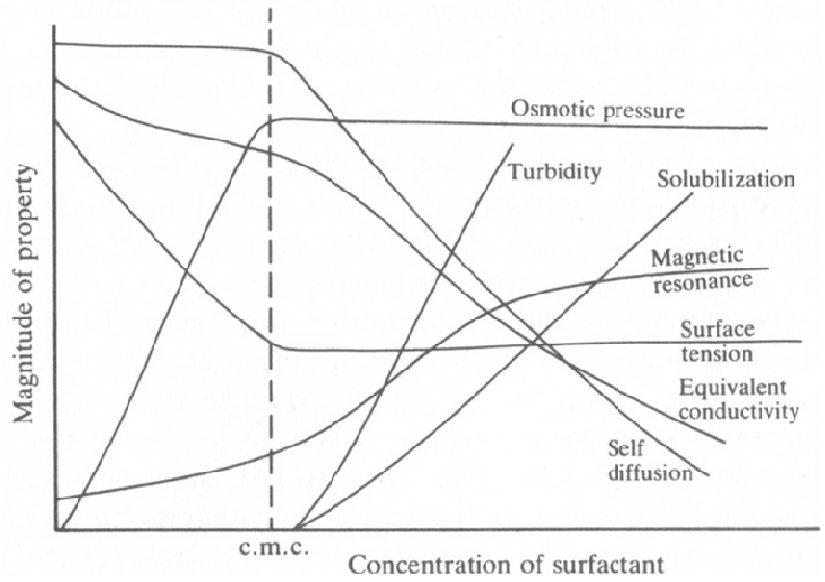

Figure 5. Schematic representation of the concentration dependence of some physical properties for solutions of micelle-forming amphiphiles. Adapted from [35].

Critical Micelle Concentration (cmc)

Micelles are formed at a concentration of surfactant called the critical micelle concentration (cmc). At the cmc and higher surfactant concentrations the monomer concentration remains relatively constant and the remaining molecules assemble into micelles. The cmc can thus be considered as a saturation concentration for monomers. It should be noted that some studies indicate that the monomer concentration decreases with increasing surfactant concentration [36, 37]. In relation to the exact determination of the cmc, it is important to realize that the cmc is not a specific concentration but a narrow range of concentrations [38]. The concept of a "critical concentration" for the exact formation of micelles from free surfactant is inexact but convenient.

An important micelle property is the number of molecules present in the micelles. This number is called the aggregation number and is around 100 for a surfactant with a dodecyl (C12) hydrocarbon chain. The aggregation number decreases with decreasing hydrocarbon chain length [28] (table 6). The typical aggregation number for SDS found in the literature is 64, however this number is concentration dependant; e.g. Quina *et. al.* [37], report aggregation numbers of 55 and 64 at SDS concentrations of 20 and 50 mM, respectively.

Table 6. Critical micelle concentrations (cmc) and aggregation numbers for a homologous series of sodium alkyl sulfates in water. Adapted from [35] and references therein.

Number of Carbon atoms	**8**	**9**	**10**	**11**	**12**	**14**	**16**	**18**
cmc in H_2O (mM)	140	60	33	16	8.6	2.2	0.58	0.23
Aggregation number	27	33		52	64	80		

The cmc is highly dependent on the properties of the given surfactant. Some general guiding rules can however be given (adapted from [27]):

- Increasing the hydrophobic part of the surfactant molecule favors micelle formation (see table 6). In aqueous media the cmc of an ionic surfactant is approximately halved by the addition of an additional CH_2 group. This effect is even more pronounced for nonionic surfactants.
- The cmc generally increases with increasing temperature.
- The addition of salt reduces the cmc of ionic surfactants. This is due to screening of the added ions. This effect is less for nonionic surfactants.
- Addition of organic molecules affects cmc in different ways dependent on the property of the given molecule. Molecules that locate to the outer area of the micelle may reduce the electrostatic repulsion of ionic surfactants, thus lowering the cmc. This effect is less for organic molecules that locate to the interior of the micelle.

How to measure the cmc

Many techniques have been used to determine the cmc, here among conductivity, surface tension, isothermal titration calorimetry (ITC) as well as the use of fluorescence probes [22, 39]. The cmc is an important parameter as it changes the property of the solution phase. Proteins interact differently with micelles as compared to monomers. E.g. some proteins can be denatured by surfactant monomers while other proteins can only be denatured by surfactant micelles [40, 41]. In order to understand the mechanism of interaction between surfactants and proteins it is thus important to determine the cmc correctly.

In this thesis the fluorescent probe pyrene [42, 43] has been used to determine the cmc of surfactants. Pyrene is a very hydrophobic probe and the fluorescence emission spectrum is sensitive to the environment. This means that when micelles are present in solution pyrene partitions into the hydrophobic interior of the micelle and the emission spectrum changes. Figure 6 shows two fluorescence emission spectra of pyrene; one in the presence of surfactant monomers and one in the presence of surfactant micelles. There are clear differences in the

two spectra and the ratio between emission peaks one (I1) and three (I3) is typically used to evaluate the polarity of the environment. E.g. in a polar environment (surfactant monomers) the I3/I1 ratio is ~0.65 while the ratio is ~0.95 in a nonpolar environment (surfactant micelles).

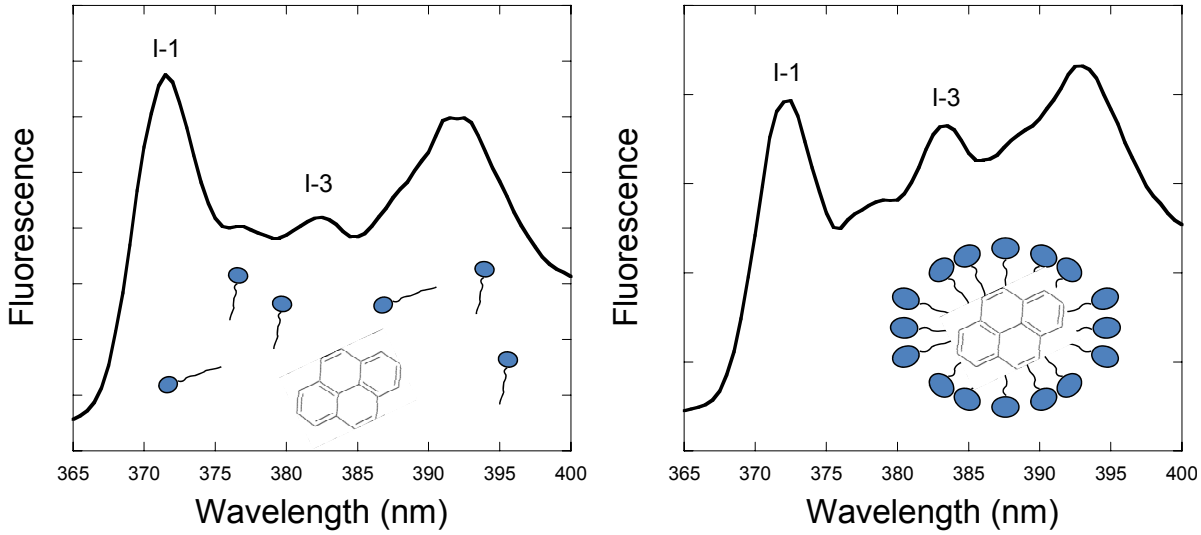

Figure 6. Fluorescence emission spectra of pyrene. (Left) In the absence of micelles the ratio between emission peak three (I-3) and one (I-1) is ~ 0.65. (Right) In the presence of micelles the I3/I1 ratio is ~0.95

Micelle Dynamics

Micelles are not static structures but are in rapid equilibrium with their monomers. Individual surfactants thus break and recombine into micelles constantly. The exchange of monomers between the bulk aqueous phase and the micelle is a very fast process on the nano- to microsecond timescale. The formation and dissociation of micelles is in the micro- to millisecond timescale [35].

"Rod-like" Micelles

As mentioned above micelle shape is dependent on parameters such as concentration, ionic strength and more. Especially high surfactant concentrations and addition of salt induce formation of large aggregates. They are usually called "rod-like" micelles but are sometimes also referred to as "worm-like", "thread-like" or even "living polymers" [44]. Although called "rod-like" they seem to be more flexible than rigid, very large, and range from a few nanometers to micrometers in length [31, 34]. See figure 7 for a structural illustration of a "rod-like" micelle.

"Rod-like" structures have been reported for all four classes for surfactants, although most reports have been on charged surfactants. In general nonionic surfactants are less prone to form "rod-like" structures. The geometry of "rod-like" micelles have been well characterized for cationic surfactants however analogous studies on anionic surfactants are still in its infancy [29]. "Rod-like" micelles are also formed when mixing surfactant with co-solvents such as short chain alcohols [45, 46]. For a more in-depth insight into the assembly of "rod-like" structures a recent review has been presented by Cècile Dreiss [34].

The structure of "rod-like" micelles has received much attention as the micelle structure changes the properties of solution phase. This has found application value in numerous industrial and technological fields, such as personal care products and the oil industry [34]. Micelle structures are mainly characterized using scattering techniques such as small angle neutron scattering (SANS) and dynamic and static light scattering [34]. Several studies over the last couple of years however report differences in micelle properties when studied in D_2O or H_2O. E.g. micelles formed in D_2O are larger than micelles formed in H_2O [15, 30, 47]. These structural differences have primarily been reported for alkyl-polysaccharides.

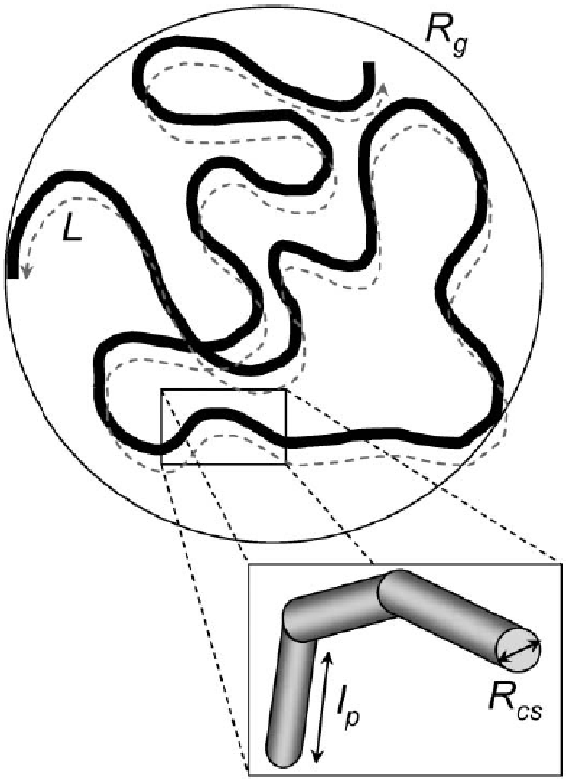

Figure 7. Schematic representation of a "rod-like" micelle showing characteristic length-scales: the overall radius of gyration R_g, the contour length L, the persistence length l_p and the cross-section radius R_{cs}. Adapted from [34]. The persistence length l_p, describes the length over which the micelles are considered rigid, and thus provides a measure of micellar flexibility

Micelle Structures of SDS and Dodecyl-Maltoside

Sodium dodecyl sulfate (SDS) and dodecyl-maltoside (DDM) are representatives of typical ionic and nonionic surfactants used in this thesis. In the following, current knowledge on micelle structure of these two surfactants will be described.

Both SDS and DDM form oblate ellipsoidal micelles [48-51] at relative low concentrations. The geometry of this structure is explained in figure 8. These structures are based on SANS studies performed in D_2O. The DDM micelles are monodisperse with an aggregation number of 132 and this number is only to very little extent influenced by surfactant concentration [49]. As mentioned above the aggregation number for especially ionic surfactants change

with increasing concentration. This is also the case for the anionic surfactant SDS. At a concentration 20 mM the aggregation numbers is 55 and at 50 mM the aggregation number is 64 [37]. Hence, although the shapes of the micelles are similar at 20 and 50 mM, the number of surfactant molecules present in the micelle is increased at 50 mM. At higher concentrations (>50 mM) SDS micelles undergo a transition from oblate ellipsoidal to "rod-like" micelles [52]. In figure 8 the geometries of oblate ellipsoidal and "rod-like" micelles are depictured. The main difference between ellipsoidal and "rod-like" micelles is that the "rod-like" micelles are significantly longer as compared to the oblate ellipsoidal micelles.

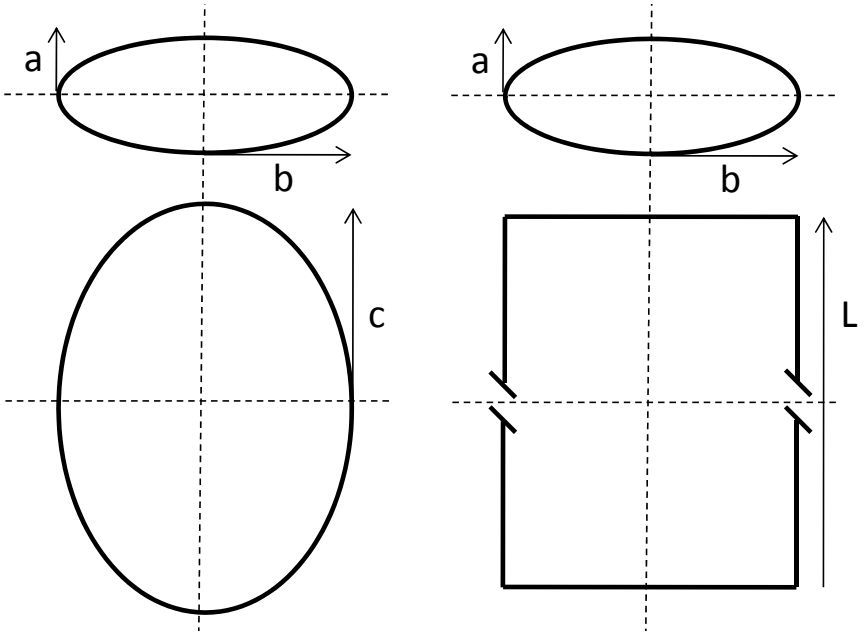

Figure 8. Schematic representations of models describing micelle structures. (Left) tri-axial ellipsoids with half axes a>b>c. This model can be used to describe both SDS and DDM micelles at low concentrations. (Right) At high SDS concentrations SDS aggregates can be described as elongated rods with an elliptical cross section. Models are adapted from [31]

At the present time, it has not been possible to gain insight into SDS micelle structure above 100 mM, as the available literature is limited in this concentration range. It is however apparent that SDS micelles can adapt a variety of different structures depending on the conditions. E.g. salt (NaCl) highly influence the structure of SDS micelles. This may especially be relevant in relation to industrial conditions were the ionic strength is quite high due to presence of builders and chelates. Magid *et. al.* [53] have studied micelle structures between 1-30 mM SDS in the presence of 1-2 M NaCl. Profound effects were observed; the contour length (length of the micelle) changes from 40 nm in 1 M of NaCl to 678 nm in 2 M of NaCl. Unfortunately they have not performed studies in the absence or at very low NaCl concentrations which would be more related to the concentrations of buffer used in the studies presented in this thesis.

Chapter III: Protein-surfactant interactions

Many industrial, biological, pharmaceutical and cosmetic systems contain both surfactants and proteins. The interplay between proteins and surfactants has thus received much attention. One of the most well known applications is SDS-PAGE [54], which is routinely used to estimate the molecular weight of proteins. Although many studies have looked at protein-surfactant interactions, the mechanism by which surfactants denature proteins is in general not well understood [55]. Most studies have been devoted to the interaction of proteins with the anionic surfactant SDS. These studies include well know model proteins such as lysozyme [56-59], bovine serum albumin (BSA) [60-68], trypsin [69] and more [70-73]. This chapter is devoted to parameters which are important in relation to protein-surfactant interactions. This includes types of interactions between proteins and surfactants and how the interactions can be described. The denaturing properties of surfactants are also compared to traditional denaturing agents such as urea and Guanidinium cloride (GdmCl). Furthermore the role of proteins are also discussed, this includes why some proteins are resistant to surfactant denaturation.

How to Denature a Protein

In the next section we shall discuss how surfactants interact with protein. Invariably these surfactants lead to denaturation of the majority of all proteins, often in a complex series of events involving initial binding, formation of complexes on the protein surface and salvation in a protein-micelle complex. The large number of conformations sampled by the protein in the course of these interactions is very characteristic for surfactants. This is probably best emphasized by briefly describing the relatively simple denaturation steps that a protein will go through under more conventional denaturation procedures. These include changing pressure, adding chemical denaturants (urea or GdmCl), thermal denaturation and acidic/alkaline unfolding [74]. For small proteins, all these processes typically occur in a simple one-step mechanism where the native and the denatured state are the two major populated species; only rarely do we find stable intermediates midway. Larger proteins usually denature irreversibly, i.e. they form aggregates and precipitate on the pathway from the denatured- to the folded state [74]. Depending on the method of denaturation the end state may be different; it is typically a completely feature-less random coil with considerable conformational freedom in chemical denaturants, while the thermally denatured state and the acid-denatured state tend to be compact and contain residual secondary structure [74]. E.g. in the case of the protein barnease, the acid denatured state seem to have some flickering α-helix in regions that are α-helical in the native state [75]. The fact that most denaturation methods lead to protein structures where some residual structure prevail is the reason why the denatured state is referred to as “D” and not “U” for unfolded. In addition, under physiological conditions proteins do not completely unfold, as this state is thermodynamically very unstable.

A major virtue of the chemical denaturants is the linear relationship between free energies of unfolding and denaturant concentration. Conventionally this is not seen to be the case for surfactants, although the present thesis uncovers several instances where similar relationships are observed [40], in addition, an empirical correlation has been observed in an increasing number of instances between denaturation potency and the mole fraction of the anionic surfactant in binary mixed micelles [76, 77].

Surfactants denature proteins differently than classical denaturants such as GdmCl and urea. This is probably best illustrated using an example. The folding mechanism for the ligand binding protein ACBP has been unraveled by studying folding kinetics. The linear relationship between refolding- and unfolding rate constants as a function of GdmCl indicate that ACBP fold in a reversible 2-state manner, where the native and the denatured state are the only two populated species (fig. 9). In contrast using the anion surfactant SDS as the denaturing agent, the folding mechanism is irreversible, and during the unfolding pathway several intermediates/complexes are found. The example presented in figure 9 is from is from paper IV where the interactions between ACBP and SDS are studied in detail at pH 8. Initially ACBP binds a few SDS molecules without denaturing. In the next step ACBP bind additional SDS, loses native structure and two individual polypeptide chains are bound to a single decorated micelle. Additional SDS binding leads to a complex where a single polypeptide chain is associated with a single decorated micelle. In the final step bulk SDS micelles are formed and the ACBP polypeptide chain associates with these micelles. The mechanism of denaturation is described in much more detail in paper IV. In all, this example clearly shows that the denaturation mechanism of small proteins can be much more complicated using surfactants as the denaturation agent as compared to classical chemical denaturants such as GdmCl or urea.

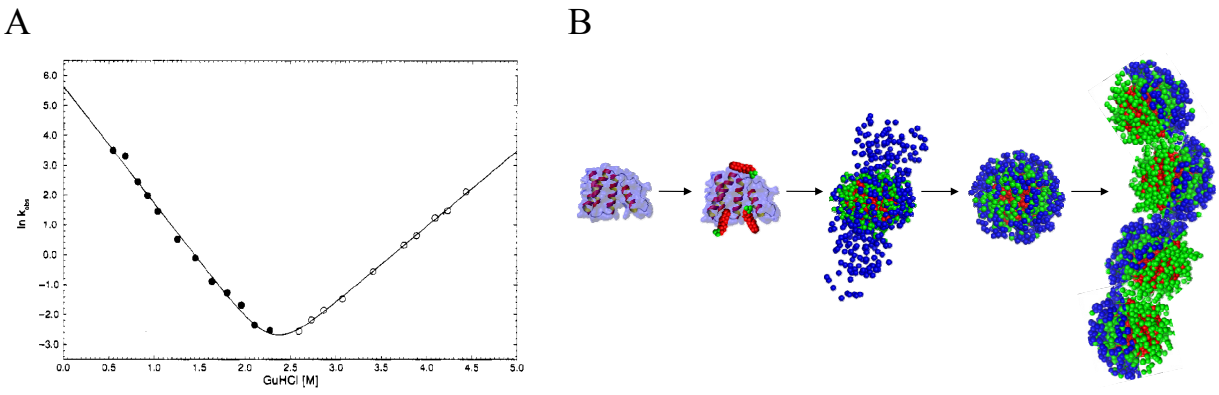

Figure 9. ACBP denaturation mechanisms in (A) GdmCl and (B) SDS. Kinetic refolding and unfolding studies in the presence of GdmCl show that ACBP folds in a reversible 2-state manner : N↔D. Adapted from [78]. B) Denaturation mechanism in SDS. Note that the process is irreversible and that denaturation proceeds in several steps. The blue color represents the ACBP polypeptide, while the red and green color represents SDS molecules. Adapted from [79].

Nature of Interactions

Both surfactants and proteins are amphiphilic molecules and strong interactions, especially, between ionic surfactants such as SDS and proteins have been noted. Non-ionic surfactants usually do not interact with proteins as they prefer to self-associate [80].

Many factors influence the interactions between surfactants and proteins. With regards to SDS, the primary surfactants used in thesis, the nature of the interactions with proteins has been found to be both electrostatic and hydrophobic [81, 82]. The interactions are much stronger as compared with other denaturants such as urea of GdmCl which act by weak interactions with the protein backbone [83]. This means that surfactants denature most proteins at millimolar concentrations, while urea and GdmCl typically denature proteins at molar concentrations. The importance of electrostatic interactions is seen by studying the effects of pH. At alkaline pH, SDS is found to interact weakly with proteins due to unfavorable electrostatic interaction between the SDS head group and negatively charges residues. At acidic pH most proteins carry a positive net charge, which facilitates interaction between positively charged residues and the anionic head group of SDS. Interactions between proteins carrying a positive net charge and SDS can lead to precipitation of the complex, because the complex is neutralized. Often it is possible to redissolve the precipitated complex by adding excess SDS; however some proteins are not readily redissolved. One example is the precipitated lysozyme-SDS complex which was found increasingly difficult to redissolve with increasing protein concentration [56].

Lysozyme has been crystallized in complex with a few SDS molecules [84]. This study revealed interactions between the hydrophobic surfactant tails and hydrophobic residues in lysozyme. In addition to showing the importance of hydrophobic interaction between surfactants and proteins the study also showed that only a few surfactant molecules are able to perturb the native structure of proteins. Binding of four SDS molecule lead to an “open-winged” conformation, where the SDS molecules were wedged into the interior of the protein.

Binding Isotherms

Binding isotherms are often used to describe to interactions of surfactants with proteins. In a binding isotherm the average number of surfactant molecules bound pr protein molecules is plotted as a function of log to the free surfactant concentration (fig. 10). For proteins such as BSA [64] and lysozyme [80] the SDS binding isotherm can be divided into four regions, which display different types of interaction. The four regions are:

I) Specific binding
II) Non cooperative binding
III) Cooperative binding
IV) Saturation

Specific binding is predominantly electrostatic [85] and takes place at low SDS concentrations. Specific binding means that surfactants bind to independent parts of the protein, in the case of SDS often to positively changed residues. The binding of a few surfactants does not necessarily perturb the native structure. Reynolds *et. al.* [86] showed that the binding sites have a specificity for different head groups; e.g. BSA bind alkyl sulfates and sulfonates strongly while the affinity is diminished for alkyl carboxylates. The length of the hydrocarbon chain also influences specific binding. Both dodecyl (C12) and decyl (C10) sulfates show specific binding to lysozyme while octyl sulfate (C8) only interact cooperatively [87]. Similar results were found for binding of alkyl trimethylammonium bromids to BSA [88]. Note that not all proteins have natural binding sites for surfactants. Non-cooperative binding follows specific binding and the region is characterized by a gradual binding of surfactant molecules. This occurs over an intermediate concentration range. The next step involves cooperative binding. Cooperative binding means that the binding affinity increases as more surfactant is bound. The concentration range over which cooperative binding takes place is usually quite narrow and a dramatic increase in binding number is observed. Cooperative binding is followed by saturation. At this point all available binding sites on the polypeptide chain are saturated with SDS. The structure of the saturated complexes formed between SDS and proteins will be described in more detail in the next section.

In general most proteins with no or reduced disulphide bonds bind ~1.4 gram SDS pr gram protein while proteins with intact disulphide bonds binds 1 gram SDS pr gram protein [68]. For proteins with reduced disulphide bounds this corresponds to roughly one surfactant molecule per two amino acid residues [89]. This is the general case however there are also reports of proteins that bind much less SDS [90, 91]. At saturation, these proteins have lost tertiary structure but retain much secondary structure. SDS binding is also influenced by glycosylation. Studies on the enzyme phytase from *Peniophora lycii* showed that the glycosylated variant bound less SDS as compared to the non-glycosylated variant [92].

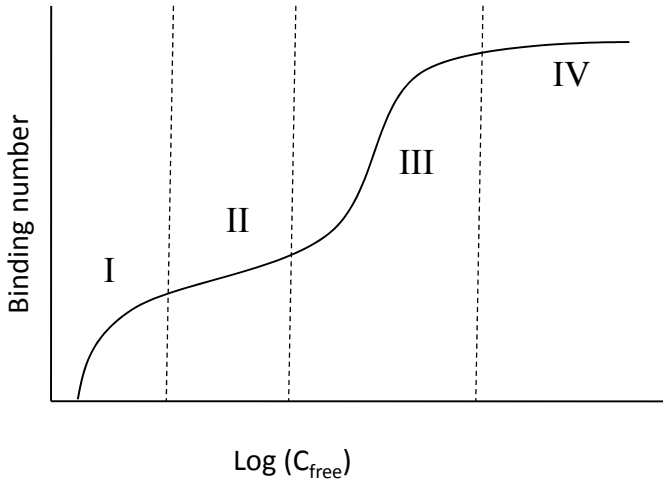

Figure 10. Schematic illustration of a surfactant binding isotherm. (I) specific binding. (II) Non-cooperative binding. (III) Cooperative binding. (IV) Saturation. Binding number is the number of surfactant molecules bound to a protein molecule and C_{free} is the concentration of free surfactant.

Saturation Complexes

Although SDS denatures the majority of globular proteins at low concentrations, most structural studies on complexes have been performed at relative high concentrations where proteins are saturated with SDS. Saturation is in general completed as the free surfactant concentration approaches the cmc [80]. Several models have been proposed here among the "rod-like particle model" [89, 93], which describes the protein-SDS complex as a rigid rod with a cross-sectional radius of about 18 Å and a length that is proportional to the length of the protein. The model which has received most support is the "bead and necklace" model (fig. 11). In this model the polypeptide chain is wrapped around SDS micelles or micelle-like clusters [94]. A variation of this model is the "decorated micelle". The main difference between the two models is that the polypeptide chain wraps around micelles in the "bead and necklace" model while the polypeptide chain passes through the micelles in the "decorated micelle" model. A few more model are discussed in [80], however these models were proposed many years ago and have not been assigned much support for a long time.

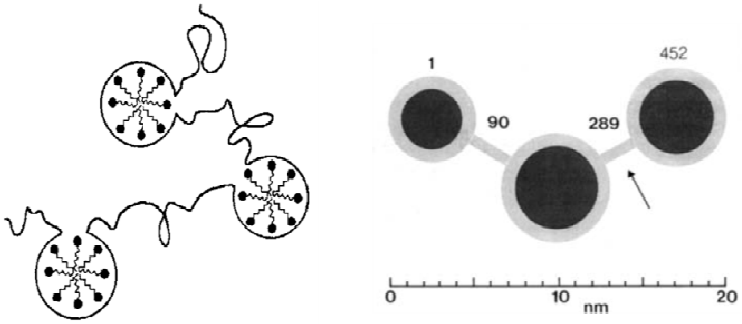

Figure 11. Schematic presentation of two models used to describe the SDS-protein complex at saturation. (Left) "Bead and necklace" model; the polypeptide chain is wrapped around SDS micelles or micelle-like clusters. Adapted from [64]. (Right) "Decorated micelle" model; the polypeptide chain passes through the micelle. Dependent on the size of the protein the polypeptide chain can pass through several micelles. Adapted from [80].

Role of Proteins

The biological role of proteins has been found to be important for the interactions between surfactants and proteins. E.g. BSA, which functions biologically as a carrier for fatty acid anions and other simple amphiphiles, has several binding sites for alkyl-sulfates [67]. This means that BSA can bind a number of SDS molecules without denaturing. In fact the binding of a few SDS molecules at specific sites can stabilize the SDS/proteins complex [95]. At high SDS concentrations BSA is eventually denatured by the large number of SDS molecules bound.

Non-ligand binding proteins, which do not have natural binding sites, will interact differently with SDS. There are two scenarios. Either the protein does not bind SDS and remains in the native state or the protein binds SDS, which often leads to disruption of the native state. Tnfn3, studied in the paper I, is an example of a protein that binds very little SDS at concentrations below the cmc and thus retains native structure [40]. This protein is thus resistant to monomeric SDS denaturation. Tnfn3 is however denatured at SDS concentrations above the cmc, which means that SDS micelles can denature the protein.

An important parameter is the amino acid composition of a given protein. Because surfactants like SDS interact strongly with positive charged residues, the interactions are highly dependent on the composition of especially charged residues. SDS interacted strongly with positively charged residues like arginine and lysine on proteins surfaces. Such interactions can lead to neutralization of the complex and precipitation as described previously [56].

Overview of Proteins

This section serve to provide an overview of the proteins studied in this thesis. In all, six proteins are studied and are listed in table 7. This table provides information such as pdb codes, molecular size, isoelectric point (pI), secondary structure composition and the number of cystine bridges. Cartoon presentations based on the pdb codes are shown in figure 13.

Table 7. Overview of proteins.

Protein	PDB	Mw (kDa)	[a]pI	[b]α-content (%)	[b]β-content (%)	Cys-Cys
ACBP	1hb6	10	6	77	-	-
Myoglobin	1wla	17.7	8.1	67	-	-
Tnfn3	1ten	10.1	4	-	53	-
TII27	1tit	10.9	4.8	-	54	-
α-lactalbumin	1f6s	14.2	4.6	56	8	-
TlL	1dt3	29.3	5	39	19	3

[a]Calculated using the tool at : http://www.iut-arles.up.univ-mrs.fr/w3bb/d_abim/compo-p.html
[b]Author-approved secondary structure [96].

The proteins have been selected not for their biological properties (which I will not dwell upon in more detail) but due to their secondary structure composition and their well characterized physiochemical properties, such as folding and stability. These parameters are helpful when comparing with denaturation in surfactants. Folding properties are found for ACBP [78, 97-99], Tnfn3 [100], TII27 [101], α-lactalbumin [102-104] and myoglobin [105-107]. Tnfn3 and TII27 are dominated by β-structure and thus serve as models for proteins with large content of β-structure. Both ACBP and myoglobin have high content of α-structure and serve as models for proteins with large content of α-structure. In addition, myoglobin is a more complex protein compared to ACBP because myoglobin is almost twice the size and binds the co-factor heme (fig. 12).

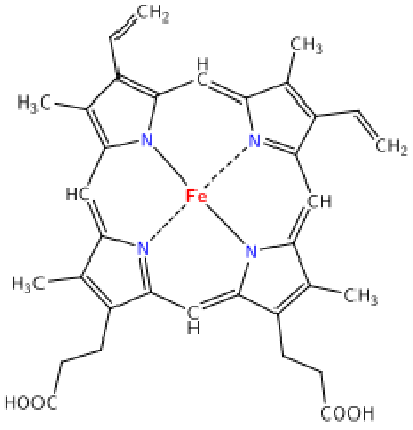

Figure 12. Structure of heme B.

In general very little literature is available on protein-surfactant interactions with proteins that contain co-factors. α-lactalbumin is the second protein is this study that can bind a co-factor. In contrast to myoglobin which binds a relative large co-factor, αLA binds the small co-factor Ca. Another significant difference between myoglobin and αLA, is that αLA has has mixed α/β-structure compared to myoglobin which is exclusively α-structured. The last protein studied in this thesis is *Thermomyces lanuginosus* lipase (TlL) [19, 22]. This enzyme is interesting since it is commercially available and used in detergents. The gene coding for this enzyme has been cloned and is commercially produced by Novozymes in *Aspergillus oryzae* [108-111]. Not much data is available on the folding properties, probably because TlL is a relative large enzyme which folding mechanism is complex. TlL is an interesting enzyme to study since is known to interact with surfactants without denaturing [22]. The enzyme thus provides a possibility to compare our model proteins with an enzyme that is known to maintain activity in the presence of surfactants.

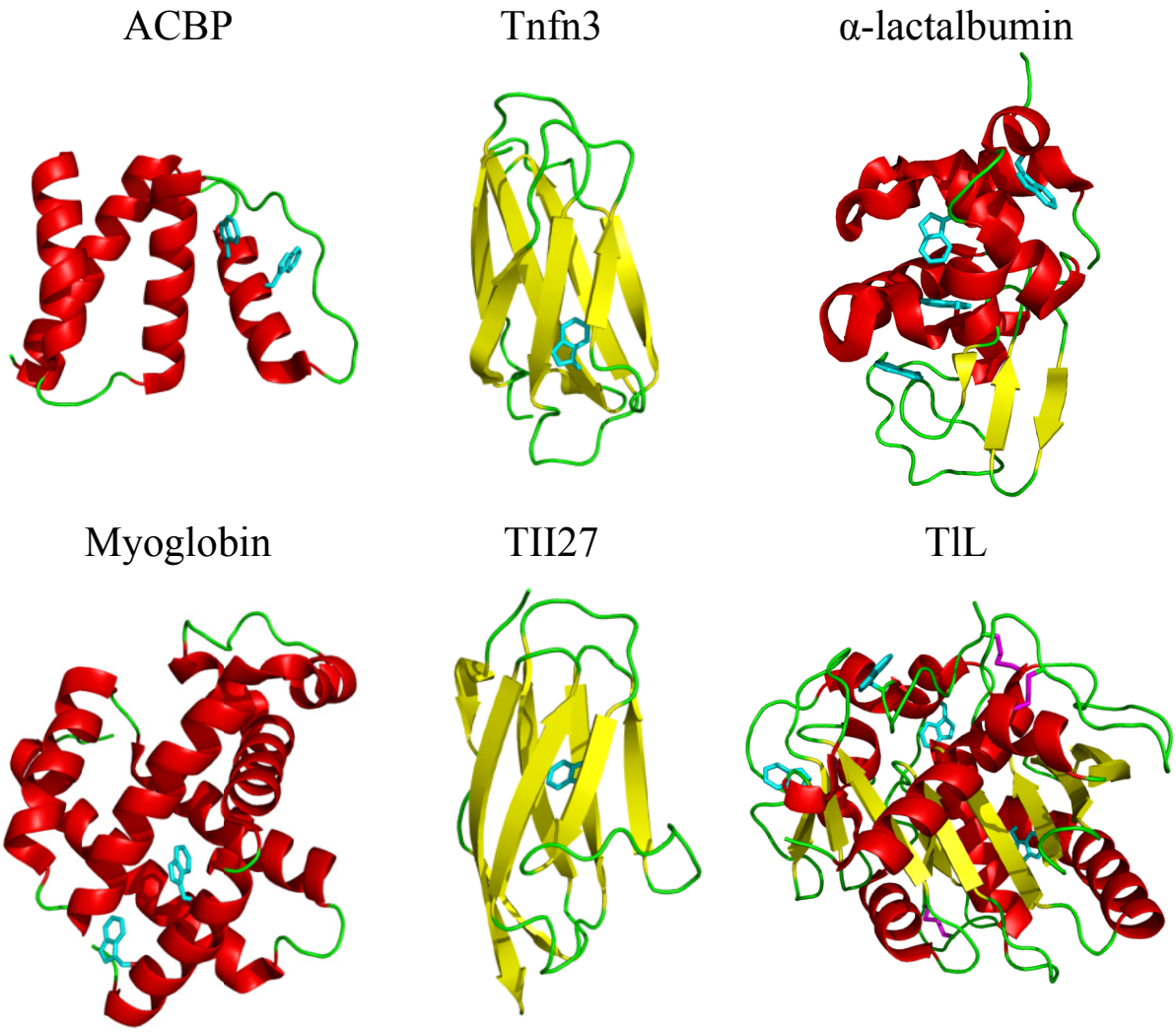

Figure. 13. Cartoon representations of the six proteins studied in this thesis. Cartoon presentations have been made in PyMOL [112], usning the pdb codes from table7. Tryptophan side chains are shown as sticks and colored cyan. Disulphide bridges are indicated in purple sticks. Co-factors as well as ligands are not depictured.

Some Proteins show SDS Resistance

While most proteins are denatured at millimolar concentrations of SDS, some proteins show natural resistance towards surfactant denaturation. This includes TlL, studied in paper VI, which clearly interacts with SDS and other surfactants, but resists surfactant denaturation. SDS actually has profound effects on the activity of TlL; at low concentrations, below the cmc and slightly above the cmc, the enzyme is activated by SDS, while higher concentrations lead to decreased activity [22]. The activation and inhibition profile is shown in figure 14.

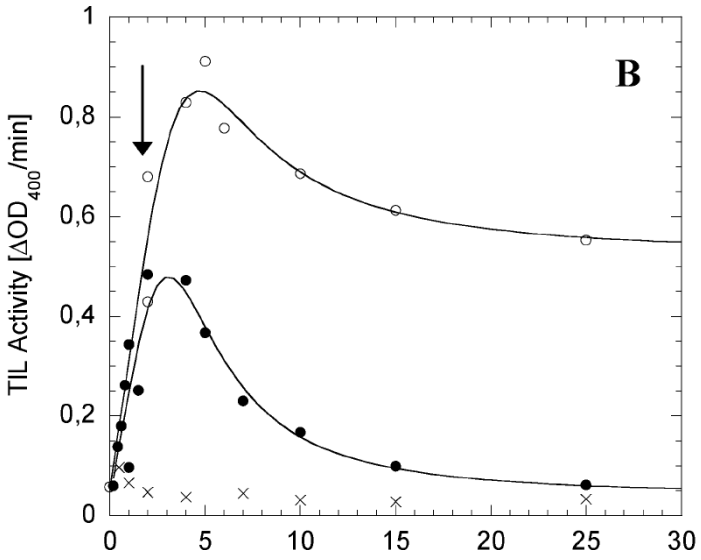

Figure 14. TlL enzymatic activity in SDS (O). Increase in activity is observed between 0 and 5mM SDS and decreases at higher concentrations. Arrow indicates the cmc in 50 mM Tris pH 8 and shows that micelles both activate and inhibit TlL. Adapted from [22]

The resistance towards surfactant denaturation has been thoroughly been studied by the group of David A. Agard [113-121]. The studies have primarily focused on the extracellular bacterial enzyme α-lytic protease (αLP). The Gram-negative soil bacterium *Lysobacter enzymogenes* secretes this enzyme which main task is to degrade other soil microorganisms [113]. While only a moderate sequence identity is found between αLP and the mammalian proteases trypsin, chymotrypsin and elastase they share the same overall three dimensional fold and are thus placed within the same family of proteases [122]. One of the main differences between αLP and its mammalian homologues is found in the N-terminal. For the mammalian proteases this region prevents premature activation, but is removed upon activation. In contrast the N-terminal pro-region (166aa) in αLP functions as a folding catalyst and is required for proper folding of the protein. After folding the pro-region is cleaved off leaving αLP in a state that is thermodynamically less favorable than the denatured state. αLP should thus converge towards to the denatured state. This is however not the case because of a very high energy barrier associated with unfolding, which leaves αLP trapped in a metastable native and active state. The scenario is illustrated in figure 15.

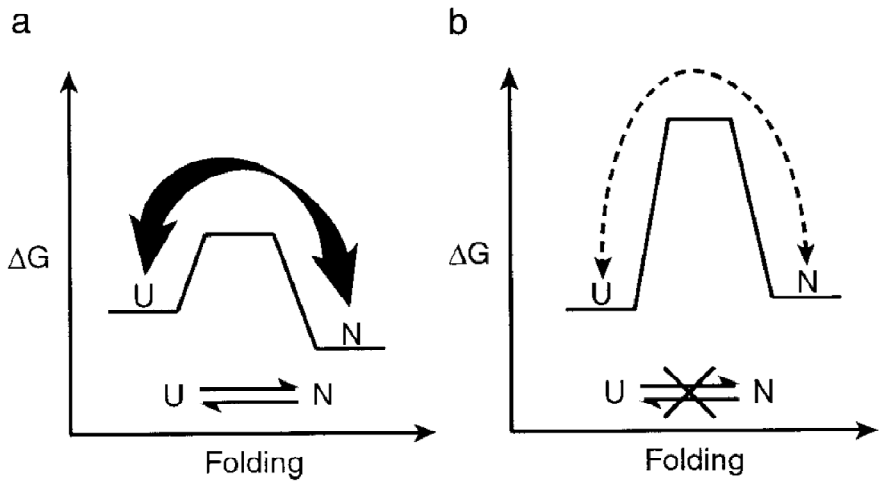

Figure 15. Advantages of kinetic stability. (a) A typical protein which native state is favored over the denatured. The energy barrier between the native and denatured state is small and the two states are thus in dynamic equilibrium. (b) Example of a protein that is trapped in the native state. The denatured state is thermodynamically favored over the native state; however the two states are not in dynamic equilibrium because of a large energy barrier between the two states. Adapted from [113].

The large energy barrier between the native and denatured state (fig. 15B), leads to very slow conversion towards the unfolded state. In the literature this is often referred to as kinetic stability. In some cases the energy barrier is so large that the dynamic equilibrium between the native and denatured state is non existing. It has been suggested that this phenomenon is an evolutionary feature intended to allow proteins to maintain activity under the extreme conditions they may encounter *in vivo* [113]. In addition because αLP functions extracellularly there is no need to regulate turnover [114]. Kinetic stability may thus also be a feature of many other secreted enzymes.

Manning and Colòn used SDS-PAGE as a method for identifying kinetically stable proteins [123]. The method is based on different migration of boiled and nonboiled protein samples in the presence of SDS. A property of kinetically stable proteins is that they are not denatured by SDS, however upon forced thermal denaturation the proteins unfolds, bind SDS and do not regain native structure upon cooling. Because the boiled and nonboiled samples bind different amounts of SDS the samples migrate with different mobilites during electrophoresis (Fig. 16). Comparing the migration of boiled and nonboiled samples can thus reveal whether or not a protein is kinetically stable. The study by Manning and Colòn identified eight kinetically stable proteins. These were: avidin, chymopapain, papain, Salmonella phage P22 tailspike protein, serum amyloid P, streptavidin, superoxide dismutase and transthyretin. The eight proteins shared two important features: firstly, a large content of β-structure and secondly, very slow unfolding rates in water. The half rates of unfolding were between 79 days and 270 years. This is very much in contrast to the non-kinetically stable proteins identified, which showed half rates between 14 minutes and 19 hours. In practical terms this means that the kinetically stable proteins, very rarely diverge from the native state. Manning and Colòn concluded that the kinetically stable proteins do not denature because SDS only binds to the unfolded state and since kinetically stable proteins do not unfold globally or locally they are practically immune to SDS denaturation.

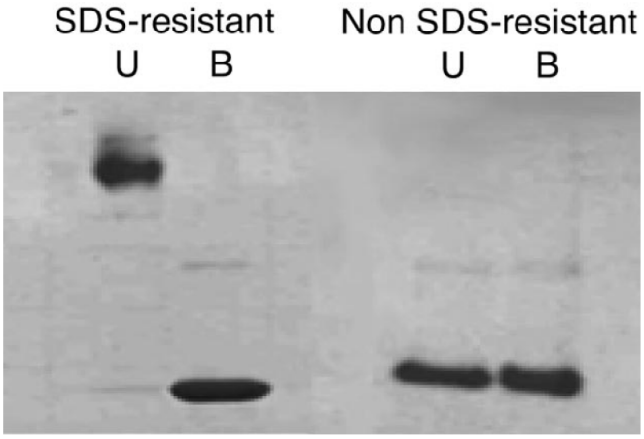

Figure 16. Identification of kinetically stable proteins by SDS-PAGE. Migration of a kinetically stable protein is shown on the left. The boiled (B) and unboiled (U) samples show different mobilities. On the right a non kinetically stable protein showed same migration no matter boiling.

To date, only very few kinetically stable proteins have been identified [123]. The number is however increasing and higher throughput techniques are being developed. E.g. using 2D SDS-PAGE the subproteome of kinetically stable proteins in *E.coli* has been investigated [124]. 50 kinetic stable proteins were indentified from *E.coli* lysate, of which 70 % were enzymes. Remarkably many of the proteins identified had previously been crystallized and the structures are thus solved. This indicates that kinetically stable proteins easily crystallize, probably because they rarely diverge from the native state. The study also showed that only very few proteins were pure α-helix proteins, and the ones found were in oligomeric assemblies. This indicates that α-helix proteins are biased against kinetic stability. β-structure, or at least long range interactions which stabilize β-structure as well as oligomeric assemblies thus have a central role in kinetic stability.

As described above kinetically stable proteins do no diverge from the native state. This has been thoroughly studied with NMR on αLP [114]. Hydrogen-deuterium exchange monitored by two-dimensional nuclear magnetic resonance (NMR) spectroscopy has been used to monitor global unfolding. After six months no exchange of protons were observed for those located in the interior of the αLP. This clearly demonstrates that the enzyme has a very rigid structure that does not undergo global unfolding.

One paper uses the term kinetic stability in connection with TlL [125]. This DSC study on native and TlL mutants indicate that TlL unfolds very slowly in water. The authors attributed this to large solvation barriers upon unfolding, i.e. the breaking of internal hydrogen bonds and penetration of water is an unfavorable process, leading to a high transition barrier. Solvation barriers are fully related to kinetic stability in that they both involve a high transition barrier; in fact solvation barriers may be a better explanation for kinetic stability than the situation depictured in figure 15. The scenario illustration in figure 15 only involves two states, the native and the denatured. This scenario can be applied to some small proteins however the folding process is much more complicated for larger proteins that fold through intermediates. Figure 15 can however be used to describe the transition which is the rate limiting step.

Kinetic stability is a relatively new phenomenon and has not been studied in much detail. The application of kinetic stability is however of potential great value. Knowledge of the mechanism of kinetic stability may be applied in the stabilization of protein for various applications such as drug stability and enzymes used in detergents.

Chapter IV: Biophysical Techniques

Protein-surfactant interactions have received much attention and a wide array of techniques has been used to study these interactions. These include conductivity [39], Nuclear Magnetic Resonance (NMR) [39], fluorescence [126], Fourier transform infrared spectroscopy (FTIR) [56], Isothermal titration calorimetry (ITC) [65, 90, 91, 127, 128], Capillary electrophoresis (CE) [129, 130], circular dichroism (CD) [39] and many more. In this thesis the primary techniques used are fluorescence, CD and ITC. In a few cases these studies have been supplemented with small angle x-ray scattering (SAXS) and capillary electrophoresis (CE) investigations in order to obtain additional valuable information. These techniques complement each other as they fundamentally report on different processes. The purpose of this chapter is to give a brief description of the principles of the primarily techniques used in this thesis.

Fluorescence

Fluorescence is the emission of light from a substance and occur from a electronically excited state [126]. The technique is considered as one of the primary research tools in biochemistry and biophysics.

The first event in fluorescence is the absorption of a photon, which leads to the excitation of an electron from the ground state. In the ground state the electron is paired with second electron in the same orbital, and the electrons have opposite spins. When one of a pair of electrons is excited to a higher energy level, either a singlet or a triplet state is formed. In the singlet state the spin of electrons is paired while in the triplet state it is unpaired (fig. 17). One main difference between the singlet and the triplet state is the lifetime. The singlet excited lifetime is in the range 10^{-5} to 10^{-8} s while the triplet state is in the range 10^{-4} to several seconds.

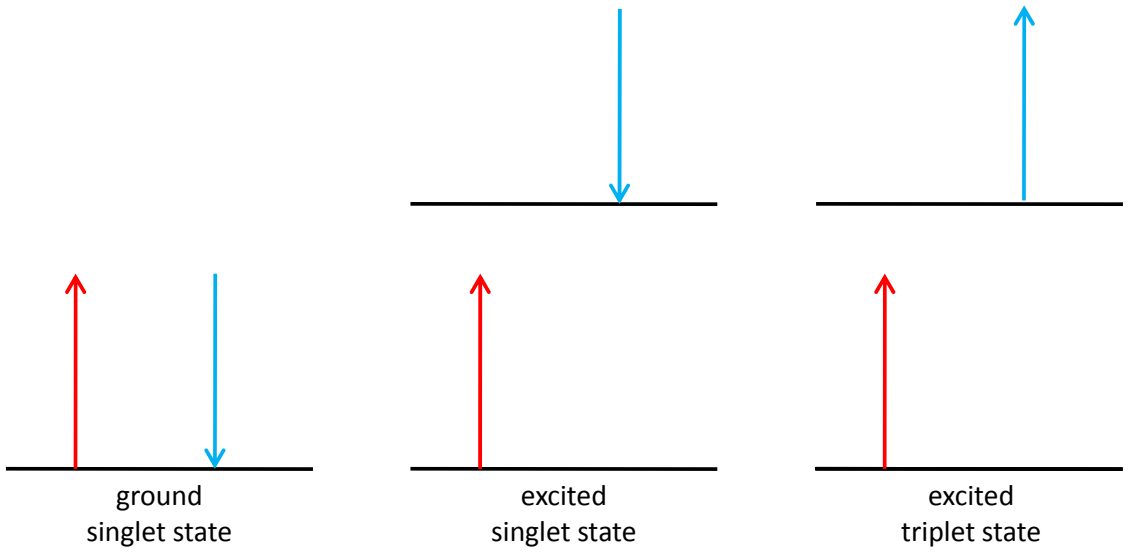

Figure 17. Electron spin and singlet/triplet excited states. Adapted from [131]

The process of electron excitation is best described using a Jablonski digram (fig. 18). S_0 is the ground state, which normally is a singlet state. The upper heavy lines are the energy levels for the ground vibrational states for the two singlet excited electronic states (S_1 and S_2). Excitation of a molecule can be brought about by absorption of two bands of radiation. The first is centered about the wavelength $\lambda_1(S_0 \rightarrow S_1)$ and the second is λ_2 $(S_0 \rightarrow S_2)$. A molecule may be excited to any of several vibrational levels during the electronic excitation process. Is solutions however, the excess vibrational energy is immediately lost due to collision with solvent, and occurs within ~10^{-12} s. This process is faster than fluorescence (~10^{-8} s) which means that fluorescence emission usually occurs from the lowest vibrational state of S_1. The electron can return to any of the vibrational levels of the ground state, which give rise to a broad emission spectrum [126].

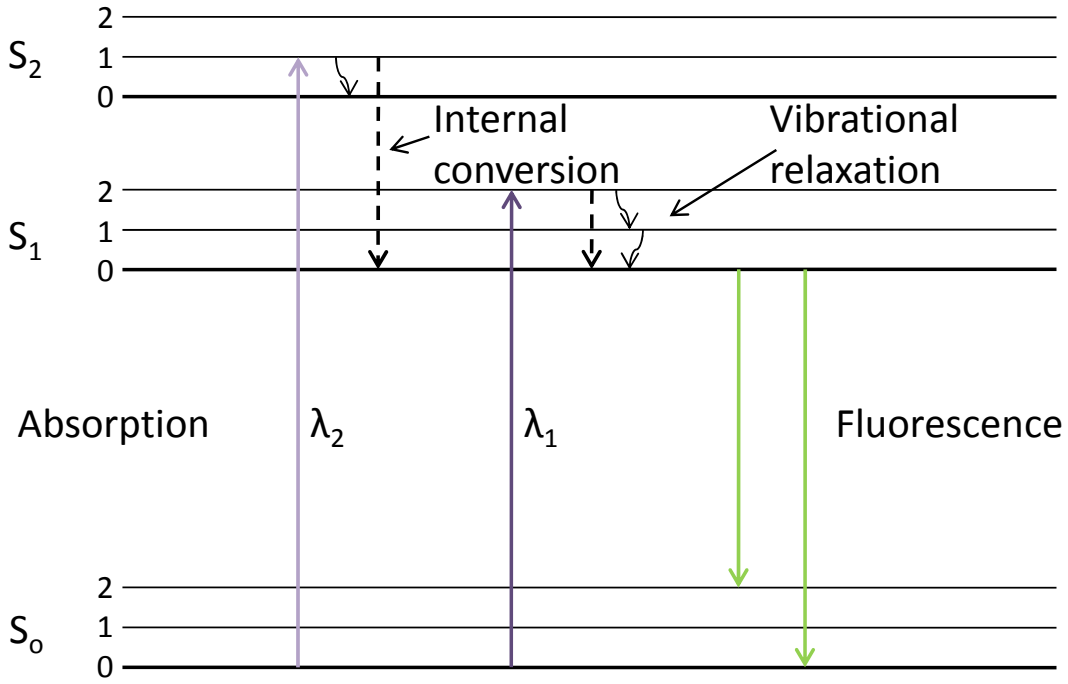

Figure 18. One form of Jablonski diagram. Adapted from [126]

Fluorophores are often divided into two classes; intrinsic and extrinsic. Extrinsic fluorophores are those added to samples. An example of an extrinsic fluorophore is pyrene which has been described in chapter II. Intrinsic fluorophores are those that occur naturally. Examples of intrinsic fluorophores in proteins are the side chains of tyrosine (Tyr) and tryptophan (Trp). The indole ring of Trp is the dominant fluorophore in proteins. It absorbs around 280 nm and emits light around 330 nm. The emission spectrum of the indole ring is highly sensitive to the polarity of the environment; Trp is thus referred to a solvatochromic fluorophore. E.g. Trp exposed to water fluoresce maximally at 350 nm while a Trp buried in the interior of a protein fluoresce maximally at 330 nm [132]. Trp can thus be used as a probe to study the local environment, and this has been used in great extent to study protein folding/unfolding mechanisms.

Fluorescence anisotropy measurements are commonly used in biochemical application of fluorescence. Anisotropy can be a powerful toll and is often used in medical ligand binding studies. The origin of anisotropy is the existence of transition moments for absorption and emission that lie along specific directions within the fluorophore structure. When exposed to polarized light, the fluorophores that have their absorption transition moment oriented along the electric vector of the incident light are preferentially excited [126]. In other words, the fluorophores that are excited are partially aligned. If the fluorophore remains immobile during the excited lifetime, the fluorescent light will be highly polarized. Most molecules in solutions however move during the time of excitation and a key feature of anisotropy is that the measurements reveal the average angular displacement of the fluorophore that occurs between absorption and subsequent emission of a photon. This angular displacement is dependent on the rate of and extent of rotational diffusion during the lifetime of the excited state. Parameters that affect rotational diffusion are viscosity of the solvent and size of the molecule [126].

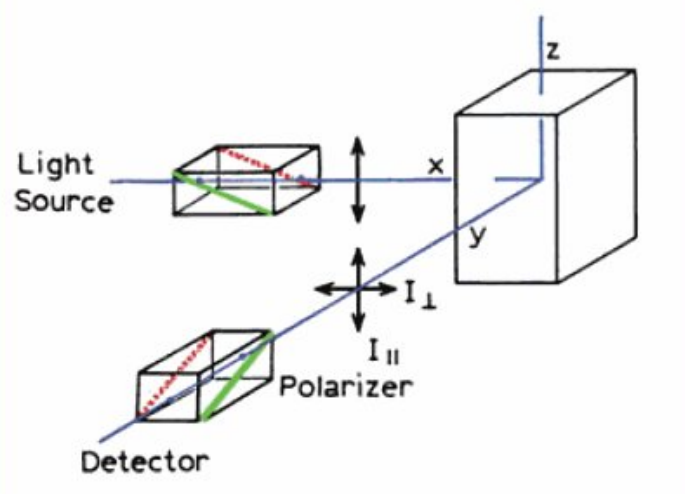

Figure. 19. Schematic diagram for measurements of fluorescence anisotropy. Adapted from [126]

I practice fluorophore are normally excited with vertical polarized light (fig. 19). The intensity of the fluorescent light is measured perpendicular through a polarizer. The polarizer can be oriented parallel or perpendicular to the direction of the polarized excitation light. The intensity of the light when the polarizer is in the parallel orientation is called $I_{||}$ and the intensity of the light when the polarizer is in the perpendicular position is called $I_\perp$. From these two intensities the anisotropy (r) can be calculated:

$$r = \frac{I_{||} - I_\perp}{I_{||} + 2 \cdot I_\perp}$$

In theory this means that a fluorophore that does not undergo rotational diffusion ($I_\perp = 0$) during the time of excitation will give a value of 1. In contrast a fluorophore which has been completely depolarized ($I_\perp = I_{||}$) will give a value of 0. Completely polarized light is only observed for oriented samples but never observed for homogeneous unoriented samples. This is due to the angular dependence of photo selection. Photo selection means that the molecule

aligned parallel to the polarized light have the highest probability of excitation. However, a fluorophores does not need to be completely aligned with the polarized light in order to absorb light. The probability of absorption is proportional to the $\cos^2\Theta$, where Θ is the angle the absorption dipole makes with the z-axis (fig. 20). This means that the molecules that are excited by polarized light are a population of molecules that are partially aligned with the z-axis.

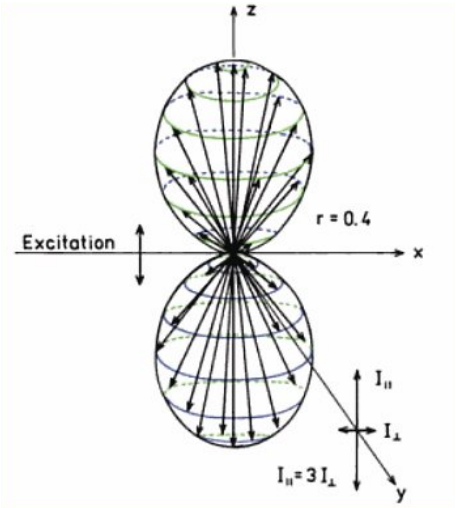

Figure 20. Excited-state distribution for immobile fluorophores. Adapted from [126]

In practice the probability distribution of excitation means that in a sample with many molecules a value of r = 1 is not obtainable. If the absorption and emission dipoles are collinear, the maximum anisotropy possible is 0.4. In theory, higher values are possible if only a single molecule is excited.

A second important factor has to be accounted for when measuring anisotropy. Only very few fluorophores show collinear absorption and emission dipoles, which means that the absorbed light is emitted in an angle different than the angle from which it was absorbed. This displacement of the emission dipole by and angle of Θ, results in a decrease in anisotropy by a factor: $(3\cos^2\Theta-1)/2$. The fundamental anisotropy of a fluorophore is thus given by:

$$r_0 = 0.4\left(\frac{3\cos^2\Theta - 1}{2}\right)$$

For some fluorophores β is close to zero; hence if no rotational diffusion occurs during the excitation lifetime r_0 is close to 0.4. If Θ is 90 degrees a negative value of -0.2 is obtained. In all, this means that practical anisotropy measurements range from 0.4 to -0.2. Selected values of β and the corresponding anisotropy are shown in table 8.

Table 8. Relationship between the angular displacement of transition moments (β) and the fundamental anisotropy.

β (degree)	0	45	54.7	90
r_0	0.4	0.1	0	-0.2

Circular Dichroism

Circular dichroism (CD) is a powerful method in structural biology that has been used to study proteins and other biomolecules since the 1960s [133]. CD is a spectroscopic method that depends upon the differential absorption of left- and right-circularly polarized light by optically active molecules [134]. A molecule is optical active (or chiral) if it can rotate the plane of polarized light [135]. In proteins there are two different contributions to optical activity; the presence of $_{L}$-amino acids and the folding of the polypeptide chain.

Far-UV CD spectra, typically in the range 250-190 nm, are determined by the peptide backbone conformation, especially secondary structure [132]. α-helix, β-sheet, and random coil structures each give rise to a characteristic shape and magnitude of CD spectrum. From Far-UV CD spectra is it thus possible to estimate the fraction of secondary structure elements. The information deducted from CD spectra does not provide information about where in the sequence the secondary structures are located but gives an average of the total content of secondary elements.

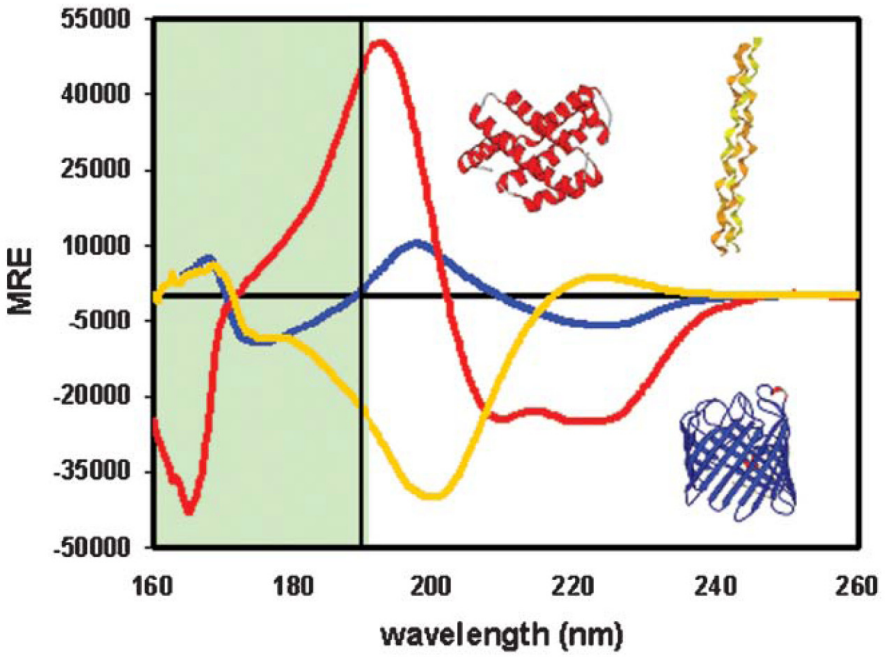

Figure 21. Synchrotron radiation CD spectra of a mostly helical protein in red, a mostly β-sheet protein in blue, and a polyproline helix (collagen) in yellow. Adapted from [134].

The far UV CD spectra of α-helical proteins are characterized by three peaks; Two negative at ~222 and ~208 nm and a stronger positive at ~192 nm [136]. In general, spectra arising from β-sheets are characterized by a small negative peak near 217 nm and a positive peak near 195 nm that has approximately half the intensity of the a-helix peak in this region [136]. β-sheets give rise to considerably less intense signals than helices and show far more variation in spectral characteristics; the latter is partly attributable to the fact that β-sheets are much more structurally diverse than a-helices, with strands which may run parallel or anti-parallel to each other, and with sheets displaying differing degrees of twisting [134].

Unordered structures (often also referred to as random coil or disordered) have variable spectra that are generally similar to the polyproline spectra shown in figure 21 [134].
While far-UV CD spectroscopy provide information on protein secondary structure, near-UV CD (250-300 nm) can be used to probe changes in tertiary structure. Aromatic side chains in asymmetric environments have optical activity in folded proteins. Signals in the region from 250-270 nm are attributable to Phe residues, signals from 270-290 nm are attributable to Tyr residues, and those from 280-300 nm are attributable to Trp. Disulfide bonds give rise to broad weak signals throughout the near-UV spectrum. A protein can retain a large degree of secondary structure without having a well defined three-dimensional structure (e.g. molten globule state). Under such circumstances the signal in the near-UV region will be nearly zero. A significant signal in the near-UV CD region is a good indication of a folded protein. In general the signal in the near-UV region is much weaker than the signal in the far-UV region. Near-UV CD thus require substantial amounts of protein compared to near-UV CD.

Isothermal Titration Calorimetry

Fluorescence and CD are excellent methods for monitoring changes in protein structure, however not all protein-surfactant interactions lead to structural changes. E.g. BSA can bind a few SDS molecules without denaturing, and this event may not be detected using the spectroscopic techniques described above. In order to detect early binding events which not necessarily leads to structural changes, spectroscopy techniques can be supplemented with ITC studies. ITC is a thermodynamic technique that directly measures the heat released or absorbed during a biomolecular binding event. This technique is used extensively in the studies presented in this thesis, and a schematic illustration of an ITC instrument from MicroCal is presented in figure 22.

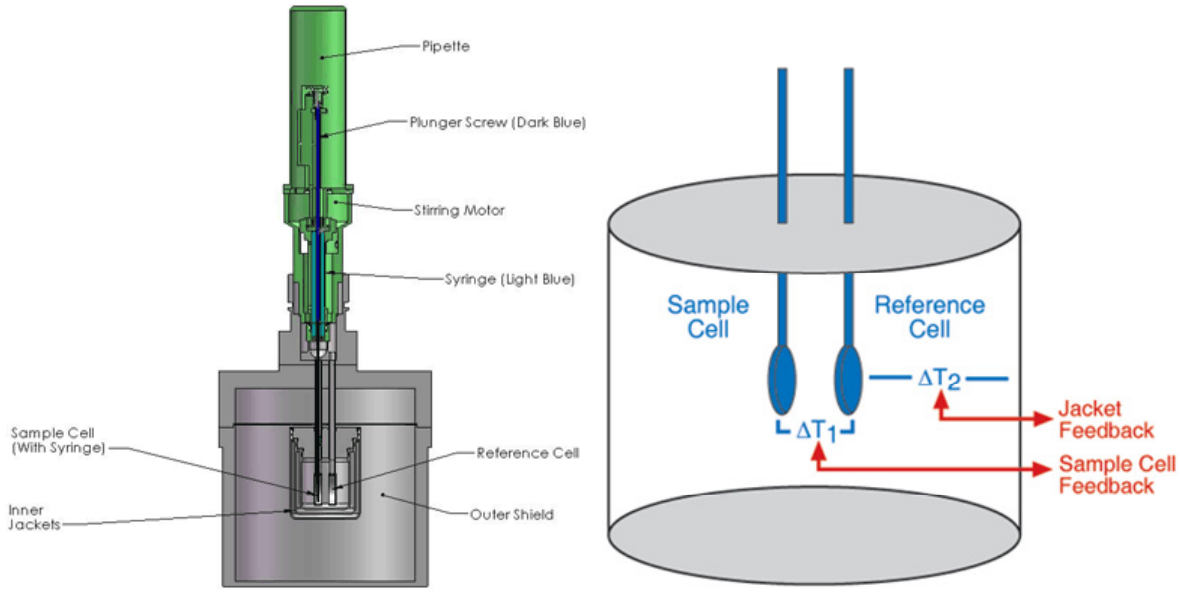

Figure 22. Left) Diagram of an ITC instrument. During a typical experiment the syringe rotates and the plunger injects precise volumes into the cell. Right) Illustration of thee sample- and reference cell. Adapted from [137].

In a typical experiment the sample cell is filled with a protein solution and the syringe is filled with surfactant. Upon injection into the cell a chemical reaction occur and heat is generated or absorbed. The temperature difference between the sample and reference cells (ΔT1) is kept at a constant value (i.e. baseline) by the addition or removal of heat to the sample cell. The integral of the power required to maintain ΔT1 = constant over time is a measure of total heat resulting from the process being studied [137]. Several events during proteins-surfactant interactions show characteristic heat flow. E.g. unfolding/denaturation of a protein is an endothermic processes and it is thus possible to separate this event from binding events that do not lead to loss of organized structure (*e.g.* early binding events).
The papers presented in this thesis show processed ITC data. An example of both raw and processed ITC data from a typical experiment is presented in figure 23. Each peak is the heat flow from a single injection of SDS to a protein solution. Data is processed such that the heat flow for each peak is integrated, and presented as a function of the SDS concentration.

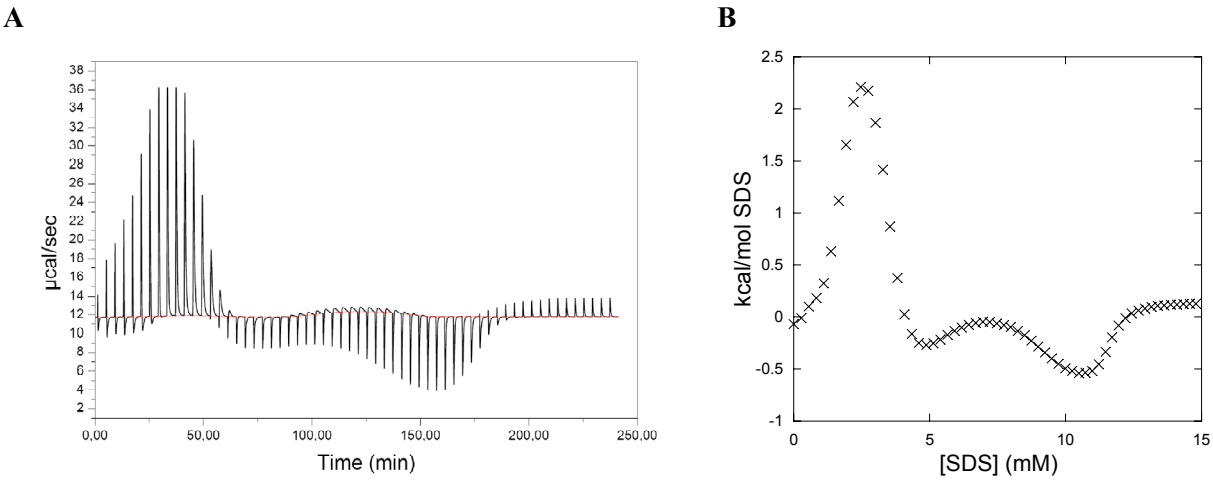

Figure 23. (A) Raw data and (B) processed data from a typical ITC experiment. A protein solution is titrated with small volumes of concentrated SDS. The interaction between protein and SDS leads to heat flow. Approximately 60 injections are performed.

Capillary Electrophoresis

Capillary electrophoresis (CE) is a family of related techniques that employ narrow-bore capillaries to perform high efficiency separations of both large and small molecules. These separations are facilitated by the use of high voltage, which may generate electroosmotic flow (EOF) and electrophoretic flow of buffer solutions and ionic species, respectively, within the capillary. The basic instrumental configuration for CE is illustrated in figure 24. The technique requires fused-silica capillary with an optical viewing window, a controllable high voltage power supply, two electrode assemblies, two buffer reservoirs, and a detector. Typical inner diameters of capillaries are in the range 25 to 75 µm. The ends of the capillary are placed in the buffer reservoirs and the optical viewing window is aligned with the detector. After filling the capillary with buffer, the sample can be introduced by replacing one of the reservoirs with a sample reservoir and applying either an electrical field or external pressure. After sample loading the capillary is placed back into the buffer reservoir. The

reservoirs contain electrodes which are used to make electrical contact between the high voltage power supply and capillaries. Separation is performed by applying an electric field, typical between 20.000 and 60.000 V, and molecules are identified as they pass the detector [138].

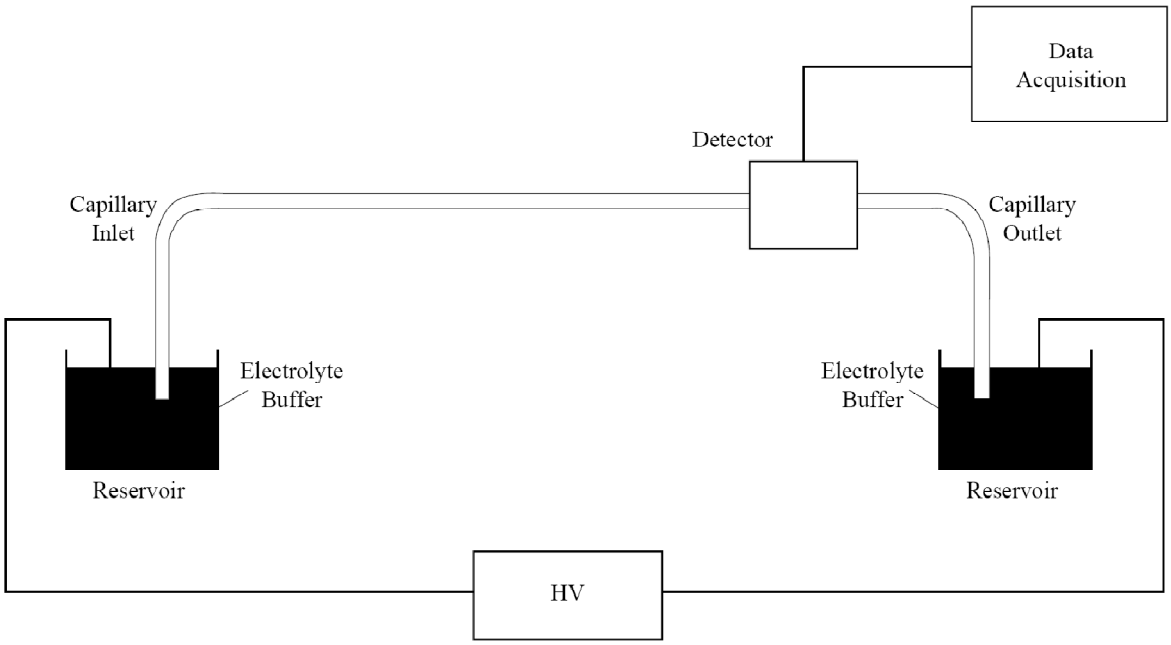

Figure 24. Basic configuration of a capillary electrophoresis system.

A fundamental constituent of CE is the electroosmotic flow (EOF). The EOF is the bulk flow of liquid in the capillary and this flow is a direct consequence of the surface charge of the interior of the capillary. In a fused-silica capillary, silanol (Si-OH) groups attached to the interior wall of the capillary are ionized to negatively charged silanoate ($Si\text{-}O^-$) groups at pH values greater than three. The negatively-charged wall attracts positively-charged ions from the buffer, creating an electrical double layer. When a voltage is applied across the capillary, cations in the diffuse portion of the double layer migrate in the direction of the cathode, carrying water with them. The result is a net flow of buffer solution in the direction of the negative electrode. At neutral to alkaline pH, the EOF is sufficiently stronger than the electrophoretic migration such that all species are swept towards the negative electrode. The order of migration is: cations, neutrals, and anions (se fig. 25).

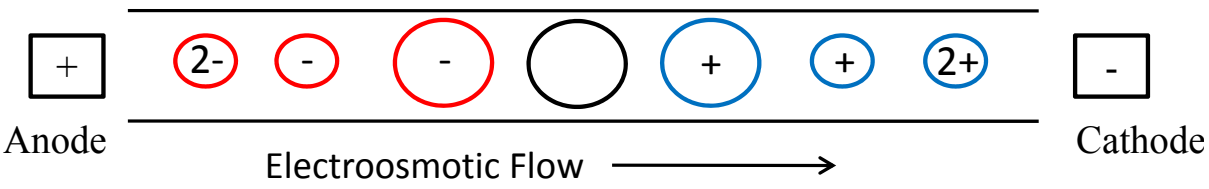

Figure 25. Diagram of the separation of charged (red/blue) and neutral (black) analytes according to their respective electrophoretic and electroosmotic flow mobilities.

The migration velocity (v) of an ion in centimeters per second in an electrical field is equal to the product of the field strength E (V cm^{-1}) and the electrophoretic mobility μ_e ($cm^2V^{-1}s^{-1}$):

$$v = \mu_e E$$

The electrophoretic mobility is proportional to the charge on the analyte and inverse proportional to the frictional retarding factors. The frictional retarding force on an analyte ion is determined by the size and shape of the ion and the viscosity of the medium. The electrical field only acts on ions which means that neutral molecules are not separated [131].
The velocity on an ion is proportional to the strength of the electrical field. The electrical field is determined by the magnitude of the applied potential (V, in volts) and the length (L) over which this potential is applied. The velocity of an ion can thus be described:

$$v = \mu_e \frac{V}{L}$$

This relationship shows that a high potential is desirable in order to achieve fast ion migration and thus also separation of molecules.
A unique feature of the EOF is the flat profile of the flow (fig. 26). This profile is different compared to the parabolic profile obtained with a laminar flow. In CE the EOF is uniformly distributed along the capillary which results in a flat profile. This flow profile is advantageous because the dispersion of the solute zone is minimized, which in turn gives good separation of molecules.

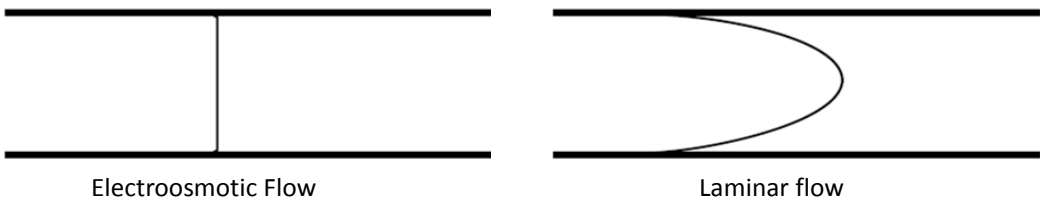

Figure 26. Electroosmotic- and laminar flow profiles.

Paper I

Unfolding of β-sheet proteins in SDS

Unfolding of β-Sheet Proteins in SDS

Mette M. Nielsen,* Kell K. Andersen,* Peter Westh,† and Daniel E. Otzen*
*Centre for Insoluble Protein Structures (inSPIN), Department of Life Sciences, Aalborg University, Aalborg, Denmark; and
†Department of Life Sciences and Chemistry, Roskilde University, Roskilde, Denmark

ABSTRACT β-Sheet proteins are particularly resistant to denaturation by sodium dodecyl sulfate (SDS). Here we compare unfolding of two β-sandwich proteins TNfn3 and TII27 in SDS. The two proteins show different surface electrostatic potential. Correspondingly, TII27 unfolds below the critical micelle concentration via the formation of hemimicelles on the protein surface, whereas TNfn3 only unfolds around the critical micelle concentration. Isothermal titration calorimetry confirms that unfolding of TII27 sets in at lower SDS concentrations, although the total number of bound SDS molecules is similar at the end of unfolding. In mixed micelles with the nonionic detergent dodecyl maltoside, where the concentration of monomeric SDS is insignificant, the behavior of the two proteins converges. TII27 unfolds more slowly than TNfn3 in SDS and follows a two-mode behavior. Additionally TNfn3 shows inhibition of SDS unfolding at intermediate SDS concentrations. Mutagenic analysis suggests that the overall unfolding mechanism is similar to that observed in denaturant for both proteins. Our data confirm the kinetic robustness of β-sheet proteins toward SDS. We suggest this is related to the inability of SDS to induce significant amounts of α-helix structure in these proteins as part of the denaturation process, forcing the protein to denature by global rather than local unfolding.

INTRODUCTION

Protein-detergent interactions highlight the multifarious ways in which proteins respond to changes in their environment (1). Ionic detergents can denature proteins by strong binding to charged and hydrophobic side chains at millimolar concentrations, unlike chemical denaturants such as guanidinium chloride or urea, which are only effective at molar concentrations, presumably due to weak binding to the protein backbone (2). These interactions are of great practical interest, since the majority of industrial enzyme production (both in terms of value and volume) is targeted to the detergent sector, primarily for laundering and dishwashing (3). Generally water-soluble proteins only interact with ionic detergents, since these proteins are not hydrophobic enough to compete with nonionic detergents' strong tendency to self-association. Nonionic detergents are mainly relevant for water-soluble proteins in so far as they can form mixed micelles with ionic detergents and thus attenuate the latter's denaturing properties (4). Ionic detergents typically bind to proteins through a mixture of electrostatic and hydrophobic interactions (5,6). The strong affinity of detergents for proteins means that detergent molecules can bind both as monomers and as micelles (7–9). Typically binding of monomeric detergents only leads to local changes in protein conformation, while global and cooperative unfolding occurs around the critical micelle concentration (cmc) (10). Unfolding in detergent usually leads to a denatured but not unstructured state that may contain significant amounts of α-helical structure (11).

While the thermodynamics of detergent binding to proteins has been studied intensely since the 1960s, unfolding kinetics—which can be used to deduce the mechanism(s) of unfolding—have received comparably less attention. Using S6 as a model system, we have previously shown that mixed α/β proteins unfold very rapidly (subsecond timescales) in sodium dodecyl sulfate (SDS) (12,13) and that the α-helix structures are unfolded first. All-α proteins such as myoglobin and Acyl CoA binding protein, also unfold very rapidly (K. K. Andersen and D. E. Otzen, unpublished observations). However, β-sheet proteins appear to be more robust. A thought-provoking study by Manning and Colón (14) established that oligomeric β-sheet proteins are particularly resistant to unfolding in SDS, possibly due to the higher content of nonlocal interactions; in addition, the authors suggested that there might be general selection for kinetically stable β-structures since partially unfolded β-sheet proteins are particularly susceptible to aggregation. We speculate that the increased sensitivity of all-α and α/β proteins toward SDS denaturation could be that α-helices, but not β-sheets, provide a good attack point for SDS micelles due to the ease of solvating independent folding units such as α-helices in an apolar environment. Thus the unfolding of α-helix-containing proteins but not that of β-sheet proteins should be distorted by SDS compared to the intrinsic unfolding behavior in GdmCl. To test this hypothesis, we have analyzed the response to SDS of two structurally similar β-sandwich proteins, TII27 (the 27th immunoglobulin domain from human cardiac titin) and TNfn3 (the third fibronectin type III domain from human tenascin). The secondary structure of both proteins contains exclusively β-sheet, turns and loops (Fig. 1 *B*). Both proteins contain a single Trp residue and no internal disulfide bridges, making them very appropriate model systems for folding studies. The equilibrium and kinetic unfolding behavior of both proteins have been extensively studied by Clarke and co-workers (15,16). Both proteins unfold under equilibrium conditions in denaturant (urea or

Submitted November 15, 2006, and accepted for publication February 6, 2007.

Address reprint requests to Daniel E. Otzen, E-mail: dao@bio.aau.dk.

0006-3495/07/05/3674/12 $2.00

doi: 10.1529/biophysj.106.101238

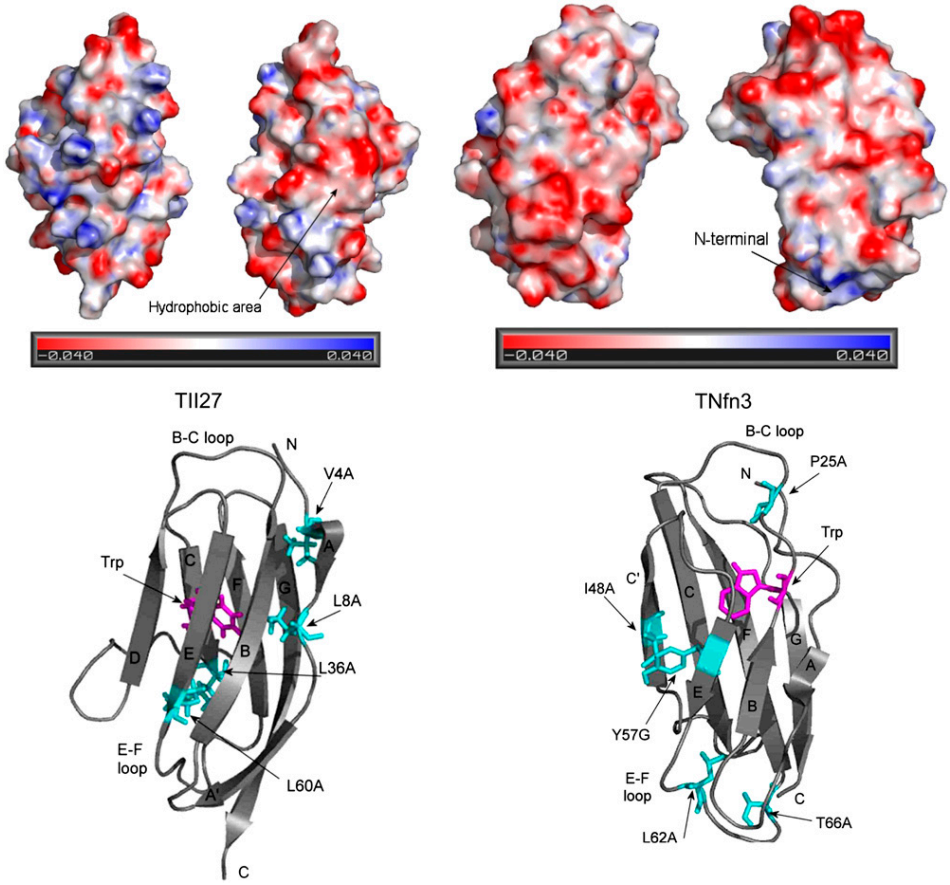

FIGURE 1 (*A*) Electrostatic potential of TII27 and TNfn3, illustrated using PyMOL. (*B*) Structures of TII27 and TNfn3, highlighting the side chains mutated in this study.

guanidinium chloride, GdmCl) according to a two-state transition with free energies of around 7 kcal/mol (15,17). TII27 but not TNfn3 folds via a kinetic intermediate, but both proteins fold according to the nucleation-condensation mechanism (18). The two proteins differ in their electrostatic surface potential. TII27 shows several areas with positive potential where SDS' sulfate headgroup could bind, some with neighboring hydrophobic areas that could interact with the detergent alkyl chain (Fig. 1 *A*). TNfn3 has fewer positively charged sites, which moreover are surrounded by negatively charged residues. This suggests that TII27 but not TNfn3 should be able to attract monomeric SDS. We show that, although the two proteins behave in a broadly similar manner, there is indeed a difference in the binding interaction of SDS with the two proteins, which translates into differences in unfolding kinetics. Importantly, the two proteins only show a small increase in α-helicity upon addition of SDS; in addition, their response to mutations is similar in SDS and denaturant, consistent with our hypothesis.

MATERIALS AND METHODS

Materials

Tris(hydroxymethyl)aminomethane (Tris) and SDS were from AppliChem (Darmstadt, Germany); *n*-dodecyl-β-D-maltoside (DDM) and thrombin, bovine high activity, were from Calbiochem (San Diego, CA); tris(2-carboxymethyl)phospine hydrochloride (TCEP) and pyrene were from Sigma-Aldrich (St. Louis, MO). All chemicals were molecular biology grade. Wild-type and mutant TII27 and TNfn3 were prepared as described (15,18,19). Both wild-type TII27 and all TII27 mutants have Thr-42 replaced by Ala, Ala-78 by Thr, and a C-terminal Arg-Ser extension (20). TNfn3 has a C-terminal Gly-Leu extension, which makes it more stable in comparison with the 90 amino acid long published protein sequence (17). Mutants of TII27 and TNfn3, as well as expression vectors for the wild-type proteins, were generously provided by Anette Steward and Jane Clarke, Cambridge University, Cambridge, UK.

Spectroscopic measurements

All experiments were conducted in 10 mM Tris pH 8.0 at 25°C using 11.7 μM TNfn3 or 7.7 μM TII27 unless otherwise stated. Solutions were left to equilibrate in detergent with 10 mM Tris, pH 8 at 25°C for at least 1 h. To avoid dimerization of TII27 via the single Cys-46, all experiments with TII27 were performed in the presence of 0.15 mM TCEP (millimolar TCEP concentrations led to precipitation in the presence of SDS).

Steady-state fluorescence measurements were performed on an LS-55 luminescence spectrometer (Perkin-Elmer Instruments, Wellesley, MA), using an excitation wavelength of 295 nm and measuring the emission between 315 and 375 nm. Measurements were performed in a 10-mm quartz cuvette (Hellma, Müllheim, Germany) as an average of three scans with a slit width of 10 nm and a scanning speed of 300 nm/min.

Far-ultraviolet (UV) circular dichroism (CD) spectra were recorded in a 1-mm quartz cuvette on a JASCO J-715 spectropolarimeter (Jasco Spectroscopic, Hachioji City, Japan) equipped with a Jasco PTC-423S temperature control unit. Wavelength scans were recorded in the wavelength range of

195–250 nm with a band width of 2 nm and a scanning speed of 50 nm/min. Five accumulations were averaged to yield the final spectrum. Background contributions from the buffer were subtracted.

Kinetics

For fluorescence studies, unfolding kinetics were studied either by manual mixing using the LS-55 instrument or on an SX18MV stopped-flow microanalyzer (Applied Photophysics, Leatherhead, UK) in a thermostatically controlled sample-handling unit, depending on the rapidity of the reaction. On the LS-55 instrument, samples were excited at 295 nm and the fluorescence intensities at 350 nm and 330 nm for TNfn3 and TII27, respectively, were followed until the signals reached a plateau. On the SX18MV instrument, proteins and detergent were mixed 1:10 to a final protein concentration of 1.2 μM, samples were excited at 280 nm, and the emission above 320 nm was monitored using a cut-off filter. Control experiments showed that the rate constants obtained by the two methods were identical within error.

For CD studies, samples were manually mixed and measured at 10-min intervals (average of five scans), 5-min intervals (average of three scans), and 1.5-min intervals (one scan) depending on the rapidity of the unfolding reaction.

The observed kinetics were fitted to single exponential functions with (TII27) and without (TNfn3) linear drift, leading to a first-order rate constant k_{obs}. The linear drift was incorporated to account for photobleaching of the Trp fluorophore in TII27, which was presumably more accessible (and hence less protected from light and oxidative reactions) in TII27 than in TNfn3. The drift was insignificant in comparison to the amplitude change caused by unfolding.

Pyrene interactions

The ratio of the intensity of pyrene emission at 372.5 and 383.5nm (I_3/I_1) can be used to evaluate the polarity of the environment, in which pyrene is solubilized. We used pyrene emission to determine if there was binding of hemimicelles to the surface of the proteins. Pyrene was excited at 335 nm and emission between 350 and 440 nm monitored. A stock solution of 20 μM pyrene in ethanol was made and added to the samples to a final concentration of ~0.05 μM. Each sample was recorded as the average of three emission scans.

Isothermal titration calorimetry (ITC)

The calorimetric measurements were conducted on a VP-ITC (MicroCal, Northampton, MA). The reference cell was filled with water and in a typical experiment, the sample cell was loaded with a solution of 8.7 and 69.8 μM TNfn3 or 32.3–114.8 μM TII27. The cell solution was titrated with aliquots of 2.5–4 μl of 99 mM SDS in 10 mM Tris, pH 8. All experiments were done at 22°C, where SDS demicellization is practically athermal (21). Therefore the enthalpic contribution from demicellization of SDS upon injection can be neglected in data analysis. The obtained heat signals from the ITC were integrated using the Origin software supplied by MicroCal.

Calculation of electrostatic potential

The electrostatic surface potential at pH 8 was calculated for the two Protein Data Bank files 1TEN (22) and 1TIT (23) to investigate possible interaction sites with SDS. pK_a values for every titratable side chain were calculated at pH 8 by the programs PDB2PQR and Propka (24,25). Electrostatic potential values were computed by the program MEAD. MEAD uses the Poisson-Boltzman equation to determine the electric potential, and incorporate details of the atomic structure into the placement of charges and dielectric boundaries (26). Finally the electrostatic map was visualized by the program PyMOL (DeLano Scientific, San Carlos, CA).

Thermal denaturation

Thermal scans were conducted on a Cary Eclipse Fluorescence spectophotometer (Varian, Mulgrave, Australia) using a 10-mm quartz cuvette. Scans were performed from 20 to 100°C using an excitation wavelength of 295 nm and an emission wavelength of 350 nm. The scan rate was 1°C/min and slit widths of 10 nm were used. Thermal scans were fitted to a thermal transition as previously described (27).

Data analysis

The observed rate constants k_{obs} vary in a characteristic manner with SDS concentration. From these characteristics, unfolding kinetics can be grouped into three different modes (12,13):

Mode 1

At low SDS concentrations (3–10 mM SDS), the rate constant for unfolding increases steeply and stabilizes at a plateau around 10 mM SDS. This behavior can be described by a minimal scheme (Scheme 1) involving rapid binding (complete within the dead time of stopped-flow mixing, ~5 ms) and subsequent global unfolding:

Scheme 1

$$P + SDS \overset{K_1}{\longleftrightarrow} P* : SDS \xrightarrow{k_{unf}^{mode\ 1}} P* : SDS^{mode\ 1}$$

where P denotes the protein, SDS a predominantly spherical SDS micelle (below 100 mM SDS (28)), K_1 the dissociation constant ($K_1 = [P][SDS]/[P^*{:}SDS]$), $P^*{:}SDS$ the protein:SDS complex, $k_{unf}^{mode\ 1}$ the rate constant for unfolding in mode 1, and $P^*{:}SDS^{mode\ 1}$ the unfolded protein:SDS complex. The magnitude of the observed rate constant k_{obs} depends on the fraction of the protein that is complexed with SDS within the dead time.

Mode 2

At intermediate SDS concentrations (10–100 mM) before the onset of mode 3, there is a decline in the unfolding rate constants for Tnfn3. Scheme 2 models this by invoking binding of additional SDS micelles to the protein:SDS complex $P^*{:}SDS$. This is analogous to uncompetitive inhibition in enzyme catalysis, whereas additional binding to unbound protein corresponds to competitive inhibition. Formation of a dead-end complex between unbound protein and SDS would not lead to a decline in unfolding rates at high SDS concentrations. In this model the dead-end complex $SDS{:}P^*{:}SDS^{mode\ 2}$ is described with a dissociation constant K_{inh}:

Scheme 2

$$\begin{array}{ccccc} & & SDS : P* : SDS^{mode\ 2} & & \\ & & K_{inh} \updownarrow SDS & & \\ P + SDS & \overset{K_1}{\longleftrightarrow} & P* : SDS & \xrightarrow{k_{unf}^{mode\ 1}} & P* : SDS^{mode\ 1} \end{array}.$$

For simplicity, it is assumed that there is no difference between the detergent micelles that bind to P and to P^*SDS, and that only one micelle binds to $P^*{:}SDS$. This means that the micellar concentration in both binding steps is described by the term ($[SDS] - cuc$) in units of monomers, where $[SDS]$ is the total SDS concentration and cuc is the critical unfolding concentration. It is assumed that unfolding only proceeds above cuc. Note that Scheme 2 is merely an attempt to present a possible model, and the data do not allow for clear conclusions about the stoichiometry of the dead-end complex.

Mode 3

Above ~100 mM SDS, the micelles gradually transform from mainly spherical to predominantly cylindrical, and the unfolding rate constants increase markedly in a manner that is linear in a double-logarithmic plot (28). This mode can also be described by rapid binding, followed by unfolding by the cylindrical micelles. Scheme 3 represents a synthesis of all three different unfolding regimes in SDS:

Scheme 3

$$\begin{array}{ccccc} & & SDS:P*:SDS^{\text{mode 2}} & & \\ & & K_{\text{inh}}\updownarrow SDS & & \\ & \xrightarrow{K_1} & P*:SDS & \xrightarrow{k_{\text{unf}}^{\text{mode 1}}} & P*:SDS^{\text{mode 1}} \\ P+SDS & & & & \\ & \xrightarrow{K_2} & P:SDS & \xrightarrow{k_{\text{unf}}^{\text{mode 3}}} & P*:SDS^{\text{mode 3}} \end{array}$$

We use two different equilibrium constants K_1 and K_2 as well as two different protein-detergent complexes P^**:SDS* and $P^{\#}$*:SDS* to emphasize the difference in micelle structure. K_2 cannot be determined directly due to the lack of an obvious saturation effect in mode 3 and is merely added for formal reasons. The three different unfolding regimes lead to the following (Eq. 1):

$$k_{\text{obs}} = \frac{k_{\text{unf}}^{\text{mode 1}}}{\frac{K_1}{[SDS]-cuc}+1+\frac{[SDS]-cuc}{K_{\text{inh}}}} + k_{\text{unf}}^{0.5\text{M SDS}}\left(\frac{[SDS]-cuc}{0.5\ \text{M}\,SDS-cuc}\right)^{\Delta n} \quad (1)$$

where $k_{\text{unf}}^{0.5\text{M SDS}}$ is the unfolding rate constant at 500 mM SDS, since 500 mM SDS is used as a reference concentration for unfolding in mode 3; Δn is a constant, which can be interpreted as the degree of cooperativity of mode 3. In cases where there is no inhibition (mode 2), the following (Eq. 2) comprises mode 1 + 3:

$$k_{\text{obs}} = \frac{k_{\text{unf}}^{\text{mode 1}}}{\frac{K_1}{[SDS]-cuc}+1} + k_{\text{unf}}^{0.5\text{M SDS}}\left(\frac{[SDS]-cuc}{0.5M\,SDS-cuc}\right)^{\Delta n} \quad (2)$$

The details of the models are not essential for the discussion of our results, but provide an opportunity to estimate key kinetic parameters for comparative purposes. In addition, they serve to emphasize the complexity of protein unfolding in detergent.

RESULTS

Equilibrium unfolding in SDS reveals hemimicellar unfolding of TII27 but micellar unfolding of TNfn3

To compare the unfolding of the two β-sheet proteins and provide a basis for an analysis of their unfolding mechanism in SDS, we start by describing their response to SDS under equilibrium conditions. Upon incubation with SDS, the fluorescence intensity maximum for both TII27 and TNfn3 shift from around 330 nm, typical of a buried Trp residue, to around 350 nm, indicative of increased exposure accompanying unfolding (Fig. 2 *A*). The fluorescence intensity of TII27 is reduced, and that of TNfn3 increased, upon unfolding. This difference probably reflects subtle conformational details relating to the immediate environment of the Trp residue in the native and denatured state.

Far-UV CD spectra show characteristic β-sheet signatures in the absence of SDS. When SDS is added, there is a general increase in ellipticity (Fig. 2 *B*). Deconvolution of the spectra using the CDSSTR algorithm (29) suggest only a very slight increase in α-helicity for TNfn3 (from 7 to 9%) and a slightly larger increase for TII27 (from 5 to 17%), accompanied by ~10% decrease in β-sheet structure and 5% increases in β-turn and unordered structure. The relatively poor accuracy of deconvolution algorithms makes it unfeasible to conclude that there are substantial differences between the conformational changes that the two proteins undergo upon unfolding in SDS.

Conformational changes associated with the stepwise addition of SDS were followed by fluorescence and far-UV CD. For TNfn3, fluorescence and CD both show a major transition around 4.8 mM SDS, which is very close to the cmc of SDS under these buffer conditions, namely 5 mM (27) (Fig. 2 *D*). However, for TII27, both techniques reveal that the transition occurs around 3 mM, and is complete before the cmc is reached (Fig. 2 *C*). Furthermore, the transition is somewhat broader for TII27, indicating a less cooperative process that involves a smaller number of SDS molecules than for TNfn3. To obtain further information about the consequences of binding of SDS at low concentrations, we also carried out thermal scans of the two proteins followed by fluorescence. For TII27, there was essentially no change in melting temperature t_{m} until 2.5 mM SDS, after which t_{m} dropped steeply and no thermal transition was observed above 3 mM SDS (Fig. 2 *C*). TNfn3 showed a constant t_{m} until around 4 mM SDS, and no transitions were observed above 4.5 mM SDS (Fig. 2 *D*). These data all suggested that monomeric SDS interacted to a greater extent with TII27 than with TNfn3, with consequent earlier unfolding.

To confirm this, we followed the change in fluorescence emission of the hydrophobic probe pyrene as a function of SDS concentration in the presence of the two proteins (Fig. 3). Pyrene's fluorescence changes as it goes from a hydrophilic (aqueous) to a hydrophobic (micellar) environment, making it a good probe for the formation of micelles as well as hemimicelles formed on protein surfaces (30). In the absence of protein, the fluorescence ratio reaches a plateau around 4–5 mM, in satisfactory correspondence with the previously determined cmc of 5 mM (27). Pyrene fluorescence is not affected by the presence of TNfn3, but when TII27 is included, the fluorescence ratio rises more steeply at low SDS concentrations (0.6–3 mM) than in the absence of SDS. This suggests that SDS molecules form hydrophobic clusters on the TII27 surface in this submicellar concentration range. An alternative interpretation is that monomeric SDS induces structural changes on TII27 that allows pyrene to bind to exposed hydrophobic surfaces. This cannot be ruled out, though we consider it less likely: such surfaces are likely to be covered by SDS molecules that would have to be out-competed by pyrene despite the 1000-fold greater concentration of SDS. Nevertheless, both interpretations indicate

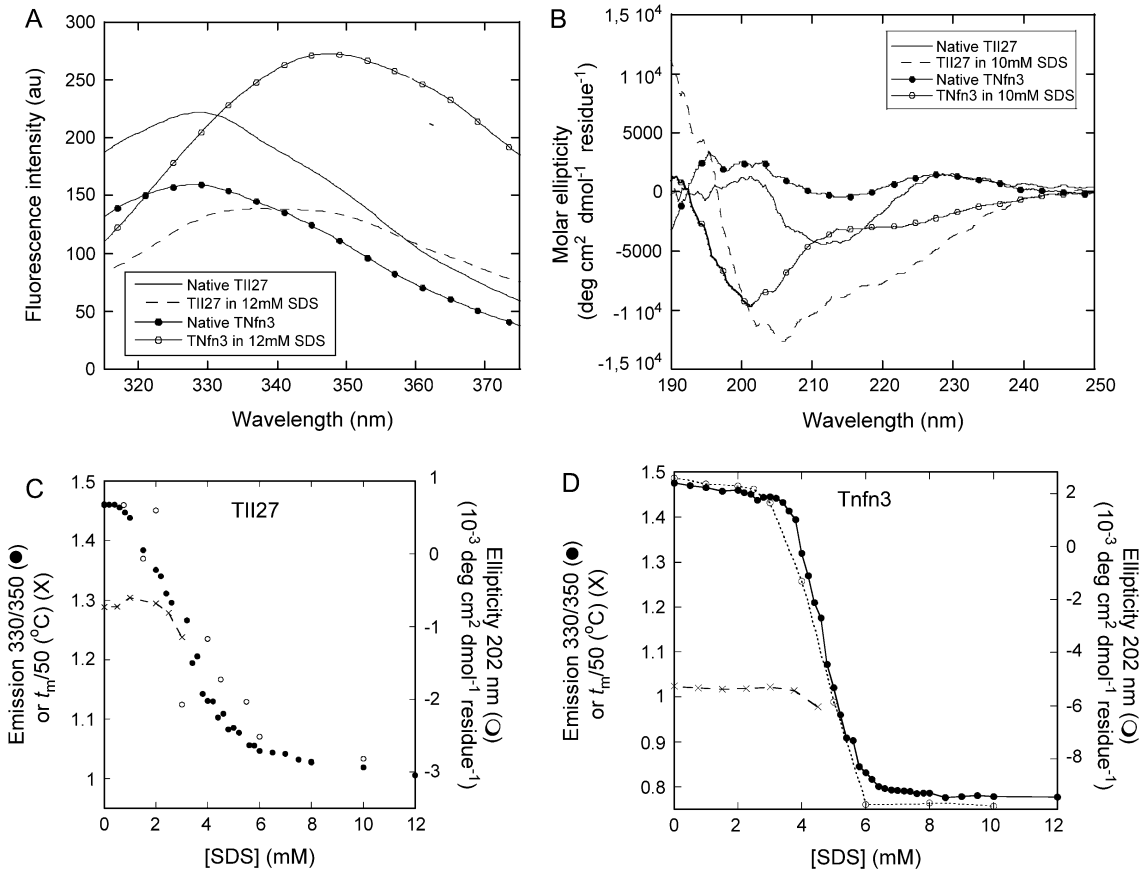

FIGURE 2 (*A*) Fluorescence and (*B*) Far-UV CD spectra of TII27 and TNfn3 in the absence and presence of SDS. (*C*) Equilibrium denaturation of TII27 and (*D*) TNfn3 followed by fluorescence, CD, and changes in the melting temperature as a function of SDS concentration. For both proteins, t_m has been divided by 50 to be compatible with the fluorescence axis.

significant interactions of submicellar SDS with TII27 but not TNfn3.

ITC reveals broadly similar stoichiometries of binding of SDS to the two proteins

ITC experiments on TNfn3 and TII27 with SDS reveal characteristic enthalpograms (Fig. 4). For TNfn3 they may be divided into four sections (*A–D*). Section *A* shows a very weak exothermic (negative) heat flow, which is essentially independent of the protein concentration. This suggests limited protein-surfactant interaction. At intermediate SDS concentrations (*B*), a strong endothermic effect sets in and peaks when [SDS] reaches 5–6 mM. This behavior has been seen for a number of other protein-SDS systems, and has been assigned the (endothermic) enthalpy change of protein denaturation (31–33) (H. L. Bagger, S. V. Hoffmann, C. C. Fuglsang, and P. Westh, unpublished data). Assuming two-state behavior for the denaturation, the maximum of the peak in section *B* will be close to the midpoint of the denaturation process. We will refer to this maximum as point I. Subsequent to the peak, the heat signal decreases and becomes negative (exothermic) around the boundary to section *C*. This type of exothermic mixing is a general observation in ITC studies on protein-SDS interactions, and it most likely reflects the association of SDS and denatured protein (31) (A. D. Nielsen, K. Borch, and P. Westh, unpublished data). The saturation of this binding is around the inflection (S-) point (point II, 8.0 mM for 69.8 μM TNfn3 in Fig. 4). This also corresponds to the apparent critical micelle concentration (cmc_{app}) in the presence of protein (21). SDS injected beyond this point mainly remains in micellar form and has far fewer protein molecules to interact with (31,34), leading to the sigmoidal course in section *C*. Finally, at high SDS concentrations (*D*), the heat flow levels out, indicating that the injected SDS remains in a micellar form and interacts only weakly with the existing protein-SDS complex.

The enthalpogram of TII27 exhibits the same four sections, preceded by a region below 1 mM SDS (denoted *A**) with a strong exothermic heat flow that rapidly tapers off as [SDS] is increased. This suggests the specific binding of a few SDS molecules to TII27. Specific binding of SDS with dissociation constants in the 0.1–1 mM range and binding enthalpies of 1–2 kcal/mol has previously been found for

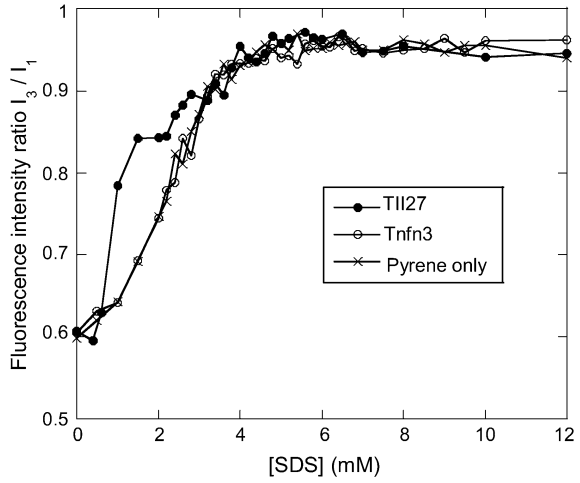

FIGURE 3 Pyrene fluorescence as a function of SDS in the absence and presence of TII27 and TNfn3. Note the steep increase in the I_3/I_1 ratio of TII27 between 0.5 and 3 mM SDS compared to protein-free pyrene and pyrene in the presence of TNfn3. This suggests that hemimicellar structures form on the TII27 surface but not on TNfn3.

a number of proteins (8,32). TII27 shows the same sections *A–D* described for Tnfn3, although the peak in section *B* was much smaller than for TNfn3.

To estimate the number of detergent molecules bound to the two proteins at point I in section *B* and point II in section *C*, we plot the total SDS concentrations ($[SDS]_{tot}$) at points I and II against the corresponding protein concentration. Provided that the SDS concentration is low enough to neglect SDS in micellar form, SDS binding at each peak can be expressed by the mass balance (Eq. 3):

$$[SDS]_{tot} = [SDS]_{aq} + [protein] * N \quad (3)$$

where $[SDS]_{aq}$ denotes aqueous (nonbound) SDS and N is the average number of bound SDS per protein molecule (21). The plots give satisfactory linear relationships (Fig. 5 *A*) and the parameters are summarized in Table 1. Point I (interpreted as the midpoint of denaturation), shows an average binding of 14.8 ± 5.2 SDS molecules for TII27 and 16.9 ± 1.5 for TNfn3. This occurs at 4.2 ± 0.4 mM SDS (in the aqueous bulk) for TII27 and 4.9 ± 0.1 mM SDS for TNfn3, which is in reasonable correspondence with the midpoint values of ~3 and 5 mM observed for the two proteins by fluorescence (Fig. 2). At binding saturation (point II), TII27 binds 44 ± 3.0 and TNfn3 binds 40 ± 1.8 SDS molecules. In both cases, this corresponds to ~1.2 g SDS per gram protein, very similar to the values seen for many other proteins (35). The SDS concentration obtained by extrapolation of point II values to zero molar protein corresponds to micellization, i.e. the cmc value, which is 5.1–5.7 mM, in good accordance with the independently determined value of 5.0 mM. The binding data are summarized in Table 1.

The amplitude of the peaks and tails also scales linearly with protein concentration although data for the comparably small peak I of TII27 is too scattered to establish an unambiguous relationship (Fig. 5 and Table 1). For peak I, it appears that the slope of these plots is much larger for TNfn3 (Fig. 5 *B*) than for TII27 (Fig. 5 *C*), and we shall return to the origin of this below. Fig. 5 *C* also shows that the size of the initial ''tail'' for TII27 is proportional to the protein concentration. This is in contrast to conventional ITC data on strongly binding pairs, and it shows that the protein (not the added ''ligand'') is the limiting reactant in section *A**. It implies that although clearly detectable in the enthalpograms, the specific binding is rather weak with low site occupancy in the submillimolar range.

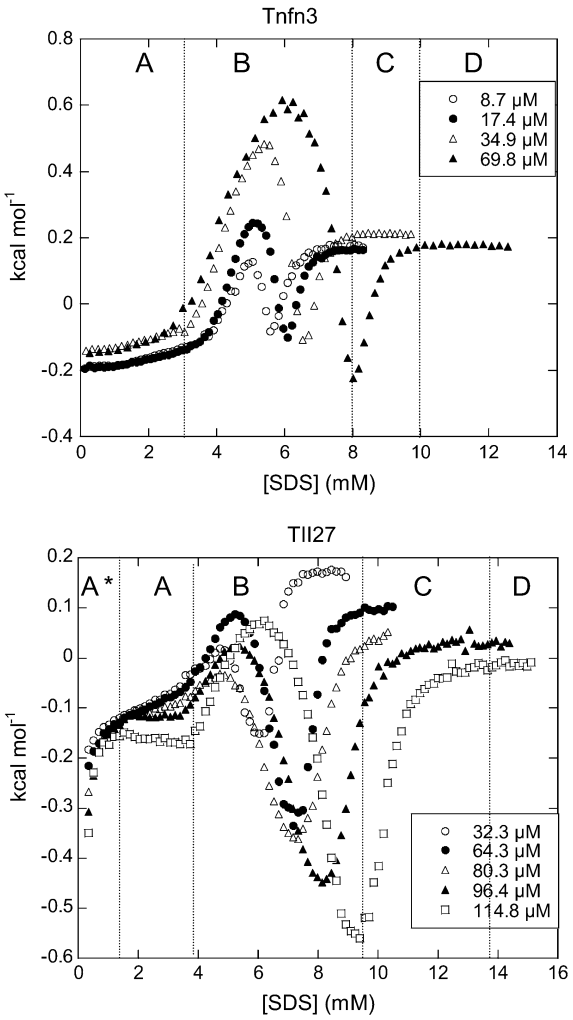

FIGURE 4 ITC enthalpograms of (*left*) Tnfn3 and (*right*) TII27 upon titration with SDS. See text for an explanations of sections *A*–D*.

Mixed micelles show that monomers are not required to unfold TII27

The previous sections had demonstrated that TII27 was unfolded by monomeric SDS and TNfn3 by micellar SDS. This raised the question as to whether the two proteins would

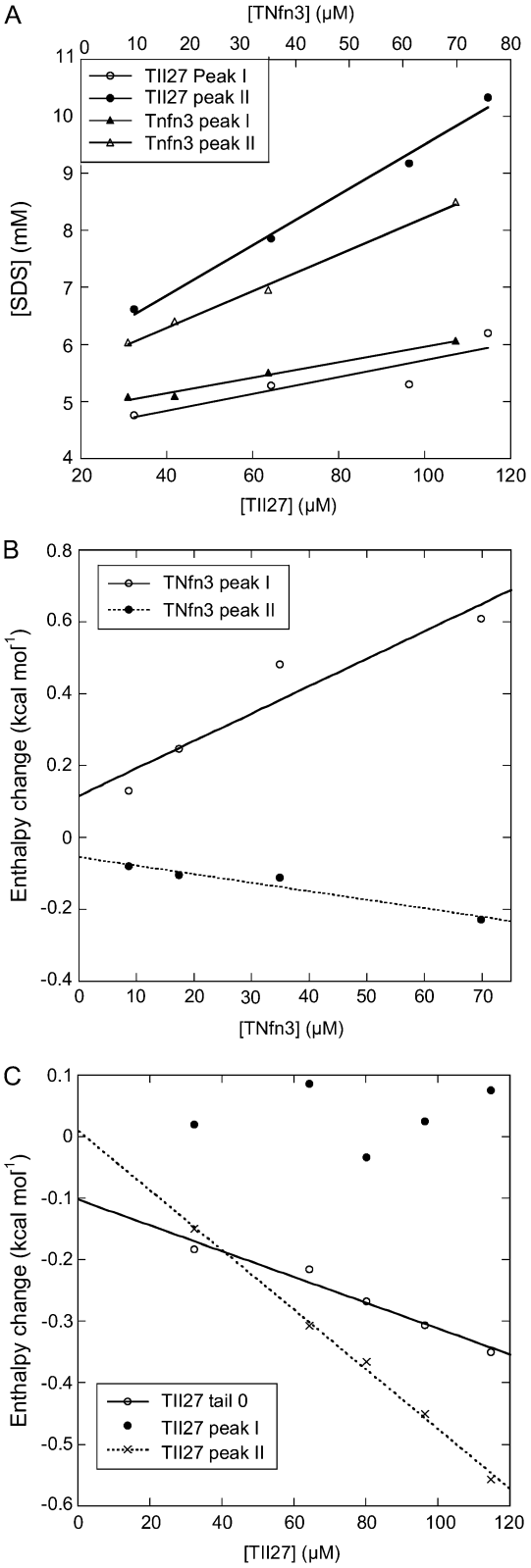

FIGURE 5 (*A*) Concentrations at which peaks I and II appear for TII27 and TNfn3 as a function of protein concentration. (*B* and *C*) Enthalpy values at peaks I and II as well as in region *A** (for TII27) as a function of protein concentration. Data are summarized in Table 1.

respond differently from each other if SDS were predominantly presented in micellar form in the absence of significant amounts of monomeric SDS. This could be done by incorporating SDS into mixed micelles with the nonionic detergent dodecyl maltoside ((DDM) cmc 0.17 mM). We used mixed micelles with SDS mole fractions of 0.75, 0.5, and 0.25. The cmc of these mixtures has previously been determined to be ~0.3, 0.18, and 0.15 mM, respectively (27), which means that there is not enough monomeric SDS present to effect any denaturation of TII27 (cfr. Fig. 2 *C*). As expected for a nonionic detergent, DDM alone does not unfold TII27 or TNfn3 (data not shown). For both proteins, titration with mixed micelles showed a clear decrease in the fluorescence ratio 330:350 nm (Fig. 6) as well as the molar ellipticity (data not shown). In addition, the aggressiveness of SDS decreases as the fraction of DM increases, with a slight deviation for TNfn3 at 0.25 mole fraction SDS. At 0.5 and 0.25 mole fraction SDS, unfolding was not completed within the probed concentration range. However, we observe slow unfolding kinetics for TII27 at all micellar mole fractions (Fig. 6 *C*). This confirms that the decrease in emission ratios represents bona fide unfolding and is not just an artifact due to changes in the polarity of the solvent (which would effect a change in fluorescence within a few milliseconds of mixing). Clearly TII27 is also unfolded by micellar SDS, and in fact retains an increased sensitivity to SDS compared to TNfn3; there is no significant native state baseline before unfolding at all SDS mole fractions (Fig. 6 *A*), whereas TNfn3 shows a cooperative unfolding in 0.75 mole fraction SDS only above ~10 mM SDS (i.e., 13.3 mM mixed detergent) (Fig. 6 *B*).

Unfolding kinetics reveal a more complex unfolding behavior for TNfn3 than TII27

Up to now, we have concentrated on the conformational changes that occur before and around the cmc of SDS under equilibrium conditions. The advantage of kinetic studies is that they provide insight into the mechanism of unfolding and also allow us to access high detergent concentrations where the rates of unfolding can vary significantly with detergent concentration, although the end conformation may be spectroscopically unchanged (12). Rate constants k_{obs} for unfolding of the two proteins as a function of SDS are shown in Fig. 7; k_{obs} measured by CD and fluorescence are essentially similar, indicating that secondary and tertiary structure is lost in parallel. Overall, k_{obs} is very low; in comparison, rate constants above 10 mM SDS lie around 2 and 10 s^{-1} for the mixed α/β proteins CI2 and S6, respectively (12), whose thermodynamic stabilities (~7 kcal/mol in water) are comparable to the β-sheet proteins TII27 and TNfn3. Clearly the variation of k_{obs} with [SDS] is more complex for TNfn3 than TII27. For both proteins, there is an initial increase in k_{obs} at 3–10 mM SDS and a power-law increase above 100 mM SDS. At 10–100 mM SDS, k_{obs} decreases slightly for TNfn3 but is essentially constant for TII27. We have observed

TABLE 1 ITC data for titration of SDS into solutions of TII27 and TNfn3

Protein*	Region	$[SDS]_{aq}$ (mM)†	N‡	ΔH_o^{SDS} (kcal mol^{-1})§	$\alpha_{\Delta H}$ (kcal mol^{-1} mM^{-1})¶
TNfn3	Peak I	4.9 ± 0.1	16.9 ± 1.5	0.117 ± 0.072	7.6 ± 1.8
TNfn3	Peak II	5.7 ± 0.1	40.2 ± 1.8	−0.054 ± 0.017	−2.4 ± 0.4
TII27	A*	‖	‖	−0.102 ± 0.020	−2.1 ± 0.2
TII27	Peak I	4.2 ± 0.4	14.8 ± 5.2	**	**
TII27	Peak II	5.1 ± 0.3	44.0 ± 3.0	0.010 ± 0.015	−4.8 ± 0.1

*All experiments in 10 mM Tris pH 8.0 at 22°C. Errors from the linear fits in Fig. 5.
†Intercept from plot of the position of the peak (mM SDS) versus protein concentration.
‡Slope from plot of the position of the peak (mM SDS) versus protein concentration.
§Intercept from plot of the height of the peak (kcal/mol) versus protein concentration.
¶Slope from plot of the height of the peak (kcal/mol) versus protein concentration (mM).
‖Not determined because no well-defined minimum available (Fig. 4 *B* and text).
**No significant linear correlation observed (Fig. 5 *C*).

similar behavior for S6 and CI2 (12), where we have classified the unfolding into three concentration regimes or modes (cfr. Scheme 3 in Materials and Methods). Mode 1 (here 3–10 mM SDS) displays saturation-type kinetics and corresponds to binding of spherical micelles, followed by global unfolding. Mode 2 (10–100 mM SDS), only observed for TNfn3, can be modeled as inhibition of unfolding due to additional binding of SDS micelles to TNfn3, although the model remains speculative. Finally, mode 3 is rationalized as increasingly rapid unfolding due to changes in the micellar structure from predominantly spherical to more cylindrical micelles. This has been supported by studies with the cationic detergent TTAB that does not form cylindrical micelles and does not give rise to mode 3 unfolding (12).

By determining k_{obs} for a number of mutants of TII27 and TNfn3, we are able to compare the effect of mutation on unfolding in SDS with intrinsic unfolding in denaturant, i.e. GdmCl for TII27 and urea for TNfn3, compiled by Clarke and co-workers (15,43). This provides information about the nature of the transition states of unfolding. We have studied four mutants of TII27 and five mutants of TNfn3 (Fig. 8, *A* and *B*). In all cases, k_{obs} increases compared to wild-type but the same unfolding pattern is retained. However, due to the complexity of the unfolding reaction and the existence of multiple equally valid interpretations of the unfolding mechanism, we will only focus on two parameters for each mutant, namely $k_{unf}^{mode\,1}$, the unfolding rate constant at plateau level before inhibition sets in (typically ~10–20 mM SDS) and $k_{unf}^{0.5M\,SDS}$, the unfolding rate constant at 500 mM SDS. These data are summarized in Table 2. For both proteins, $k_{unf}^{mode\,1}$ and $k_{unf}^{0.5M\,SDS}$ correlate significantly with each other (Fig. 8 *C* and Table 3), indicating that the two unfolding modes are fundamentally the same, since the transition states for unfolding by the two modes are affected in a similar manner by mutation. Similarly, both rate constants show a reasonable linear correlation with the unfolding rate k_{unf} in water extrapolated from unfolding rate constants in GdmCl and urea (Fig. 8 *D* and Table 3) (15,17), suggesting an overall similar transition state of unfolding in denaturant versus detergent.

DISCUSSION

Differences and similarities between two structurally similar β-sheet proteins

In this study, we have focused on the SDS-induced unfolding of two structurally similar β-sandwich proteins TII27 and TNfn3. Despite their similarity, the two proteins show significantly different electrostatic surface potential, with TII27 possessing more positively charged regions than TNfn3. This suggests that TII27 should be able to attract negatively charged detergent molecules to a greater extent than TNfn3, and this expectation is borne out by equilibrium denaturation studies, which show that TII27 denatures, and loses the ability to undergo a cooperative thermal transition, below cmc while TNfn3 only shows significant structural changes as well as a decrease in thermal stability, around the cmc. Similar effects of electrostatics have been observed for, e.g., carbonic anhydrase, whose resistance to SDS increased dramatically upon peracetylation of the lysine side chains (6).

The ability of SDS to denature TII27 at submicellar concentrations can be explained by its ability to form hemimicelles on the protein surface, as demonstrated by pyrene fluorescence experiments. Nevertheless, the presence of monomeric SDS is not essential for unfolding of TII27 but merely provides an early start, since mixed micelles with DDM (where the amount of monomeric SDS is negligible) are also able to denature TII27. Nonionic detergents only react weakly if at all with water-soluble proteins because their low cmc values indicate that detergent-detergent interactions are more thermodynamically favorable than protein-detergent interactions. The SDS-DDM micelles also have low cmc values (0.15–0.3 mM) but still interact with TII27 and TNfn3, although to a smaller extent. Clearly the concentration of negative charge in the micelle is very important for denaturing potency, since there is a fourfold increase in the amount of detergent needed to cause denaturation when the SDS mole fraction decreases 25% (from 100 to 75%).

Mixed SDS-DDM micelles are increasingly being used to quantitate membrane protein stability (36,37) and folding kinetics (4,38). The reported midpoint values of denaturation

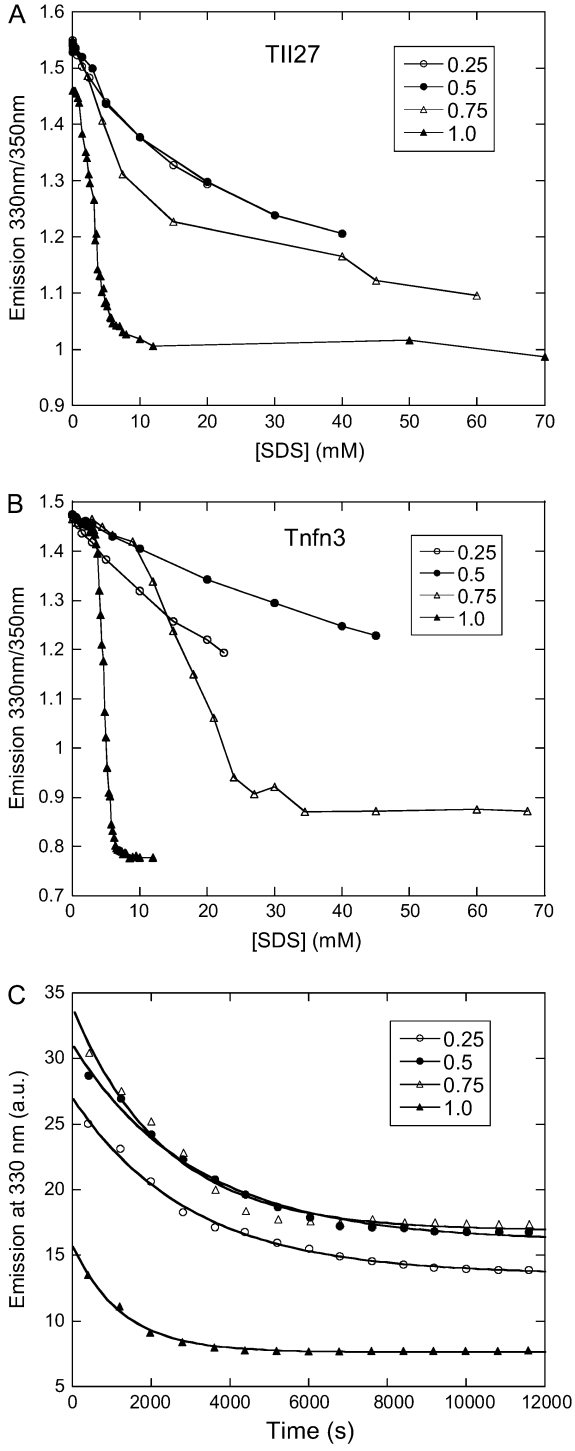

FIGURE 6 Unfolding of (*A*) TII27 and (*B*) TNfn3 in mixed micelles of SDS and DDM at SDS mole fractions 0.25–1 followed by the change in emission ratio 330:350 nm. (*C*) Kinetics of unfolding of TII27 in 80 mM detergent containing 0.25–1 mole fraction SDS.

vary from 30 to 70%. However, an important difference between membrane proteins and water-soluble proteins is the former's uncompromising requirement for amphiphiles to stay in solution and consequent very high affinity for micelles.

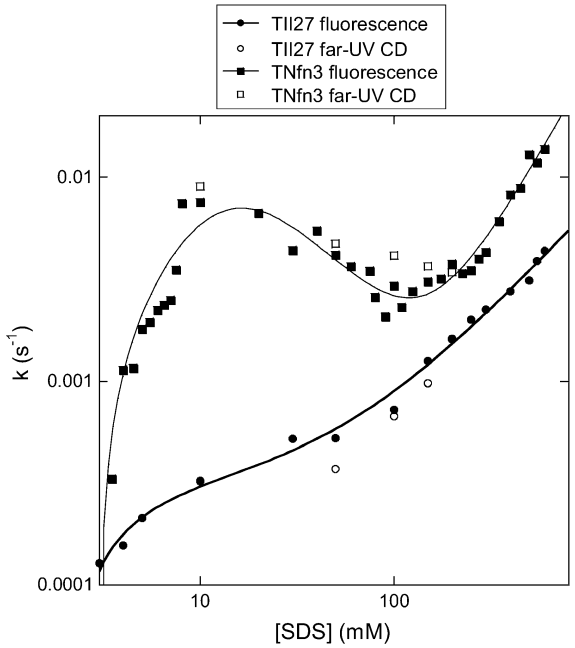

FIGURE 7 Rate constants of unfolding of TII27 and TNfn3 as a function of SDS concentration. Data for TII27 are fitted to mode 1 + 3 unfolding, whereas data for TNfn3 are fitted to mode 1 + 2 + 3 unfolding (Scheme 3).

Thus, all membrane proteins will be bound in micelles even at low micelle concentrations provided there is a stoichiometric amount of detergent micelles present, and varying the absolute SDS concentration has no effect on the unfolding of diacyl glycerate kinase stability provided the mole fraction is kept constant (36). In contrast, unfolding of TII27 and TNfn3 in mixed SDS-DM micelles only occurs above a certain SDS concentration (Fig. 6), highlighting the equilibrium between free and bound protein for both TII27 and TNfn3.

Differences between the two proteins are also evident from the calorimetric titration trials. An early binding event below 1 mM SDS occurs only for TII27, and this again is in accord with the analysis of the electrostatic potentials discussed above. At higher [SDS], both proteins show an endothermic transition, which is ascribed to the surfactant-induced denaturation. In accordance with the spectroscopic measurements, this transition occurs at higher [SDS] for TNfn3. The ITC data further showed that the robustness toward SDS of these proteins did not rely on a particularly low affinity for the surfactant. In fact, the saturation binding level (~1.2 g/g) was identical to that typically found for globular protein with no (or reduced) cysteines (35,39). The conspicuous difference in the unfolding rates (Fig.7) is not reflected in the binding stoichiometry either, since both proteins bind around 15 SDS molecules at the transition midpoint. This similarity in the binding isotherm is also relevant for the interpretation of the slopes, $\alpha_{\Delta H}$, in Fig. 5 (listed in Table 1). This function quantifies the change in enthalpy of the system upon a small change in the amount of both protein and surfactant.

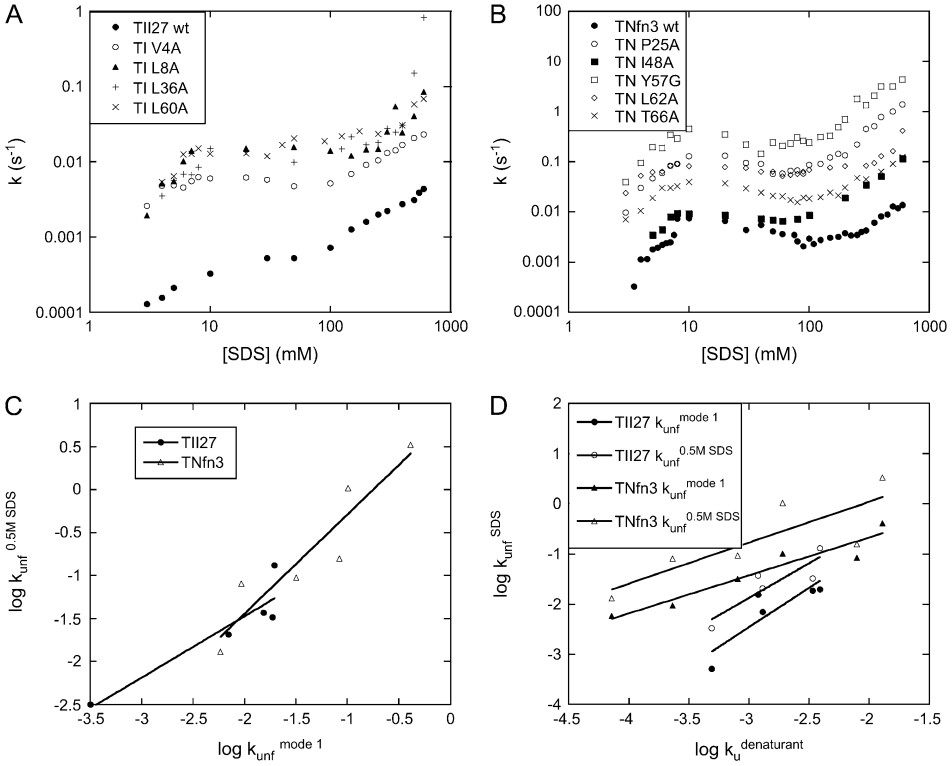

FIGURE 8 Unfolding rate constants for mutants of (*A*) TII27 and (*B*) TNfn3 as a function of SDS. Data are summarized in Table 2. Correlation of unfolding rate constants in SDS (*C*) with each other and (*D*) with unfolding rate constants in buffer extrapolated from unfolding rate constants in denaturant. The slopes, intercepts, and correlation coefficients for the best linear fits are summarized in Table 3.

In other words it is proportional to the second derivative $(d^2H)/(dn_{\text{protein}}dn_{\text{SDS}})$, where n denotes number of moles and the subscripts defines the compound. This derivative is a measure of the enthalpy of protein-surfactant interactions in solution (40,41). The distinctive positive $\alpha_{\Delta H}$ for peak I of TNfn3, for example, indicates a pronounced endothermic nature of the TNfn3-SDS interaction around peak I. Because the binding affinity for the two proteins are similar, we interpret this as a stronger effect of SDS on the denaturation equilibrium of TNfn3. Thus, in the transition zone, the population of denatured TNfn3 molecules increases more steeply with [SDS], than in the case of TII27. This higher degree of cooperativity for SDS denaturation of TNfn3, which is also reflected in a steeper CD and fluorescence unfolding curve

TABLE 2 Changes in stability and unfolding kinetics for TII27, TNfn3, and their mutants in SDS and chemical denaturants

Protein	$\Delta\Delta G_{\text{D-N}}$*	$k_{\text{unf}}^{\text{denat}}$ †	$k_{\text{unf}}^{\text{mode1}}$ ‡	$k_{\text{unf}}^{0.5\,\text{M SDS}}$ §
TNfn3 wild-type	$\equiv 0$	$7.21 \pm 0.26 \times 10^{-5}$	5.81×10^{-3}	1.3×10^{-2}
TN P25A	1.73 ± 0.13	$1.92 \pm 0.46 \times 10^{-3}$	1.02×10^{-1}	1.04
TN I48A	2.19 ± 0.12	$2.32 \pm 0.33 \times 10^{-4}$	9.3×10^{-3}	8.09×10^{-2}
TN Y57G	4.14 ± 0.10	$1.29 \pm 0.22 \times 10^{-2}$	4.12×10^{-1}	3.32
TN L62A	4.22 ± 0.11	$7.91 \pm 1.40 \times 10^{-3}$	8.39×10^{-2}	1.57×10^{-1}
TN T66A	1.96 ± 0.12	$8.11 \pm 1.80 \times 10^{-4}$	3.2×10^{-2}	9.41×10^{-2}
TII27 wild-type	$\equiv 0$	$4.9 \pm 0.6 \times 10^{-4}$	$3.22 \pm 2.1 \times 10^{-4}$	$3.17 \pm 0.23 \times 10^{-3}$
TI V4A	2.45 ± 0.10	$1.3 \pm 0.1 \times 10^{-3}$	6.98×10^{-3}	2.07×10^{-2}
TI L8A	2.45 ± 0.10	$1.2 \pm 0.2 \times 10^{-3}$	$1.54 \pm 0.54 \times 10^{-2}$	$3.72 \pm 0.89 \times 10^{-2}$
TI L36A	3.3 ± 0.10	$3.9 \pm 0.3 \times 10^{-3}$	$1.96 \pm 0.19 \times 10^{-2}$	$1.31 \pm 0.00 \times 10^{-1}$
TI L60A	4.88 ± 0.08	$3.4 \pm 0.3 \times 10^{-3}$	$1.87 \pm 0.22 \times 10^{-2}$	$3.26 \pm 0.37 \times 10^{-2}$

*The mutation-induced change in the difference in free energy between the denatured state, D, and the native state, N, on mutation (kcal·mol^{-1}), relative to wild-type protein. Obtained from Fowler and Clarke (15) (TII27) and Hamill et al. (43) (TNfn3).

†The $k_{\text{unf}}^{\text{denat}}$ (s^{-1}) values are obtained from Fowler and Clarke (15) (TII27, GdmCl) and Hamill et al. (43) (TNfn3, Urea). For TII27 the authors determined $k_{\text{unf}}^{\text{denat}}$ by linear extrapolation of log $k_{\text{unf}}^{\text{denat}}$ at different denaturant concentrations to zero molar denaturant; $k_{\text{unf}}^{\text{denat}}$ for TNfn3 mutants was calculated from Hamill et al. (43) by use of the following equation: $\Delta G_{\text{D-N}}^{(\text{H2O})}(\text{mutant}) = -RT\ln(k_u/k_f)_{\text{mutant}}$.

‡Unfolding rate constant (s^{-1}) in SDS at the plateau level (TII27) and at the highest level before inhibition sets in (TNfn3) (cfr. Figs. 7 and 8). Errors are from the direct fits to Eq. 2 (TNfn3) or Eq. 3 (TII27). In several cases, it was not possible to obtain a stable fit, making it necessary to estimate the value by visual inspection.

§Unfolding rate constant (s^{-1}) interpolated to 500 mM SDS.

TABLE 3 Correlations between kinetic parameters for unfolding in SDS and denaturant

Protein	Independent variable	Dependent variable	Slope	Intercept	R
TII27	$k_{unf}^{mode\ 1}$	$k_{unf}^{0.5\ M\ SDS}$	0.71 ± 0.17	−0.04 ± 0.40	0.92
TNfn3	$k_{unf}^{mode\ 1}$	$k_{unf}^{0.5\ M\ SDS}$	1.15 ± 0.23	0.87 ± 0.34	0.93
TII27	$k_{u}^{denaturant}$*	$k_{unf}^{mode\ 1}$	1.57 ± 0.52	2.25 ± 1.47	0.87
TII27	$k_{u}^{denaturant}$*	$k_{unf}^{0.5\ M\ SDS}$	1.38 ± 0.42	2.27 ± 1.19	0.88
TNfn3	$k_{u}^{denaturant}$*	$k_{unf}^{mode\ 1}$	0.76 ± 0.12	0.85 ± 0.36	0.95
TNfn3	$k_{u}^{denaturant}$*	$k_{unf}^{0.5\ M\ SDS}$	0.82 ± 0.28	1.68 ± 0.83	0.83

*Unfolding rates extrapolated to zero molar denaturant. Values determined as in Table 2. Errors are from the linear fits.

than TII27 (Fig. 2), may rely on the transition zone's location close to cmc and the micelle-driven unfolding.

Differences in unfolding kinetics

There are two important differences between TII27 and TNfn3 as regards kinetics. Firstly, TNfn3 but not TII27 undergoes an inhibition of unfolding. Secondly, although the mutants' unfolding rate constants in SDS (k_{unf}^{SDS}) are linearly correlated to unfolding rate constants in denaturant (k_{unf}^{denat}), the slopes of the two correlations are significantly different (Fig. 8 *D*).

The first observation clearly illustrates that inhibition of unfolding, previously reported for both S6 and CI2 (12), is not a general detergent phenomenon but is a specific reflection of protein properties. The effect can be modeled by the binding of additional SDS micelles to TNfn3—but not TII27—in the mode 2 region (10–100 mM SDS). It is difficult to come up with straightforward explanations for this difference. It is possible that the different abilities to bind monomeric SDS may affect the ability to bind more SDS molecules at higher concentrations. The ground state from which unfolding occurs could be different for the two proteins if for example TII27 is partially covered by hemimicellar structures that block access to additional (inhibiting) micelles within the dead time of mixing before unfolding occurs, in contrast to TNfn3, which does not attract submicellar structures.

The second observation relates to the nature of binding of SDS to proteins. It is safe to assume that k_{unf}^{denat}, which are obtained from extrapolations from unfolding rates in denaturant (GdmCl or urea) represent the intrinsic and denaturant-independent unfolding rates. Consequently, the changes in k_{unf}^{denat} upon mutation must reflect absolute changes in the energy of the transition state. However, the degree to which changes in k_{unf}^{denat} correlate to changes in k_{unf}^{SDS} (the slopes in Fig. 8 *D*) will depend on how efficiently SDS can bind to and denature the protein. The fact that changes in k_{unf}^{SDS} for TII27 mutants are more sensitive than those of TNfn3 to changes in k_{unf}^{denat} must illustrate that SDS is more efficient at destabilizing TII27 than TNfn3 (even though the total amount of SDS bound is the same, namely 1.2 g SDS per gram protein). This ties in well with our previous observations that TII27 generally is more sensitive to SDS than TNfn3, presumably facilitated by the altered electrostatic potential.

A general model for SDS unfolding of all-β versus helix-containing proteins

Generally, denaturation in SDS tends to increase the amount of α-helix structure in proteins with high native content of β-structure (11). This corresponds to the formation of a ''bead-on-a-string'' structure, where SDS micelles attach to individual segments of the protein and preferentially stabilize isolated structural elements with independent hydrogen-binding abilities (42). However, the SDS-unfolded states of TII27 and TNfn3 only show a relatively insignificant increase in α-helical structure. An important corollary of the linear correlations established in Fig. 8 is that the transition states for unfolding are broadly similar in SDS and denaturant. That is, we do not need to postulate a ''distorted'' transition state for unfolding in SDS compared to unfolding in denaturant, as opposed to, e.g., the mixed α/β protein S6 (13).

In combination with the low α-helicity of the SDS-denatured states, our data have inspired us to present the following working hypothesis for β-sheet unfolding in SDS. There are no SDS-specific attack points for the unfolding of β-sheet proteins, rather SDS has to rely on the global unfolding behavior of this class of proteins to destabilize them. In contrast, for proteins containing significant elements of α-helical structure such as S6, the α-helices may provide a first line of attack for SDS micelles. As demonstrated experimentally for S6, α-helices can quite easily be ripped out of the intact tertiary structure since they constitute independent folding units that are stable as isolated entities in micelles due to their ability to form internal hydrogen bonds, whereas β-sheet structures rely on global contacts and are therefore less easily disrupted, unless the entire protein is unfolded. This may provide an underlying structural reason for the observation by Manning and Colón on the enhanced robustness of β-sheet proteins, and particularly oligomeric structures, toward SDS (14). However, we emphasize that the present data, although consistent with this hypothesis, are insufficient to establish the validity of the model in detail. We are therefore currently pursuing experimental strategies to resolve this question.

We are very grateful to Annette Steward and Jane Clarke for generously providing mutants of TNfn3 and TII27 as well as expression vectors for the wild-type proteins.

D.E.O. is supported by the Danish National Research Foundation (inSPIN) and by the Villum Kann Rasmussen Foundation (BioNET). K.K.A. is supported by the BIOPRO Innovation Consortium. P.W. acknowledges support from Carlsberg Foundation and the Danish Research Agency (grants 26-02-0160 and 21-04-0087).

REFERENCES

1. La Mesa, C. 2005. Polymer-surfactant and protein-surfactant interactions. *J. Coll. Int. Sci.* 286:148–157.

2. Timasheff, S. 2002. Protein hydration, thermodynamic binding, and preferential hydration. *Biochemistry*. 41:13473–13482.
3. Kirk, O., T. V. Borchert, and C. C. Fuglsang. 2002. Industrial enzyme applications. *Curr. Opin. Biotechnol.* 13:345–351.
4. Sehgal, P., and D. E. Otzen. 2006. Thermodynamics of unfolding of an integral membrane protein in mixed micelles. *Prot. Sci.* 15:890–899.
5. Otzen, D. E., L. Christiansen, and M. Schülein. 1999. A comparative study of the unfolding of the endoglucanase Cel45 from *Humicola insolens* in denaturant and surfactant. *Prot. Sci.* 8:1878–1887.
6. Gitlin, I., K. L. Gudiksen, and G. M. Whitesides. 2006. Peracetylated bovine carbonic anhydrase (BCA-Ac18) is kinetically more stable than native BCA to sodium dodecyl sulfate. *J. Phys. Chem. B*. 110:2372–2377.
7. Jones, M. N., and P. Manley. 1979. Binding of *n*-alkyl sulphates to lysozyme in aqueous solution. *J. Chem. Soc. Faraday Trans.* 75:1736–1744.
8. Jones, M. N. 1992. Surfactant interactions with biomembranes and proteins. *Chem. Soc. Rev.* 21:127–136.
9. Reynolds, J. A., S. Herbert, H. Polet, and J. Steinhardt. 1967. The binding of divers detergent anions to bovine serum albumin. *Biochemistry*. 6:937–943.
10. Tanford, C. 1980. The Hydrophobic Effect. Formation of Micelles and Biological Membranes. Wiley & Sons, New York.
11. Takeda, K., H. Sasaoka, K. Sasa, H. Hirai, K. Hachiya, and Y. Moriyama. 1992. Size and mobility of sodium dodecyl-sulfate bovine serum-albumin complex as studied by dynamic light-scattering and electrophoretic light-scattering. *J. Coll. Int. Sci.* 154:385–392.
12. Otzen, D. E. 2002. Protein unfolding in detergents: effect of micelle structure, ionic strength, pH, and temperature. *Biophys. J.* 83:2219–2230.
13. Otzen, D. E., and M. Oliveberg. 2002. Burst-phase expansion of native protein prior to global unfolding in SDS. *J. Mol. Biol.* 315:1231–1240.
14. Manning, M., and W. Colón. 2004. Structural basis of protein kinetic stability: resistance to sodium dodecyl sulfate suggests a central role for rigidity and a bias toward beta-sheet structure. *Biochemistry*. 43: 11248–11254.
15. Fowler, S. B., and J. Clarke. 2001. Mapping the folding pathway of an immunoglobulin domain: structural detail from Phi value analysis and movement of the transition state. *Structure*. 9:355–366.
16. Clarke, J., E. Cota, S. B. Fowler, and S. J. Hamill. 1999. Folding studies of immunoglobulin-like beta-sandwich proteins suggest that they share a common folding pathway. *Structure*. 7:1145–1153.
17. Hamill, S. J., A. E. Meekhof, and J. Clarke. 1998. The effect of boundary selection on the stability and folding of the third fibronectin type III domain from human tenascin. *Biochemistry*. 37:8071–8079.
18. Geierhaas, C. D., E. Paci, M. Vendruscolo, and J. Clarke. 2004. Comparison of the transition states for folding of two Ig-like proteins from different superfamilies. *J. Mol. Biol.* 343:1111–1123.
19. Clarke, J., S. J. Hamill, and C. M. Johnson. 1997. Folding and stability of a fibronectin type III domain of human tenascin. *J. Mol. Biol.* 270:771–778.
20. Carrion-Vazquez, M., A. F. Oberhauser, S. B. Fowler, P. E. Marszalek, S. E. Broedel, J. Clarke, and J. M. Fernandez. 1999. Mechanical and chemical unfolding of a single protein: a comparison. *Proc. Natl. Acad. Sci. USA*. 96:3694–3699.
21. Nielsen, A. D., L. Arleth, and P. Westh. 2005. Analysis of protein-surfactant interactions—a titration calorimetric and fluorescence spectroscopic investigation of interactions between *Humicola insolens* cutinase and an anionic surfactant. *Biochim. Biophys. Acta*. 1752:124–132.
22. Leahy, D. J., W. A. Hendrickson, I. Aukhil, and H. P. Erickson. 1992. Structure of a fibronectin type III domain from tenascin phased by MAD analysis of the selenomethionyl protein. *Science*. 258:987–991.
23. Improta, S., J. K. Krueger, M. Gautel, R. A. Atkinson, J. F. Lefevre, S. Moulton, J. Trewhella, and A. Pastore. 1998. The assembly of immunoglobulin-like modules in titin: implications for muscle elasticity. *J. Mol. Biol.* 284:761–777.
24. Li, H., A. D. Robertson, and J. H. Jensen. 2005. Very fast empirical prediction and rationalization of protein pKa values. *Proteins*. 61:704–721.
25. Dolinsky, T. J., J. E. Nielsen, J. A. McCammon, and N. A. Baker. 2004. PDB2PQR: an automated pipeline for the setup of Poisson-Boltzmann electrostatics calculations. *Nucleic Acids Res.* 32:W665–W667.
26. Bashford, D. 2004. Macroscopic electrostatic models for protonation states in proteins. *Front. Biosci.* 9:1082–1099.
27. Sehgal, P., J. E. Mogensen, and D. E. Otzen. 2005. Using micellar mole fractions to assess membrane protein stability in mixed micelles. *Biochim. Biophys. Acta*. 1716:59–68.
28. Croonen, Y., E. Geladé, M. Van der Zegel, M. Van der Auweraer, H. Vandendriessche, F. C. De Schryver, and M. Almgren. 1983. Influence of salt, detergent concentration and temperature on the fluorescence quenching of 1-methylpyrene in sodium dodecyl sulfate with *m*-dicyanobenzene. *J. Phys. Chem.* 87:1426–1431.
29. Lobley, A., L. Whitmore, and B. A. Wallace. 2002. DICHROWEB: an interactive website for the analysis of protein secondary structure from circular dichroism spectra. *Bioinformatics Applications Note*. 18:211–212.
30. Turro, N. J., and A. Yekta. 1978. Luminescent probes for detergent solutions. A simple procedure for determination of the mean aggregation number of micelles. *J. Am. Chem. Soc.* 100:5951–5955.
31. Nielsen, A. D., L. Arleth, and P. Westh. 2005. Interactions of Humicola insolens cutinase with an anionic surfactant studied by small-angle neutron scattering and isothermal titration calorimetry. *Langmuir*. 21:4299–4307.
32. Lad, M. D., V. M. Ledger, B. Briggs, R. J. Green, and R. A. Frazier. 2003. Analysis of the SDS-lysozyme binding isotherm. *Langmuir*. 19:5098–5103.
33. Kelley, D., and D. J. McClements. 2003. Interactions of bovine serum albumin with ionic surfactants in aqueous solutions. *Food Hydrocolloids*. 17:73–85.
34. Paula, S., W. Sus, J. Tuchtenhagen, and A. Blume. 1995. Thermodynamics of micelle formation as a function of temperature—a high-sensitivity titration calorimetry study. *J. Phys. Chem.* 99:11742–11751.
35. Reynolds, J. A., and C. Tanford. 1970. The gross conformation of protein-sodium dodecyl sulfate complexes. *J. Biol. Chem.* 245:5161–5165.
36. Lau, F. W., and J. U. Bowie. 1997. A method for assessing the stability of a membrane protein. *Biochemistry*. 36:5884–5892.
37. Faham, S., D. Yang, E. Bare, S. Yohannan, J. P. Whitelegge, and J. U. Bowie. 2004. Side-chain contributions to membrane protein structure and stability. *J. Mol. Biol.* 335:297–305.
38. Otzen, D. E. 2003. Folding of DsbB in mixed micelles: a kinetic analysis of the stability of a bacterial membrane protein. *J. Mol. Biol.* 330:641–649.
39. Pitt-Rivers, R., and F. Impiombato. 1968. Binding of sodium dodecyl sulphate to various proteins. *Biochem. J.* 109:825–830.
40. Westh, P., and Y. Koga. 1997. Intermolecular interactions of lysozyme and small alcohols: a calorimetric investigation. *J. Phys. Chem.* 101B:5755–5758.
41. Trandum, C., P. Westh, K. Jørgensen, and O. G. Mouritsen. 2000. A thermodynamic study of the effects of cholesterol on the interaction between liposomes and ethanol. *Biophys. J.* 78:2486–2492.
42. Ibel, K., R. P. May, K. Kirschner, H. Szadkowski, E. Mascher, and P. Lundahl. 1990. Protein-decorated micelle structure of sodium-dodecyl-sulfate-protein complexes as determined by neutron scattering. *Eur. J. Biochem.* 190:311–318.
43. Hamill, S. J., A. Steward, and J. Clarke. 2000. The folding of an immunoglobulin-like Greek key protein is defined by a common-core nucleus and regions constrained by topology. *J. Mol. Biol.* 297:165–178.

Paper II

Global study of myoglobin-surfactant interactions

Global Study of Myoglobin−Surfactant Interactions

Kell K. Andersen,[†,§] Peter Westh,*[,‡] and Daniel E. Otzen*[,†,§]

Interdisciplinary Nanoscience Centre, Aarhus University, Gustav Wieds Vej 10C, DK-8000 Aarhus C, Denmark, and NSM, Research Unit for Functional Biomaterials, Roskilde University, Building 18.1, DK-4000 Roskilde, Denmark, and Department of Life Sciences, Aalborg University, Sohngaardsholmsvej 49, DK-9000 Aalborg

Received May 24, 2007. In Final Form: October 23, 2007

Surfactants interact with proteins in multifarious ways which depend on surfactant concentration and structure. To obtain a global overview of this process, we have analyzed the interaction of horse myoglobin (Mb) with an anionic (SDS) and cationic (CTAC) surfactant, using both equilibrium titration techniques and stopped-flow kinetics. Binding and kinetics of conformational changes can be divided into a number of different regions (five below the cmc and one above) with very distinct features (broadly similar between the two surfactants, despite their difference in head group and chain length), which nuance the classical view of biphasic binding prior to micellization. In stage A, fairly weak interactions lead to a linear decrease in thermal stability. This gives way to a more cooperative process in stage B, where aggregates (presumably hemimicelles) start to form on the protein surface, leading to global denaturation (loss of a thermal transition) and biphasic unfolding kinetics. This is consolidated in stage C with titratable surfactant adsorption. Adsorption of this surfactant species leads to significant changes in kinetics, namely, inhibition of unfolding kinetics in CTAC and altered unfolding amplitudes in SDS, though the process is still biphasic in both surfactants. Stage D commences the reduction in exothermic binding signals, leading to further uptake of 5 (SDS) or 31 (CTAC) surfactant molecules without any major changes in protein conformation. In stage E many more surfactant molecules (46 SDS and 39 CTAC) are bound, presumably as quasi-micellar structures, and we observe a very slow unfolding phase in SDS, which disappears as we reach the cmc. Above the cmc, the unfolding rates remain essentially constant in SDS, but increase significantly in CTAC, possibly because binding of bulk micelles removes the inhibition by hemimicellar aggregates. Our work highlights the fascinating richness of conformational changes that proteins can undergo in the presence of molecules with self-assembling properties.

Introduction

Ionic surfactants can denature proteins by strong binding to charged and hydrophobic side chains at millimolar concentrations.[1] The consensus view[2−5] is that binding below the critical micelle concentration (cmc) proceeds through one to two different regions, starting in some but not all cases[6] with specific binding of surfactant to a few high-affinity sites on the protein surface (probably through both hydrophobic and electrostatic interactions). This causes some expansion in the protein structure to form a separate intermediate species[7] and is followed by unspecific and uncooperative binding before the protein binds a dramatically larger number of surfactant molecules and unfolds cooperatively. Beyond this point (typically around the cmc[2,3,6,8−11]), no further unfolding occurs and excess surfactant simply leads to normal micelle formation. However, kinetic studies may provide mechanistic information both above and below the cmc.[6,12,13]

We report a combined equilibrium−kinetic analysis of the interactions between horse myoglobin (Mb) and an anionic (sodium dodecyl sulfate, SDS) and cationic (cetyl trimethylammonium chloride, CTAC) surfactant. Mb's heme group provides an independent spectroscopic probe, monitoring structural changes around the heme group, in addition to the intrinsic fluorescence arising from Trp7 and Trp14, which probably reflect more global changes in structure. Smulevich and co-workers combined electronic absorption, fluorescence, and tensiometry to conclude that Mb/surfactant complexes display multiple interaction modes, giving rise to conformational changes which can be interpreted in terms of different degrees of protein unfolding.[14] Low concentrations of SDS or CTAC induced the formation of a heme six-coordinated, low-spin (6cLS) species. However, only SDS was active as a monomer toward Mb, whereas CTAC was only active as micelles. Higher concentrations led to dissociation of heme from the protein.[14]

Here, we focus on the stoichiometry, thermodynamics, kinetics, and mechanistics of the Mb−surfactant interactions to better characterize various Mb/surfactant species formed at different stages and surfactant concentrations. We use isothermal titration calorimetry (ITC) to quantify the gradual increase in the number of surfactant molecules bound per molecule of Mb. ITC will also detect binding of SDS molecules that do not fortuitously elicit changes in the Trp fluorescence, and we show that although the

* Authors to whom correspondence should be addressed. E-mail: pwesth@ruc.dk (P.W.); dao@inano.dk (D.E.O.).

† Aarhus University.

‡ Roskilde University.

§ Aalborg University.

(2) LaMesa, C. *J. Colloid Interface Sci.* **2005**, *286*, 148−157.

(3) Turro, N. J.; Lei, X.-G.; Ananthapadmanabhan, K. P.; Aronson, M. *Langmuir* **1995**, *11*, 2525−2533.

(4) Tanford, C. *The hydrophobic effect. Formation of micelles and biological membranes*, 2nd ed.; Wiley & Sons: New York, 1980; pp 18−20.

(5) Jones, M. N. *Biochem. J.* **1975**, *151*, 109−114.

(6) Ananthapadmanabhan, K. P. Protein-surfactant interactions. In *Interactions of surfactants with polymers and proteins*; Goddard, E. D., Ananthapadmanabhan, K. P., Eds.; CRC Press: Boca Raton, FL, 1993; pp 319−365.

(7) Nielsen, M. M.; Andersen, K. K.; Westh, P.; Otzen, D. E. *Biophys. J.* **2007**, *92*, 3674−3685.

(8) Maestro, B.; Sanz, J. M. *FEBS Lett.* **2007**, *581*, 375−381.

(9) Reynolds, J. A.; Herbert, S.; Polet, H.; Steinhardt, J. *Biochemistry* **1967**, *6*, 937−943.

(10) Jones, M. N.; Skinner, H. A.; Tipping, E. *Biochem. J.* **1975**, *147*, 229−234.

(11) Gimel, J. C.; Brown, W. *J. Chem. Phys.* **1996**, *104*, 8112−8117.

(12) Takeda, K.; Sasaoka, H.; Sasa, K.; Hirai, H.; Hachiya, K.; Moriyama, Y. *J. Colloid Interface Sci.* **1992**, *154*, 385−392.

(13) Otzen, D. E. *Biophys. J.* **2002**, *83*, 2219−2230.

(14) Otzen, D. E.; Oliveberg, M. *J. Mol. Biol.* **2002**, *315*, 1231−40.

(15) Tofani, L.; Feis, A.; Snoke, R. E.; Berti, D.; Baglioni, P.; Smulevich, G. *Biophys. J.* **2004**, *87*, 1186−1195.

10.1021/la702890y CCC: $40.75
Published on Web 12/11/2007

different stages involved in the binding of SDS to Mb can be detected by fluorescence to the same extent as by ITC, the ITC measurements provide better resolution of the binding steps of CTAC than fluorescence. We also extend the binding studies at very low surfactant concentrations using thermal scans since the denaturation temperature t_m is highly sensitive to binding of micromolar amounts of surfactant. We use stopped-flow kinetics to observe transient states, and thus to obtain more insight into the mechanisms involved in these structural changes. In our previous studies of the unfolding of the proteins S6, CI2, Tnfn3, and TII27[6,12,13] in SDS and LTAB, unfolding involved only one relaxation phase which followed a rapid binding reaction in the dead time of the experiment. The situation is significantly more complex in the case of Mb despite its comparably small size and simple fold. Several relaxation phases are observed which undergo significant changes in rate constant and amplitudes as the surfactant concentration is varied, highlighting the contribution of cofactors to the unfolding behavior of proteins.

Materials and Methods

Materials. Horse Mb was purchased from Sigma (St. Louis, MO) (Reinheitszahl = 5.2) and used without further purification. The protein was dissolved in 20 mM 4-morpholinepropanesulfonic acid (MOPS) buffer (Boehringer Mannheim, Ingelheim am Rhein, Germany), pH 8.0. The solutions were filtered with Millex SV filters (Millipore, Billerica, MA) before use. The concentration of the protein was determined spectrophotometrically using $\epsilon = 157\ cm^{-1}\ mM^{-1}$ at 409 nm.[15] CTAC was purchased from Aldrich Chemicals (St. Louis, MO). SDS (99% purity) was purchased from Merck (Darmstadt, Germany).

ITC. Calorimetric titrations were conducted at 25 °C in two different instruments (VP-ITC and MCS-ITC, both from MicroCal Inc., Northhampton, MA) with cell volumes of respectively 1.42 and 1.32 mL. No systematic differences between the two instruments were detected. The calorimetric cell was initially cleaned and rinsed with buffer and 500 μL of Mb solution. Then 1800 μL of the protein solution was loaded into the calorimeter and titrated with 1−5 μL aliquots of surfactant solution from a 250 μL syringe. All solutions were degassed by stirring under vacuum prior to use. Concentrations of protein and buffer throughout the trials and enthalpy changes for each injection were calculated with the Origin-ITC software package provided by the instrument manufacturer. This also takes into account dilution of protein during the titration procedure.

Fluorescence Spectroscopy. Steady-state fluorescence measurements were performed on an LS-55 Luminescence spectrometer (Perkin-Elmer Instruments, Wellesley, MA) at 25 °C, using an excitation wavelength of 295 nm and measuring the emission between 310 and 400 nm. Measurements were performed in a 10 mm quartz cuvette (Hellma, Müllheim, Germany) as an average of two scans with a slit width of 10 nm and a scanning speed of 200 nm/min. Samples of 72 μM Mb were left to equilibrate with SDS or CTAC for at least 1 h before measurement.

Pyrene Interactions. Four micromolar Mb was equilibrated with SDS or CTAC for 1 h before addition of pyrene. Pyrene was added to a final concentration of 1 μM from a stock solution of 200 μM in ethanol. The solution was excited at 335 nm and emission between 350 and 440 nm monitored. Each sample was recorded as the average of two emission scans.

Stopped-Flow Fluorescence. Stopped-flow (both absorption and fluorescence) experiments were carried out on 3 μM Mb solutions using a SX18MV stopped-flow microanalyzer (Applied Photophysics, Leatherhead, UK), provided with a diode array, in a thermostatically controlled sample-handling unit at 25 °C. The reaction was followed by (1) excitation at 275 nm with a 305 nm cutoff filter, (2) absorption at 410 nm, and (3) collection of transient absorption spectra. Typically, at least five runs were averaged at each SDS concentration to increase the signal:noise ratio. With use of the software provided by the manufacturer, kinetic data at single wavelength were fitted to double or triple exponential functions, depending on the surfactant concentration (see Results and Discussion). This provided both the amplitudes and rate constants associated with each relaxation phase. Subsequently, the data from two separate series of measurements were averaged.

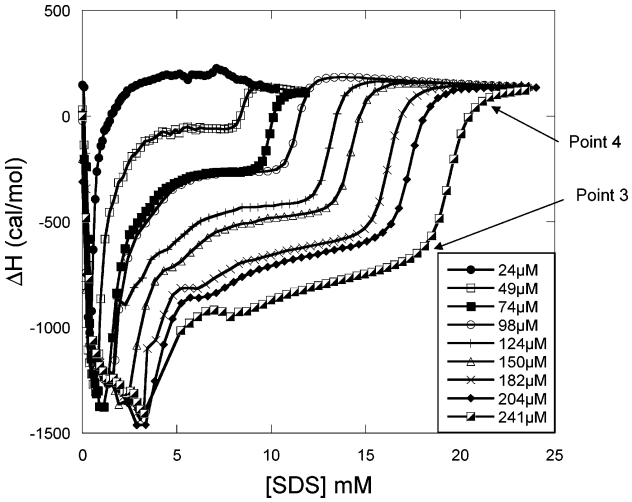

Figure 1. Isotherms for the calorimetric titrations of Mb solutions (24−241 μM) with 130 mM SDS at pH 8.0 and 25 °C. The ordinate is the enthalpy change, ΔH, per mole of SDS added and the abscissa is the total concentration of SDS in the sample. Points 3 and 4 (used for determining the stoichiometry of SDS binding in Table 1) are indicated for the 241 μM curve. Their exact values are determined by the intersections of the two tangents before and after each point.

Results

Submicellar SDS Binds to Mb in Multiple Steps. We start by determining Mb's surfactant binding profile using ITC. Titrations of Mb with millimolar concentrations of SDS lead to isotherms with several characteristic and reproducible transitions (Figure 1, S1A and S1B in the Supporting Information). There is an initial decrease in enthalpy between 16 and 50 μM SDS to a plateau, whose enthalpy value (interpolated to 0.1 mM SDS for comparative purposes) increases linearly with [Mb] (Figure S2). Subsequently, there is a steep decrease (Figure S1A) from 0.2 to 0.4 mM SDS. The heat signal in this range is not titratable in the sense that it does not depend on protein concentration. Thus, while Mb−SDS interactions in this range are clearly exothermic, the net affinity is too weak to involve the adsorption of stoichiometrically detectable amounts of SDS on the protein. However, between 0 and 0.3 mM SDS, Mb loses the ability to undergo cooperative thermal stability (described in the Supporting Information and Figure S3), suggesting interactions in this concentration range.

At intermediate concentrations (∼1−3 mM SDS), the enthalpograms follow a common line with a somewhat shallower negative slope. At a point, which is titratable since it is displaced to the right with increasing protein concentration, the enthalpograms curve steeply upward and reach a plateau with no or a slightly positive slope. Finally, the enthalpograms (Figure 1) show a sigmoidal (S-shaped) course between 10 and 20 mM SDS, and all merge to one horizontal line at the highest investigated surfactant concentrations due to formation of free micelles.[6,16,17] The enthalpy just before the onset of the sigmoidal

(16) Antonini, E.; Brunori, M. In *Hemoglobin and Myoglobin and Their Reactions with Ligands*; Neuberger, A., Tatum, E. L., Eds.; North-Holland Publishers: London, 1971; pp 541−548.

(17) Lad, M. D.; Ledger, V. M.; Briggs, B.; Green, R. J.; Frazier, R. A. *Langmuir* **2003**, *19*, 5098−5103.

course increases with [Mb] in a manner which is very similar to the 0.1 mM SDS plateau (Figure S2). All these transitions are mirrored by changes in Trp fluorescence, except that the changes are much more distinct by ITC (see Supporting Information and Figure S4A). Tofani et al.[14] observed an additional transition between ca. 8 and 80 mM SDS according to Trp fluorescence which was attributed to the loss of the heme group. This process is enthalpically invisible, as indicated by the plateau at higher SDS concentrations in Figure 1.

We analyze these data using a simple mass balance approach[6,17] where the total [SDS] concentration, $[SDS]_{tot}$, may be partitioned into a free ($[SDS]_{aq}$) and a protein bound ($=N$[Mb]) population with binding number N (eq 1):

$$[SDS]_{tot} = [SDS]_{aq} + N[Mb] \quad (1)$$

Plotting the location of different transition points in the SDS titration (illustrated in Figure 2A) as a function of [Mb] (Figure 2B) leads to N and $[SDS]_{aq}$ (Table 1). The transition points Z and 0 (onset and end of steep decline at low SDS concentrations, respectively), which do not change with [Mb], occur around 0.19 and 0.4 mM SDS, respectively. Subsequently, massive adsorption to the protein sets in, particularly between point 0 and 1 where about 16 SDS bind to each protein molecule with little concomitant increase in the bulk surfactant concentration. Five additional molecules of SDS bind until point 2. This corresponds to the first phase of the biphasic course typically observed for proteins−SDS binding isotherms.[2,18] Following this, there is a large region where more SDS binds until saturation occurs between points 3 and 4. Between points 2 and 3, around 32 molecules of SDS bind, and only 5−6 molecules bind during the final saturation phase. The free SDS concentration at point 3 (5.6 mM, Table 1) corresponds to the cmc, in perfect agreement with independent ITC measurements of cmc in protein-free solution (data not shown). No further binding to Mb can be detected by ITC when the bulk concentration of the surfactant reaches cmc. The binding number at saturation translates into 1.14 ± 0.02 g of SDS/g of protein, in excellent agreement with the average binding level (1.1−1.2 g/g) found for a range of globular proteins.[3,8]

Formation of SDS Aggregates on the Mb Surface Monitored by Pyrene Fluorescence. Increasing affinity of SDS for Mb at increasing SDS concentrations can be explained by cooperative binding, which would involve formation of aggregated surfactants on the Mb surface. This can be investigated using the hydrophobic probe pyrene, whose ratio for the emission peaks I_3 and I_1 changes as it goes from a hydrophilic (aqueous) to a hydrophobic (micellar) environment[19] such as submicellar (or hemimicellar) aggregates formed on the protein surface. Pyrene could also bind to hydrophobic pockets exposed on the protein surface by SDS denaturation, but these are likely to be populated by SDS molecules due to their much greater concentration compared to pyrene. I_3/I_1 increases above protein-free level already around 0.2 mM in the presence of Mb (Figure 3A), leveling off to an intermediate plateau around 0.6 mM before rising between 2 and 5 mM SDS to converge with the protein-free titration as pyrene incorporates into proper micelles. This confirms a critical aggregate concentration around 0.2 mM (cfr.[14]), above which SDS starts to form complexes on the Mb surface.

CTAC Binding to Mb. The calorimetric analysis of this system was analogous to that of SDS discussed above. Demicellization and dilution of CTAC gives a stronger thermal signal than SDS, but this merely shifts the overall level of the enthalpic signal, rather than affecting the individual steps. The CTAC isotherms (Figure 4A) are distinctively different from SDS. They commence with a sharp transition at very low CTAC concentrations,

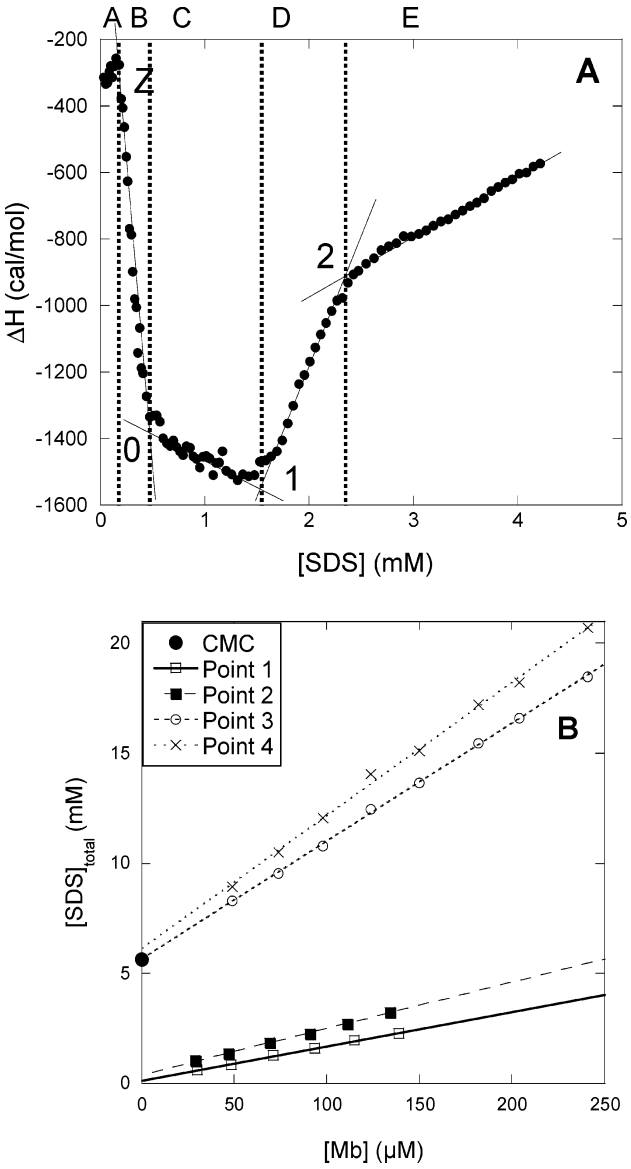

Figure 2. (A) Illustration of the different titration transition points used to estimate the amount of bound SDS, and their associated regions. Region F corresponds to the region above cmc. (B) Total concentrations of SDS, $[SDS]_{tot}$, at the different points indicated in Figures 1 and 2A, plotted as a function of the protein concentration, [Mb]. Binding numbers and free SDS concentrations are derived from eq 1. Data summarized in Table 1. The cmc determined by ITC also indicated.

Table 1. Binding Parameters for SDS−Mb; Transition Points Indicated in Figures 1 and 2B[a]

transition point	binding number N	SDS bound per protein (g/g)	$[SDS]_{aq}$ (mM)
1	15.6 ± 0.3	0.26 ± 0.01	0.13 ± 0.03
2	21.1 ± 0.4	0.35 ± 0.01	0.37 ± 0.04
3	61.2 ± 0.6	1.03 ± 0.01	5.64 ± 0.09
4	67.6 ± 1.0	1.14 ± 0.02	5.65 ± 0.12

[a] All data are obtained at pH 8.0 and 25 °C.

(18) Nielsen, A. D.; Arleth, L.; Westh, P. *Biochim. Biophys. Acta* **2005**, *1752*, 124−132.
(19) Takagi, T.; Tsujii, K.; Shirahama, K. *J. Biochem.* **1975**, *77*, 939−947.
(20) Kalyanasundaram, K.; Thomas, J. K. *J. Am. Chem. Soc.* **1977**, *99*, 2039−2044.

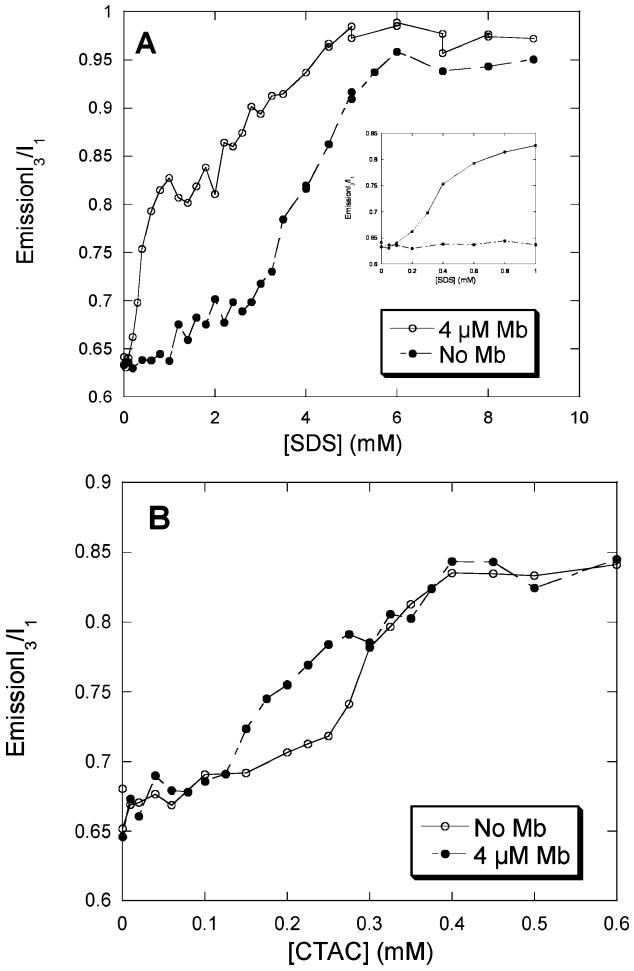

Figure 3. Pyrene emission ratios I_3/I_1 in different concentrations of (A) SDS and (B) CTAC with and without 4 μM Mb present. For both detergents, there is a clearly visible concentration range where detergent structures formed in the presence of Mb allow pyrene to sequester in a hydrophobic environment well below the cmc.

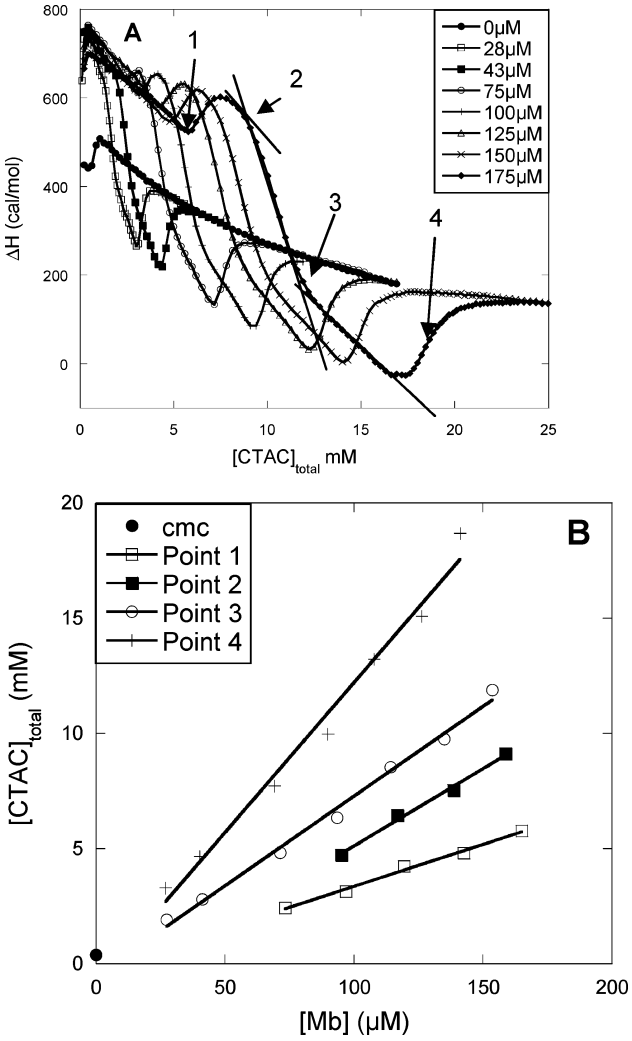

Figure 4. (A) Enthalpy change, ΔH, in cal/mol CTAC for the titration of a range of Mb solutions with CTAC at pH 8.0 and 25 °C. The characteristic points used for calculating SDS binding stoichiometries are indicated. (B) Characteristic point concentrations plotted versus [Mb]. Data summarized in Table 2.

completed within 0.4 mM CTAC (Figure S4B), in which the signal is independent of the protein concentration, as for SDS. At intermediate [CTAC], a number of transitions occur at locations that are displaced to the right with increasing [Mb]. Finally, analogous to SDS, all enthalpograms for CTAC end with an S-shaped course, after which they merge into one common curve that superimposes with the control experiment (CTAC titrated into buffer). This superposition makes it safe to assume that the inflection point prior to this merging represents saturation. These transitions are much more diffuse in Trp fluorescence titration (Figure S4B), highlighting ITC's superior ability to monitor detergent binding. Linear analysis as in Figure 2B (shown in Figure 4B and summarized in Table 2) shows 130 molecules (about 2.58 g of surfactant/g of protein) bound at saturation. Stoichiometric binding occurs primarily between 0.2 and 0.8 mM CTAC (see Supporting Information).

As with SDS, CTAC shows a linear decrease in the thermal melting temperature t_m until around 0.14 mM CTAC, after which the protein no longer unfolds cooperatively (Figure S3B). Also analogous to SDS, this corresponds to the midpoint of the first titration monitored by Trp fluorescence.[14]

Time-Resolved Spectroscopic Studies: SDS. We now turn to a time-resolved study of the interactions between myoglobin and surfactant to provide a more mechanistic understanding of how these interactions take place. Mb provides probes both for

Table 2. Binding Parameters for CTAC−Mb[a]

transition point	binding number N	CTAC bound per protein (g/g)
1	36.40 ± 1.81	0.72 ± 0.03
2	67.02 ± 4.05	1.33 ± 0.08
3	77.82 ± 3.01	1.54 ± 0.06
4	130.1 ± 7.44	2.58 ± 0.15

[a] All data are obtained at pH 8.0 and 25 °C.

the heme environment (monitored by changes in absorption at 410 nm) and the overall protein conformation (fluorescence). With an excitation wavelength of 275 nm and a cutoff filter of 305 nm, we can follow changes involving both of the two Trp residues (position 7 and 14) and the two Tyr residues (positions 103 and 146). Both the number and the relative amplitudes of the relaxation phases are unaffected by switching to an excitation wavelength of 295 nm and a cutoff filter of 320 nm, which only reports on Trp fluorescence (data not shown). We therefore conclude that the observed fluorescence signals mostly refer to variations in the Trp environments. Note that Trp fluorescence will be affected not only by the protein environment but also by the proximity of surfactant molecules. Therefore, one cannot a

priori conclude that a fluorescence change is caused by a conformational change around the Trp residues rather than simple surfactant binding.[20] However, the absorption of Trp is not perturbed by surfactants to nearly the same extent as fluorescence. As we will see below, absorption and fluorescence changes generally follow each other closely, suggesting that we are in fact monitoring large conformational changes which affect both Trp residues and the heme.

When Mb is mixed with SDS, a minimum of around 0.1 mM surfactant is needed to elicit spectroscopic changes with time. Above this concentration level, several relaxation phases are seen. Typical fluorescence and absorption time profiles are illustrated in Figure S5A−S5C, showing that the fluorescence signal increases with time, while the absorption signal decreases.

The number of relaxation phases varies with SDS concentration. In the range 0.1−1 mM only two phases are observed, whereas a total of three phases are seen between 1 and 10 mM SDS. Above 10 mM, only two phases can be detected. Note that in all experiments there is close temporal correspondence between fluorescence and absorption. This is illustrated by the two linear regions in the absorption versus fluorescence plot (Figure S5D), where the time dimension is eliminated. We term the three phases the fast, intermediate, and slow phase, respectively, with associated rate constants k_{fast}, k_{inter}, and k_{slow}. Although the rate constants from fluorescence and absorption measurements are essentially identical, the amplitudes differ. The three phases are described in more detail in the Supporting Information, but may be summarized as follows: k_{fast} increases hyperbolically with [SDS], plateauing around 50−55 s^{-1}, and its concentration dependence can be fitted to a simple binding scheme (Figure 5A) with a pre-equilibrium binding step that saturates around 4 mM SDS and an apparent binding constant of 0.5−1 mM (Table S2). The development in the corresponding fluorescence amplitude (Figure 5B), which reflects the difference in fluorescence between the start and end species, suggests that the dead time species changes with increasing SDS concentration. k_{interm} increases from 0.2 to ca. 15 s^{-1} up to 20 mM, after which it declines to 4−6 s^{-1} (Figure 5C); the signs for the fluorescence and absorption amplitudes are opposite that of the fast phase between 1 and 10 mM but similar outside this range (Figure 5D). The slow phase is observed only between 0.5 and 10 mM SDS, with the k_{slow} constant around 1 s^{-1} (Figure 5E). Its amplitude peaks around 2.5 mM SDS (Figure 5F) and is larger for absorption than fluorescence, suggesting that this phase mainly involves the heme environment.

Time-Resolved Spectroscopic Studies: CTAC. Mb−CTAC kinetics differ substantially from those of Mb−SDS. First, the changes are several orders of magnitude slower (Figure S6A,B), typically taking 500 s to reach completion, in contrast to the few seconds required in SDS. Second, there are only two predominant phases throughout the concentration regime, which are indicated as intermediate and slow. In addition, a fast phase (with rate constants around 5−15 s^{-1}) can be discerned in a relatively narrow interval between 0.2 and 0.8 mM CTAC (on each side of the cmc of about 0.4 mM), but the signal is not very reproducible. Third, the rate constants in CTAC show a much more variable concentration dependence than in SDS (Figure 6A,C). The amplitudes (Figure 6B,D) suggest that most of the structural changes at the protein level occur in the intermediate phase, whereas the changes in the heme environment dominate the slow phase. This is discussed further in the Supporting Information.

(21) Otzen, D. E. *J. Mol. Biol.* **2003**, *330*, 641−649.

Discussion

We have performed a multidisciplinary analysis of the interactions of the two surfactants SDS and CTAC with Mb. Many different steps are involved, but a closer inspection reveals a good correlation between the different techniques. Let us start with a description of the SDS−Mb system. This may be divided into six regions, A−F, delimited by the following concentrations of free SDS and encapsulated for illustrative purposes in Figure 7 (cfr. Figure 2 for an ITC-based summary of regions A−E; region F is above the cmc).

In region A, around 0−0.15 mM SDS, no interactions are detected by Trp fluorescence, pyrene, or kinetics, indicating no major conformational changes or clustering of SDS. This is confirmed from thermal scanning data, which show that Mb is able to unfold cooperatively throughout this region (Figure S3B). The decline in thermal stability most likely stems from an increased affinity of SDS for the denatured state compared to the native state, a phenomenon that is observed only at high temperatures where the denatured state becomes more significantly populated. The negative slope (for 0.1 mM SDS) in Figure S2 reveals exothermic protein−surfactant interactions, and the enthalpy of interaction increases with protein concentration. However, as the transition from region A to region B is independent of the protein concentration (Figure S1B), no stoichiometric adsorption of the surfactant could be detected through region A (i.e., $N \sim 0$ in eq 1), presumably because of a weak net affinity of surfactant for the protein. This implies that the favorable (exothermic) enthalpy of interaction is balanced out by an entropic penalty ($\Delta S < 0$), thus giving a small free energy of interaction. These thermodynamic parameters speak against a hydrophobic nature of the interactions in this range and rather point toward (nonspecific) columbic interactions between charges on the protein and the sodium- and dodecylsulfate ions in solution. This binding corresponds to the first (specific) binding region in the classical analysis of protein−surfactant interactions.[5−8] Possible binding regions with charge complementary to the dodecylsulfate group are highlighted in Figure S8A based on the calculated electrostatic potential surface.

The surfactant concentration range following the specific binding region is traditionally ascribed to noncooperative and fairly weak binding of surfactant regions. However, we find that for Mb this range can be divided into a number of different regions with very distinct features, both in terms of equilibrium and kinetics, which strongly nuance this rather simple view.

Region B, spanning 0.15−0.4 mM SDS, leads to major changes. The enthalpograms exhibit a strong exothermic signal which (in contrast to region A) is remarkably independent of the protein concentration (Figure S1B). The superposition of the curves (Figure S1B) signifies the absence of stoichiometric binding and indeed any enthalpic effect of protein−surfactant contacts in this region. The distinctive negative slopes of the enthalpograms are therefore likely to arise from SDS-induced changes in the protein conformation. This is probably the change from 6cHS to 6cLS coordination of the heme group previously shown to occur in this range of SDS concentrations.[12] Moderate changes in the protein conformation are also deduced from the loss of the ability to unfold cooperatively (Figure S3B), the start of the rise of Trp fluorescence (Figure S4B) and the ability to monitor unfolding kinetics (Figure 5). The pyrene fluorescence data (Figure 3A) further show that region B is where the initial nucleation of SDS aggregates on the protein occurs. However, the invariance of point 0 (Figure 2A) with regards to protein concentration shows that the binding number is too low to be quantified by ITC.

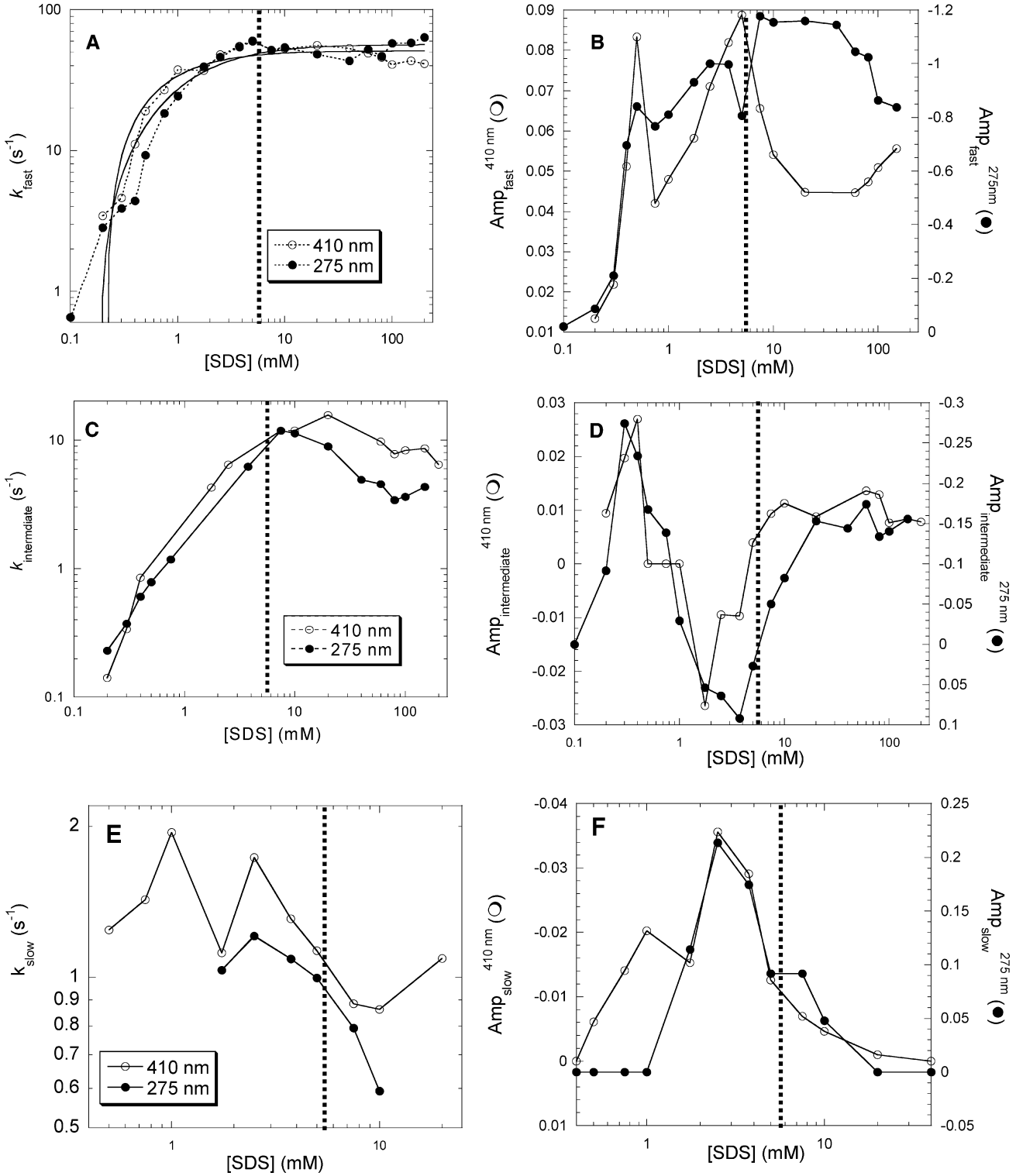

Figure 5. Rate constants for the different relaxation phases seen upon mixing Mb with SDS, followed by absorption (410 nm) and fluorescence (275 nm). The cmc is indicated by a stippled line. (A) k_{fast} with associated amplitude in (B). The joined lines are the best fit of the data to eq A (Supporting Information). (C) $k_{intermediate}$ with associated amplitude in (D). (E) k_{slow} with associated amplitude in (F).

These changes are consolidated and modified in region C (0.4−1.2 mM SDS), where around 16 molecules of SDS are bound, leading to further increases in pyrene fluorescence, a very strong change in Trp fluorescence and an interesting shift in the kinetics revealed by the amplitudes: the amplitude of the fast phase undergoes a shift in its magnitude, while that of the intermediate phase declines steeply. In addition, the fluorescence of the dead-time species from which unfolding occurs (Figure S7A) starts to rise from 0.4 mM SDS onward, indicating binding of a significant number of SDS molecules prior to unfolding. While the molecular origins of these kinetic changes remain obscure in the absence of, e.g., protein engineering studies (cfr. the approach used in refs 6 and 13), they indicate that binding of a defined number of SDS molecules affects the mechanism of unfolding.

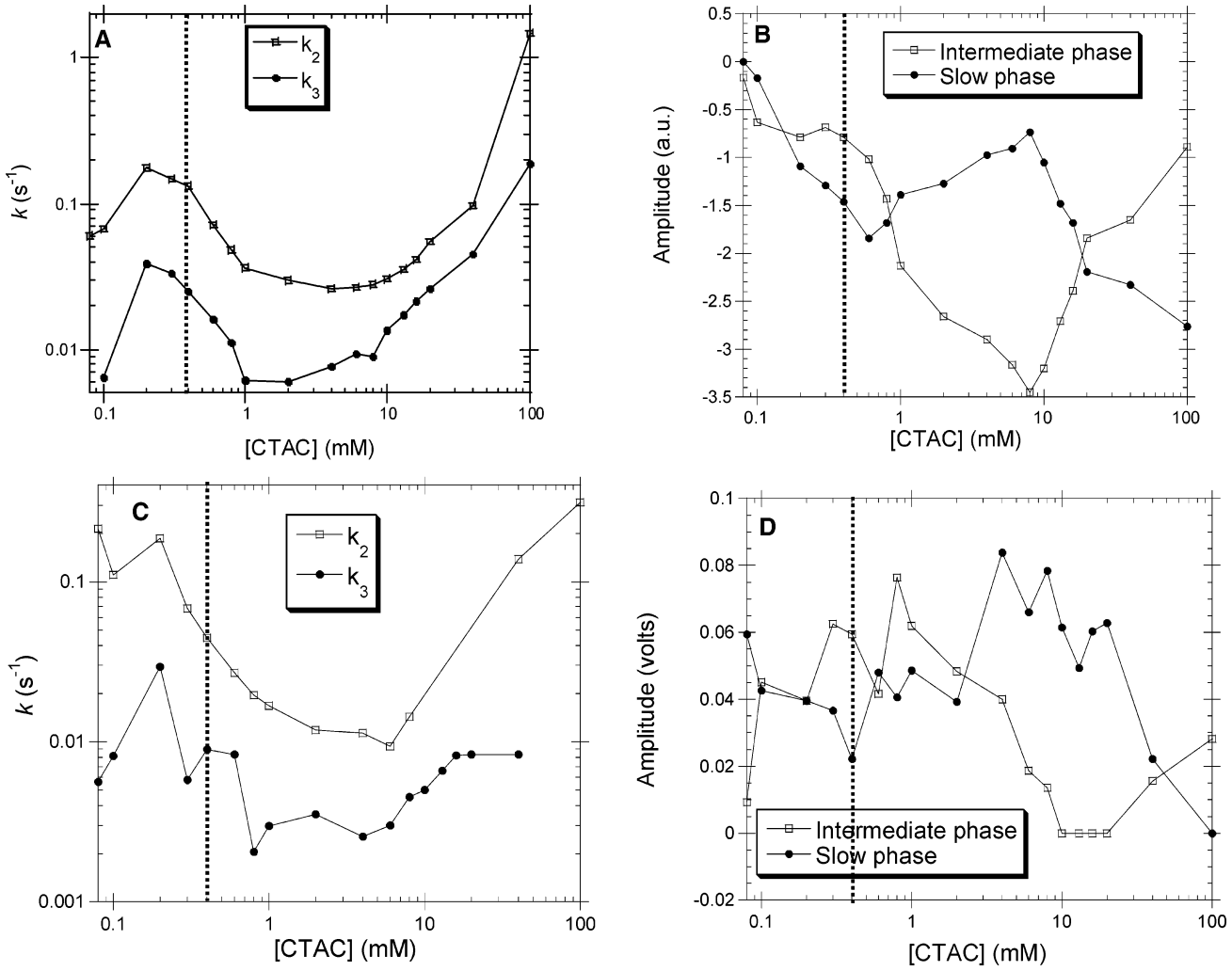

Figure 6. Amplitudes and rates for the two relaxation phases seen upon mixing Mb with CTAC monitored by (A) and (B) fluorescence or (C) and (D) absorption. The cmc is indicated by a stippled line.

In region D (1.2−2 mM SDS) an additional five molecules of SDS (16−21) are bound. This represents a "calorimetric turning point" as SDS binding changes quite abruply from a highly exothermic process (region C) to a marked decline in exothermal signal. This is mirrored by a less steep rise in Trp fluorescence with SDS concentration. This would suggest that the five new SDS molecules bind in a markedly different fashion from the preceding 16. However, this does not translate into major changes in clustering since the pyrene fluorescence or unfolding kinetics do not change.

Finally, region E takes us from 2 mM SDS up to the cmc, in which SDS increasingly binds as more conventional micellar structures with binding numbers around 68 so that the pyrene fluorescence converges to that of micellar SDS. In this region, there is only a small decline in the steady-state Trp fluorescence (since the protein has already been effectively denatured at 2 mM SDS), but there is a characteristic rise and decline of a slow kinetic phase within this region. It is possible that there are two parallel unfolding pathways, where the fast one is driven by small-cluster SDS molecules, while micelle-like clusters on the surface, which only form in this region, trap Mb in a slowly folding pathway. The intermediate unfolding phase may also be involved in this pathway since its amplitude is only negative in this region.

Above cmc in region F, the changes in the amplitude of the fast and intermediate phases as well as a small but significant decrease in the intermediate rate constant reveal the transition to a new unfolding pathway, driven by micellar SDS perhaps in cooperation with monomeric SDS, where unfolding is fast and biphasic. The strong similarity between kinetic data (rates as well as amplitude changes) obtained by Trp fluorescence and heme absorption indicates that the changes are global in nature and affect the heme environment and the aromatic residues to the same extent.

Importantly, the number of transitions for Mb is considerably higher than for other proteins analyzed in a similar fashion. For example, the two β-sheet proteins TII27 and Tnfn3 show only a single symmetrical enthalpy peak prior to micellization (although this is preceded by a small specific binding step)[6] and a correspondingly simple fluorescence titration and single-phase unfolding kinetics. Similar observations have been made for the enzyme cutinase.[17] It is possible that the presence of the heme cofactor induces a higher degree of complexity in the system and thus extends the range of conformational transitions.

For CTAC, we see some remarkable similarities as well as differences compared to SDS. Overall, unfolding is 2 orders of magnitude slower despite the longer tail length of CTAC compared to SDS. While anionic and cationic surfactants unfold S6 with comparable rates,[12] CI2 cannot be unfolded by cationic surfactants at all. Since SDS and CTAC must prefer to bind to oppositely charged residues on Mb, it is clear that Mb regions with clusters of positive charge must be better nuclei for unfolding

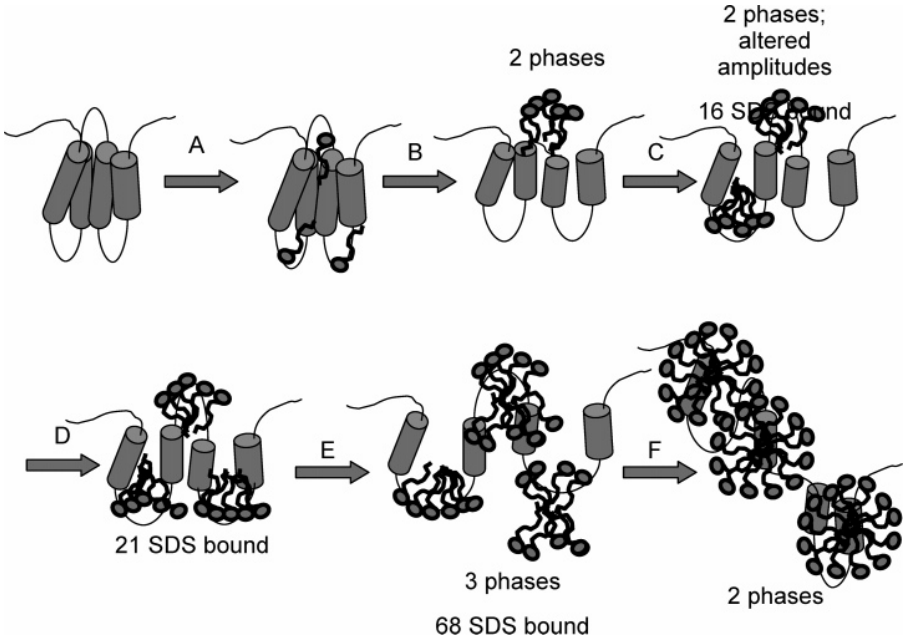

Figure 7. Model of the different stages of unfolding of Mb by different concentrations of SDS. In region A (0−0.15 mM SDS), weak (but not stoichiometrically quantifiable) binding is observed only by ITC and may correspond to the first phase of binding of SDS via specific electrostatic interactions. In region B (0.15−0.4 mM SDS), strong (but nonstoichiometric as in A) exothermic binding occurs in parallel with the loss of cooperative unfolding, initial formation of aggregates, and two-phase unfolding kinetics. Region C (0.4−1.2 mM SDS) leads to binding of 16 SDS molecules coupled with a large increase in Trp fluorescence and changes in the amplitudes of the two unfolding phases, probably due to increased dead-time binding of SDS. During region D (1.2−2 mM SDS), an additional five SDS molecules bind, forming a transition to region E (2−5.6 mM SDS), where an additional 47 SDS molecules bind (possibly with size between the region C aggregates and true SDS micelles) and lead to the appearance of a slow kinetic phase, possibly related to the binding of the micelle-like species. This phase disappears in region F (above 5.6 mM SDS), where intact SDS micelles coupled with monomeric SDS are probably the main driving force in unfolding Mb.

than the negatively charged regions. The electrostatic potential surface (Figure S8A) does not provide any obvious structural clues for this, probably because initial binding is only part of the unfolding reaction.

As with SDS, we observe two distinct binding regions prior to the stoichiometrically well-defined regions. The exact concentration regimes are difficult to ascertain, as the low cmc of CTAC prevents us from estimating concentrations of free CTAC accurately from ITC data. The following concentration regions are therefore only rough guidelines. In region A (between 0 and 0.12 mM CTAC), neither kinetics nor pyrene and Trp fluorescence indicate any interactions, while ITC suggests nonstoichiometrical and thus unspecific interactions with the native state, whose existence is again confirmed by cooperative thermal transitions. As for SDS, putative binding regions can be identified from the electrostatic potential surface (Figure S8B). These thermal transitions disappear in region B (ca. 0.12−0.3 mM), suggesting the disappearance of the native state. This occurs as the rise in the exothermal signal levels off, clusters form on the surface (pyrene), and profound Trp fluorescence changes start to be observed. The conformational changes have a distinct kinetic profile in this region, as the rate constants for both phases rise while the amplitudes change.

This changes in region C (ca. 0.3−1 mM), where the first stoichiometric signals are accumulated as 36 CTAC molecules bind. Interestingly, it is in this region that we observe a clear decline in the rate of unfolding, similar to what we have observed for S6 in the cationic surfactant LTAC (lauryl-trimethyl ammonium chloride).[12] We previously rationalized this as the binding of distinct species of LTAC clusters which inhibit the protein in a slowly unfolding state, and we can now substantiate this species as the distinct stoichiometric cluster of, in this case, 36 CTAC molecules, although we cannot ascertain whether this is a single cluster or the CTAC molecules are distributed among several clusters. Subsequently, there is a transition region D (1−1.5 mM) observed by both steady-state and kinetic fluorescence data as well as ITC, in which a substantial number of CTAC molecules (ca. 31) bind without large effects on the conformational transitions. In regions E and F an additional 63 molecules bind in two different stages (11 in region E and 52 in region F) until the cmc is reached. In contrast to SDS, significant mechanistic changes occur above the cmc. Having declined to a plateau in regions C−F, the rate constants subsequently start to rise above 10 mM CTAC. The simplest explanation for this phenomenon is that the micelles can out-compete the inhibitory clusters on the surface and act as more effective unfolding species. This is in clear contrast to the unfolding of S6 by LTAC, where the unfolding rates decline continuously up to 1 M surfactant.[12] In the case of S6, however, all unfolding occurs above the cmc (10 mM LTAC), and inhibition is not observed before 20 mM. Therefore, the inhibitory activity toward S6 can be caused only by micelles and will not change at higher concentrations. Again this underlines that different proteins have different susceptibilities toward unfolding by cationic surfactants.

In summary, we have demonstrated the existence of multiple Mb−surfactant interaction regimes, which reflect the buildup of different types of surfactant−protein complexes with varying stoichiometries and different mechanistic pathways. This represents an expansion of the classical view of biphasic surfactant binding prior to formation of micellar structures. The variety of interactions may reflect the contribution of the heme cofactor to the conformational properties of Mb.

Acknowledgment. K.K.A. is funded by the BIOPRO innovation consortium. D.E.O. gratefully acknowledges support from the Danish Research Foundation and the Villum Kann

Rasmussen Foundation. Support to P.W. from the Carlsberg Foundation, the Danish Research Foundation, and the Danish Research Agency (Grants 26-02-0160 and 21-04-0087) is acknowledged. We thank G. Smulevich and M. Coletta for helpful discussions. K.K.A. performed and analyzed thermal stability and equilibrium fluorescence titration experiments, P.W. performed and analyzed ITC experiments, D.E.O. performed and analyzed kinetic experiments, D.E.O. and P.W. wrote the article, and D.E.O. revised the article.

Supporting Information Available: Supporting Information describes the following aspects in more detail: (1) Fluorescence-based analysis of thermal stability of Mb at low concentrations of SDS and CTAC. (2) Direct comparison of ITC and fluorescence data for titration of Mb with SDS and CTAC. (3) Titration of Mb with CTAC using the mass balance equation. (4) Detailed descriptions of the time-resolved changes upon titration of Mb with different concentrations of SDS and CTAC, including the three different phases observed by SDS and the two phases observed by CTAC. Data include both rate constants, associated amplitude changes, and calculated start and end points. This information is available free of charge via the Internet at http://pubs.acs.org.

LA702890Y

Paper II - Supplementary material

SUPPLEMENTARY MATERIAL

MATERIALS AND METHODS

Calculation of myoglobin's electrostatic potential: This was performed using the programme MEAD and the pdb file of horse myoglobin (1WLA) as described [1].

Thermal denaturation: Thermal scans were conducted on a Cary Eclipse Fluorescence spectophotometer (Varian, Mulgrave, Australia) using a 10mm quartz cuvette. Scans were performed from 20 to 100°C using an excitation wavelength of 295nm and an emission wavelength of 350nm. The scan rate was 1°C/min and a slit width of 10nm was used. Samples of 4μM Mb were left to equilibrate with SDS or CTAC for at least 1 hour before measurement. Thermal scans were fitted to a thermal transition as previously described [2].

RESULTS

Detection of binding of μM amounts of SDS by changes in thermal stability

The data in Fig. S1B suggest some interaction at concentrations below 0.2 mM, but the modest size of the signals and the inability to assign a definite number of bound SDS molecules suggest that the binding is relatively weak, and make it appropriate to investigate this by alternative means. One approach is to measure the thermal stability at different SDS concentrations, since the denaturation temperature t_m is typically sensitive to even small solvent perturbations. Mb undergoes a characteristic increase in fluorescence upon denaturation (Fig. S3A), since denaturation removes the heme group from the vicinity of the two Trp residues (residues 7 and 14) and thus reduces its ability to quench their fluorescence. This makes it possible to determine the temperature of denaturation t_m

with acceptable precision. t_m decreases linearly with [SDS] between 0 and ca. 0.3 mM SDS (Fig. S3B), after which no transition is observed, indicating a loss of native structure. The loss of cooperative unfolding corresponds to the midpoint of the first transition observed by Trp fluorescence [3], indicating that after this stage there is no longer sufficient native protein left to give rise to an unfolding signal. Thus SDS interacts with Mb at concentrations as low as 10 μM, but global denaturation is not observed until above 0.3 mM SDS. We also observe that if we increase the myoglobin and SDS concentrations from 10 to 30 μM while keeping the molar ratio 1:1, the t_m declines continuously (Table S1). In accordance with the ITC data, this suggests non-specific interactions (rather than stoichiometric binding) at low [SDS].

Direct comparison of ITC data and changes in Trp fluorescence for SDS

Previous fluorescence titration of Mb by SDS had revealed transitions at a very low SDS concentrations compared to our ITC data [3]. However, the experiments by Tofani *et al.* were carried out at relatively low (8μM) Mb concentrations, where the amount of SDS complexed by Mb is insignificant compared to the total SDS concentration. We therefore repeated these fluorescence titrations at 72 μM Mb, where binding of SDS to Mb will lower the amount of free SDS to a significant extent, and found that the transitions can be correlated satisfactorily with the ITC data, although the different spectroscopic transitions are more distinct by ITC (Fig. S4A). Direct comparison reveals that regions A and B (see Fig. S4A), which seems to be connected to nonspecific interactions, do not lead to any significant changes in Mb conformation, commensurate with the observation that Mb retains its ability to thermally unfold cooperatively in this region. In contrast, the ensuing zone C, during which Mb binds 16 SDS molecules and the enthalpic signal remains large and exothermic, is where the largest conformational changes occurs. In the subsequent zone D, only 5 more SDS molecules are bound, leading to a decrease in the enthalpic

signal and a distinct second phase in the fluorescence curve with a smaller signal change. Finally, zone E (which continues to the saturation point outside the range of Fig. S4A) is assigned to the binding of a large number of SDS molecules (ca. 46) but with a much smaller enthalpic signal, corresponding to an only slightly decreasing fluorescence signal.

Titration of Mb with CTAC using the mass balance equation (Table 2)

The free CTAC concentrations could not be determined with satisfactory precision since the regression standard error for the parameter $[CTAC]_{aq}$ was 0.2-0.5 mM. This is comparable with the cmc(~0.4mM) for this more hydrophobic surfactant. However, given that we have a concentration-independent binding phase which completes around 0.2 mM CTAC, stoichiometric binding of CTAC to Mb appears primarily to occur between 0.2 and 0.8 mM CTAC. This is corroborated by pyrene-binding data (Fig. 4B), which also indicate a region (around 0.15-0.3 mM CTAC) where hemi-micellar structures are formed on the Mb surface.

Description of time-resolved changes upon binding of SDS to Mb

Fast phase: For the fast phase, the observed rate constant k_{fast} increases from ca. 0.6 to 50 s^{-1} between 0.1 and around 10 mM SDS, after which it remains constant (Figure 5A).

The hyperbolic behaviour seen in the plot of k_{fast} versus [SDS] suggests that the observed k_{fast} is related to a simple binding and unfolding scheme:

$$Mb_N + \mathrm{SDS} \overset{K_{SD}}{\rightleftharpoons} Mb_N : SDS \xrightarrow{k_d} Mb_A : SDS \qquad \text{(Scheme 1)}$$

where Mb_N and Mb_A denote the native and (partially) unfolded state of Mb, K_{SDS} = .[SDS]/[Mb_N:SDS] is a preequilibrium corresponding to a very fast phase barely observed at the lowest SDS concentrations (see below) and k_d is the rate constant for the conformation change following binding. (Note that we do not imply that Mb_A is completely unfolded, but it must have undergone some structural change relative to Mb_N). This leads to the following equation:

$$k_{obs} = k_d * \frac{([SDS] - [SDS]_o)}{K_{SDS} + ([SDS] - [SDS]_o)} \qquad \text{(A)}$$

Here we take into account that the SDS concentration needs to be above a critical threshold concentration $[SDS]_o$ to allow the second process (characterized by k_d) to occur. This concentration is not necessarily related to the critical concentrations for aggregate or micelle formation, which are 0.2-0.4 mM and 5.6 mM, respectively. The fact that k_{fast} levels off at SDS concentrations which are close to the cmc indicates that the fast phase mostly concerns SDS monomers and SDS/protein aggregates rather than bulk micelles. The data from both fluorescence and absorption fit reasonably to eq. A (curve fits shown in Figure 5A) and lead to the values in Table S1, in which absorption and fluorescence values agree reasonably well.

The fluorescence amplitude increases more or less monotonically up to 10 mM SDS, after which it slightly declines (Fig. 5B). This amplitude is the difference in fluorescence between the start species (the state formed in the dead-time of mixing in the stopped-flow apparatus) and the end species (the state formed during the fast phase). The amplitude difference suggests that the species forming within the dead-time is not the same at different SDS concentrations. This is corroborated by calculating the fluorescence level at the beginning of the unfolding reaction (Fig. S7A) which shows an increase in the fluorescence level between 1 and 10 mM SDS. This is probably due to the accumulation of micelles which bind to Mb, altering its fluorescence properties.

The amplitude for absorption shows a more complex (but reproducible) behaviour, with local maxima around 0.5 and 5 mM and a slight increase above 40 mM SDS (Fig. 5B). The dead-time absorption start values also show a steep rise around 0.4 mM SDS (Fig. S7A), indicating a change in the structural environment of the heme group.

Intermediate phase: For the intermediate phase, the rate constant $k_{\text{intermediate}}$ increases from 0.2 to ca. 15 s^{-1} up to 20 mM, after which it declines to 4 - 6 s^{-1} (Fig. 5C). For both fluorescence and absorption, the amplitude sign of this phase is opposite of that for the fast phase between 1 and 10 mM SDS, whereas it is the same below 1 mM and above 10 mM SDS (Fig. 5D).

Slow phase: This phase is only observed between 0.5 and 10 mM SDS. The rate constants remain essentially constant around 1 s^{-1} (Fig. 5E). The amplitude of this phase peaks very clearly around 2.5 mM (Fig. 5F), where it constitutes almost half of the amplitude of the two other phases according to absorption data, but less than a quarter of the fluorescence phases. This suggests that the slow phase primarily involves the heme environment, with smaller structural repercussions for the Trp residues. This is further strengthened by two observations: firstly, the slow phase starts to appear at a lower SDS concentration when measured by absorbance (0.5 mM) than when using fluorescence (1.75 mM), indicating either that (i) a threshold (minimum) proportion of the Mb molecules have to undergo the conformational change around the heme for the effect to be visible by Trp fluorescence or (ii) the change in the heme environment occurs in two steps, the first of which (between 0.5 and 1.0 mM) does not affect the Trp environment, whereas the second one (between 1.75 and ca. 10 mM) does. Secondly, the slow phase is completely absent when SDS is mixed with apoMb (data not shown).

The end-points of the absorption and fluorescence time profiles both show two transitions; one with a plateau at 0.5-2 mM and the other with a plateau at 20 mM SDS and above (Fig. S7A). As

expected, these transitions are very similar to those seen for titration of Mb under equilibrium conditions. The fluorescence change can be rationalized as follows: both the fluorescence end point (*i.e.* the fluorescence level at equilibrium) and the starting point (the fluorescence level from which the reaction kinetics starts) increase with SDS concentration. However, at high [SDS] the starting point increases more steeply than the end point, in other words more and more SDS molecules bind to the Mb molecule within the deadtime of the stopped-flow experiment (in accord with Scheme 1), leading to a dead time fluorescence increase which increasingly eclipses the subsequent conformational change.

Description of time-resolved changes upon binding of CTAC to Mb

The two slow phases in CTAC follow a much more variable pattern than those of SDS: at low [CTAC], the rate constants initially increase, then decline with increasing surfactant concentration, reaching a minimum between 1 and 10 mM CTAC, before rising again (Fig. 6A and 6C). Particularly above ca. 2 mM CTAC, absorbance rate constants are consistently slightly lower than those for fluorescence, suggesting that protein conformational changes precede those of the heme group. This is illustrated nicely in Fig. S6D, which shows how the heme signal in 10 mM CTAC continues to change after the fluorescence signal has reached a plateau, in contrast to the development at 0.4 mM CTAC (Fig. S6C). These interpretations are supported by the amplitudes (Fig. 6B and 6D): the amplitude of the intermediate phase dominates the fluorescence signal between 1 and 10 mM, whereas the opposite is the case for the absorption signal. This would suggest that most of the structural changes at the protein level occur in the intermediate phase, whereas the changes in the heme environment dominate the slow phase. Interestingly, the dead time species shows a gradual increase in fluorescence above 0.3 mM CTAC whereas the absorption level essentially switches from one plateau level below 0.4 mM CTAC to another above 0.4 mM CTAC

(Fig. S7B), also highlighting differences in the effect of CTAC on protein and heme structure. There is a correspondence between Trp fluorescence measured at equilibrium and resolved in time, since the end point fluorescence levels at different CTAC concentrations (Fig. S7B) correspond very well to the transitions observed under equilibrium conditions [3].

REFERENCES

(1) Nielsen, M. M.; Andersen, K. K.; Westh, P.; Otzen, D. E., *Biophys. J.* **2007,** *92*, 3674–3685.
(2) Sehgal, P.; Mogensen, J. E.; Otzen, D. E., *Biochim Biophys Acta* **2005,** *1716*, 59-68.
(3) Tofani, L.; Feis, A.; Snoke, R. E.; Berti, D.; Baglioni, P.; Smulevich, G., *Biophys. J.* **2004,** *87*, 1186-1195.

FIGURES

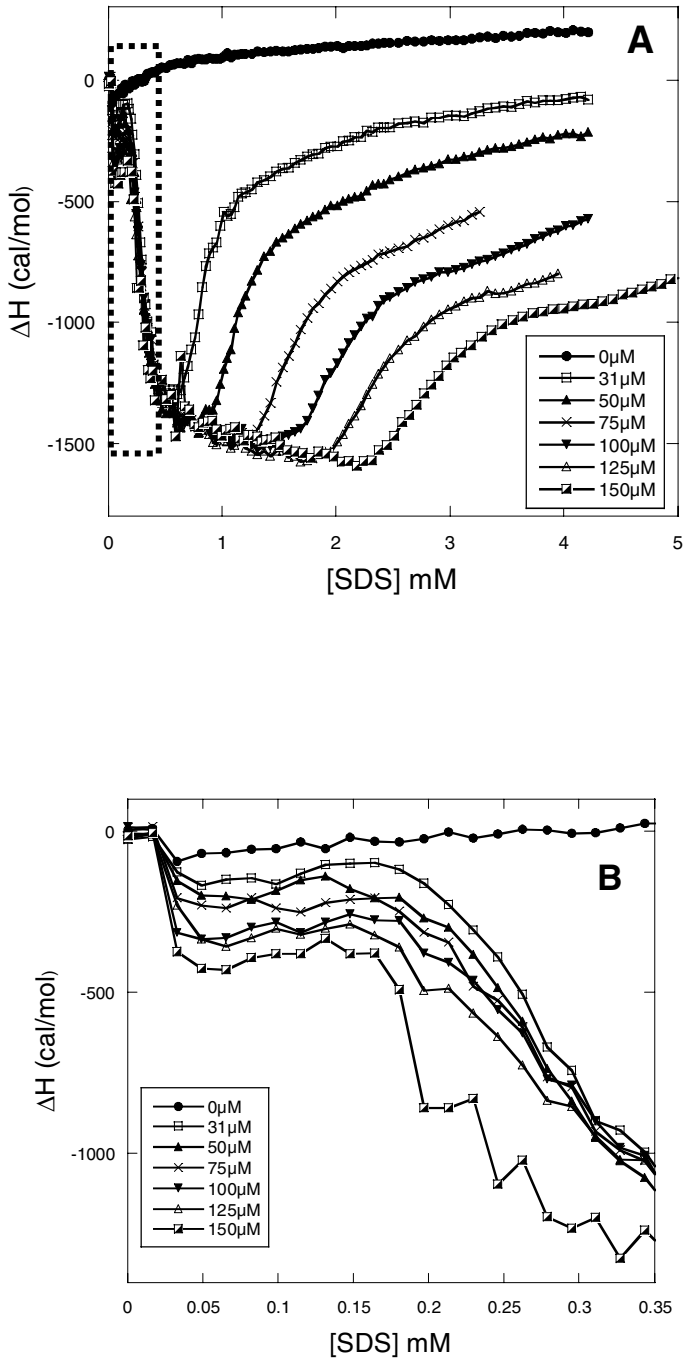

Figure S1. (A) An independent set of isotherms focusing on lower SDS concentrations than in Fig. 1A. The stippled box indicates the region shown in magnification in the panel (B).

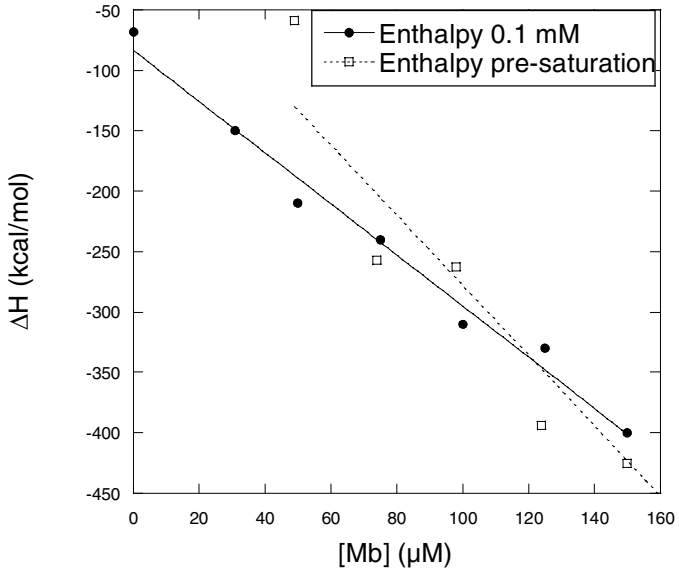

Figure S2.

Interpolated enthalpy values at the first plateau (0.1 mM SDS) and at the level just before the inflection curve leading to saturation versus [Mb]. Notice the close similarity in values.

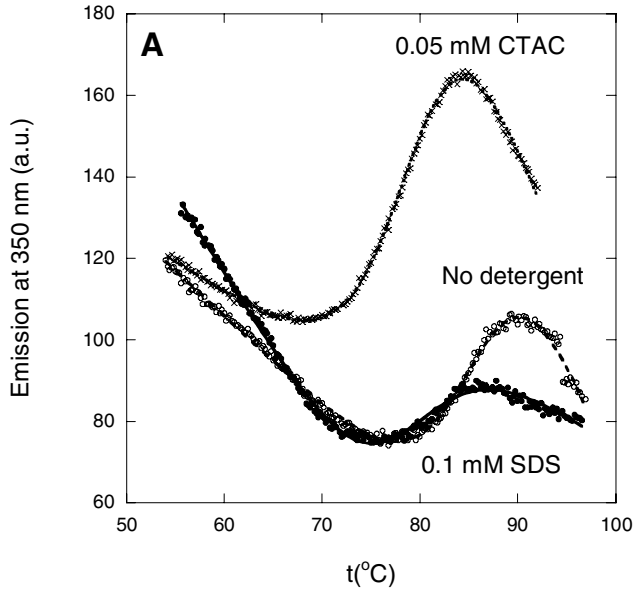

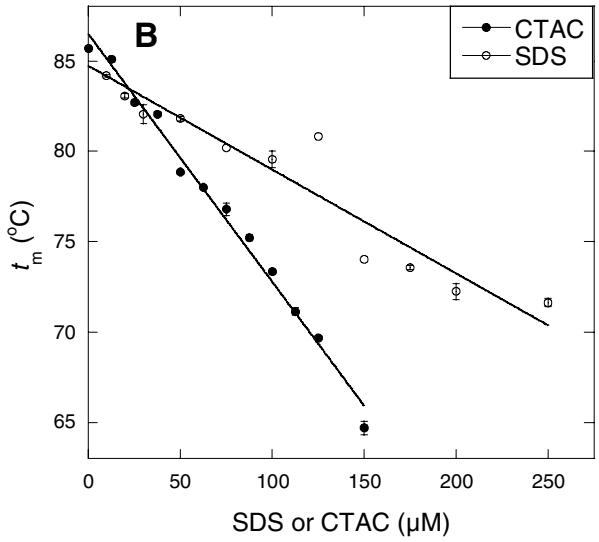

Figure S3

(A) Thermal scans of myoglobin in the presence of detergent. The melting temperature t_m is determined by fitting the data as described in Materials and Methods.

(B) At low detergent concentrations, Mb's t_m declines linearly with detergent concentration for both SDS and CTAC. No clear transitions are seen above 0.25 mM SDS or 0.15 mM CTAC.

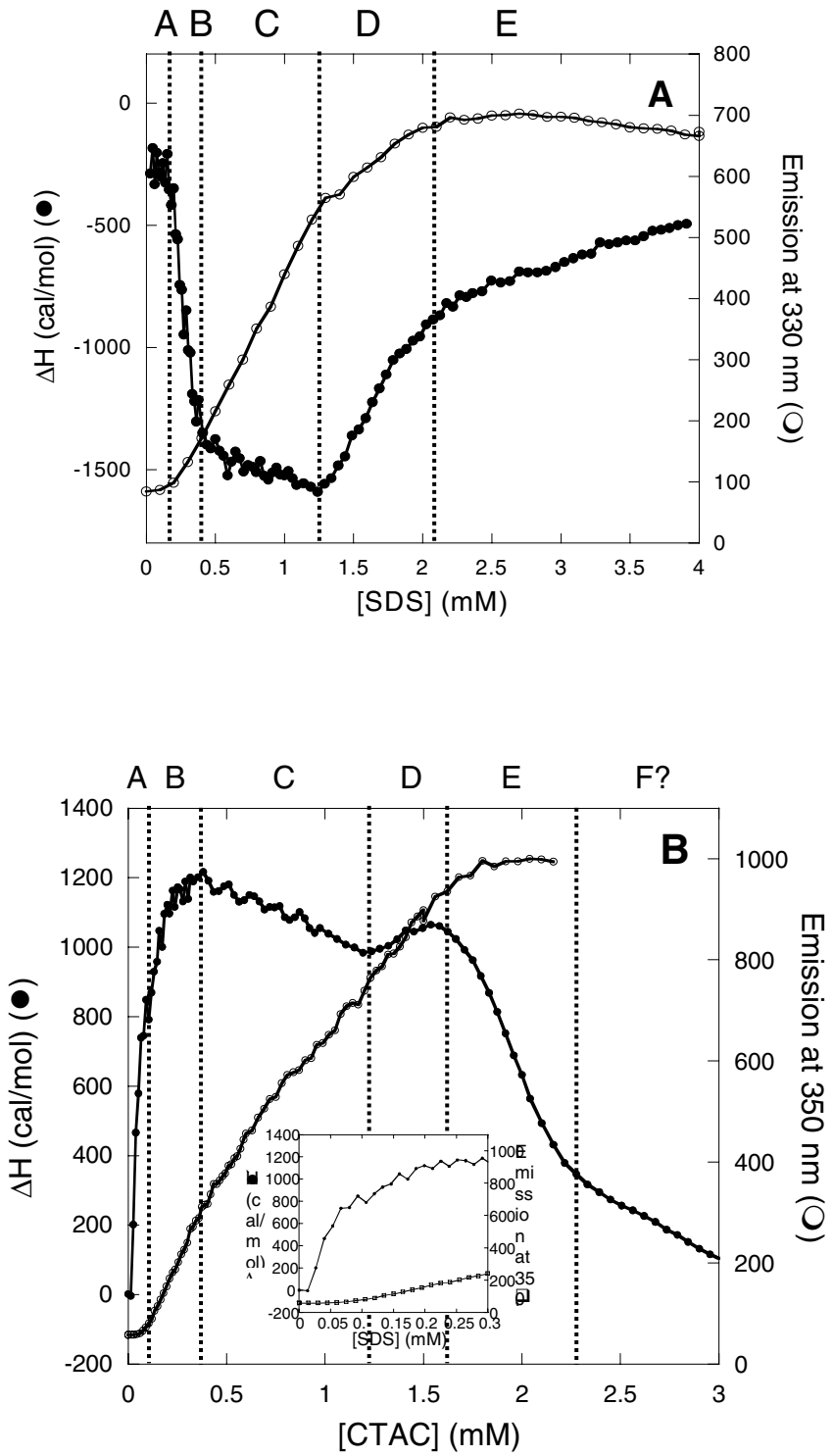

Figure S4. Comparison of titration of Mb with (A) SDS and (B) CTACmonitored by ITC and Trp fluorescence. Stippled lines divide the transitions into different regions referred to in the text.

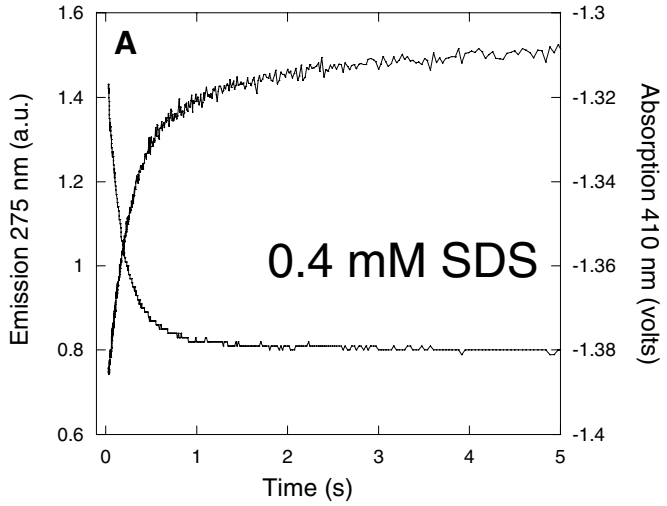
A
0.4 mM SDS
Emission 275 nm (a.u.)
Absorption 410 nm (volts)
Time (s)
1.6
1.4
1.2
1
0.8
0.6
-1.3
-1.32
-1.34
-1.36
-1.38
-1.4
0
1
2
3
4
5

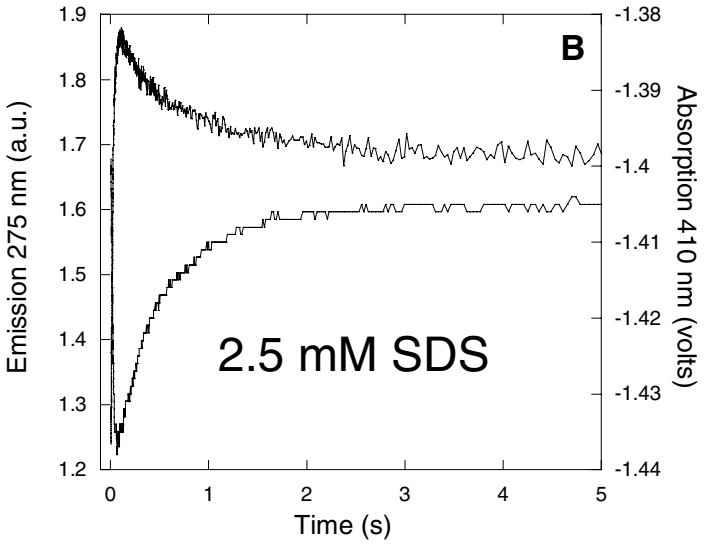
B
2.5 mM SDS
Emission 275 nm (a.u.)
Absorption 410 nm (volts)
Time (s)
1.9
1.8
1.7
1.6
1.5
1.4
1.3
1.2
-1.38
-1.39
-1.4
-1.41
-1.42
-1.43
-1.44
0
1
2
3
4
5

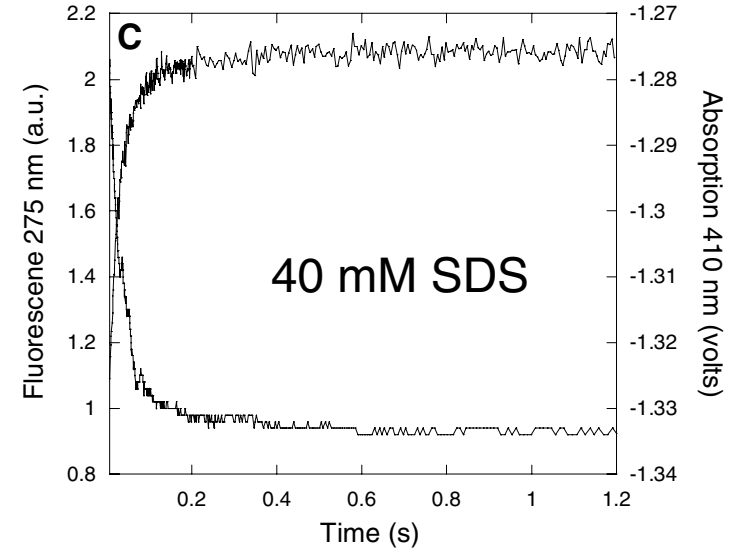

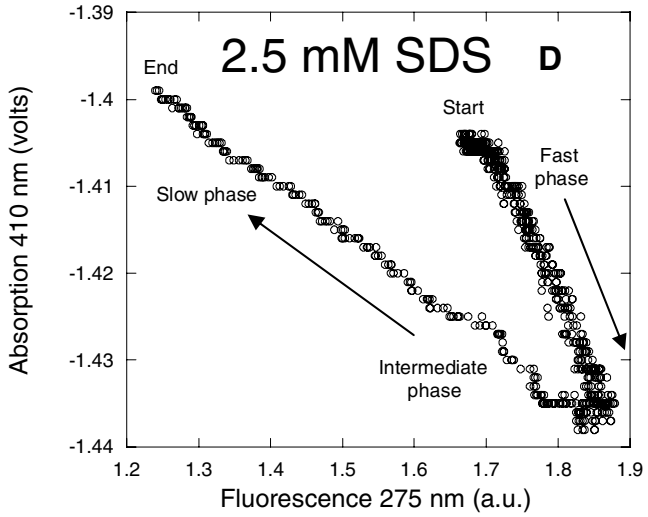

Figure S5.

(A)-(C): Time profiles for changes in the Trp environment (fluorescence emission upon excitation at 275 nm) and the heme environment (absorption at 410 nm) of Mb upon mixing with 0.4, 2.5 and 40 mM SDS, respectively. (D) Plot of absorption versus fluorescence for Mb with indication of time's arrow.

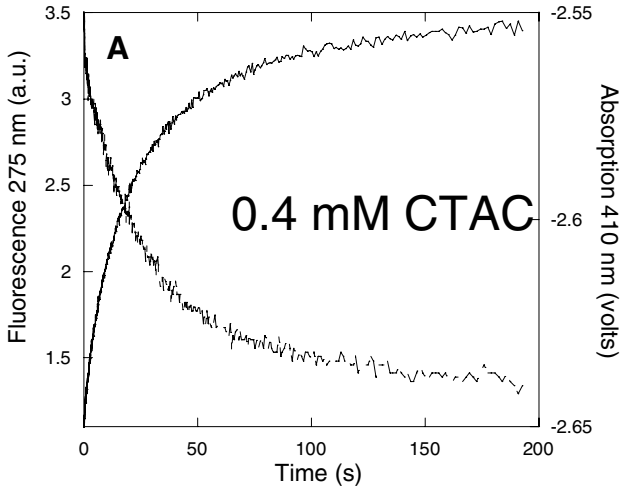
A
0.4 mM CTAC
Fluorescence 275 nm (a.u.)
Absorption 410 nm (volts)
Time (s)
3.5
3
2.5
2
1.5
-2.55
-2.6
-2.65
0
50
100
150
200

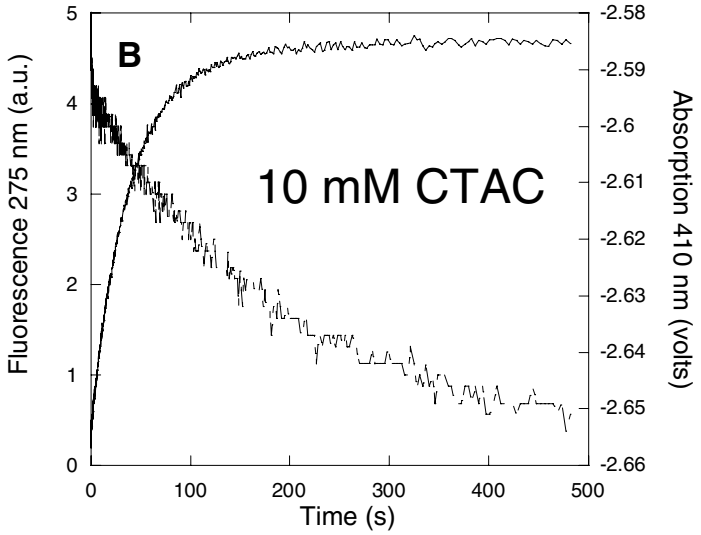
B
10 mM CTAC
Fluorescence 275 nm (a.u.)
Absorption 410 nm (volts)
Time (s)
5
4
3
2
1
0
-2.58
-2.59
-2.6
-2.61
-2.62
-2.63
-2.64
-2.65
-2.66
0
100
200
300
400
500

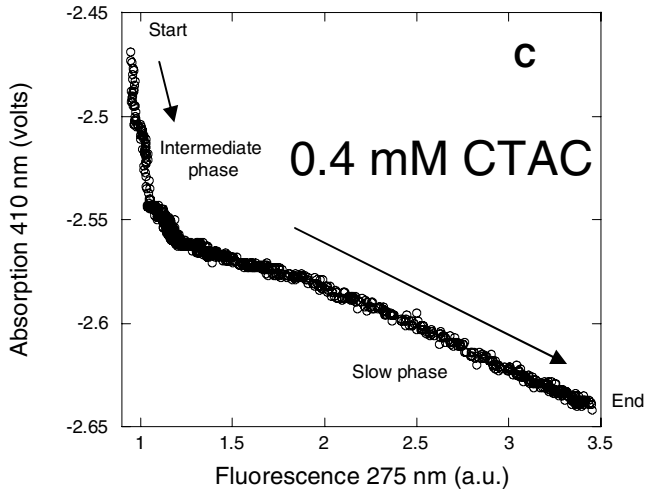

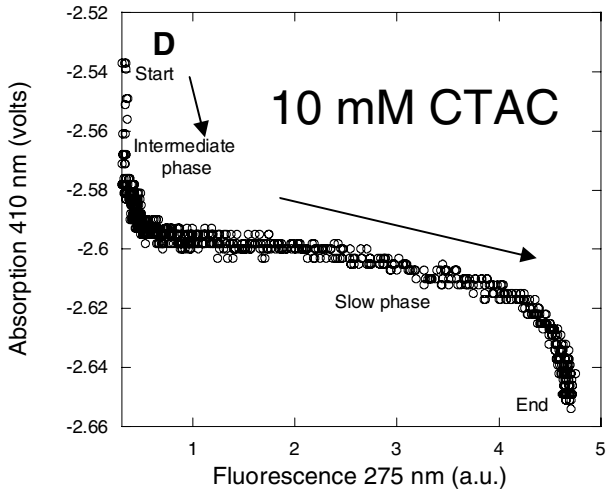

Figure S6

(A) and (B): Time profiles for changes in the Trp environment (fluorescence emission upon excitation at 275 nm) and the heme environment (absorption at 410 nm) of Mb upon mixing with 0.4 and 10 mM CTAC.

(C) and (D): Associated plots of absorption versus fluorescence with indication of time's arrow.

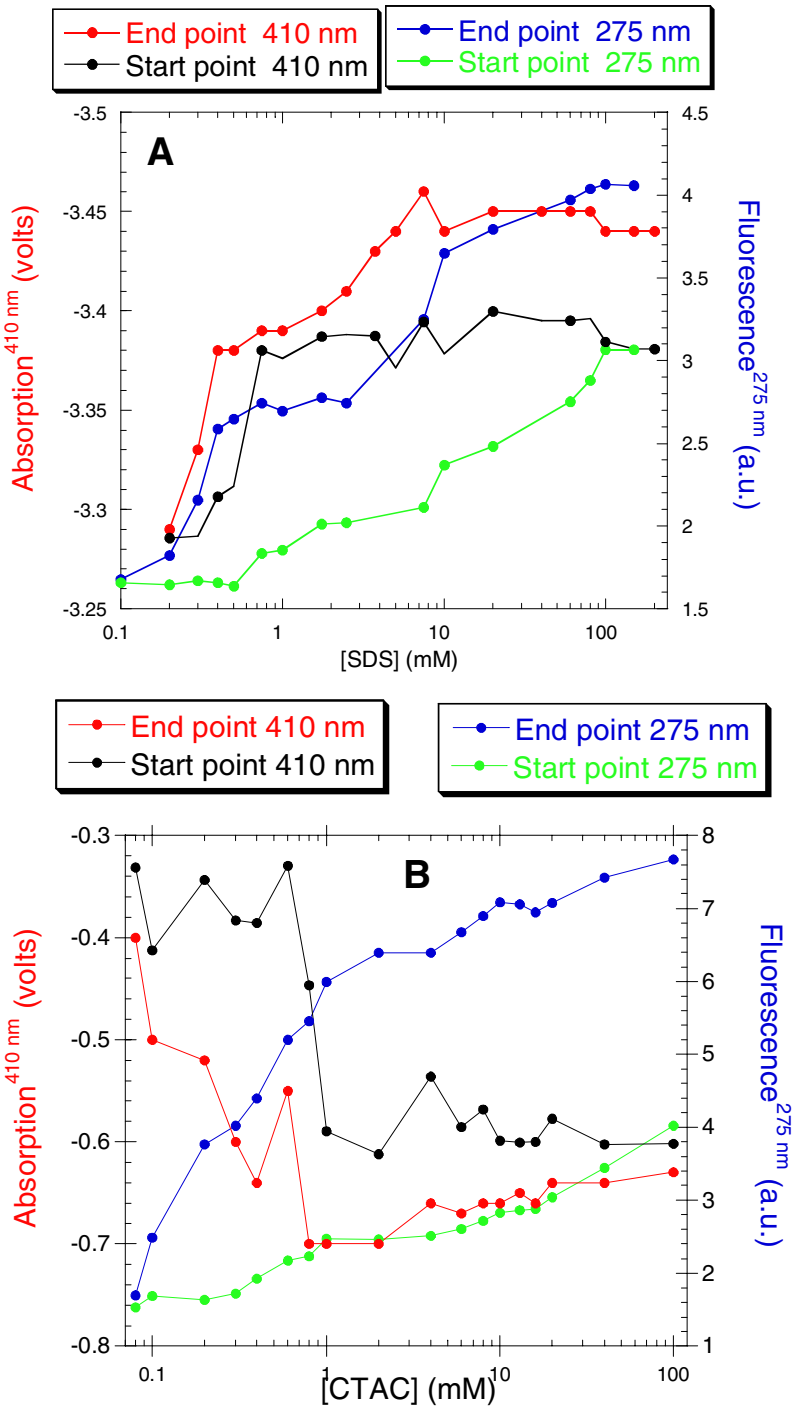

Figure S7.

Start and end absorption (410 nm) and Trp fluorescence (275 nm) values for unfolding of Mb in (A) SDS and (B) CTAC. Start values obtained by extrapolating exponential fits back to time $t = 0$. End point values taken as plateau values of exponential fits.

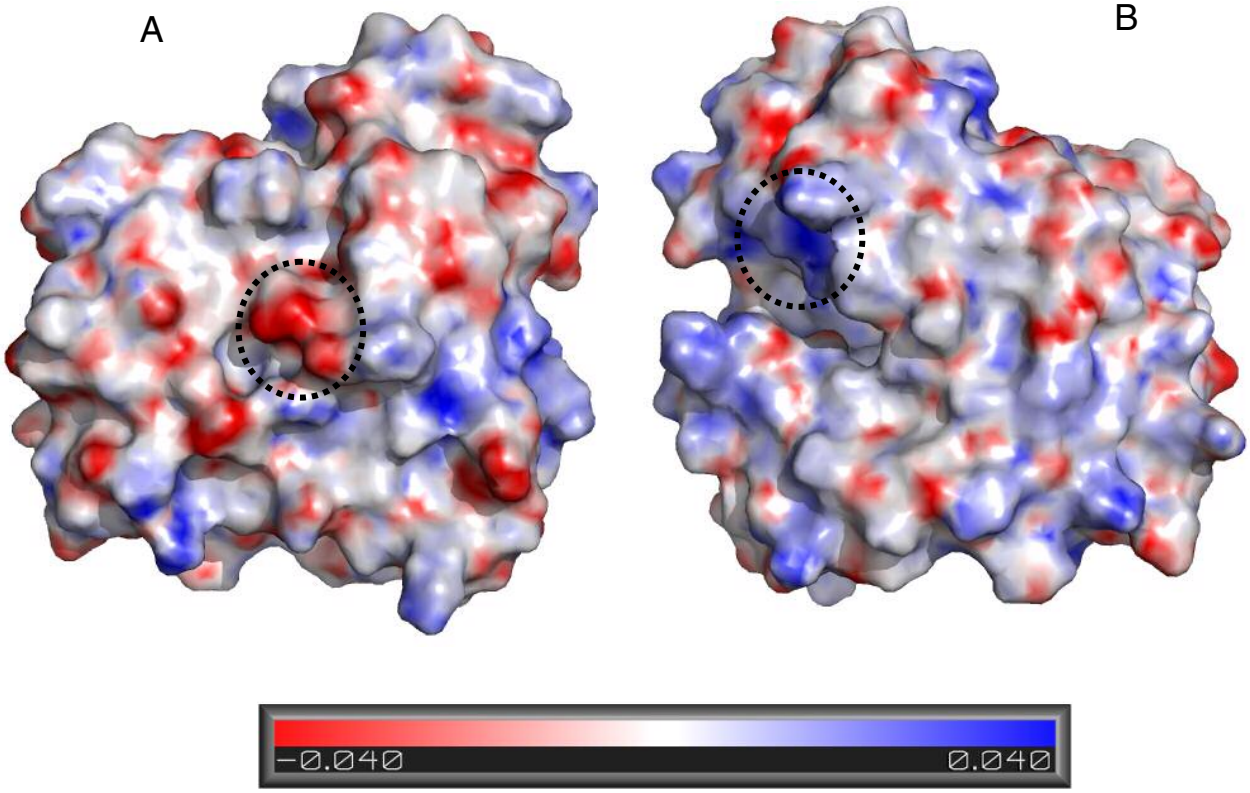

Figure S8. Two views of the electrostatic potential surface of myoglobin calculated using MEAD. Two possible binding patches with particularly high electrostatic potential are highlighted with stippled circles, namely (A) Asp109 and Glu105 and (B) Lys45 and Lys63.

Table S1

Melting temperatures for Mb in the presence of equimolar amounts of SDS but different absolute concentrations. The decline in t_m indicates that SDS does not bind in a strong titratable fashion but rather in a weak saturable fashion.

[Myoglobin] (μM)	[SDS] (μM)	Tm (^{o}C)
20	0	85.70±0.15
10	10	84.17±0.08
20	20	83.05±0.12
30	30	82.06±0.54

Table S2

Kinetic parameters for the fast phase in the binding of SDS to Mb. Parameters obtained by fitting data in Fig. 5A to eq. A.

Parameter	Absorption at 410 nm	Trp fluorescence
k_d (s^{-1})	51.1±2.2	56.8±2.4
K_{SDS} (mM)	0.40±0.12	0.90±0.22
$[SDS]_o$ (mM).	0.21±0.04	0.18±0.06

Paper III

Stable intermediates determine proteins' primary unfolding sites in the presence of surfactants

Stable Intermediates Determine Proteins' Primary Unfolding Sites in the Presence of Surfactants

Jonas Høeg Hansen,[1] Steen Vang Petersen,[2,3*] Kell Kleiner Andersen,[1,2,3] Jan J. Enghild,[2,3] Ture Damhus,[4] Daniel Otzen[1,2,3]

[1] *Department of Life Sciences, Aalborg University, Sohngaardsholmsvej 49, Aalborg DK-9000, Denmark*

[2] *Center for Insoluble Protein Structures (inSPIN), University of Aarhus, Gustav Wieds Vej 10C, Aarhus C DK-8000, Denmark*

[3] *Interdisciplinary Nanoscience Centre (iNANO), Department of Molecular Biology, University of Aarhus, Gustav Wieds Vej 10C, Aarhus C DK-8000, Denmark*

[4] *R&D, Detergent Applications, Novozymes A/S, Bagsvaerd DK-2880, Denmark*

Received 14 October 2008; revised 23 November 2008; accepted 24 November 2008
Published online 15 December 2008 in Wiley InterScience (www.interscience.wiley.com). DOI 10.1002/bip.21125

ABSTRACT:

Despite detailed knowledge of the overall structural changes and stoichiometries of surfactant binding, little is known about which protein regions constitute the preferred sites of attack for initial unfolding. Here we have exposed three proteins to limited proteolysis at anionic (SDS) and cationic (DTAC) surfactant concentrations corresponding to specific conformational transitions, using the surfactant-robust broad-specificity proteases Savinase and Alcalase. Cleavage sites are identified by SDS-PAGE and N-terminal sequencing. We observe well-defined cleavage fragments, which suggest that flexibility is limited to certain regions of the protein. Cleavage sites for α-lactalbumin and myoglobin correspond to regions identified in other studies as partially unfolded at low pH or in the presence of organic solvents. For Tnfn3, which does not form partially folded structures under other conditions, cleavage sites can be rationalized from the structure of the protein's folding transition state and the position of loops in the native state. Nevertheless, they are more sensitive to choice of surfactant and protease, probably reflecting a heterogeneous and fluctuating ensemble of partially unfolded structures. Thus, for proteins accumulating stable intermediates on the folding pathway, surfactants encourage the formation of these states, while the situation is more complex for proteins that do not form these intermediates. © *2008 Wiley Periodicals, Inc. Biopolymers 91: 221–231, 2009.*

Keywords: Savinase; Alcalase; surfactant; flexibility; N-terminal sequencing; unfolding; protein substrates

This article was originally published online as an accepted preprint. The "Published Online" date corresponds to the preprint version. You can request a copy of the preprint by emailing the Biopolymers editorial office at biopolymers@wiley.com

INTRODUCTION

Anionic surfactants such as sodium dodecyl sulfate (SDS) or linear alkylbenzenesulfonates typically denature proteins at low millimolar concentrations, in contrast to the molar amounts required by weakly binding chemical denaturants such as guanidinium chloride or urea. For example, more than 90% of all *E. coli* proteins can be denatured in SDS at low millimolar concentrations.[1] Structural studies of proteins complexed with individual surfactant molecules at sub-denaturation concentrations reveal that the high affinity is achieved by a combination

Correspondence to: Daniel Otzen; e-mail: dao@inano.dk
**Present address:* Institute of Medical Biochemistry, Ole Worms Allé, Aarhus C DK-8000, Denmark.
Contract grant sponsors: Novo Scholarship, Danish Research Foundation (inSPIN), Ministry of Science, Technology and Innovation (Innovation Consortium BioPRO headed by Dr. Torben Madsen).

of electrostatic and hydrophobic interactions, in which the sulfate head and alkyl chain contact Lys/Arg and hydrophobic residues, respectively.[2] Even the individual binding of a small number of surfactant molecules can induce substantial conformational changes, since the surfactant molecules can wedge themselves into the interior of the protein, leading in the case of lysozyme to a wing-like opening.[2] On each protein, there will be a spectrum of binding sites with different affinities. Therefore an increase in the surfactant concentration below the critical micelle concentration (cmc) leads to a number of different binding transitions, which result in protein denaturation and subsequent expansion of the polypeptide chain as micelle-like structures (hemi-micelles) form on the protein.[3,4] Generally speaking, most proteins follow the same sequence of binding events, in which surfactant monomers bind individually at low concentrations, followed by formation of surfactant clusters that grow in size and number as the surfactant concentration increases. However, the exact number of binding events and associated conformational changes will depend on the structure and amino acid composition of the protein in question.[5–7]

In view of this idiosyncratic binding behavior, it is of interest to identify the sites, which first start to become flexible and locally unfolded due to surfactant binding, as they are likely to hold the key to the subsequent denaturation process. These sites cannot be identified by conventional spectroscopic or calorimetric approaches which only focus on the surfactant binding steps and associated conformational changes. Structural analysis of surfactant binding by X-ray crystallography, although hugely informative, will be biased by the inability to accommodate significant flexibility within the existing crystal lattice, and analysis by NMR (which is limited by protein size and usually requires large amounts of isotope-labeled protein samples) will be complicated by the existence of multiple conformations. Hydrogen-deuterium exchange in combination with NMR can provide information on the stabilities of secondary structure elements in the protein under different conditions,[8] but this approach requires prior assignment of all protein residues and an efficient approach to remove surfactant after the completion of the exchange. Furthermore, there may not be a simple correspondence between hydrogen-deuterium exchange and local flexibility in loop areas which lack regular hydrogen-bonding features. Although cyclodextrins rapidly sequester surfactants[9] without the need for dialysis, they may also form complexes with proteins and perturb the NMR signal.[10] To circumvent these complications and provide a rapid and low-tech approach that is independent of the properties of the protein to be examined, we have adopted a simple functional identification assay based on limited proteolysis. For a protein to act as substrate for a protease, it has to possess regions of sufficient flexibility to allow the protease to dock such a region into its binding site where it can form a localized intermolecular β-sheet structure.[11,12] Typically up to 12 residues need to unravel to facilitate this binding.[13] The flexible regions identified in this way generally correspond well to data obtained by other approaches.[14] Its simplicity and low substance requirements has made limited proteolysis the method of choice for identifying domain structures,[15,16] exposed regions of membrane-bound proteins,[17] core regions within amyloid fibrils[18,19] and flexible regions within proteins partially denatured by perturbants such as alcohol, low pH or SDS.[20–22] The ideal protease for these experiments should be as nonspecific as possible to avoid bias towards certain sequences and should also remain active under the conditions inducing substrate flexibility. To satisfy these requirements, we have chosen to use the two subtilisin proteases Alcalase and Savinase. Alcalase is the trade name of the 27 kDa alkaliphilic (pI 8.4) Subtilisin Carlsberg secreted by *B. licheniformis*, which is relatively nonspecific, cleaving after hydrophobic and hydroxyl residues as well as Met, Glu, and Lys.[23] Savinase is a closely related alkaliphilic (pI 10) subtilisin secreted by *B. lentus* which is able to cleave after both hydrophobic and hydrophilic residues.[24] Both enzymes are used in the detergent industry because of their broad substrate specificity and relative robustness toward surfactants.[25] By comparing data from two different proteases, it is easier to rule out artifacts based on partial sequence specificity.

We have chosen to study the effect of limited proteolysis on a number of proteins, whose unfolding in surfactant has already been documented extensively. These are the all-α protein myoglobin,[5,26] the all-β protein Tnfn3[6] and the mixed α/β protein α-lactalbumin (αLA). We find that cleavage sites differ significantly from one protein to another in terms of the secondary structure elements. However, in all cases the cleavage sites are found in regions shown to be flexible in previously identified intermediate or transition states. This suggests that despite their unique combination of electrostatic and hydrophobic binding, surfactants encourage the formation of the same type of partially unfolded state as other denaturing conditions such as low pH or the presence of alcohols or chemical denaturants.

RESULTS AND DISCUSSION

Protease Stability and Activity is Sensitive to Surfactant but the Proteases Remain Active at Several Millimolar Surfactant

To ensure that the proteases remained active during the limited proteolysis conditions, the thermal stabilities of Alcalase and Savinase were determined in the presence of different

surfactant concentrations. Although the melting temperature t_m declines steeply as the SDS concentration is increased, it was possible to obtain a cooperative denaturation transition for both proteases in up to 10 m*M* SDS and 25 m*M* DTAC (Figure 1A) with a low-temperature baseline starting at the same ellipticity value irrespective of surfactant concentration (Figure 1B). Although some intermediate states can also unfold cooperatively,[27] the gradual reduction in melting temperature, combined with retention of significant enzymatic activity (see below), is consistent with the presence of native structure at 20°C. In the absence of surfactant, the initial steep thermal transition gives way to a denatured state plateau baseline, but at higher SDS concentrations the initial thermal transition ends at a lower ellipticity level and the subsequent baseline shows a clear linear increase. This is probably because the SDS, which generally stabilizes nonnative α-helical structure in proteins at sufficiently high surfactant concentrations,[6,28,29] induces a certain level of α-helical structure in the denatured protease (cfr. the effect of SDS on the thermally denatured state of other β-rich proteins such as AIDA[27]), and this structure only melts out slowly as the temperature increases.

The reduction in stability is mirrored by the reduced activity towards the small peptide substrate sAAPF-pNA (Figure 1C). The reduction in activity starts well below the onset of micelle formation (around 3.3 m*M* for SDS and 12.2 m*M* for DTAC in our buffer conditions) and so cannot be explained by a trivial uptake of substrate into micelles and consequent sequestering from the protease. Because the peptide is too small to have any persistent structure, any change in activity is likely to reflect changes to the protease rather than the substrate. *A priori* one would only expect a loss in activity when the melting temperature decreases so much that there is a substantial amount of denatured protein under the conditions of the activity assay (which are conducted at 25°C, well below the melting temperatures measured under most of the surfactant concentrations in Figure 1). The similar dependence of stability and activity on surfactant concentration suggests that the changes leading to a reduction in melting temperature also reflect an increased binding of surfactant, which either directly inhibits the protein by binding to the active site or leads to conformational changes that transmit to the active site.

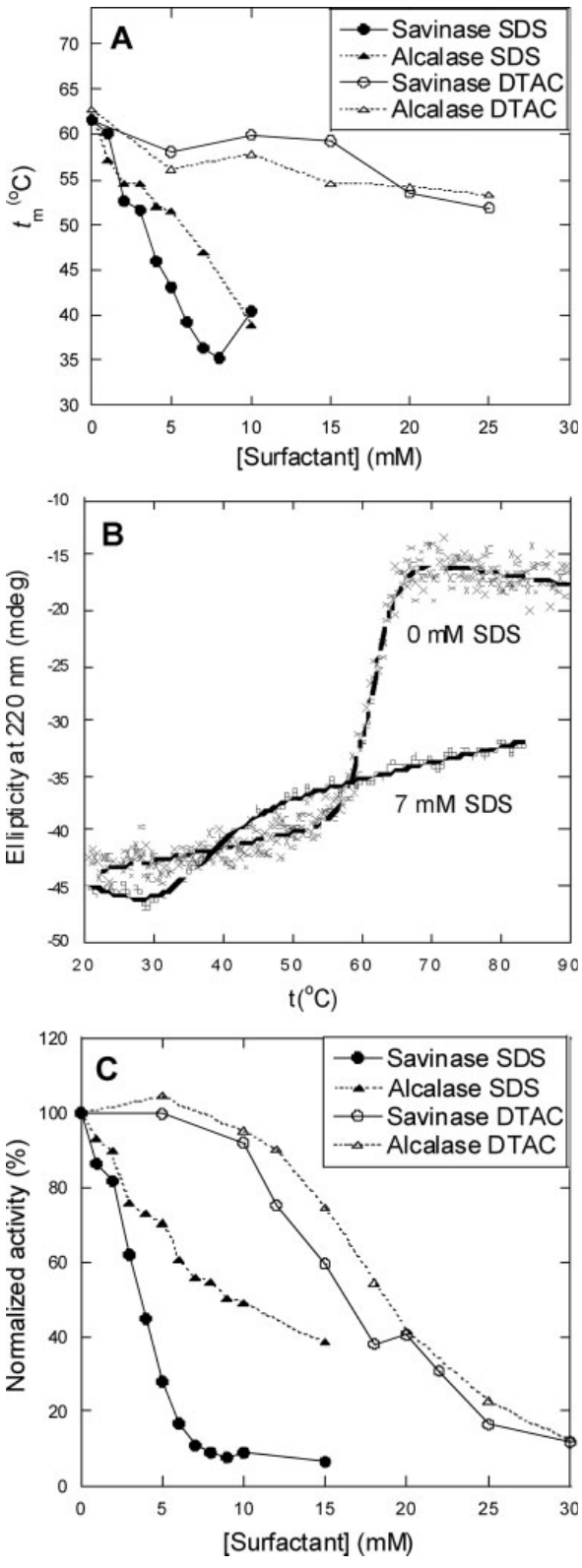

FIGURE 1 (A) Thermal stability of Savinase and Alcalase as a function of surfactant concentration in 20 m*M* Tris pH 7. (B) Thermal scan of Savinase in 0 and 7 m*M* SDS. (C) Activity of Savinase and Alcalase toward the substrate sAAPF-pNA as a function of surfactant concentration.

Table I Overview of the Cleavage Sites of αLA, Myoglobin, and Tnfn3

Protein	Cleavage Sites	2° Structure[a]	Protease[b]	Surfactant	Position in Protein Structure
αLA	S_{34}	Loop	Al	SDS	β-domain
αLA	Q_{39}, E_{49}, F_{53}	St	Sa	SDS	β-domain
αLA	Q_{39}, N_{56}, F_{53}	St	Sa	DTAC, UM,C_7PC	β-domain
Myoglobin	S_{58},H_{93}	He	Sa	SDS	58: between helices D and E 93: helix F
Myoglobin	T_{70},L_{72}	Hm	Sa	DTAC	Middle of helix E
Myoglobin	L_{72},H_{93}	Hm	Al	DTAC	93: helix F
Tnfn3	G_{60}	Lo	Sa	SDS	End of strand E
Tnfn3	K_{39}	Lo	Al	SDS	Between strands C and C′
Tnfn3	K_{11}	Lo	Al	DTAC	Second half of strand A

[a] He, helix end; St, strand; Hm, helix middle; Lo, loop.
[b] Al, Alcalase; Sa, Savinase.

Note that DTAC is much less effective at reducing t_m or activity than SDS. The concentration at which activity has declined to 50% ($C^{50\%}$) can be read from Figure 1C as 3.5 and 8 m*M* SDS for Savinase and Alcalase, respectively, while the corresponding concentrations for in DTAC are 16 and 18 m*M*. This most likely reflects the electrostatics at pH 7, where Lys and Arg are positively charged, leading to electrostatic attraction to SDS and repulsion from DTAC. In agreement with this, increasing the pH to 10 (close to the Lys side chain pK_a of 10.5) makes the protein more resistant to SDS, increasing $C^{50\%}$ to 7.5 and 22 m*M* SDS in Savinase and Alcalase, respectively (data not shown). The higher positive charge of Savinase at neutral pH may also explain its increased susceptibility to SDS compared to Alcalase. Savinase has 13 basic (Lys or Arg) residues and 10 acidic (Asp or Glu) residues; the corresponding numbers for Alcalase are 13 and 14. We therefore conclude that at pH 7, Alcalase retains activity up to at least 10 m*M* SDS and 20 m*M* DTAC, whereas Savinase, though equally active in DTAC, is restricted to the region up to 5 m*M* SDS.

Proteolysis of Proteins in SDS and DTAC Reveals Distinct Cleavage Sites

We now turn to the proteolysis of our model proteins in SDS and DTAC. An initial proteolytic cleavage event will generate two substrate fragments, each of which will be less stable than the parent protein molecule because of a more flexible backbone around the cleavage site, and therefore more susceptible to further unfolding and cleavage. These events, which are not directly relevant for the unfolding of the intact protein, can obscure the initial site of attack. Therefore it is important to be able to identify the very first cleavage fragments. We ensure that this occurs in two ways. First, we use time-based analyses, in which the substrate protein was incubated with protease (substrate in 200–2000-fold excess) and aliquots are removed at appropriate time points and analyzed by gel electrophoresis. Provided that samples are removed at appropriate time intervals and the initial cleavage products are not rapidly degraded, we are likely to identify the initial cleavage event. Second, we can ascertain whether both fragments from the identified cleavage reaction can be seen on the gel, to verify that we observe the result of only one cleavage event. The samples are run on the gel in ca. 3 m*M* SDS under reducing conditions to ensure that cleaved proteins held together by disulfide bonds (of which there are four in αLA but none in myoglobin and Tnfn3) migrate as separate fragments.

The appropriate concentration of surfactant to use for the proteolysis experiment is based on the conformational transitions that the proteins are known to undergo at different surfactant concentrations. All experiments are run with both Savinase and Alcalase, which in all cases except a few (see below) gave rise to the same bands, thus underlining their general usefulness as "generic proteases." We will now discuss the individual proteins in turn. The cleavage data are summarized in Table I and on the structures of the three proteins in the appropriate figures (see later).

Note that the purpose of this study is structural rather than energetic. That is, in order to compare surfactants and other destabilizing conditions in terms of how they affect protein conformation, it is sufficient to identify which part(s) of the proteins become more flexible in the presence of surfactants. We do not intend to determine the actual degree of flexibility and local instability induced by surfactant, as that will depend on specific conditions such as surfactant concentration, temperature etc. and is beyond the scope of the present work. However, these aspects could be

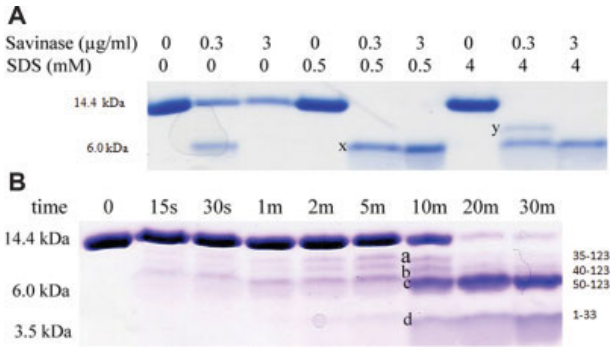

FIGURE 2 (A) Degradation of 0.5 mg/ml αLA after 30 min incubation with 0–3 μg/ml Savinase in 0–4 m*M* SDS at pH 7. Bands x and y were not N-terminally sequenced. (B) Time profile of degradation of 0.5 mg/ml αLA with 0.3 μg/ml Alcalase in 4 m*M* SDS at pH 7. Numbers indicate sequences identified by N-terminal sequences of bands a–d (the C-termini of the fragments are conjectured to be the end of the intact protein, based on the size of the fragment).

addressed in the future using *e.g.* quantitative proteolysis approaches such as developed by Wang and Kallenbach, in which protease-exposed cytochrome *c* was exposed to mildly denaturing conditions which led to the spectroscopically detected denaturation of the cleaved but not intact protein.[30]

α-Lactalbumin

αLA is a mixed α/β protein with a distinct bipartite structure,[31–33] consisting of a contiguous α-domain (residues 1–33 and 85–123) separate from the β-domain (residues 34–57) and a domain predominantly consisting of loops (58–84) In the acid-denatured state, the α-domain remains structured whereas the β-domain becomes very flexible and vulnerable to proteolysis.[34–36] A similar domain distinction is seen for the partially folded states formed in the presence of trifluoroethanol (TFE), oleic acid or when the apo-form of αLA is thermally destabilized.[22]

The 123-residue αLA (αLA) undergoes a two-step loss of structure in SDS: between 0 and 0.5–0.8 m*M* SDS, there is a major change in both tertiary and secondary structure, leading to a marked reduction in organized structure, which gives way to a second transition between 0.5 and 4 m*M* SDS.[37–39] These two steps correspond to the uptake of around 10 and 36 SDS molecules, respectively.[39] We therefore incubated αLA with 0, 0.5, and 4 m*M* SDS and initially focused on the end-product after 30 min of incubation. Because of the inherently flexible nature of αLA, there was already some degradation in the absence of SDS, but the intact state only disappeared completely in the presence of SDS (Figure 2A), leading to cleavage products around 10 and 7 kDa. As the 7 kDa band was seen irrespective of SDS concentrations, whereas the 10 kDa band appeared only at 4 m*M* SDS (and not in the absence of SDS), we carried out a time-series study at 4 m*M* SDS. This identified numerous bands at 7–10 kDa which accumulate in parallel over the first 10 min, indicating parallel rather than consecutive cleavage reactions (Figure 2B). The band around 7 kDa is formed most rapidly, and after 10 min the higher order fragments (particularly the largest fragment) appear to degrade to this band, indicating that this state is the most stable fragment. N-terminal sequencing of the three bands reveals that Alcalase cleaves after S_{34}, Q_{39}, E_{49}, and F_{53} (the latter only to a minor extent), whereas Savinase cleaves after Q_{39}, F_{53}, and N_{56} (minor fragment). The sizes of the bands estimated from the gels suggest that the C-terminus is intact and that no other cleavages occur in these fragments. Thus the two proteases cleave the same region, namely the β-domain (residues 34–57). In all cases except residue 49, the cleaved peptide bonds are located in loops rather than in strands (see Figure 3). The 7 kDa band corresponds to a fragment representing the end of the β-domain to the C-terminus of the intact protein, in other words the fragment where most of the flexible β-domain has been removed. In addition, an approximately ∼4 kDa band with the N-terminus of intact αLA is observed. This fragment corresponds to the N-terminal α-domain (residues 1–33) which is also known to be well-structured in the intact protein. Larger fragments (e.g. 1–57) do not appear as distinct bands but are presumably quickly degraded to the fragment comprising the first 33 residues.

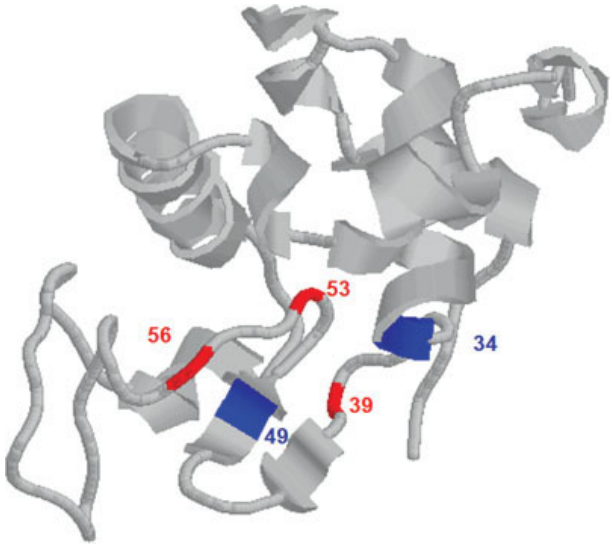

FIGURE 3 Structure of bovine α-lactalbumin (PDB file 1F6S), highlighting SDS cleavage sites in blue (residues 34 and 49) and sites cleaved both in SDS and DTAC in red (39, 53, and 56).

We now turn to the proteolysis of αLA in the cationic surfactant DTAC. The ratio between the fluorescence emission at 330 and 350 nm changes dramatically between 0 and 2 m*M* DTAC, after which it remains constant (Figure 4A), but the actual emission intensity of αLA, which rises steeply up to 2 m*M* DTAC, continues to rise more slowly up to around 16 m*M* DTAC (Figure 4B). We have elsewhere shown by spectroscopy and NMR that this binding is accompanied by loss of organized tertiary structure[39] and therefore corresponds to actual denaturation. This suggests that denaturation occurs in two steps, one between 0 and 2 m*M* DTAC, and the second between 2 and 16 m*M* DTAC. Based on this, we selected 2 and 16 m*M* DTAC for analyses. They show essentially the same degradation pattern (data not shown), indicating that the same regions are flexible at the two different surfactant concentrations. We therefore focus on the lower concentration. A time-series analysis in 2 m*M* DTAC (Figure 4C) reveals a time course, which is very similar to that of SDS, except that the higher molecular weight fragment around 9–10 kDa (band a) accumulates more rapidly than the 7 kDa species (band b) at the very beginning, but is subsequently degraded to the 7 kDa band over time. In addition to the 4 kDa band (band y), there is also a transient accumulation of an intermediate band x around 5 kDa. Thus there are subtle changes in the degradation kinetics, which probably reflect slightly altered binding sites for DTAC in the β-domain where cleavage occurs, but the overall hierarchy of cleavage sites is still observed. N-terminal sequencing identifies Savinase-cleavage sites Q_{39}, F_{53}, and N_{56} (minor), which are identical to those in SDS. Similar cleavage sites are observed in the presence of the zwitterionic surfactant diheptanoyl-phosphocholine and the nonionic surfactant undecyl maltoside (data not shown), which have also been shown to denature αLA according to other spectroscopic techniques.[39]

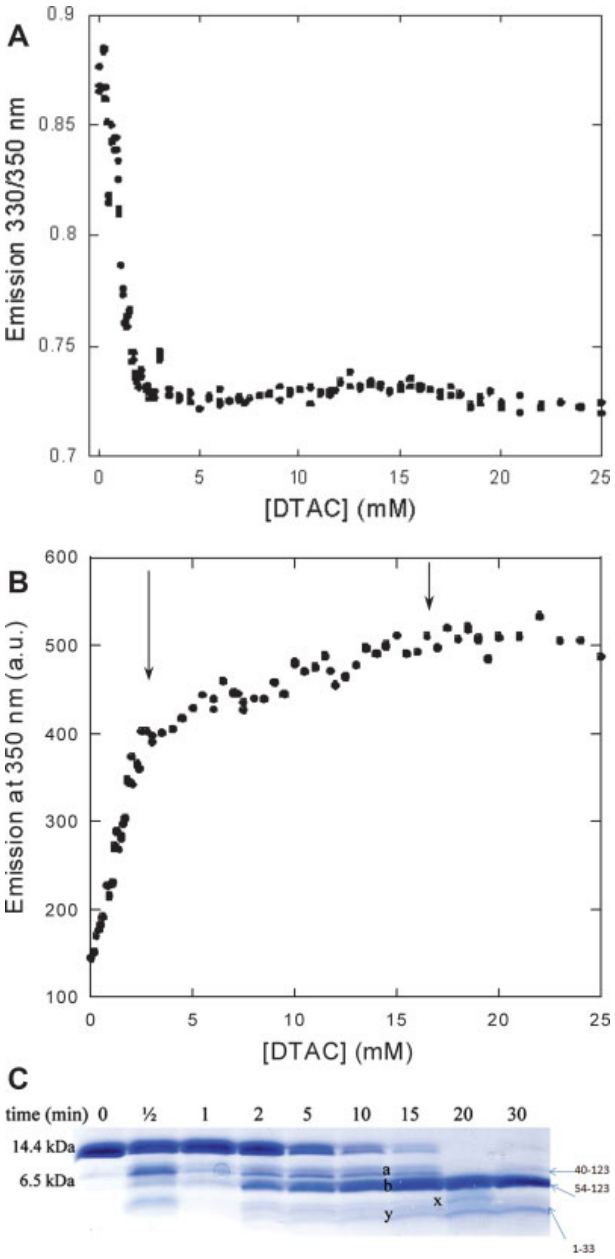

FIGURE 4 Degradation of αLA in DTAC at pH 7. (A) Ratio of fluorescence emission at 330 and 350 nm, highlighting that the shift in emission is completed by the end of the first transition. (B) Titration of αLA with DTAC followed by fluorescence emission at 350 nm. Arrows indicate approximate end of first and second transition. (C) Time profile of degradation of 0.5 mg/ml αLA with 0.3 μg/ml Savinase in 2 m*M* DTAC. Sequences for bands a, b and y indicated (x could not be sequenced). Sequence numbers constructed as in Figure 2.

Myoglobin

The all-helical 153-residue heme-protein myoglobin is known to form partially folded intermediate states both under equilibrium conditions (*e.g.* in the apo-form at pH 4) and during the folding process.[40–42] These states, though formed under different conditions, have a number of features in common, namely a well-structured core formed by helices A, H and G as well as part of helix B. In contrast, the C-D loop, the boundary of the D and E helices, the C-terminal half of the E helix and helix F are much more dynamic and flexible. Myoglobin unfolds in SDS in a very complex series of transitions involving at least six stages.[5] For simplicity, they can be split up into three steps. From 0 to 0.5 m*M* SDS, a small number of SDS molecules bind specifically producing strong exothermic signals, leading to minor conformational changes. From 0.5 to 2 m*M* SDS, 21 SDS molecules bind, leading to clustering on the surface and major changes in Trp

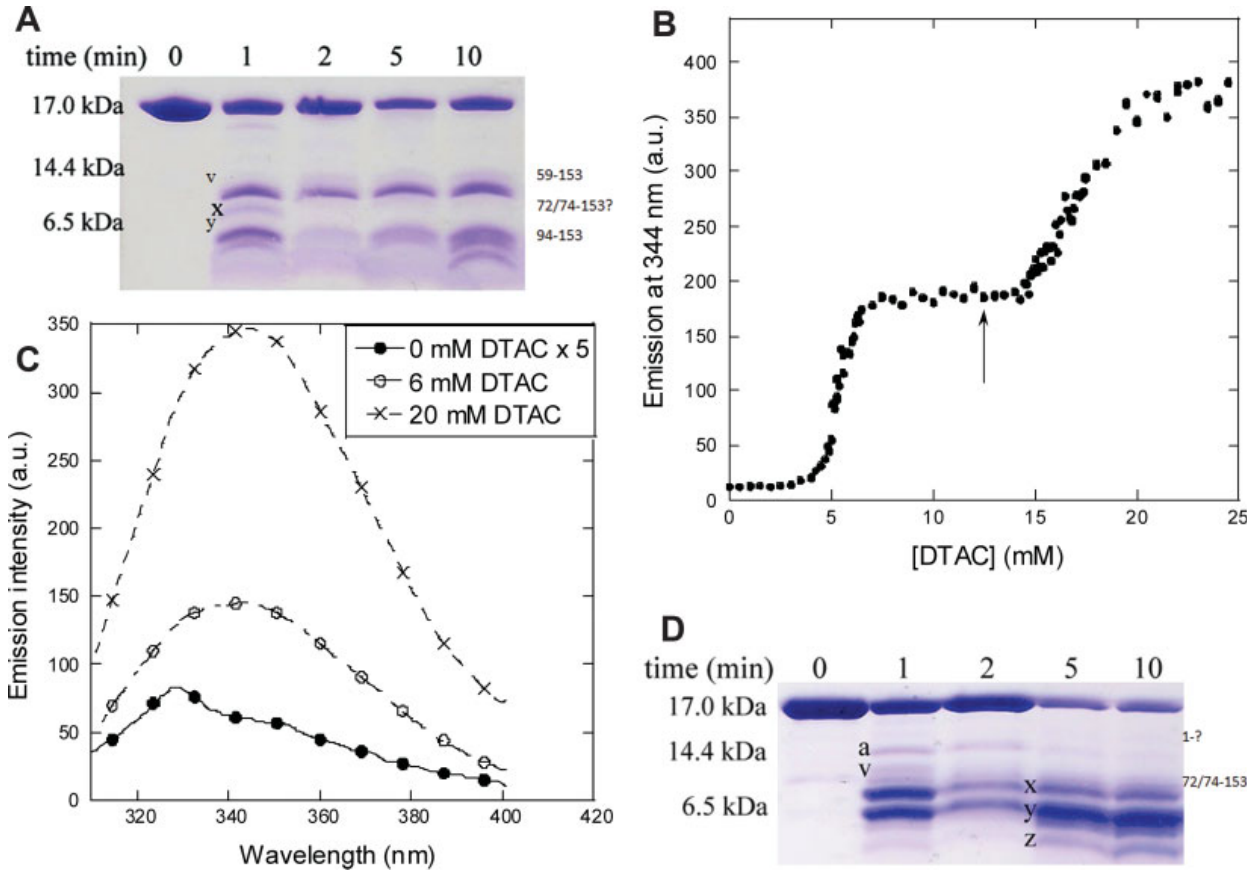

FIGURE 5 Degradation of myoglobin in SDS and DTAC at pH 7. Sequence numbers constructed as in Figure 2. (A) Time profile of degradation of 0.5 mg/ml myoglobin with 0.3 μg/ml Savinase in 0.5 mM SDS. Only bands v and y could be sequenced (band x could not be sequenced, but is assumed to be the same as in panel D). (B) Titration of myoglobin with DTAC, following the fluorescence emission at 334 nm. (C) Emission spectra of myoglobin at different DTAC concentrations. (D) Time profile of degradation of 0.5 mg/ml myoglobin with 0.3 μg/ml Alcalase in 6 mM DTAC. Only band x could be sequenced.

fluorescence. Up to 4 m*M* SDS, an additional ~50 SDS molecules bind, with consequences mainly for the kinetics of unfolding. Therefore we monitored proteolysis of myoglobin at 0.5, 2, and 4 m*M* SDS. Although myoglobin is completely impervious to proteolysis in the absence of surfactants, it is extensively degraded at 0.5 m*M* SDS, and this pattern does not change with increasing SDS concentrations (data not shown). A time course of the degradation (Figure 5A) shows the appearance of two major bands, one around 10 kDa (v), the other around 6 kDa (y), as well as a transient and faint species around 8 kDa (x). This band could not be sequenced, but it corresponds well to a much stronger band seen after proteolysis in DTAC (see later), whose N-terminus is at T_{70} and L_{72} (middle of helix E). Band v has an N-terminus at S_{58} (the loop between helices D and E, shown in Figure 6), while band y starts at H_{93} (inside helix F), matching the gel band masses very well (the complementary fragments, which also have molecular weights around 6 and 10 kDa, were not detected, presumably because they are degraded more extensively). These regions are also known to be flexible in the intermediate state at low pH.[42] At longer time scales, additional fragments appear which are not of interest in this context where we focus on the initial cleavage sites.

In DTAC, we have determined two clear transitions according to Trp fluorescence (Figure 5B), the first one around 4–6 m*M* DTAC, corresponding predominantly to protein unfolding, and the second around 15–20 m*M* due to release of heme.[26] Both are accompanied by an increased red shift of the fluorescence spectrum (Figure 5C). The time-dependent proteolysis in 6 m*M* DTAC leads for both

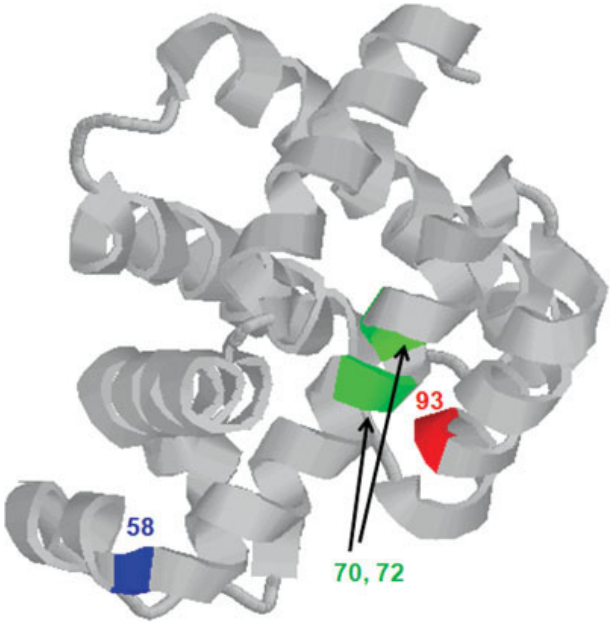

FIGURE 6 Structure of myoglobin (PDB file 1WLA), highlighting SDS cleavage site in blue (residue 58), DTAC cleavage sites in green (residues 70 and 72) and the cleavage site found both in SDS and DTAC in red (residue 93).

proteases to a cleavage pattern that is somewhat different from that in SDS. There is a transient band around 14 kDa (a) with an intact N-terminus, as well as a faint band (v) similar to the somewhat stronger 59–153 band in SDS (but which we could not sequence in DTAC) (Figure 5D). The major band x (only observed faintly marked x in the gel with SDS) is the result of cleavage at after T_{70} and L_{72}, whereas the other one (y) stems from cleavage after H_{93} (helix F) and becomes the major band after several minutes of incubation. A low molecular weight band (z) around 4 kDa is observed in both surfactants. Thus a change from SDS to DTAC leads to a change in the sequence of cleavage events but does not appear to lead to a radical shift in cleavage sites. In all cases, the cleavage sites occur in regions known to be flexible in the intermediate state formed under other conditions.

Tnfn3

Having tested a mixed α/β protein (αLA) and an all-α protein (myoglobin), we finally turn to the 91-residue all-β protein Tnfn3. This protein is interesting in two ways. Firstly, it is rich in β-sheet structure. Essentially all proteins known to be robust against SDS denaturation are all-β proteins.[43] Secondly, it does not accumulate a stable or even a transient folding intermediate[44] under any known conditions. The only partially folded state between the denatured and native

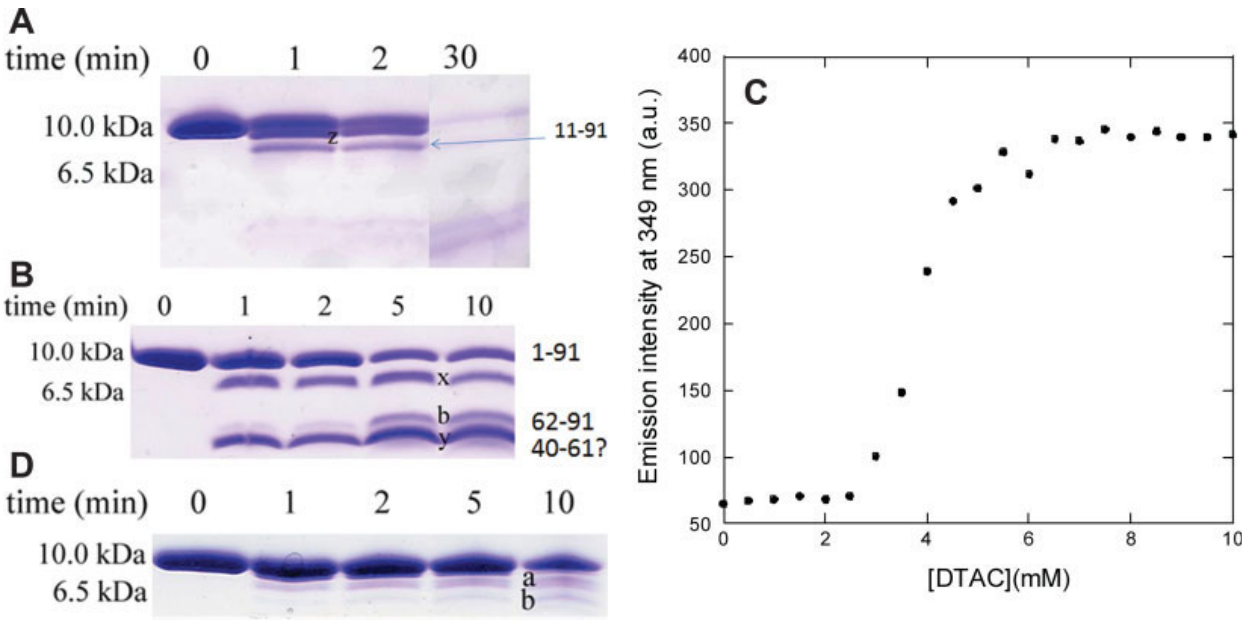

FIGURE 7 Degradation of Tnfn3 in SDS and DTAC. Sequence numbers constructed as in Figure 2. Time profile of degradation of 0.5 mg/ml Tnfn3 with 0.3 μg/ml (A) Alcalase and (B) Savinase in 5 m*M* SDS. Band x could not be sequenced. (C) Titration of Tnfn3 with DTAC, following the fluorescence emission at 349 nm. (D) Time profile of degradation of 0.5 mg/ml Tnfn3 with 0.3 μg/ml Alcalase in 3 m*M* DTAC. Bands a and b could not be sequenced.

state is the very fleeting transition state of folding, whose structure has been elucidated by a combination of computational[45] and experimental[44] approaches. In the transition state, the β-sheet composed of strands C′-C-F-G is significantly ordered; whereas the β-sheet containing strands A-B-E is largely disordered.

Tnfn3 is only unfolded in the presence of micellar amounts of SDS, *i.e.* >4 m*M* SDS, and unfolds several orders of magnitude slower than helix-containing proteins.[6] The protein is robust against both proteases in the absence of surfactant, and only unfolds in 5–8 m*M* SDS, where it gives identical cleavage patterns (data not shown). The time-course of proteolysis in 5 m*M* SDS shows some divergence between the different proteases (Figures 7A and 7B). In Alcalase, hardly any cleavage products are observed before the intact protein band disappears, but in Savinase two major cleavage points are identified based on sequencing of bands b and y, identifying residues 39 (between strands C and C′, which are ordered in the transition state) and 61 (end of strand E, which is largely disordered in the transition state). A band running close to the intact protein cannot be identified by sequencing.

According to fluorescence spectroscopy, Tnfn3 undergoes a simple two-state unfolding with a midpoint around 4 m*M* DTAC (Figure 7C). However, both proteases only give rise to a very modest cleavage in 6 m*M* DTAC. Two major bands close to the full-length protein result from proteolysis in 10 m*M* DTAC (shown for Alcalase in Figure 5D). Both bands have N-termini around residue 11, corresponding to the middle of strand A. The different cleavage sites are shown in Figure 8.

Thus, in Alcalase we witness an all-or-none degradation where very few fragments accumulate before the intact state disappears, whereas Savinase accumulates well-defined species in SDS but not in DTAC. A possible explanation is that Tnfn3 is only partially denatured in surfactant[6] and retains a very compact surfactant-bound state, so that small differences in cleavage specificity and efficiency between the two proteases may determine the efficiency and extent of degradation. Nevertheless, the cleavage sites are not unlikely sites of attack. The protein is either cleaved in a loop (a structural element which can be expected to become more flexible if the protein expands slightly in general upon surfactant binding) or in two strands (A and E) identified as flexible in the transition state.

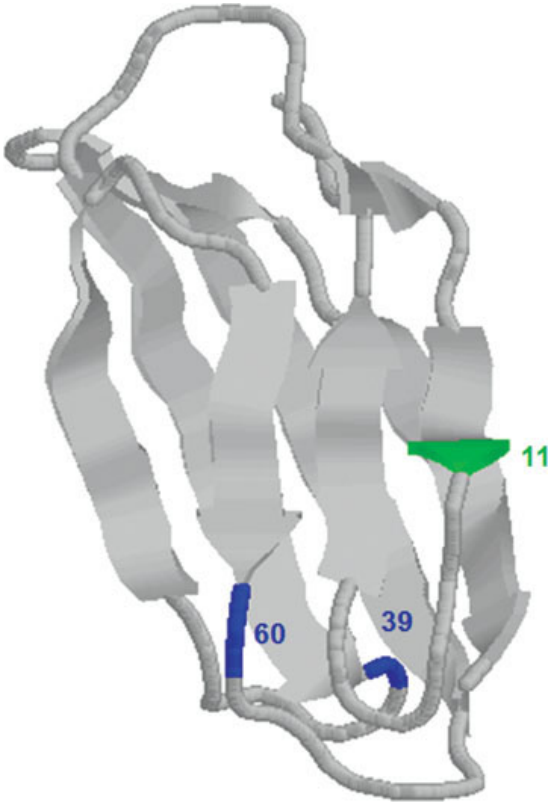

FIGURE 8 Structure of Tnfn3 (PDB file 1TEN), highlighting SDS cleavage sites in blue (residues 39 and 60) and DTAC cleavage site in green (residue 11).

CONCLUSION

The purpose of this study was to use limited protease digestion to identify initial binding sites for surfactants, based on the increased flexibility induced by surfactants. Cleavages occur in regions corresponding to many different elements of structure in the native state, namely both loops, helices and strands, and the sites overlap between SDS and DTAC despite their opposite charges and consequently different binding preferences. However, all this apparent variation can be reconciled in a very simple manner: For the two proteins which form stable intermediates, namely αLA and myoglobin, the cleavage sites identify regions which are known to be unstructured under other partially denaturing conditions, *e.g.* low pH, organic solvents or in the thermally destabilized apo-form. There are subtle differences between the results from SDS and DTAC in terms of the sequence of cleavage events, but overall they confirm that surfactants merely encourage the intrinsic propensity of certain regions of the protein to unfold, rather than stabilizing a non-native state substantially different from that formed under other denaturing conditions. For αLA we also see parallel formation of several fragments formed by cleavage within the same flexible region, implying multiple sites of initial attack followed by whittling down to the minimal structured species. The initial sites of binding of SDS and DTAC at low sub-micellar concentrations are expected to differ because of their opposite

charges, but they must represent specific ligand binding events, which does not lead to significant structural changes in the protein and consequent increased sensitivity to proteolysis. The conformational changes that occur at higher concentrations of surfactant clearly converge to the same flexible state for the two surfactant types.

Thus the situation is very straightforward for proteins that form stable intermediates. The situation is somewhat different for the all-β protein Tnfn3 which does not populate a partially folded state under known conditions. This makes it difficult to predict which areas of the protein are most likely to become flexible. In accordance with this, it is not possible to draw any general conclusions from our cleavage data. Although the available structure of the transition state makes it possible to rationalize two of the three cleavage sites, the cleavage patterns differ from one protease to the other in SDS, and there is very little cleavage in DTAC, only around the N-terminal β-strand. Our interpretation of these data is that in the absence of a predetermined stable intermediate, the ensemble of partially unfolded structures available to Tnfn3 is heterogeneous and in rapid equilibrium, so that changes in terms of the nature of the surfactant and the protease can skew the population in different directions, leading to different cleavage patterns. This opens up for the possibility of the judicious use of surfactants to accumulate a wide array of different protein conformations for this class of proteins in order to shed more light on the remarkable conformational diversity of proteins.

MATERIALS AND METHODS

Materials

All surfactants as well as horse myoglobin and bovine αLA were from Sigma Aldrich (St. Louis, MO). Recombinant Tnfn3 was purified as described[46] using an expression vector generously donated by Dr. J. Clarke. Alcalase and Savinase were commercial products provided by Novozymes A/S. Protease concentration in these products is determined by activity measurements, calibrating with known concentrations (communication by Novozymes A/S).

Determination of the cmc Value Using Pyrene

In the presence of micelles, pyrene undergoes a shift in the emission intensity at 383.5 nm (I_3) and 372.5 nm (I_1) upon excitation at 335 nm, allowing us to use the I_3/I_1 ratio to measure the cmc value.[47] Pyrene was added to a final concentration of 0.2 μM from a 20 μM stock solution in ethanol. The solution was excited at 335 nm and the emission between 350 and 440 nm was monitored. Each measurement was recorded as an average of three emission scans in a 10 mm quartz cuvette (Helma) on a LS-55 Luminescence spectrometer (Perkin Elmer instruments, UK). The cmc values in 20 mM Tris pH 7 were determined to be 3.3 mM for SDS and 12.2 mM for DTAC.

Protease Activity Toward sAAPFpNA

The activity of Alcalase and Savinase toward the substrate Suc-Ala-Ala-Pro-Phe-*p*-nitroanilide (sAAPFpNA) was measured at 25°C. Proteolytic release of the pNA group leads to increased absorbance at 410 nm. Reactions were performed in a volume of 1 ml, containing various concentrations of SDS or DTAC, 2 mM substrate [from a 40 mM stock in dimethylsulfoxide (DMSO)], 20 mM Tris-HCl pH 7 and 10–100 nM protease. The absorbance at 410 nm was recorded over 3 min using a Lambda 2 UV/VIS spectrometer (Perkin Elmer instruments, UK). The relative activity is given in katal/mol of enzyme added, where one katal equals 1 mol pNA released per second. The activity was calculated using a molar extinction coefficient of 8489 M^{-1} cm^{-1}. $C^{50\%}$ denotes the surfactant concentration where 50% of the protease activity is lost.

Thermal Stability of Savinase and Alcalase Measured by Far-UV CD Measurements

All far-UV CD wavelength and temperature scans were recorded using a JASCO J-810 spectropolarimeter (Jasco Spectroscopic Co. Ltd., Japan) in a quartz cuvette (Helma) with a path length of 1 mm using 12 μM protease in 20 mM Tris buffer (pH 7). Wavelength scans were an average of six accumulations from 200 nm to 250 nm, recorded at 20°C using a scan speed of 50 nm/min and a bandwidth of 1. Temperature scans were recorded at 218 nm with a temperature slope of 60°C/h from 20 to 90°C. The contribution of buffer and surfactants were subtracted as a blank. The midpoint of denaturation was determined as described.[48]

Trp Fluorescence Studies of the Interaction Between Proteins and Surfactants

A final concentration of 5 μM protein was mixed in 20 mM Tris-Cl pH 7 with 0–25 mM surfactant, left to equilibrate for at least 45 min and an emission spectrum between 310 and 400 nm was recorded with an excitation of 295 nm. Measurements were performed as duplicates using a slit width of 7 nm and a scan speed of 250 nm/min. All experiments were recorded using a 10 mm quartz cuvette (Hellma). Background surfactant contributions were subtracted.

Limited Proteolysis

These were performed at 20°C in 20 mM Tris-Cl pH 7. 0.5 mg/ml protein substrate was mixed with various concentrations of surfactants. αLA is supplied by the manufacturer with ca. 35% bound Ca^{2+}. To ensure a homogeneous population, hydrolysis of αLA was therefore carried in 5 mM EDTA to remove the bound Ca^{2+} ions. After equilibrating for 15 min to reach a state of conformational equilibrium (1 h for the more slowly unfolding protein Tnfn3), Savinase or Alcalase was added to final concentrations of 0, 0.3, and 3 μg/ml (11 and 110 nM). At appropriate time points, the reaction was stopped by adding phenylmethanesulfonyl fluoride (PMSF) to 1 mM from a 20 mM stock solution in ethanol.

Gel Electrophoresis

The peptide fragments were separated by Tris/tricine SDS-PAGE gel electrophoresis according to Schägger and von Jagow[49] with the

slight modification that the separation gel was made by using 16% w/v acrylamide and 0.84% bisacrylamide, 10% glycerol, 0.1% w/v SDS, and 1*M* Tris-Cl pH 8.45. On top of the separation gel, a 1 cm spacer gel composed of 11% acrylamide gel without glycerol was polymerized followed by the stacking gel composed of 0.75*M* Tris-Cl pH 8.45, 4% acrylamide, and 0.1% bis acrylamide. For analysis of cleavage reactions, 15 μl (7.5 μg protein) from each digest was mixed with 5 μl 4X Tricine sample buffer (200 m*M* Tris-Cl pH 6.8, 1.6% w/v SDS, 50% v/v glycerol, 62 mg/ml DTT, and 0.4 mg/ml Coomassie Blue), heated to 95°C for 10 min, and applied to the gel. Protein MW markers with the range 2.5–200 kDa (Mark 12, Invitrogen), 1.8–23 (Polypeptide SDS-Page Molecular Weight Standards, Bio-Rad) and 10–200 kDa (#SM0661, Fermentas) were used. The separation was performed for 105 min at 140 V. The gel was stained for 45 min in a solution containing 50% v/v ethanol, 7% v/v acetic acid, and 0.2% w/v Coomassie Brilliant Blue G-250 in milli Q water, subsequently destained overnight in 40% v/v ethanol and 10% v/v acetic acid and washed in milli Q water.

N-Terminal Sequencing

The digested samples were mixed with sample buffer and heated to 95°C, separated by Tris/tricine gel electrophoresis[49] and electroblotted to a PVDF membrane using Towbin buffer (25 m*M* Tris, 192 mM glycine, 20% methanol, pH 8.3) containing 0.01% SDS. Bands were visualized by Coomassie Brilliant Blue staining, excised and analysed by automated Edman degradation using a Procise 494HT amino acid sequencer (Applied Biosystems) with on-line phenylthiohydantoin analysis.

REFERENCES

1. Xia, K.; Manning, M.; Hesham, H.; Lin, Q.; Bystroff, C.; Colón, W. Proc Natl Acad Sci USA 2007, 104, 17329–17334.
2. Yonath, A.; Podjarny, A.; Honig, B.; Sielecki, A.; Traub, W. Biochemistry 1977, 16, 1418–1424.
3. Tanford, C. The hydrophobic effect. Formation of Micelles and Biological Membranes; Wiley: New York, 1980.
4. Ibel, K.; May, R. P.; Kirschner, K.; Szadkowski, H.; Mascher, E.; Lundahl, P. Eur J Biochem 1990, 190, 311–318.
5. Andersen, K.; Westh, P.; Otzen, D. E. Langmuir 2008, 15, 399–407.
6. Nielsen, M. M.; Andersen, K. K.; Westh, P.; Otzen, D. E. Biophys J 2007, 92, 3674–3685.
7. Nielsen, A. D.; Arleth, L.; Westh, P. Biochim Biophys Acta 2005, 1752, 124–132.
8. Clarke, J.; Itzhaki, L. S. Curr Opin Struct Biol 1998, 8, 112–118.
9. Otzen, D. E.; Oliveberg, M. J Mol Biol 2001, 313, 479–483.
10. Aachmann, F. L.; Otzen, D. E.; Larsen, K. L.; Wimmer, R. Prot Eng 2003, 16, 1–8.
11. Schechter, I.; Berger, A. Biochem Biophys Res Comm 1967, 27, 157–162.
12. Branden, C. I.; Tooze, J. Introduction to Protein Structure; Garland: New York, 1999.
13. Hubbard, S. J. Biochim Biophys Acta 1998, 1382, 191–206.
14. Fontana, A.; De Laureto, P. P.; Spolaore, B.; Frare, E.; Picotti, P.; Zambonin, M. Acta Biochim Pol 2004, 51, 299–321.
15. Zhang, F.; Kartner, N.; Lukacs, G. L. Nat Struct Biol 1998, 5, 180–183.
16. Zaltash, S.; Johansson, J. FEBS Lett 1998, 423, 1–4.
17. Mogensen, J. E.; Ferreras, M.; Petersen, S. V.; Enghild, J. J.; Otzen, D. E. Biochemistry 2007, 46, 3356–3365.
18. Frare, E.; Mossuto, M. F.; De Laureto, P. P.; Dumoulin, M.; Dobson, C. M.; Fontana, A. J Mol Biol 2006, 3651, 551–561.
19. Kheterpal, I.; Williams, A. D.; Murphy, C.; Bledsoe, B.; Wetzel, R. Biochemistry 2001, 40, 11757–11767.
20. Horowitz, P. M.; Xu, R. F. J Biol Chem 1992, 267, 19464–19469.
21. De Laureto, P. P.; Tosatto, L.; Frare, E.; Marin, O.; Uversky, V. N.; Fontana, A. Biochemistry 2006, 45, 11523–11531.
22. De Laureto, P. P.; Frare, E.; Gittardo, R.; Fontana, A. Proteins: Struct Funct Genet 2002, 49, 385–397.
23. Doucet, D.; Otter, D. E.; Gauthier, S. F.; Foegeding, E. A. J Agr Food Chem 2003, 53, 6300–6308.
24. Georgieva, D. N.; Stoeva, S.; Voelter, W.; Genov, N.; Betzel, C. Arch Biochem Biophys 2001, 387, 197–201.
25. Maurer, K. H. Curr Opin Biotechnol 2004, 15, 330–334.
26. Tofani, L.; Feis, A.; Snoke, R. E.; Berti, D.; Baglioni, P.; Smulevich, G. Biophys J 2004, 87, 1186–1195.
27. Mogensen, J. E.; Tapadar, D.; Schmidt, M. A.; Otzen, D. E. Biochemistry 2005, 44, 4533–4545.
28. Jirgensons, B. Arch Biochem Biophys 1961, 94, 59–67.
29. Parker, W.; Song, P. S. Biophys J 1992, 61, 1435–1439.
30. Wang, L.; Kallenbach, N. R. Protein Sci 1998, 7, 2460–2464.
31. Peng, Z. Y.; Kim, P. S. Biochemistry 1994, 33, 2136–2141.
32. Wu, L. C.; Peng, Z. Y.; Kim, P. S. Nat Struct Biol 1995, 2, 281–286.
33. Schulman, B. A.; Kim, P. S.; Dobson, C. M.; Redfield, C. Nat Struct Biol 1997, 4, 630–634.
34. Alexandrescu, A. T.; Evans, P. A.; Pitkeathly, M.; Baum, J.; Dobson, C. M. Biochemistry 1993, 32, 1707–1718.
35. Chyan, C. L.; Wormald, C.; Dobson, C. M.; Evans, P. A.; Baum, J. Biochemistry 1993, 32, 5681–5691.
36. Shimizu, A.; Ikeguchi, M.; Sugai, S. Biochemistry 1993, 32, 13198–13203.
37. Hamada, S.; Takeda, K. J Prot Chem 1993, 12, 477–482.
38. Gudiksen, K. L.; Gitlin, I.; Whitesides, G. M. Proc Natl Acad Sci USA 2006, 103, 7968–7972.
39. Otzen, D. E.; Sehgal, P.; Westh, P. J Colloid Interface Sci 2009, 329, 273–283.
40. Jennings, P. A.; Wright, P. E. Science 1993, 262, 892–896.
41. Hughson, F. M.; Wright, P. E.; Baldwin, R. L. Science 1990, 249, 1544–1548.
42. Eliezer, D.; Yao, J.; Dyson, H. J.; Wright, P. E. Nat Struct Biol 1998, 5, 148–155.
43. Manning, M.; Colón, W. Biochemistry 2004, 43, 11248–11254.
44. Geierhaas, C. D.; Paci, E.; Vendruscolo, M.; Clarke, J. J Mol Biol 2004, 343, 1111–1123.
45. Paci, E.; Clarke, J.; Steward, A.; Vendruscolo, M.; Karplus, M. Proc Natl Acad Sci USA 2003, 100, 394–399.
46. Clarke, J.; Hamill, S. J.; Johnson, C. M. J Mol Biol 1997, 270, 771–778.
47. Kalyanasundaram, K.; Thomas, J. K. J Am Chem Soc 1977, 99, 2039–2044.
48. Mogensen, J. E.; Ibsen, H.; Lund, J.; Otzen, D. E. Biochemistry 2004, 43, 3357–3367.
49. Schägger, H.; von Jagow, G. Anal Biochem 1987, 166, 368–379.

Reviewing Editor: Stephen Blacklow

Paper IV

The role of decorated SDS micelles in sub-cmc protein denaturation and association

The role of decorated SDS micelles in sub-cmc protein denaturation and association

Andersen K.K.[1,2], Oliveira, C.L.P.[3], Larsen, K.L.[2], Poulsen, F.M.[4], Callisen, T.H.[5], Westh P.[6], Pedersen, J.S.[6], Otzen D.E.[1*].

[1] Interdisciplinary Nanoscience Centre, University of Aarhus, Gustav Wieds Vej 10C, DK – 8000 Aarhus C.
[2] Department of Life Sciences, Aalborg University, Sohngaardsholmsvej 49, DK-9000 Aalborg, Denmark
[3] Department of Chemistry, iNANO Interdisciplinary Nanoscience Center and Centre for mRNP Biogenesis and Metabolism, University of Aarhus, Langelandsgade 140, DK – 8000 Aarhus C.
[4]Structural Biology and NMR Laboratory, Department of Molecular Biology, University of Copenhagen, DK-2200, Copenhagen, Denmark
[5]Novozymes A/S, DK – 2880 Bagsværd, Denmark
[6] NSM Functional Biomaterials, Roskilde University, P.O. Box 260, DK-4000 Roskilde, Denmark

*To whom correspondence should be addressed. Telephone + 45 89 42 50 46, fax + 45 98 12 31 78, e-mail dao@inano.dk

Resubmitted to Journal of Molecular Biology

ABSTRACT

We have combined spectroscopy, chromatography, calorimetry and small-angle X-ray scattering (SAXS) to provide a comprehensive structural and stoichiometric description of the SDS-induced denaturation of the 86-residue α-helical bovine Acyl-coenzyme A-binding protein (ACBP). Denaturation is a multi-step process. Initial weak binding of 1-3 SDS molecules per protein molecule below 1.3 mM does not perturb the tertiary structure. Subsequent binding of ~13 SDS molecules per ACBP molecule leads to the formation of SDS aggregates on the protein and changes in both tertiary and secondary structure. SAXS data show that at this stage a decorated micelle links two ACBP molecules together, leaving about half of the polypeptide chain as a disordered region protruding into the solvent. Further titration with SDS leads to the additional uptake of 26 SDS molecules which according to SAXS forms a larger decorated micelle bound to a single ACBP molecule. At the critical micelle concentration (cmc), we conclude from a reduced tumbling and increased fluorescence anisotropy that each ACBP molecule becomes associated with more than one micelle. At this point 56-60 SDS molecules are bound per ACBP molecule. Our data provide key structural insights into decorated micelle complexes with proteins, revealing a remarkable diversity in the different conformations they can stabilize. The data highlight that a minimum decorated micelle size exists, which may be a key driving force for intermolecular protein association. This may also provide a structural basis for the known ability of submicellar surfactant concentrations to induce protein aggregation and fibrillation.

Keywords: ACBP, surfactant, isothermal titration calorimetry, Small Angle X-ray Scattering, dimerization

INTRODUCTION

Protein-surfactant interactions have both fundamental and applied interest. They play a significant role in food industry, pharmaceutical industry and not least in the fabric and homecare detergent industry. Enzymes such as proteases, amylases, lipases and cellulases are typically present in many detergency formulations [1; 2]. Furthermore, protein-surfactant interactions reveal new facets about the types of conformational changes that proteins may undergo in response to changing environment. While both nonionic and ionic surfactants can increase the activity of lipases [3; 4], ionic surfactants generally denature proteins at low concentrations through a combination of ionic and hydrophobic interactions [5; 6]. The classical model of protein denaturation by SDS is based on Tanford's pioneering work [7] and confirmed by more recent reports [8]. In this model, individual SDS molecules at low surfactant concentrations first bind to a number of high-affinity sites accompanied by a limited degree of structural change, followed by a plateau in the binding isotherm before a massive uptake of SDS occurs in a cooperative step. However, many details of the binding and accompanying structural changes remain to be elucidated. This particularly relates to the coupling between protein structure and susceptibility to SDS. Generally, SDS resistance cannot be linked to primary structure [9] or thermodynamic stability [10], but appears to be more strongly correlated with rigidity and lack of "breathing". This is particularly found in proteins rich in β-sheet structure, often in combination with oligomeric

assemblies, possibly due to the elaborate network of global hydrogen bonding between β-strands. In contrast, the predominance of local interactions stabilizing α-helical structure allows SDS micelles to solubilize individual α-helices and thus unravel the tertiary structure of an α-helical protein while keeping the secondary structure more or less intact. In support of this, our previous studies suggest that proteins containing mixed α/β structure such as S6 [11] and α-lactalbumin [12] are more susceptible to denaturation than proteins consisting of all-β secondary structure [13], which also unfold significantly more slowly [9; 14]. All α-helix proteins unfold readily in SDS but the mechanistic details can vary significantly. Our study of the interactions between SDS and the 7-helix heme protein myoglobin revealed multistep denaturation [15], considerably more complex than the behavior of the archetypal surfactant-binding protein BSA [16; 17].

In addition to providing new insight into protein conformational changes at the level of the individual molecule, surfactants may also provide more insight into the driving forces behind protein aggregation. While surfactant micelles show strong dispersive or solubilizing abilities, sub-micellar concentrations of SDS show a remarkable propensity to stimulate protein aggregation. This is particularly pronounced at low pH where aggregation appears to lead to amorphous precipitates [18], but also occurs at neutral pH, leading to orderly or fibrillar aggregate structures for proteins as diverse as Aβ [19], β_2-microglobulin [20], S6 [18] and lysozyme [21]. The increased aggregation propensity is undoubtedly related to the ability of SDS to stabilize aggregation-prone structures which represent species at the very early stage of the aggregation process. As such, the mechanism by which surfactants stimulate aggregation may provide important information about aggregation pathways in biological contexts. However, the details of how surfactant and protein cooperate to facilitate this process remain obscure.

The present study is devoted to the interactions of SDS with a simple α-helix protein containing no cofactor, namely the 86-residue 4-helix bundle bovine Acyl-coenzyme A-binding protein (ACBP). ACBP has several properties, which make it interesting in protein-surfactant studies: its unfolding behaviour in denaturants under equilibrium and kinetic conditions has been well characterized [22; 23; 24], and it has a binding site for amphiphilic ligands with K_d values for C_{14}-C_{22} acyl-CoA around 2-10 nM [25] which might provide sites for initial SDS binding. In the present study, we combine a number of complementary techniques which uncover both molecular, mesoscopic, thermodynamic and stoichiometric information, to piece together the details of the different binding steps involved in SDS-denaturation of ACBP. Our work also provides low-resolution structural information on SDS-protein complexes, which we term decorated micelles, including a species in which two protein molecules are bridged by a cluster of SDS molecules. This sheds new light on the role that SDS may play in promoting protein-protein interactions.

RESULTS

ACBP unfolding in SDS proceeds through several transitions according to spectroscopy and capillary electrophoresis

Our aim is to provide as complete a description as possible of the multiple structural transitions that ACBP undergoes in the presence of SDS. We start with conventional fluorescence spectroscopy, since the intensity *I* and peak position of the emission spectrum (λ_{max}) can be very informative about the Trp side chain environment. Two closely spaced tryptophans (Trp55 and Trp58) are present in the primary sequence of ACBP. Upon titration of ACBP with SDS at pH 8, profound changes are observed in both *I* and λ_{max} (Fig. 1A). No apparent change in fluorescence intensity or λ_{max} is observed in the concentration range 0 ~ 1 mM SDS. Between 1 and 3

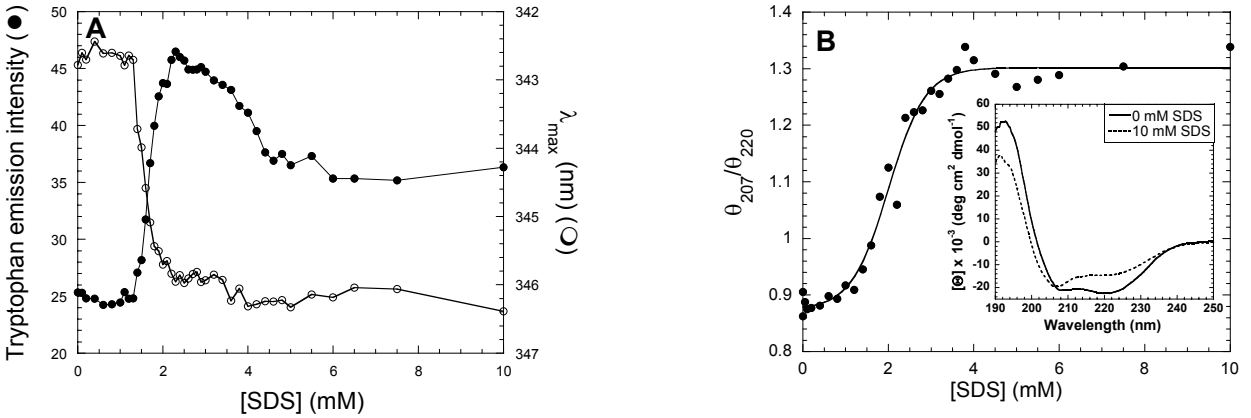

Figure 1. ACBP denaturation follow by tryptophan fluorescence and far-UV CD. (A) Tryptophan fluorescence intensity and λ_{max} are unaffected in the SDS concentration range 0~1mM SDS, followed by increased fluorescence intensity and a blue shift in lambda max (transition 1). Transition 2 is observed between 3 and 5 mM SDS characterized by fluorescence decrease with only little change in λ_{max}. (B) Far-UV circular dichroism data, plotted as the ratio between ellipticity at 207 nm and 220 nm, report on secondary change in transition 1 while transition 2 cannot be detected. Insert: Far-UV CD spectra of ACBP in 0 and 10 mM SDS.

mM there is an increase in *I* and λ_{max} blueshifts, while further titration to 5 mM SDS resulted in a decrease in fluorescence with only a little change in λ_{max}. No significant change in fluorescence is observed above the cmc (~5 mM, see below). The baseline region (0~1 mM) prior to the first transition shrinks with decreasing pH down to pH 4 (data not shown). In part this reflects an increased affinity of SDS at lower pH due to increased protonation of anionic side-chains [11]; a reduction in protein stability is less likely as ACBP remains stably folded until pH 3.5 [26]. Far-UV CD spectra at pH 8 show that both native and SDS-denatured ACBP possess a high degree of α-helix secondary structure as indicated by the two minima at 207 and 220 nm (Fig. 1B). Using the ratio of these two wavelengths, we only observe one transition, which corresponds to the change in fluorescence emission intensity and λ_{max} between 1 and 3 mM. Thus the 1-3 mM transition shows joint changes in secondary and tertiary structure, whereas the 3-5 mM transition is restricted to changes in the aromatic environment.

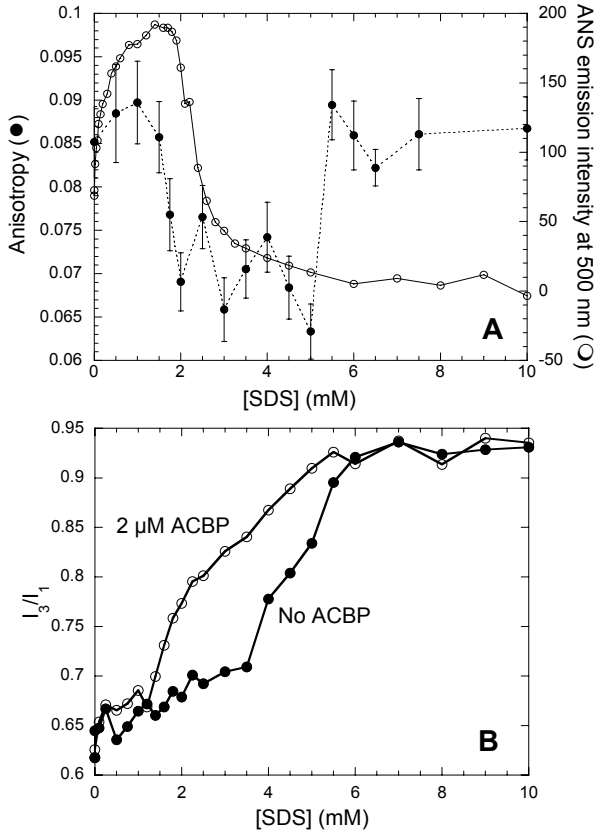

Figure 2. (A) Tumbling of ACBP in SDS as shown by fluorescence anisotropy (left y-axis) and ANS fluorescence vs. SDS concentration (right y-axis). The tumbling of ACBP is described in three states. Native-structured in the interval 0 to 1 mM SDS, followed by a decrease in anisotropy, indicating a less ordered and denatured structure in the range 2~4.5 mM SDS. Finally associations with SDS micelles, at which point the anisotropy increases. ANS binds in the absence of SDS indicating a hydrophobic area present on the surface of ACBP. ANS/SDS co-binding is observed up between 0 and 1,75 mM SDS, followed by decreased ANS fluorescence indicating denaturation of ACBP. (B) Formation of SDS aggregates on the protein surface is revealed by the increase in the I_3/I_1 ratio of the fluorescent probe pyrene around ~1.5 mM SDS.

We used fluorescence anisotropy to measure the changes in the Trp side chains' rotational diffusion or tumbling upon titration with SDS (Fig. 2A). In the range 0~1 mM SDS, no obvious change was observed, however, increasing the SDS concentration to 2-3 mM decreased anisotropy, most likely due to a faster tumbling of the aromatic residues and increased structural flexibility. This observation corresponds well to the increase in fluorescence intensity and change in secondary structure. Anisotropy levels stayed constant up to around 5 mM SDS, after which it increased to the initial native-state level. This change in tumbling coincides with the formation of bulk SDS micelles (at the cmc). It is likely that denatured ACBP associates with SDS micelles forming a large aggregate and thus has slower tumbling. Unlike our SAXS data for the sub-cmc ACBP:SDS complexes (see below), we do not have any direct structural information on the complex between ACBP and bulk micelles. However, it is worth mentioning that several structures have been suggested for complex between proteins and SDS above the cmc. On balance, there is most support for the "necklace and bead" model, which involves an unfolded and elongated protein that wraps around several micelles [27].

The fluorescent probe pyrene was used to investigate whether or not small SDS aggregates, which we designate as decorated micelles, are formed on the surface of ACBP. Pyrene is a highly hydrophobic molecule with low solubility in water (2-3 μM); the ratio of the intensity of its emission at 372.5 and 383.5 nm (I_3/I_1) can be used to evaluate the polarity of its environment [28]. In the absence of protein, this ratio changes from ~0.65 to ~0.93 (Fig. 2B) when pyrene partitions into SDS micelles, indicating micelle formation in the concentration range 4-6 mM SDS. In the presence of 2 μM ACBP, it is clear that pyrene experiences a more hydrophobic environment than water in the range 1.25 to 6 mM SDS. We explain this by the formation of SDS aggregates on ACBP, into which pyrene can partition. The point at which these aggregates are detected agrees very well with the concentration where we observe an increase in tryptophan fluorescence and change in secondary structure by CD. Put together, these studies indicate that denaturation of ACBP is due to formation of hydrophobic clusters of SDS on ACBP.

A second extrinsic probe, ANS, was used to study the initial binding of SDS and denaturation. ANS binds to hydrophobic regions on protein surfaces with a many-fold increase in fluorescence intensity [29]. This has made it a very good indicator for partially folded states [30], which tends to expose contiguous hydrophobic regions that are buried in the native state. However, ANS will also bind to natively formed

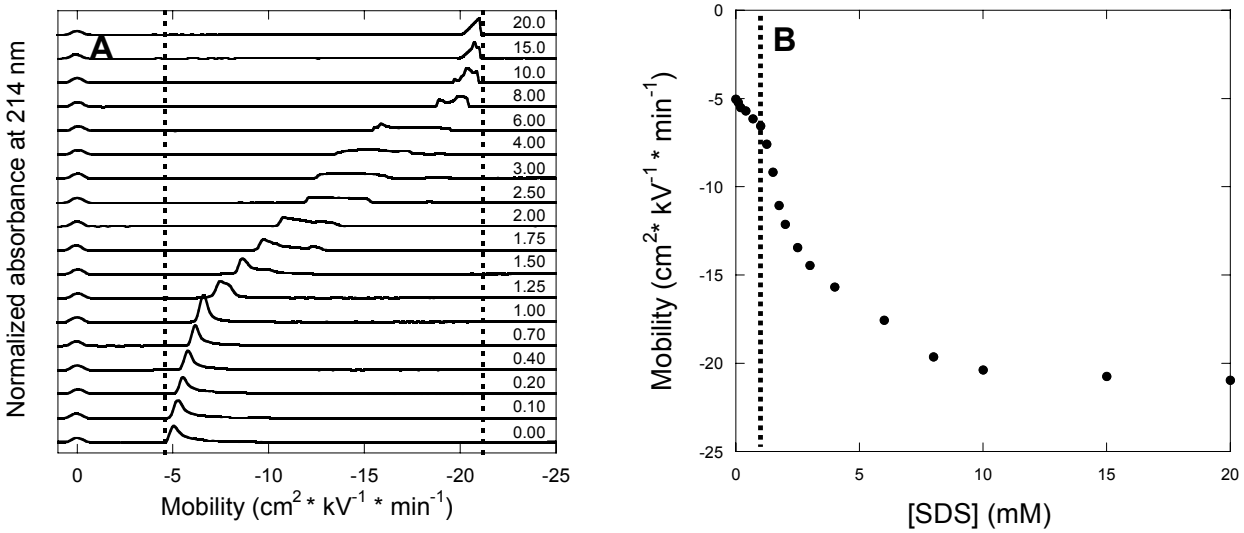

Figure 3. (A) Electropherograms showing the mobility of ACBP at SDS concentrations from 0-20mM. Lines indicate mobility of native ACBP and ACBP saturated with SDS, respectively. Figures indicate SDS concentration in mM. (B) Mobility of ACBP, defined as the midway between the baseline before and after the peak region, plotted against SDS concentration. The broken line indicates the onset of the fluorescence-based transitions seen in Fig. 1A.

hydrophobic patches such as active sites or ligand-binding pockets [31]. We also see ANS binding to native ACBP (Fig. 2A). This agrees with independent observations that ANS binds to the active site of ACBP, reflecting the protein's high affinity for hydrophobic substrates such as long chain acyl-CoA esters (B.B. Kragelund and F.M.P., unpublished observations). Upon titration of ACBP with SDS, ANS fluorescence increases in the interval 0-1.5 mM SDS, due either to co-binding of ANS and SDS or to exposure of hydrophobic patches upon denaturation (Fig. 2A). Further titration results in a decrease in fluorescence which coincides with denaturation of the native structure. As opposed to Trp fluorescence, which did not show any change in the interval 0-1 mM SDS, a significant change in ANS fluorescence was observed in this range. This suggests that initial SDS binding takes place in the absence of significant changes in the aromatic environment.

To obtain independent information on this early binding event, we used capillary electrophoresis (CE), where solute mobility is based on a combination of hydrodynamic drag and charge, making it sensitive to binding of even small amounts of charged ligands [32; 33]. Electropherograms show changes in the mobility of ACBP at 0-1 mM SDS without concomitant broadening of the ACBP peak (Fig. 3A), indicating that ACBP binds SDS without denaturing the protein. Above 1 mM SDS, a shoulder on the right side appears and increases with SDS concentration, merging with the main peak around 2.5 mM SDS until only a large smear is observed, indicating denatured ACBP with a range of bound SDS molecules. Finally, between 10 to 20 mM SDS, ACBP is fully saturated with SDS and thus retains a constant mobility over this concentration range. When plotting the mobility of ACBP, defined as the midway between the baseline before and after the peak region, against SDS concentration, we observe an almost linear increase in mobility in the range 0-1 mM SDS, followed by a steep increase in mobility, which eventually levels out at 10-20 mM SDS (Fig. 3B). The broken lines indicate the onset of the fluorescence based transitions seen in Fig. 1A. CE data generally support the spectroscopic techniques describes above very well, apart from the continued shift in peak position between 4 and 10 mM SDS, which is not reflected in the fluorescence data. This may reflect additional binding of SDS, *e.g.* as a necklace and bead structure, without concomitant structural changes on ACBP (see discussion).

Isothermal titration calorimetry resolves the stoichiometry of SDS binding

Fluorescence and circular dichroism focus predominantly on ACBP's structural changes. To obtain information about the stoichiometry and thermodynamics of binding, we turned to isothermal titration calorimetry (ITC), which measures the heat flow associated with binding, even in the absence of structural changes [15; 34; 35]. Enthalpograms from titrations of ACBP with SDS revealed a number of characteristic and reproducible transitions (Fig. 4A). Each titration curve is generally described by a large endothermic process peaking at 1.5-2.5 mM followed by a dip to a minimum at 3-5 mM, a second peak around 4-7 mM and a dip at 6-11 mM SDS. At higher SDS concentrations, the signal levels out, indicating no further interaction, as the binding process has reached saturation at this stage; thus, all added SDS (injected as micelles) remains in a micellar form and do not lead to any additional detectable heat flow.

Each of the observed transitions represent distinct SDS binding transitions, which we have described for other proteins such as cutinase [34], myoglobin [15] and the all-β proteins TII27 and Tnfn3 [35]. The second endothermic peak may be visualized more clearly in Fig. 4B, where the broken line indicates the plateau that is seen for the other studied

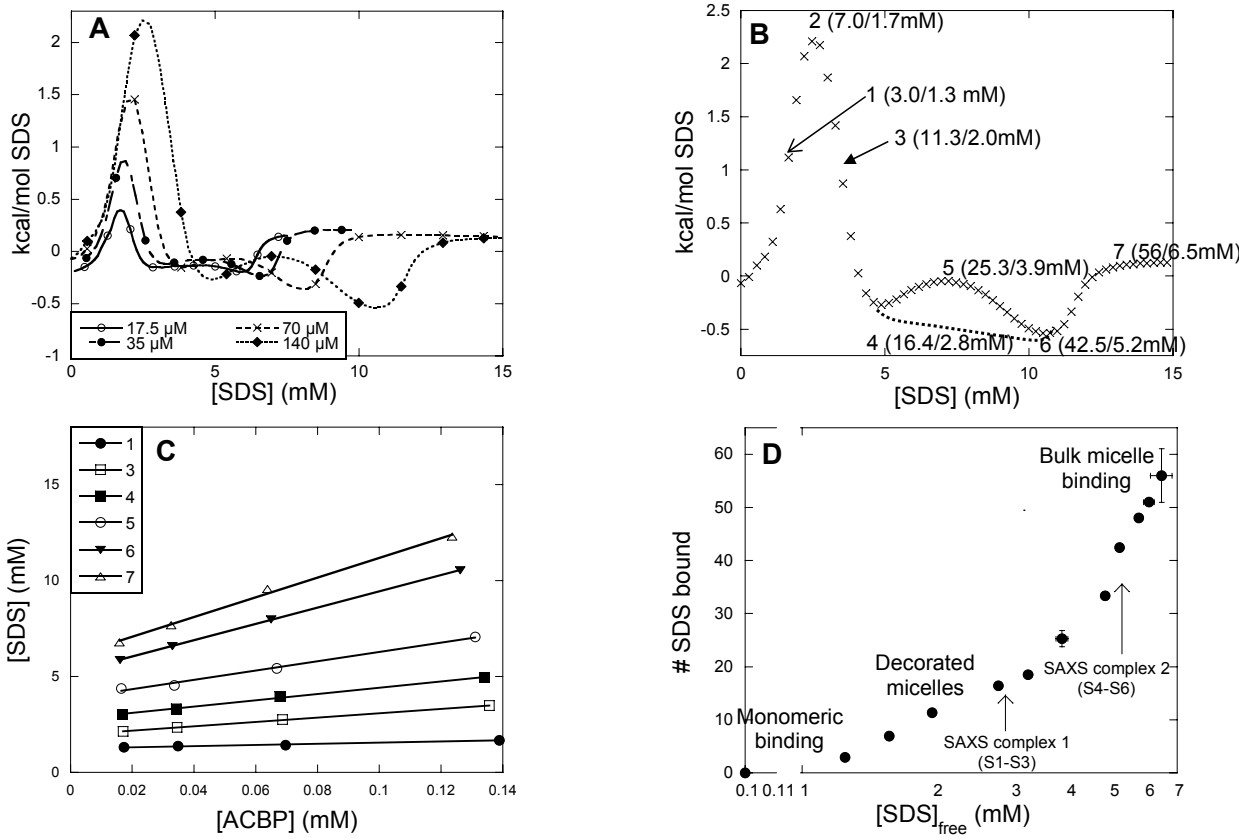

Figure 4. (A) ITC enthalpograms for the titration of SDS (99 mM) into four different ACBP solutions. Each trial comprised sixty 4µl titrations, but for clarity only a few points are marked along the dashed line identifying each enthalpogram. The experimental resolution is illustrated in panel B, which shows all data points for the trial with 140µM ACBP. (B) Enthalpogram for 140 mM ACBP with indication of the binding stoichiometry and the free SDS concentration calculated according to eq. (1) at different stages of the process. The molecular interpretation of point 1-7 based on small angle scattering and spectroscopy is discussed in the main text. The dotted line between points 4 and 6 is inserted as a visual guide to highlight the second endothermic peak with maximum at point 5. (C) Total concentrations of SDS, at the different transition points indicated in figure A, plotted as a function of ACBP concentration. Binding numbers and free SDS concentrations are derived from eq. 1, and summarized in Table 1. (D) Free SDS concentration plotted versus the number of bound SDS molecules. This plot corresponds to Tanford's classical SDS binding isotherm [7]. Different types of protein-SDS complexes are indicated in the appropriate concentration range. The two arrows refer to the conditions (including sample names described in Table 3) under which the SAXS data were recorded.

proteins, typically taking place after an exothermic peak [15; 35; 36]. This plateau was investigated in some detail for SDS titrated intocutinase [37] and it was concluded that it reflected the hydrophobically driven association of SDS and denatured protein, which is exothermic at room temperature and becomes endothermic above 30-40°C. We interpret the second endothermic peak as a specific structural change in the protein-SDS complex occurring on top of a more general accretion of SDS. Details of this change will be discussed below in light of the SAXS results.

The stoichiometry of SDS binding (the binding isotherm) can be derived from a series of titrations into solutions with different protein concentration as described previously[34]. Briefly, the underlying principle is that a given trait or anomaly in the enthalpogram reflects a certain stage or transition in the titration (e.g. protein unfolding, binding saturation etc as discussed above). As more SDS is required to satisfy the stoichiometry of a certain transition the higher the concentration of protein, the location of a transition will be shifted to the right with increasing [ACBP]. This tendency is clearly seen in Fig 4A and it may be quantified by a mass-conservation approach, which separates the total SDS concentration, $[SDS]_{tot}$, into a free and a protein bound population. Thus, at a certain stage (defined by a maximum, minimum or inflexion in Fig. 4A) of the titration we may write

$$[SDS]_{tot} = [SDS]_{free} + N[ACBP] \qquad (1)$$

where N is the number of SDS molecules bound per protein. In Fig. 4C we have plotted $[SDS]_{tot}$ as a function of [ACBP] for the seven transitional points defined in Fig. 4B, and indeed find the linear relation stipulated by eq. (1). Hence the slope and intercept listed in Table 1 specifies the free SDS concentration and binding number at the seven transition points. 3 SDS molecules bind at a free SDS concentration of up to 1.3 mM, during which time ACBP does not undergo any significant changes. The major endothermic process occurs over a free SDS range of 1.3-2.8 mM, which corresponds nicely to the main denaturation profile and the formation of

Table 1. Stoichiometry of binding at different stages of ITC titration

Transition point[b]	No. of bound SDS[c]	$[SDS]_{free}$ (mM)[c]
1	2.97±0.28	1.25±0.02
2	6.95±0.06	1.57±0.00
3	11.33±0.14	1.96±0.01
4	16.44±0.62	2.77±0.05
5	25.27±1.53	3.85±0.12
6	42.47±0.32	5.19±0.02
7	56±5.07	6.46±0.36
Final point (EGPC)	60.0	(cmc)

Notes:
[a] All data in 10 mM Tris pH 8.0 at 22°C.
[b] See Fig. 4B for definitions.
[c] Based on fits to eq. 1.

decorated micelles, and is accompanied by the binding of ~16 SDS molecules. The second endothermic peak, spanning 2.8-5.2 mM free SDS and leading to 42 molecules bound SDS, coincides with the second fluorescence titration with minor changes in λ_{max}. Finally, accretion of large micelle-like clusters occurs up to the cmc completion around 6.5 mM, with 56 SDS molecules bound and the resumption of increased anisotropy (Fig. 2A). The enthalpies scale essentially linearly with protein concentration (data not shown), as would be expected in a process where each binding reaction contributes to the calorimetric signal.

Plotting the number of bound SDS molecules versus free SDS concentration (Fig. 4D) reveals the characteristic multi-step binding isotherm described in Tanford's classical treatment[7]. Thus an initial strong (or "high-energy") binding at low SDS is followed by a slow-rising part of the binding isotherm at intermediate concentrations with a binding level of about 0.4 g SD /g protein. Eventually, as the free SDS concentration approaches the cmc, massive uptake (traditionally referred to as cooperative binding) sets in, leading to a final binding level of about 1.7 g SDS/ g protein. Although the final amount of SDS bound is significantly above the average value of 1.2 g SDS/g protein[7], this binding profile mimics the generic SDS binding isotherm [8], and the spectroscopic and SAXS results from the current work identifies several of the structural details involved in the associated protein-SDS interactions. Some of these are delineated in the graph and discussed further below.

Independent verification of the binding stochimetry by eluent gel permeation chromatography (EGPC)

To verify the saturation binding number (56±5) obtained by ITC, we turned to EGPC [38]. In this approach, a column is equilibrated with a certain concentration of a desired ligand, in our case 9.0 mM SDS, which is distributed between ~5 mM monomer (the cmc) and ~4 mM micelles (the exact cmc value is not essential for the accuracy of the binding number). The micelle concentration is monitored by the refractive index (RI). We then inject samples of 50 μM ACBP in different concentrations of SDS onto the column, which leads to two RI peaks. The large positive peak around 23 minutes (also seen by absorption at 280 nm) corresponds to ACBP saturated with SDS, whereas the smaller peak around 31 minutes (invisible by 280 nm absorption) corresponds to micelles. As illustrated in Fig. 5, if there is less than 9.0 mM free (i.e. monomeric or micellar) SDS in the ACBP sample injected into the column, then the micelle concentration will be less than ~4 mM (the concentration in the column buffer which is the background concentration on the column) and this will be reflected in a negative micelle peak at 31 minutes. Conversely, more than 9.0 mM free SDS in the ACBP sample leads to a positive micelle peak. By plotting micelle peak area against total SDS concentration in the ACBP sample, we obtain a clear linear dependence (Fig. 5 insert), which intersects the *x*-axis at 12.0 mM SDS. Thus, at a total SDS concentration of 12.0 mM in the ACBP sample, the free concentration of SDS is 9.0 mM, which means that 3.0 mM SDS is bound. Given that the ACBP concentration is 50 μM, the stoichiometry of binding must be 60.0 SDS to one ACBP molecule. Within error, this value (which we estimate to have 5% uncertainty) is identical to the value (56±5) obtained from ITC.

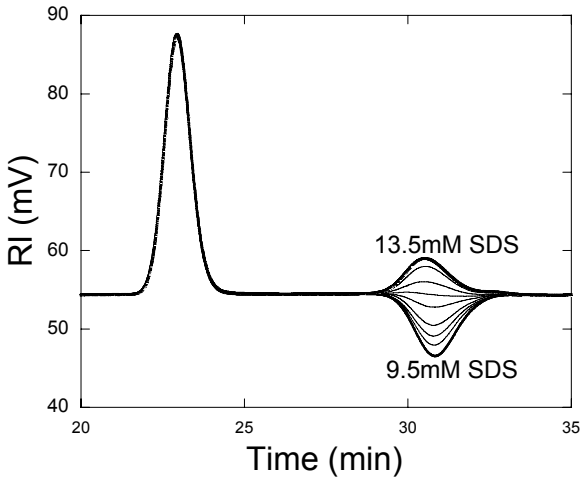

Figure 5. ACBP-SDS binding stoichiometry measured by eluent gel permeation chromatography. An elutent containing 9mM SDS (5mM monomer and 4mM micelles) passes through a gel filtration column, and change in micelle concentration is measured with a refractive index detector. Samples of 50μM ACBP incubated with 9.5-13.5 mM SDS are passed onto the column. A micelle concentration smaller or higher than 4mM results in a decrease or increase in the refractive index respectively. Insert show area of the micelle peak as a function of SDS concentration. The intersect at 12mM indicate that 3mM SDS is bound to 50μM ACBP, which gives a binding stoichiometry of 60 SDS molecules to one ACBP molecule.

Small Angle X-ray Scattering identifies both dimeric and monomeric ACBP:SDS complexes

In the previous sections we have obtained information about the conformational changes that ACBP undergoes at increasing SDS concentrations, as well

as the number of SDS molecules bound at the various transitions. Based on these data, we identify two central points where it is particularly relevant to obtain structural information about the SDS:ACBP complexes by SAXS. These are (1) after the first endothermic peak where ~16 SDS molecules are bound (and where ACBP has undergone significant changes in secondary and tertiary structure), and (2) after the second endothermic peak where a total of ~42 SDS molecules are bound, accompanied by a more modest change in tertiary structure and no secondary structure change. These are points 4 and 6 in Fig. 4B and correspond to distinct parts of the Tanford binding isotherm depicted in Fig. 4D. We reason that the additional uptake of SDS molecules must be reflected in a structural rearrangement of the SDS:ACBP complex, which SAXS can shed light on.

In order to give a comprehensive presentation of the investigations of the complexes by SAXS, we have also performed SAXS on the native ACBP protein, and on pure SDS samples. The study of the native protein is important with respect to addressing whether the samples with ACBP and SDS consist of mixtures or if they are homogenous with only one type of complexes. The samples of pure SDS serves to demonstrate that the new modeling method that we use for analyzing the SAXS data from the complexes, which is based on Monte Carlo simulation integration, is applicable for describing SAXS from SDS micellar structures.

The analysis of the SAXS data from the SDS micelles and the complexes progresses in two steps: First the Indirect Fourier Transformation (IFT) method [39; 40] is used for obtaining model-independent information on the structures of the objects. Secondly, structural models are constructed, partly based on the model-independent information from IFT and partly on the information from the spectroscopic, chromatographic and calorimetric titration experiments and on the knowledge of the constituting molecules and their concentrations within the samples.

The IFT methods provides the pair distance distribution function $p(r)$, which gives direct information about the structure in real space. The function is a histogram of all distances between pair of points within the particles weighted by the excess electron density relative to the buffer (which can be both positive and negative) at each point. The function goes to zero at $r = D_{max}$, where D_{max} is the maximum distance within the scattering objects. A micelle-like structure of SDS has a negative excess scattering length density in the core as the electron density of hydrocarbon chains is lower than that of the buffer and a positive excess scattering length density in the headgroup region as the electron densities of the sulfate and sodium ions are larger than that of the buffer. Therefore the pair distance distribution function $p(r)$ of micelle-like structures of SDS will have characteristic oscillations with a main maximum close to the diameter of the headgroup + counter ion shell. For proteins, the $p(r)$ function gives the maximum size of the protein and, by comparison with $p(r)$ functions for objects of know shape, also low-resolution information on the structure of the protein.

The new modelling method is very similar to traditional modelling of SAXS data in which a geometric structure is assumed and parameters describing the geometry are optimized by weighted least-squares methods when the scattering intensity of the model is fitted to the experimental data[41]. Constraints can be included in the model in terms of partial specific volumes and excess scattering length densities of the various parts of the molecules, and in terms of concentrations. This allows the scattering intensity to be calculated on absolute scale and good quality fits ensure models that are consistent with the prior knowledge of the samples. The main difference between the traditional modelling approach and the new one introduced here is that Monte Carlo simulation techniques are used for integrating over the volume of the objects in connection with the calculation of the scattering intensity[42,43]. A finite set of points generated by Monte Carlo methods is used for representing the structure. Note that it is straightforward to introduce smeared distributions or interfaces in the model by adding random vectors with a certain distribution to the points. The implementation used in the present work employs smeared distributions in terms of Gaussians as well as constraints so that the SAXS intensity was fitted on an absolute scale. The Monte Carlo method has the great advantage that one can apply very complex structural models since one is not limited to structures for which the intensity can be calculated analytically.

SAXS data for pure native ACBP protein in solution are shown in Supplementary Figure S1. The data decay monotonically with increasing q and most of the decays is beyond q = 0.1 Å^{-1}. The $p(r)$ function

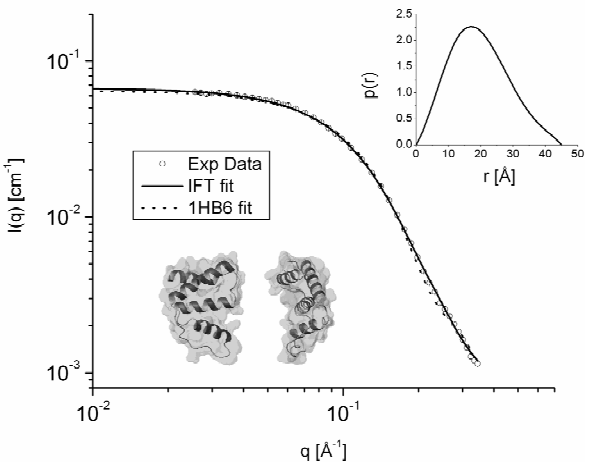

Figure 6. SAXS results for native ACBP in solution at 5 mg/mL. Experimental data (open circles), IFT fit (solid line) and fit using atomic resolution crystal structure model (doted line). Inserts: Upper – Pair distance distribution function for ACBP; Lower – Atomic structure of ACBP protein (1HB6.pdb)

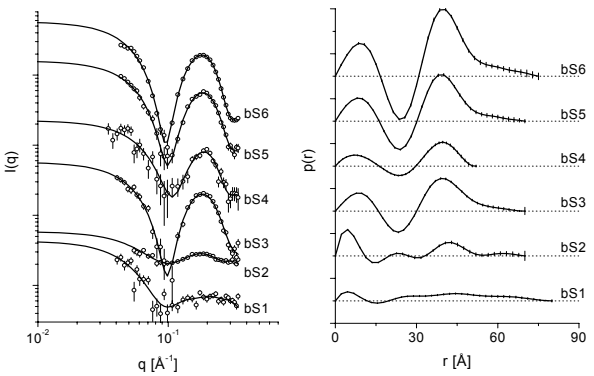

Figure 7. SAXS results for pure SDS micelles. (A) The experimental SAXS data are shown as open circles and the model fits using the methods described in the text as solid lines. The overall SDS concentrations are given. The same structure was used for fitting the samples bS2-bS6 but it was only fully optimized against the bS5 and bS6 data sets. The structure had to be slightly modified to fit the data for bS1 for which the concentration is very close to cmc. The structures of the micelles are shown as spheres at the position of the Monte Carlo points. The hydrocarbon tail region is represented by red spheres, whereas headgroup and counterion region is represented by green spheres. 500 points are used for each of the two contributions (SDS headgroup+counterions and SDS C12 tails, respectively). (B) Pair Distance Distribution functions obtained from the

(inset) obtained by the IFT analysis shows that the protein in solution forms a compact, slightly flattened structure. Comparing the experimental SAXS data with the theoretical intensity for the protein in solution calculated for the atomic coordinates of the protein (pdb entry 1HB6) using the program CRYSOL [44], we obtain good agreement (Fig. 6). This shows that the native protein in solution has a similar shape as in the crystal structure.

The experimental data for pure SDS samples are displayed in Fig. 7 (left). The characteristic bump at high scattering vectors q originates from a core-shell micelle structure with a negative scattering length density in the core and a positive scattering length density in the shell [45]. At low q, the SAXS data at high SDS concentrations display a decrease as q goes to zero due to inter-particle interference effects caused mainly by electrostatic repulsion between the micelles. The $p(r)$ functions obtained by IFT are displayed in Fig. 7 (right panel). The $p(r)$ functions have a characteristic bump at short distances and an oscillatory behavior that originates from the core-shell structure of the micelle. The functions furthermore demonstrate that the maximum diameter of the micelles is about 60−70 Å.

The Monte Carlo modelling method was applied to the SAXS data from pure SDS solutions. The micelles structure was described by a core-shell ellipsoidal model with a constant thickness of the headgroup shell and core semi axis of (R_m,R_m,εR_m). A fit parameter was used for describing the concentration of SDS in micelles. This value can be compared to the expected value estimated from the overall concentration and the estimated cmc of 4 mM (Table 2). It was necessary to fit the number of headgroup excess electrons in terms of a scale factor Se_{head} to account for the reduction in excess electrons due to dissociation of the sodium counter ions. As illustrated in Table 2, the approach gave good fits to the data and micelle aggregation numbers of 66±1 for oblate ellipsoids with R_m = 20.3±0.3 Å and ε = 0.663±0.005, except at the lowest concentration where the micelles appear more flattened. The number of headgroup excess electrons is reduced by a factor of about 0.86 and this parameter was kept fixed during the fit to the data from the complexes described below. The obtained parameters for the SDS micelles are in good agreement with those obtained in a previous work by Vass et al[45] by a more traditional modeling approach. The results demonstrate that the model can describe the scattering from SDS micelles very well and we can proceed to applying it for modeling the complexes.

The experimental SAXS data for ABCP:SDS complexes are shown in Fig. 8A for all studied concentrations. A characteristic bump at high scattering vectors q demonstrates that in all cases we have the formation of micelle-like structures. At low q, the SAXS data at high protein concentrations as for the pure micelles display a decrease as q goes to zero due to interparticle interference effects. The $p(r)$ functions obtained by IFT are shown in Fig. 8B and they have a characteristic bump at short distances and an oscillatory behavior. The functions are similar to those obtained for the pure micelle solutions, however

Table 2. Parameters obtained by model fits to the SAXS data for the pure SDS micelles[a].

	Sample					
Fit Results	bS1	bS2	bS3	bS4	bS5	bS6
c_{SDS}-cmc (mM)	1.8 (0.8)	2.8 (4.5)	12.4 (15.7)	3.7 (6.1)	16.1 (15.3)	52.0 (44.6)
N_{agg} [b]	67±5	69±1	66±1	66±1	66±1	66±1
R_m (Å) [c]	22.9±2.8	20.7±0.9	20.3*	20.3*	20.3±0.3	20.3±0.2
ε [c]	0.476±0.03	0.663*	0.663*	0.663*	0.663±0.005	0.662±0.01
Se_{head} [d]	1.06±0.21	0.878*	0.878*	0.878*	0.878±0.07	0.855±0.003

Notes:
[a] Nominal concentrations assuming a cmc of 4 mM are given in parentheses. Parameters with a star were kept fixed.
[b] Number of SDS molecules per micelle.
[c] Parameters referring to the oblate ellipsoid formed by the micelles with long axis length R_m and axis scaling factor e.
[d] Scale factor accounting for the reduction in excess electrons due to dissociation of Na^+ counter ions.

without negative portions. The similarity shows that there is a micelle-like core-shell structural organization in the complexes. The functions furthermore demonstrate that the maximum diameter of the complexes are 60-80 Å with a clear tendency of larger diameters for the complexes with less SDS bound (samples S1-S3, corresponding to point 4 in Fig. 4B) as compared to the complexes with more SDS bound (samples S5-S6, corresponding to point 6 in Fig. 4B). We note that the SAXS intensities as well as the $p(r)$ functions are both very different from those of the native protein and much more similar to those of the pure micellar samples. If the samples have a significant part of heterogeneity in terms of complexes and native protein, which *a priori* could be expected in particular for the samples with a low SDS to protein ratio (samples S1-S3), the bump at high q in the SAXS data and the oscillatory behaviour of $p(r)$ would be much less pronounced. We can therefore already from the data and the model-independent analysis conclude that the samples are quite homogeneous and we will use this in the modeling.

The Monte Carlo modeling approach was also applied to the five SAXS data sets from the protein-SDS complexes. A large set of possible structures were tested for the ACBP+SDS complexes and their scattering intensities compared with the experimental SAXS data. The models consisted of cylindrical structures (both long and flat) for the protein and various structures for the SDS contribution: Micelles of SDS associated with the cylinder, rims of SDS, and hemi-rims of SDS. The surfactant aggregate was placed at several positions around the protein contribution. However, none of the structures could reproduce the experimental SAXS intensities or the $p(r)$. After further tests, it was realized that only a core-shell structure could give the features observed in $p(r)$. For the data at high SDS concentration, a Janus-type particle consisting of an ellipsoidal SDS micelle with the protein as a shell covering part of the surface of the micelle and mixing with the SDS headgroups could perfectly reproduce the data. The micelle core structure is described as an ellipsoid of revolution with axes $(R_i, R_i, \varepsilon R_i)$. The protein covers the full angular range around the z axis except the range between $-\alpha$ and α, a region between $-w_p$ and w_p along z and has a thickness of W_p. The fits for the ACBP:SDS complex at high SDS-to-protein ratio are shown in Fig. 8A (S5 and S6), which also shows the resulting structures of the complexes. The model reproduces the experimental SAXS data very well. Table 3 displays the fitting results and aggregation numbers derived from them. The model has one ACBP molecule per decorated micelle, and the aggregation number of the micelle is 35-38 in very good agreement with the value obtained by ITC (42.5). The protein almost fully cover the surface of the micelle and such a distribution is in good agreement with the loss of tertiary structure and the conservation of part of the secondary structure as observed by the spectroscopic techniques. Note that the micellar cores are nearly spherical with a small prolate tendency and thus the micelles are quite different from those formed in pure SDS solutions. The volume of the distribution of the protein can also

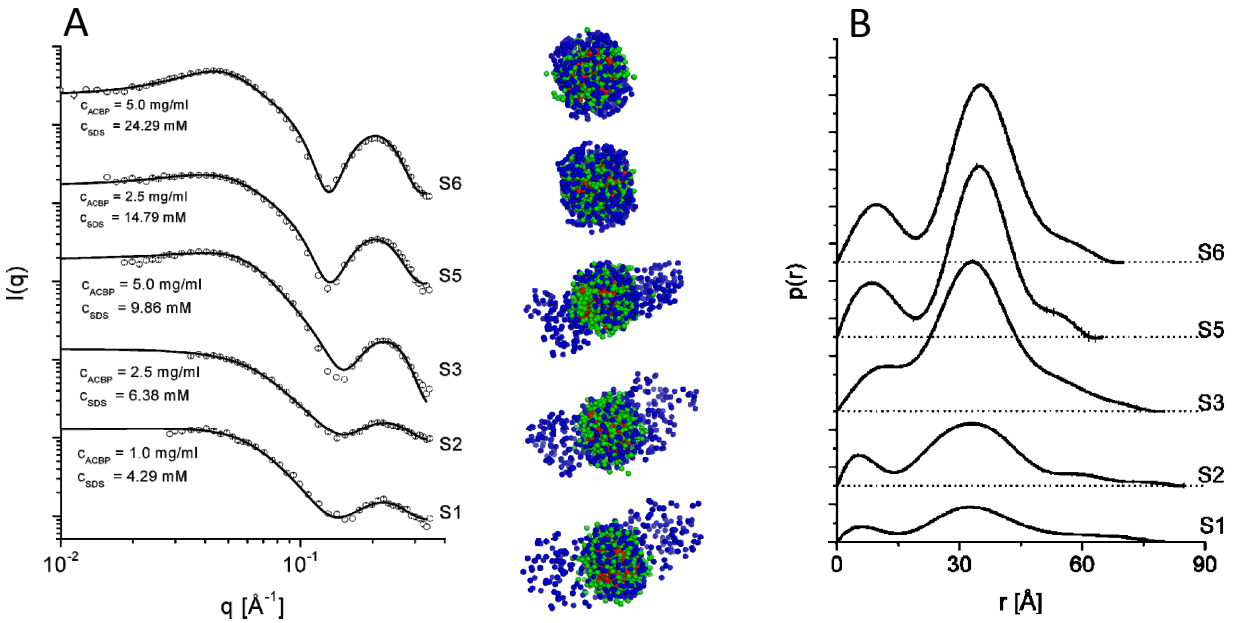

Figure 8. SAXS intensities and associated IFT results for the ACBP+SDS complexes. The experimental data are shown as open circles and the theoretical fits as solid lines. (A) Model fits and data for the different ACBP-SDS complexes. Concentrations of ACBP in mg/mL (1 mg/mL corresponds to 100 µM ACBP) and SDS in mM indicated in brackets. The sample concentrations are indicated for each case. The sketch of the proposed model is shown as inset and near to each curve is shown the resulting model. The red points represent the hydrocarbon tails of the SDS, the green points represent the headgroup and counterions of SDS, and the blue points represent the protein distribution. (B) Pair distance distribution functions obtained from the indirect Fourier Transformation fit of each experimental data.

Table 3. Parameters obtained by model fits to the SAXS data for the ACBP protein + SDS micelles

	Sample				
Fit Results	S1	S2	S3	S5	S6
C_p [mg/mL][a]	1.0	2.5	5.0	2.5	5.0
C_{SDS} [mM][b]	4.3	6.4	9.9	14.8	24.3
N_{agg}[c]	25±14	18.6±1.1	18.7±0.7	37.6±4.1	40.1±1.3
M_W per compl [kDa][d]	20	20	20	10	10
W_p [Å][e]	5.2±1.2	8.6±0.8	8.1±0.2	14.2±0.2	14.2±0.4
w_p [Å][e]	14.3±2.8	18.6±2.3	20.4±1.6	21.8±3.0	20.8±1.3
α [rad][e]	3.86±1.4	3.43±0.18	3.40±0.19	1.92±0.21	3.26±0.12
R_i [Å][f]	14.2±0.8	13.6±0.3	14.2±0.2	11.8±0.4	12.1±0.2
ε[f]	1.42±0.84	1.26±0.07	1.12±0.04	1.92±0.21	1.90±0.06
S_{RW} [Å][g]	12±4	16±2	16.2±0.7	-	-
r_{RW} [Å][g]	12±6	9.1±0.9	8.5±0.4	-	-

Notes:
[a] ACBP concentration.
[b] SDS concentration.
[c] Number of SDS molecules in the complex.
[d] Protein mass per complex.
[e] In the SAXS model, the protein molecule covers the full angular range around the z axis except the range between $-\alpha$ and α, a region between $-w_p$ and w_p along the z axis and has a thickness of W_p
[f] The micelle core structure is described as an ellipsoid of revolution with axes $(R_i, R_i, \varepsilon R_i)$ where ε is a constant defined in the Table.
[g] These parameters refer to the random configurations of ACBP outside the SDS micelle. The random walks were constructed using step lengths of S_{RW} with spheres of radius r_{RW} at each point of the walk.

be estimated from the fit results. The protein distribution as displayed in Fig. 8A is partly mixed with the SDS headgroups but these only contribute about 5000 Å^3. As mentioned, the distribution covers almost the full surface area on the decorated micelle and it has a thickness of about 14 Å. It has a volume 70-80,000 Å^3, which is 6-7 times that of the dry protein (12,000 Å^3), suggesting that a large fraction (~80%) of this volume is water.

For the data at low SDS-to-protein ratio, the same structure could reproduce the data quite well, however, very importantly, the total amount of SDS required was much higher than what was present in the samples. Such a model is clearly inconsistent and has to be disregarded. Calculations showed that there either has to be free protein in solution or that two proteins have to be associated with each decorated micelle. Further test showed that in the former case, the free protein has to be associated in dimers and either have a large dilute structure or a shell-like structure. As none of these possibilities seems likely, they were discarded. For the second case with two proteins associated with each decorated micelle, a significant part of the protein should only contribute to the scattering at low q as it would otherwise mask the scattering at high q from the micelle-like structure. This is possible if parts of the protein are disordered. In order to describe this, a model was made with two ACBP molecules per micelle with half of each protein located in a shell around the micelle and the other two halves in random configurations protruding into the solvent on opposite sides of the micelle. The random configurations were generated as random walks starting from a flat surface and only occupying half of the space. The walks had each 10 points and a step length of S_{RW}. A small ensemble of 10 different configurations for the complex was generated. The walks were placed at two opposite sides of the decorated micelle along the z axis. A finite volume was associated with the random walks by placing spheres of radius r_{RW} at each point of the walk.

The model with two proteins bound per decorated micelle was fitted to the data at low SDS-to-protein ratio. The results are given in Table 3 and the fits and structures are displayed in Fig. 8A (S1, S2 and S3). The model fits the SAXS data well. Importantly, the structure is also in agreement with the larger size of the structures at low SDS concentration as observed in the $p(r)$ functions, which underlines that this 'dimer' model is correct. As already mentioned, the model employs molecular constraints and therefore we can calculate the amount of SDS per ACBP as well as the overall SDS concentration. For the model with two ACBP proteins per complex, the protein as well as the overall SDS concentrations are in agreement with the actual sample concentrations and the model is thus consistent. For the samples S1, S2 and S3 with low SDS-to-protein ratio, the number of associated SDS molecules per ACBP, given as N_{agg} in Table 3, is 15-17 which agrees very well with the 16 molecules determined by ITC. The core of the SDS micelles structure is also for these samples close to spherical, however, with a small tendency towards a slightly oblate shape. The distribution of the protein in the structures is in good agreement with the loss of tertiary structure and the conservation of part of the secondary structure as observed by the spectroscopic techniques. We note that the dimeric association of the ABCP in the model for the ACBP:SDS complexes is similar to the behaviour of cutinase at low SDS

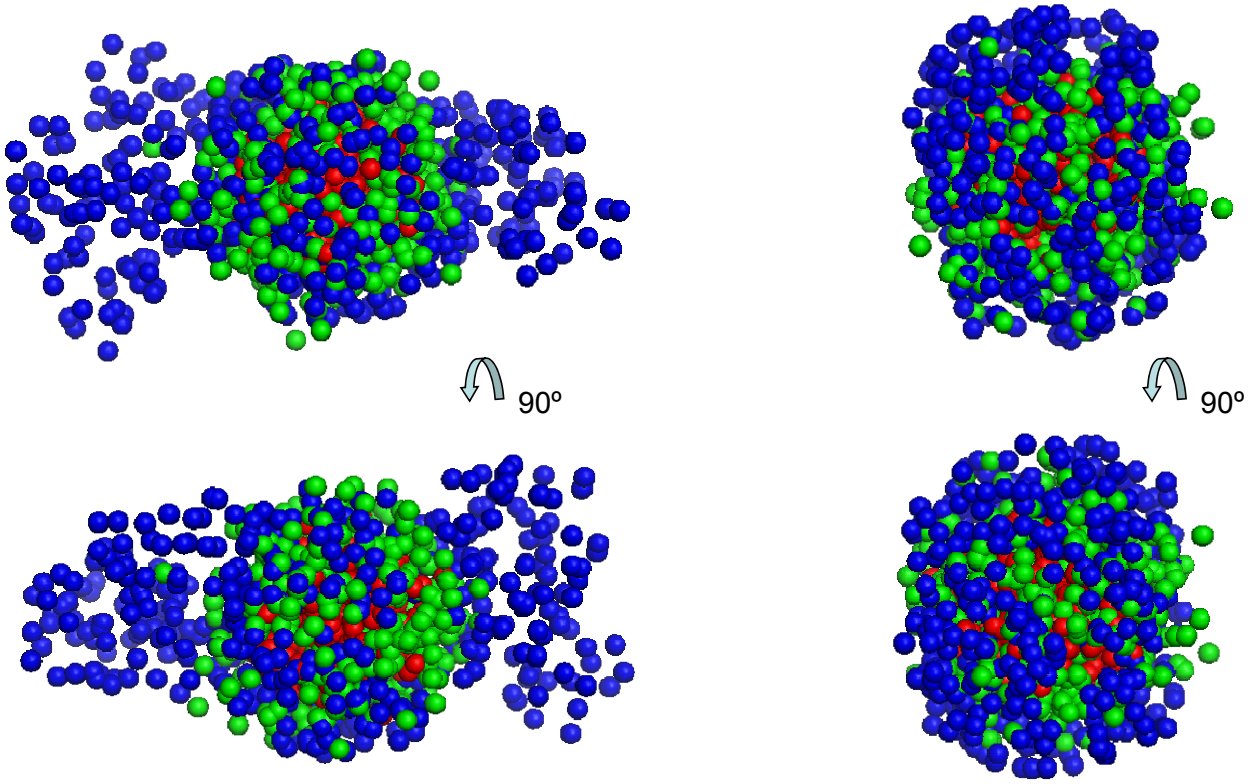

Figure 9. Model representation of the ACBP+SDS complex structures using the spheres at the position of the the MC points used in the analysis of the SAXS data. Note that 500 points are used for each of the three contributions (SDS headgroup+counterions, SDS C12 tails, and protein, respectively). Green points represent the headgroup and counterions of SDS, red points the hydrocarbon tails of the SDS, and the blue points represent the protein distribution. Left: Configuration for low concentrations for SDS. Right: .configuration for high concentration of SDS. For details, see text.

concentrations [36] where dimers also are found.

The volume of the distribution of the protein for the low SDS-to-protein ratio samples (S1-S3) is 40-50,000 $Å^3$, which is about twice the volume of two proteins (2 x 12,000 $Å^3$), meaning that the protein distribution is somewhat spread out on the surface of micelle. The protein distribution as displayed in Fig. 8A also includes the SDS headgroups but these only contribute about 2200$Å^3$. Thus there is also in these distributions a significant amount of water present. The protein layer on the micelle is only about 9 Å thick, corresponding to the thickness of a single α-helix.

The models derived from the SAXS data for the low and high SDS-to-protein ratio samples for the formed complexes are displayed in two different views in Fig. 9. Although the decorated micelle SAXS models are of low resolution, the figure provides a visual impression of the characteristic features of the complexes formed between the ABCP protein and the SDS micelles. It should be noted that the models agree both with SAXS data and all the additional information that we have available from spectroscopic, chromatographic, and calorimetric measurements and that despite extensive tests on alternative structures we have not been able to find any other models that could fit the data.

DISCUSSION

We have used a wide variety of techniques to characterize the changes in ACBP's structure and extent of binding of SDS molecules over a range spanning the whole bulk pre-micellar regime. This allows us to compare ACBP with a large number of other proteins and establish a general pattern of protein-surfactant interactions. We will start by describing the individual ACBP-SDS binding steps in more detail. An overview is provided by the tentative structures given in Fig. 10 and the summary in Table 4. It should be noted that the denaturing steps and structures given in the figure are base on interpretation of all the experimental evidence in the paper, as direct structural investigations by SAXS have only been perfomed on the structures at stage B and C.

Stage A (0~1.3mM SDS): no change in tryptophan fluorescence, pyrene fluorescence or secondary structure is observed, indicating that ACBP retains its native structure. ANS fluorescence and CE, however, clearly reveal the binding of SDS molecules without accompanying denaturation. It is very difficult to determine the exact number of SDS molecules bound to ACBP by ITC because the number is very low, leading to a very low heat flow. A reasonable approximation would be between 1 and 3 SDS molecules. Individual SDS molecules bind to specific

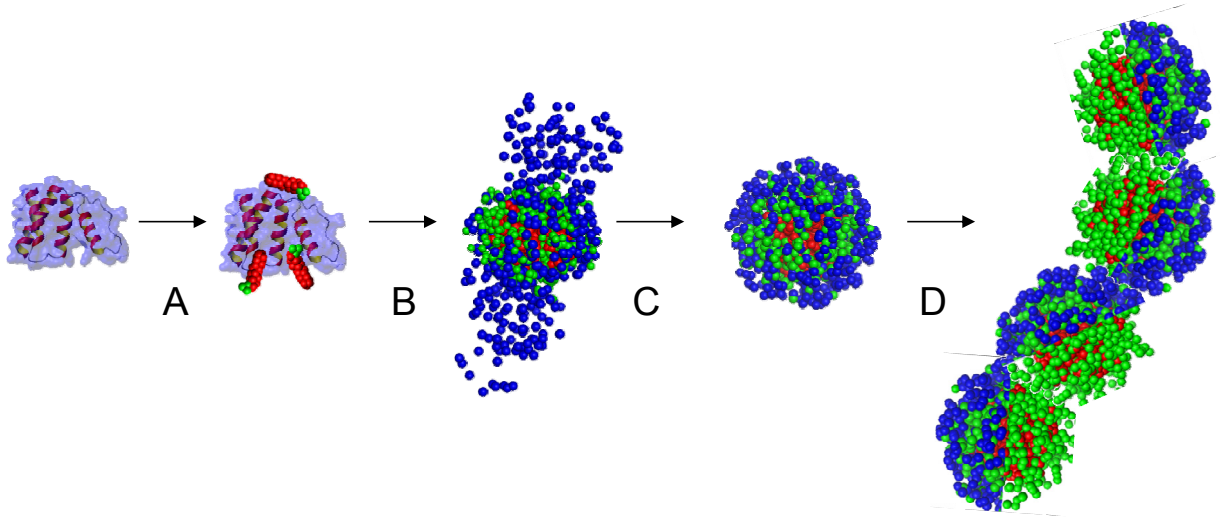

Figure 10. Schematic representation of the different stages of ACBP denaturation. In stage A ACBP binds between 1 and 3 SDS molecules without losing native structure. Stage B involves the formation of a decorated micelle of 37 SDS molecules that binds 2 ACBP molecules. Further binding of SDS to a total of 40 in stage C leads to monomeric ACBP with a shell like structure of SDS. The structure presented in stage D is speculative, however, represents the "beads on a string" model that has been proposed for proteins interaction with SDS micelles above the cmc.

sites on the surface of the native state, probably around the ligand-binding site where we have identified several positively charged patches. The binding behavior in this region is considerably less complex than that of SDS towards myoglobin, where the pre-denaturation zone can be divided into two regions (0-0.15 and 0.15-0.4 mM SDS). SDS-Myoglobin interactions are detected by ITC already at 0.05-0.1 mM SDS [15] and decorated micelles start to form around 0.15-0.4 mM SDS although it is not possible to determine the stoichiometry of binding on myoglobin until around 0.4-1.2 mM SDS. It is possible that the presence of pre-determined hydrophobic ligand binding sites on the surface makes this process stoichiometrically more well-defined for ACBP while stoichiometric binding to myoglobin only sets in above a critical SDS concentration of about 0.15 mM.

Stage B (1.3~2.8mM SDS): In this region proper denaturation occurs: there are changes in both Trp fluorescence intensity, λ_{max} and secondary structure, as well as formation of SDS decorated micelles from an uptake of 3-16 SDS molecules. Anisotropic measurements show that the Trp side-chain tumbles faster, probably due to loss of structure in its surroundings. Also ANS fluorescence decreases at this stage, showing that the structural changes that take place in this region is severe enough to disrupt the ANS binding site(s). At the end of this transition structural characterization by SAXS revealed formation of a decorated micelle, containing about 33 SDS molecules, which links two ACBP molecules together. Part of the protein is bound to the decorated micelle and part of it protrudes into the solvent.

Table 4. Summary of conformational changes that ACBP undergoes in SDS[a].

Stage	Event	Methods	#SDS bound [b]	$[SDS]_{free}$ (mM) [b]
A	Binding of few molecules (around active site, possibly making ANS site more hydrophobic). No significant structural or calorimetric impact.	ANS, CE	3	1.25
B	Major alterations in secondary and tertiary structure, decrease in anisotropy and displacement of ANS. Endothermic interactions leading to formation of decorated micelles.	ITC, Trp, CD, CE, ANS, anisotropy, pyrene	16 (ITC), 18-19 (SAXS)	2.8
C	Second exothermic series of interactions, minor changes in tertiary structure, possibly second phase of ANS displacement.	ITC, Trp (λ_{max}), ANS	42 (ITC), 38-40 (SAXS)	5.8
D	No changes in ACBP structure. Onset of micellization.	ITC, CE, anisotropy	56±5 (ITC), 60±6 (EGPC)	6 (cmc)

Notes:
[a] All data at 25°C in 10 mM Tris pH 8.0.
[b] Based on ITC data fitted to eq. 1 unless otherwise stated.

Clearly ACBP has lost (most of) its tertiary structure at this point.

Stage C (2.8-5.2mM SDS) A massive uptake of additional 26 SDS molecules to a total of 42 is accompanied by a decrease in Trp fluorescence. There are no additional changes in secondary structure. An endothermic process, observed by ITC, suggests an event involving bond breaking, which probably involves further unfolding. However, the enthalpy of this process is not as large as observed for the initial denaturation step, indicating that the structural loss is minor as compared to the initial denaturation in stage B. The changes in Trp fluorescence and slow decline in ANS fluorescence may reflect rearrangements of SDS micelles or tertiary changes. Both may occur according to SAXS, which reveals an ACBP-SDS complex with only one protein per decorated micelle and all of the protein located in a shell-like structure around the micelle.

Stage D (>5.2mM SDS) involves formation of bulk SDS micelles and binding of 56-60 (according to ITC/EGPC) SDS molecules, leading to large micellar structures where Trp has reduced tumbling. CE also indicates that SDS molecules continue to accumulate on ACBP all the way up to 10 mM SDS, possibly as large protein micelle complexes are formed with ACBP bridging between micelles. The fact that ITC does not report on this interaction is probably due to the weak interaction of this binding.

Two-stage SDS denaturation is seen for several but not all α-helix containing proteins and requires binding of a critical amount of SDS

The enthalpogram profile for ACBP resembles the ITC profiles not only for an all α-helix protein such as BSA [17] but also the mixed α/β protein lysozyme [46]. Although the studies on lysozyme and BSA have not used the same collection of techniques as in the present study, the ITC titration profile is in both cases described by two endothermic peaks, as is the case for ACBP. Endothermic processes correspond to a loss of organized protein structure, while the formation of electrostatic protein-SDS contacts leads to an exothermic signal; in contrast, hydrophobic protein-SDS contacts are enthalpically essentially invisible [7; 47].

We propose that these proteins follow a common denaturation mechanism, in which initial denaturation at relatively low SDS concentrations, driven by the formation of organized SDS aggregates on the protein surface, leads to the first endothermic peak. The minor second peak may then be due to condensation of the protein molecule on the micellar interface (*i.e.* step 3 in Fig. 10). This second rearrangement is accompanied by smaller structural changes but a larger number of SDS molecules per protein molecule. It is difficult to say whether the first step in all cases requires the formation of a protein dimer bridged by the decorated SDS micelle. If dimerization occurs over the entire protein range probed by the ITC scans, it will not show up as a protein concentration dependence phenomenon. The ability to dimerize may depend on the details of the protein surface chemistry and the availability of other domains on the protein which could fold back onto the decorated micelle to form an "internal arrangement". Other α-helix containing protein such as myoglobin [15] and S6 [18] do not show this double endothermic peak at pH 8.0, indicating that particular conditions need to be fulfilled to allow this process to happen. SDS-induced dimerization detected by small angle (neutron) scattering was also reported for cutinase, and this was hypothesized to rely on decreased intermolecular repulsion as the positively charged cutinase molecules were gradually neutralized by the anionic surfactant [36]. However, charge estimates for ACBP based on the primary structure (www.expasy.ch) suggests a negative charge of 2-3 at pH 8, and it follows that the mechanism suggested for cutinase cannot account for the current results. Rather, transition from stage B to C (Fig. 10) for ACBP appears to be driven by attractive interactions of the denatured protein and the micellar interface, and hence require a critical area of available interface to occur. Interestingly, this may be directly reflected in the ITC results. Thus, the thermograms for cutinase were similar to those for ACBP in Fig 4A in the early parts of the titration, but did not show any signs of the second endoterm found for ACBP. The binding of SDS to cutinase saturated at 0.5 g SDS/g protein which is about 2-3 times lower than typical values [48].This correlation between low binding numbers and the lack of the second transition supports the view that a critical amount of surfactant must be associated with the protein to support the condensed structure (stage C in Fig. 10). This interpretation is corroborated by a number of previously investigated proteins including phytase [49], which has low saturation binding and no second endoterm (like cutinase) and lysozyme [50; 51], BSA [17], α-lactalbumin [12] and myoglobin [15] which all show normal saturation binding (~1 g/g) and a conspicuous second endotherm (*i.e.* like ACBP). While a final conclusion awaits further experimental back-up, the current results suggest (*i*) that the transition between the two forms in Fig. 9 requires a critical amount of SDS (in the 0.5-1 g/g protein range) onto which the protein can bind, and (*ii*) that this transition may be identified as the second endotherm in the ITC trials.

α-helix structure may be a prerequisite for multi-step unfolding

All the proteins described above contain α-helix structure and interact strongly with SDS under the critical micelle concentration. Previously we have studied proteins with a high content of β-structure which only showed weak interactions with monomeric SDS, and were only fully denatured by micellar SDS [35]. Thus, for Tnfn3 we did not observe any endothermic processes below the cmc, showing that micelles were required to denature the proteins while

monomeric SDS showed no denaturing effect. This highlights a fundamental difference between all β-proteins and proteins containing α-helical elements, namely that the α-helical segments are much more prone to take up pre-micellar SDS with dramatic conformational consequences. We have previously used protein engineering approaches to identify the α-helix as a preferred site of attack in the unfolding mechanism of the mixed α/β protein S6 in SDS [52]. In addition, S6 also forms pre-micellar SDS aggregates and undergoes a series of conformational changes according to tryptophan fluorescence [18], which is remarkably similar to that of ACBP. The tryptophan fluorescence profile, which is a fluorescence intensity increase followed by an intensity decrease, is also observed for cutinase [34], α-lactalbumin [12] and myoglobin [15; 53], albeit the fluorescence decrease in the latter case is rather faint, probably due to the heme group whose dissociation leads to a subsequent rise in fluorescence. In all cases where pyrene fluorescence experiments have been conducted (for α-lactalbumin, S6 and ACBP), the increase in tryptophan fluorescence is associated with the formation of decorated micelles. Cutinase, myoglobin and α-lactalbumin do not show any fluorescence baseline prior to unfolding, probably due to high susceptibility to SDS binding. As ACBP is designed to bind anionic substrates with hydrophobic tails, it may be able to bind SDS at very low concentrations but without significant conformational changes.

For all-β proteins, the fluorescence and far-UV CD signals change in parallel, indicating a simple binding mechanism [35], in contrast to α og α/β proteins where CD and fluorescence signals do not show an identical number of steps. Since the β-proteins are only denatured by micelles, the denaturation process takes place around the cmc. This means that the proteins bind a large amount of SDS in one step around the cmc and as a consequence secondary and tertiary structure change in parallel. In contrast α and α/β structured proteins denature at SDS concentrations well below the cmc. This leads to a more gradual denaturation process as the binding of SDS takes place over a wider range of SDS concentrations. As a consequence several stages in the denaturation process can be observed for α and α/β proteins, as emphasized by the present study.

Decorated micelles linking protein molecules may provide a structural explanation for sub-micellar protein aggregation with physiological parallels

The SAXS analysis shows the formation of decorated micelles with an aggregation number of about 33, since two proteins is associated with each decorated micelle at the lower SDS concentrations investigated. It is likely that these micelles are the smallest ones that can be formed and thus, one can conclude that the structure of the formed complexes is dominated by the properties of SDS. The initial binding of SDS at very low concentration is predominately by electrostatic interactions as single molecules. These bound SDS molecules have lost their mixing entropy with the solvent. Although they presumably bind primarily to the most hydrophobic part of the protein facilitated by the loss of protein tertiary structure, they are likely to have their hydrophobic tails at least partially exposed to the solvent. They are therefore prone to form micelle-like structures at concentrations much below that of the bulk cmc value of SDS. In order to form energetically favorable micelle-like structures with sufficient space and conformational entropy for the C12 tails, the aggregation number has to exceed a minimum value. A way to achieve this is to link up with SDS molecules bound to another protein molecule. Thus, unsatisfied "hydrophobic bonds" drives the formation of intermolecular contacts with another protein molecule. Furthermore, the disordered regions of ACBP outside the micelle-decorated region, which are exposed to the solvent, may also by themselves provide anchor points to other proteins, since conformational flexibility is a prerequisite for initial contacts in protein aggregation [54]. Note that these phenomena only occur within a narrow SDS concentration range. Once the SDS concentration of SDS is high enough to facilitate formation of full micellar structures on each protein surface or bulk micelles are available for binding, the motivation for aggregation is removed and SDS can revert to its role as an agent of dispersion and solubilization.

Ultimately, decorated micelles in combination with flexible protein regions, in which protein-SDS interactions are mediated by electrostatic interactions while hydrophobic interactions mediate intermolecular protein contacts, may be the force that drives the accumulation of higher-order protein aggregates at certain critical SDS concentrations. Although ACBP does not form higher-order aggregates with SDS at pH 8.0, this may only be a matter of altering *e.g.* pH, since even small alterations in the ionization of side chains can strongly affect the ability of SDS to bind, unfold [11] and aggregate [18] proteins. Suitable aggregation conditions with sub-micellar SDS, some at neutral pH, have been identified for other proteins such as S6 [18], Aβ [19], β_2-microglobulin [20], collagen [55] and lysozyme[21]. Similar types of amphiphile-driven aggregation may occur *in vivo*. For example, fatty acids such as oleic acid can form higher-order complexes with α-lactalbumin and related proteins with potent anti-cancer properties [56]. The large number of oleic acid molecules bound per protein leaves plenty of room for the formation of decorated micelles.

MATERIALS AND METHODS

Chemicals: Tris(hydroxymethyl)aminomethane (Tris) and sodium dodecyl sulfate (SDS) were from AppliChem (Darmstadt, Germany). ACBP was purified as described previously [57]. Pyrene and ANS (1,8-anilino-nathphalene-sulfonic acid) were from Sigma-Aldrich (St. Louis, MO). All chemicals were of

the highest grade available. All experiments were performed in 10 mM Tris pH 8.

Fluorescence measurements: All experiments were conducted in a 10 mm quartz cuvette (Hellma) on a LS-55 Luminescence spectrometer (Perkin-Elmer Instruments, UK) at 25°C using 2 µM ACBP (except for fluorescence anisotropy, for which 20 µM ACBP was used). Solutions were recorded with 200 nm/min scan speed and 3 accumulations after at least 30 min of equilibration.

Tryptophan fluorescence: Excitation was at 295 nm and emission at 345 nm using 10 nm slit widths for both excitation and emission wavelengths. For anisotropy, 15 measurements for each sample were averaged using an integration time of 10 seconds.

Pyrene fluorescence: A stock solution of 200 µM pyrene in ethanol was made and added to the samples to a final concentration of 1 µM. Excitation was at 335 nm using excitation and emission slit widths of 3.5 nm. The ratio of the intensity of the emission at 372.5 and 383.5 was used for further analysis.

ANS fluorescence: 2 µM ACBP was incubated with 0-10 mM of SDS and 40 µM ANS. Contributions from buffer and SDS were subtracted at each SDS concentration. Excitation was at 350 nm and emission at 500 nm with excitation and emission slit widths of 7.5 nm.

Circular dichroism (CD): Far-UV CD spectra were recorded, using 10 µM ACBP, in a 1.0 mm quartz cuvette on a JASCO J-715 spectropolarimeter (Jasco Spectroscopic Co. Ltd., Japan) equipped with a Jasco PTC-423S temperature control unit. Wavelength scans were recorded in the wavelength range of 185-250 nm with a band width of 2 nm and a scanning speed of 50 nm/min. Five accumulations were averaged to yield the final spectrum. Background contributions from the buffer were subtracted.

Capillary electrophoresis (CE): CE was carried out on a Beckman PACE-MDQ system using a capillary with an inner diameter of 25 µm. Total length of the capillary was 60 cm and the length to the detector was 50 cm. The running buffer consisted of 10 mM Tris pH 8 and SDS in the range 0 to 20 mM. The sample contained 1 mg/mL ACBP and 1 mM dimethylformamide (DMF) in order to monitor the electroosmotic flow. In each run a plug corresponding to 3% of the capillary length was injected and electrophoresis was performed at 30 kV. The mobility of ACBP was followed using absorbance at 214 nm.

Isothermal titration calorimetry (ITC): Calorimetric measurements were conducted on a VP-ITC (MicroCal Inc., Northampton, MA, USA). The reference cell was filled with water and in a typical experiment, the sample cell was loaded with a solution of 18-141 µM ACBP. The cell solution was titrated with aliquots of 2.5-4 µl of 99 mM SDS in 10 mM Tris, pH 8. All experiments were done at 22°C, where SDS demicellization is practically athermal [34]. Therefore the enthalpic contribution from demicellization of SDS upon injection can be neglected in data analysis. The obtained heat signals from the ITC were integrated using the Origin software supplied by MicroCal Inc.

Eluent Gel Permation Chromatography (EGPC): Measurements were carried out using an eluent buffer containing 9 mM SDS in 10 mM Tris pH 8. The eluent was passed onto a 24 mL Superose 6 (GE Healthcare) gel filtration column with a flow rate of 0.5 mL/min. Following the column, a Hitachi L-4250 UV detector measured absorbance at 280 nm and an Agilent 1100 detector measured the refractive index. A probe series of 50 µM ACBP was incubated with varying SDS concentrations in the range 9.5-14 mM SDS for 1 hr. After equilibration of the column with eluent, a probe sample was injected onto the column, and absorbance at 280nm and the refractive index were followed over time.

Small Angle X-ray scattering (SAXS): The SAXS experiments were performed on the in-house instrument in the Chemistry Department of University of Aarhus [58]. All experiments were performed at 25ºC in 10 mM Tris pH 8. For comparison, experiments were performed on the native protein at a concentration of 5 mg/mL, on pure SDS micellar solutions at six different concentrations (given in Fig. 6) and on samples with ACBP:SDS complexes at five different concentrations (see legend to Fig. 8A). The exposure times were 1800 s and the data treatment, background subtraction of buffer and normalization to absolute scale were performed using homemade software. The resulting data on absolute scale are displayed as a function of the modulus of the scattering vector $q = (4\ \pi/\lambda)\ \sin(\theta)$, where $\lambda = 0.154$ nm is the x-ray wavelength and 2θ is the angle between the incident and scattered X-rays.

The SAXS data was first analyzed by the Indirect Fourier Transformation (IFT) method[39; 40], which provides the pair distance distribution function $p(r)$. It gives direct information about the structure in real space. The function is a histogram of all distances between pair of points within the particles weighted by the excess electron density (which can be both positive and negative) at the points. Structural information derived from the $p(r)$ function can be used for indentifying structural features that have to be incorporated in a model for the micelles and the complexes. The influence of interparticle interference effects was eliminated by omitting the low q-part of the data.

A new modelling method was developed and implemented in order to describe the SAXS data from the complexes. The approach is inspired by the work of Hansen [42] and Spinozzi and coworkers [43]. The method is similar to traditional modelling of SAXS data in which a structure is assumed and parameters describing the structure are optimized by weighted least-squares methods when fitting the scattering intensity of the model to the experimental data[41]. The main difference for the new method introduced here is that Monte Carlo simulation techniques are used for

integrating over the volume of the objects in connection with the calculation of the scattering intensity[42,43]. This is accomplished by using a finite set of points generated by Monte Carlo methods for representing the structure. The Monte Carlo method has the great advantage that one can apply very complex structural models since one is not limited to structures for which the intensity can be calculated analytically. This allows us to test a large number of different structures against the experimental data. The new approach was used for analyzing both the SAXS data for puse SDS solutions and for the solutions with the SDS-protein complexes.

In the new approach a large set (10^8) statistically uniformly distributed points are first generated by Monte Carlo simulation within a cubic search volume of volume $(2R_{max})^3$, where R_{max} is the expected maximum radius of the structure. R_{max} can be estimated from the $p(r)$ function and should fulfil $R_{max} > D_{max}/2$, where D_{max} is the distance at which $p(r)$ goes to zero. Additional three-dimensional random vectors with a Gaussian distribution are calculated, so that these later can be used for smearing the distributions of components in the model. Note that when the vectors with a Gaussian distribution are added to the points in the distribution of a component, it corresponds to a convolution of the distribution of a component with the Gaussian. For each of the components of the structure, a subset of the points is selected by geometrical conditions for the coordinates. The subset is defined by parameters that can be varied during a least-squares optimization. The parameters also define the various components of the model (hydrocarbon core of the micelle, shell describing the surfactant headgroups and counterions, and protein, respectively) which each have a different scattering length density. For each component, 5000 points are selected and these points are divided into 10 subsets with 500 points. An excess electron density is associated with each point so that the known number of excess electrons is obtained. The molecular values used for calculating the values were as follows: SDS headgroup + counter ion, volume of 60.53 Å^3 with 59 electrons, C12 tailgroup of 355.1 Å^3 with 97 electrons [45]. The protein volume was calculated from the protein sequence, and corresponds to a theoretical partial specific volume of 0.7372 cm^3/gram. The excess electron density of 2.0 x 10^{10} el./gram was used for the estimation of the molecular weight (J.S. Pedersen and C.L.P. Oliveira, unpublished). The buffer electron density was set to 0.3334 el./Å^3 so that the number of excess electrons per headgroup, tail and protein was 38.8, –21.4, and 1178, respectively. The core volume of the micelle/decorated micelles is expected to be dry and therefore it was used for calculating an aggregation number by dividing the volume with that of a C12 tail.

The pair distance distribution $p(r)$, which is a histogram over distances between the points weighted by the electron density of the points, was calculated for each subset and added. The resolution of $p(r)$ was chosen to be 0.1 Å. Note that the distributions functions are calculated for each subset and merged rather than calculating it for the full set. The procedure using subsets is faster by a factor of 10. The convergence of $p(r)$ is quite good as the distances are more independent in the subsets (private communication, S.L. Hansen). The function $p(r)$ is calculated in a subroutine call before the q dependence is calculated by a simple Fourier transformation of $p(r)$. The resulting intensity on absolute scale is calculated by multiplying the Fourier transform by the number concentration of particles and the square of the Thomson radius of the electron (0.282 x 10^{-12} cm).

For the points representing the headgroup+counterions and the micelle core smearing of the distributions were introduced, as already mentioned, by adding random vectors with a Gaussian distribution to the position of the points with scale factors for the width of the Gaussian distribution. A width of σ_{head} for the interfaces of the headgroup+counter ion distribution and a width σ_{core} for the surface of the core were used. The width of the distribution generated for the headgroup region was fixed at 3.0 Å and σ_{head} and σ_{core} were fixed at, respectively, 4.0 Å and 2.0 Å in accordance with previous studies [45].

Parameters for the structure and a background were optimized using a standard Levenberg-Maquard weighted least-squares algorithm[41]. Despite the discretization of structures into limited sets of points, the gradients required for the least-squares algorithm can be calculated for all parameters without any problems.

The final intensity expression on an absolute scale that was used for fitting the experimental data was:

$$I(q) = nP(q)S(q) \qquad (2)$$

where n is the number density of particles, $P(q)$ is the Fourier transform of the $p(r)$ function multiplied by the square of the Thomson radius, $S(q)$ is the average structure factor of the system describing effects of interparticle interactions. As the particle are charged, the structure factor for a screened Coulomb potential[59] was used.

ACKNOWLEDGEMENTS

K.K.A. is supported by a pre-doctoral grant from the innovation consortium BIOPRO (headed by Dr. Torben Madsen, DHI), financed by the Danish Ministry of Science, Technology and Innovation. P.W. is grateful for support from the Carlsberg Foundation, the Danish Research Foundation and the Danish Research Agency (grants 26-02-0160 and 21-04-0087 to P.W.). D.E.O. is grateful for long-term support from the Danish Research Foundation (inSPIN) and the Villum Kann Rasmussen Foundation (BioNET). We thank Dr. S. Vass for very helpful discussions on SDS micellar structures.

REFERENCES

1. Stoner, M. R., Dale, D. A., Gualfetti, P. J., Becker, T. & Randolph, T. W. (2006). Surfactant-induced unfolding of cellulase: kinetic studies. *Biotechnol Prog* **22**, 225-32.
2. Kirk, O., Borchert, T. V. & Fuglsang, C. C. (2002). Industrial enzyme applications. *Curr Opin Biotechnol* **13**, 345-51.
3. Mogensen, J. E., Sehgal, P. & Otzen, D. E. (2005). Activation, inhibition, and destabilization of Thermomyces lanuginosus lipase by detergents. *Biochemistry* **44**, 1719-30.
4. Sonesson, A. W., Callisen, T. H., Elofsson, U. M. & Brismar, H. (2007). Imaging the detergency of single cotton fibers with confocal microscopy: The effect of surfactants and lipases. *J. Surfact. Deterg.* **10**, 211-218.
5. Gitlin, I., Gudiksen, K. L. & Whitesides, G. M. (2006). Peracetylated bovine carbonic anhydrase (BCA-Ac18) is kinetically more stable than native BCA to sodium dodecyl sulfate. *J Phys Chem B* **110**, 2372-7.
6. Otzen, D. E., Christiansen, L. & Schulein, M. (1999). A comparative study of the unfolding of the endoglucanase Cel45 from Humicola insolens in denaturant and surfactant. *Protein Sci* **8**, 1878-87.
7. Tanford, C. (1980). *The hydrophobic effect. Formation of micelles and biological membranes*. 2nd Edition edit, Wiley & Sons, New York.
8. Turro, N. J., Lei, X.-G., Ananthapadmanabhan, K. P. & Aronson, M. (1995). Spectroscopic probe analysis of protein-surfactant interactions: the BSA/SDS system. *Langmuir* **11**, 2525-2533.
9. Manning, M. & Colon, W. (2004). Structural basis of protein kinetic stability: resistance to sodium dodecyl sulfate suggests a central role for rigidity and a bias toward beta-sheet structure. *Biochemistry* **43**, 11248-54.
10. Nelson, C. A. (1971). The binding of detergents to proteins. *The journal of biological chemistry* **246**, 3895-3901.
11. Otzen, D. E. (2002). Protein unfolding in detergents: Effect of micelle structure, ionic strength, pH, and temperature. *Biophys. J.* **83**, 2219-2230.
12. Otzen, D. E., Sehgal, P. & Westh, P. (2009). α-lactalbumin is unfolded by all classes of detergents but with different mechanisms. *J. Coll. Int. Sci.* **329**, 273-283.
13. Nielsen, M. M., Andersen, K. K., Westh, P. & Otzen, D. E. (2007). Unfolding of beta-sheet proteins in SDS. *Biophys J* **92**, 3674-85.
14. Cunningham, E. L., Jaswal, S. S., Sohl, J. L. & Agard, D. A. (1999). Kinetic stability as a mechanism for protease longevity. *Proc Natl Acad Sci U S A* **96**, 11008-14.
15. Andersen, K., Westh, P. & Otzen, D. E. (2008). A global study of myoglobin-surfactant interactions. *Langmuir* **15**, 399-407.
16. Nielsen, A. D., Borch, K. & Westh, P. (2000). Thermochemistry of the specific binding of C12 surfactants to bovine serum albumin. *Biochim Biophys Acta* **1479**, 321-31.
17. Kelley, D. & McClements, D. J. (2003). Interactions of bovine serum albumin with ionic surfactants in aqueous solutions. *Food Hydrocolloids* **17**, 73-85.
18. Otzen, D. E., Nesgaard, L., Andersen, K. K., Hansen, J. H., Christiansen, G., Doe, H. & Sehgal, P. (2008). Aggregation of S6 in a quasi-native state by monomeric SDS. *Biochim Biophys Acta* **1784**, 400-414.
19. Rangachari, V., Reed, D. K., Moore, B. D. & Rosenberry, T. L. (2006). Secondary structure and interfacial aggregation of Amyloid-β(1-40) on sodium dodecyl sulfate micelles. *Biochemistry* **45**, 8639-8648.
20. Yamamoto, S., Kasegawa, K., Yamaguchi, I., Tsutsumi, S., Kardos, J., Goto, Y., Gejyo, F. & Naiki, H. (2004). Low concentrations of sodium dodecyl sulfate induces the extension of beta-2-microglobulin-related amyloid fibrils at neutral pH. *Biochemistry* **43**, 11075-11082.
21. Moosavi-Movahedi, A. A., Pirzadeh, P., Hashemnia, S., Ahmadian, S., Hemmateenejad, B., Amani, M., Saboury, A. A., Ahmad, F., Shamsipur, M., Hakimelahi, G. H., F.Y., T., Alijanvand, H. H. & Yousefi, R. (2007). Fibril formation of lysozyme upon interaction with sodium dodecyl sulfate at pH 9.2. *Colloids Surf. B Biointerfaces* **60**, 55-61.
22. Kragelund, B. B., Poulsen, K., Andersen, K. V., Baldursson, T., Kroll, J. B., Neergard, T. B., Jepsen, J., Roepstorff, P., Kristiansen, K., Poulsen, F. M. & Knudsen, J. (1999). Conserved residues and their role in the structure, function, and stability of acyl-coenzyme A binding protein. *Biochemistry* **38**, 2386-94.
23. Kragelund, B. B., Osmark, P., Neergaard, T. B., Schiodt, J., Kristiansen, K., Knudsen, J. & Poulsen, F. M. (1999). The formation of a native-like structure containing eight conserved hydrophobic residues is rate limiting in two-state protein folding of ACBP. *Nat Struct Biol* **6**, 594-601.
24. Kragelund, B. B., Robinson, C. V., Knudsen, J., Dobson, C. M. & Poulsen, F. M. (1995). Folding of a four-helix bundle: studies of acyl-coenzyme A binding protein. *Biochemistry* **34**, 7217-24.
25. Knudsen, J. (1990). Acyl-CoA-binding protein (ACBP) and its relation to fatty acid-binding protein (FABP): an overvi. *Mol. Cell. Biochem.* **98**, 217-223.
26. Thomsen, J. K., Kragelund, B. B., Teilum, K., Knudsen, J. & Poulsen, F. M. (2002). Transient Intermediary States with High and Low Folding

Probabilities in the Apparent Two-state Folding Equilibrium of ACBP at Low pH. *J. Mol. Biol.* **318**, 805-814.
27. Hazra, P., Chakrabarty, D., Chakraborty, A. & Sarkar, N. (2004). Probing protein-surfactant interaction by steady state and time-resolved fluorescence spectroscopy. *Biochem Biophys Res Commun* **314**, 543-9.
28. Kalyanasundaram, K. & Thomas, J. K. (1976). Environmental Effects on Vibronic Band Intensitiesin Pyrene Monomer Fluorescence and Their Application in Studies of Micellar Systems. *Journal of the American Chemical Society* **99:7**, 2039-2044.
29. De, S., Girigoswami, A. & Das, S. (2005). Fluorescence probing of albumin-surfactant interaction. *J Colloid Interface Sci* **285**, 562-73.
30. Semisotnov, G. V., Rodinova, N. A., Razgulyaev, O. I., Uversky, V. N., Gripas, A. F. & Gilmanshin, R. I. (1991). Study of the "Molten Globule" Intermediate State in Protein Folding by a Hydrophobic Fluorescent Probe. *Biopolymers* **31**, 119-128.
31. Mogensen, J. E., Wimmer, R., Larsen, J. N., Spangfort, M. D. & Otzen, D. E. (2002). The major birch allergen, Bet v 1, shows affinity for a broad spectrum of physiological ligands. *J. Biol. Chem.* **277**, 23684-23692.
32. Stutz, H., Wallner, M., Malissa, H., Jr., Bordin, G. & Rodriguez, A. R. (2005). Detection of coexisting protein conformations in capillary zone electrophoresis subsequent to transient contact with sodium dodecyl sulfate solutions. *Electrophoresis* **26**, 1089-105.
33. Gudiksen, K. L., Gitlin, I. & Whitesides, G. M. (2006). Differentiation of proteins based on characteristic patterns of association and denaturation in solutions of SDS. *Proc Natl Acad Sci U S A* **103**, 7968-72.
34. Nielsen, A. D., Arleth, L. & Westh, P. (2005). Analysis of protein-surfactant interactions - a titration calorimetric and fluorescenc spectroscopic investigation of interactions between *Humicola insolens* cutinase and an anionic surfactant. *Biochim Biophys Acta* **1752**, 124-132.
35. Nielsen, M. M., Andersen, K. K., Westh, P. & Otzen, D. E. (2007). Unfolding of β-sheet proteins in SDS. *Biophys. J.* **92**, 3674–3685.
36. Nielsen, A. D., Arleth, L. & Westh, P. (2005). Interactions of Humicola insolens cutinase with an anionic surfactant studied by small-angle neutron scattering and isothermal titration calorimetry. *Langmuir* **21**, 4299-4307.
37. Nielsen, A. D., Borch, K. & Westh, P. (2007). Thermal Stability of *Humicola insolens* Cutinase in aqueous SDS. *J. Phys. Chem. B* **111**, 2941-7.
38. Draper, M., Savage, M., Collett, J. H., Attwood, D., Price, C., Booth, C. & Wang, Q. G. (1995). Solubilisation of drugs in micellar systems studied by eluent gel permeation chromatography. *Pharm. Res.* **12**, 1231-1237.
39. Pedersen, J. S., Hansen, S. & Bauer, R. (1994). The Aggregation Behavior of Zinc-free Insulin Studied by Small-angle Neutron Scattering. *Eur. Biophys. J.* **23**, 379-389.
40. Glatter, O. (1977). A new method for the evaluation of small-angle scattering data. *J. Appl. Crystall.* **10**, 415-421.
41. Pedersen, J. S. (1997). Analysis of Small-angle Scattering Data from Polymeric and Colloidal Systems: Modelling and Least-squares Fitting. *Adv. Coll. Int. Sci.* **70**, 171-201.
42. Hansen, S. (1990). Calculation of small-angle scattering profiles using Monte-Carlo simulation. *J. Appl. Crystall.* **23**, 344-346.
43. Spinozzi, F., Carsughi, F., mariani, P., Teixeira, C. V. & Amaral, L. Q. (2000). SAS from inhomogeneous particules with more than one domain of scattering density and arbitrary shape. *J. Appl. Crystall.* **33**, 556-559.
44. Svergun, D. I., Barberato, C. & Koch, M. H. (1995). CRYSOL - A program to evaluate x-ray solution scattering of biological macromolecules from atomic coordinates. *J. Appl. Crystall.* **28**, 768-773.
45. Vass, S., Plestil, J., Laggner, P., Gilanyi, T., Borbely, S., Kriechbaum, M., Jakli, G., Decsy, Z. & Abuja, P. J. (2003). Models of micellar structure tested by SANS and SAXS (from a Kratky camera) in Cesium dodecyl sulfate solution. *J. Phys. Chem. B* **107**, 12752-12761.
46. Chatterjee, A., Moulik, S. P., Majhi, P. R. & Sanyal, S. K. (2002). Studies on surfactant-biopolymer interaction. I. Microcalorimetric investigation on the interaction of cetyltrimethylammonium bromide (CTAB) and sodium dodecylsulfate (SDS) with gelatin (Gn), lysozyme (Lz) and deoxyribonucleic acid (DNA). *Biophys Chem* **98**, 313-27.
47. Kauzmann, W. (1959). Some factors in the interpretation of protein denaturation. *Adv. Prot. Chem.* **14**, 1-63.
48. Pitt-Rivers, R. & Impiombato, F. (1968). Binding of Sodium Dodecyl Sulphate to Various Proteins. *Biochem. J.* **109**, 825-830.
49. Bagger, H. L., Hoffmann, S. V., Fuglsang, C. C. & Westh, P. (2007). Glycoprotein-surfactant interactions: a calorimetric and spectroscopic investigation of the phytase-SDS system. *Biophys. Chem.* **129**, 251-258.
50. Chatterjee, A., Moulik, S. P., Majhi, P. R. & Sanyal, S. K. (2002). Studies on surfactant-biopolymer interaction. I. Microcalorimetric investigation on the interaction of cetyltrimethylammonium bromide (CTAB) and sodium dodecylsulfate (SDS) with gelatine (Gn), lysozyme (Lz) and deoxyribonucleic acid (DNA). *Biophys. Chem.* **98**, 313-327.

51. Lad, M. D., Ledger, V. M., Briggs, B., Green, R. J. & Frazier, R. A. (2003). Analysis of the SDS-lysozyme binding isotherm. *Langmuir* **19**, 5098-5103.
52. Otzen, D. E. & Oliveberg, M. (2002). Burst-phase expansion of native protein prior to global unfolding in SDS. *J Mol Biol* **315**, 1231-40.
53. Tofani, L., Feis, A., Snoke, R. E., Berti, D., Baglioni, P. & Smulevich, G. (2004). Spectroscopic and interfacial properties of myoglobin/surfactant complexes. *Biophys J* **87**, 1186-95.
54. Pedersen, J. S., Christiansen, G. & Otzen, D. E. (2004). Modulation of S6 fibrillation by unfolding rates and gatekeeper residues. *J. Mol. Biol.* **341**, 575–588.
55. Dombi, G. W. & Halsall, H. B. (1985). Collagen fibril formation in the presence of sodium dodecyl sulphate. *Biochem. J.* **228**, 551-556.
56. Svanborg, C., Ågerstam, H., Düringer, C., Fischer, W., Gustafsson, L., Hallgren, O., Leijonhuvud, I., Linse, S., Mossberg, A.-K., Nilsson, H., Pettersson, J., Svensson, M., Aronson, A. & Bjerkvig, R. (2003). HAMLET kills tumor cells by apoptosis - cellular, molecular and therapeutic aspects. *Adv. Cancer Res.* **88**, 1-29.
57. Mandrup, S., Højrup, P., Kristiansen, K. & Knudsen, J. (1991). Gene synthesis, expression in *Escherichia coli*, purification and characterization of the recombinant bovine acyl-CoA-binding protein. *Biochem. J.* **276**, 817-823.
58. Pedersen, J. S. (2004). A flux- and background-optimized version of the NanoSTAR small-angle x-ray scattering camera for solution scattering. *J. Appl. Crystall.* **37**, 369-380.
59. Hayter, J. B. & Penfold, J. (1981). An analytic structure factor for macroion solutions. *Mol. Phys.* **42**, 109-118.

Paper V

How chain length and charge affect surfactant denaturation of ACBP

How chain length and charge affect surfactant denaturation of ACBP

Kell K. Andersen[1,2] and Daniel E. Otzen[1,2 *].

[1] Interdisciplinary Nanoscience Centre, University of Aarhus, Gustav Wieds Vej 10C, DK – Aarhus C.
[2] Department of Life Sciences, University of Aalborg, Sohngaardsholmsvej 49, DK-9000 Aalborg, Denmark

* To whom correspondence should be addressed. Tel. + 45 89 42 50 46, fax + 45 86 12 31 78, e-mail dao@inano.dk

Abbreviations: ACBP, Acyl Coenzyme A Binding Protein; DDM, dodecyl maltoside; SXS, sodium alkyl sulfate;

Manuscript in preparation

ABSTRACT

Because of their high affinity for proteins and self-assembling properties, anionic surfactants such as sodium dodecyl sulfate (SDS) denature proteins by mechanisms that are fundamentally different from those of weakly binding chemical denaturants. In this way they expand the range and kinetic accessibility of conformations available to the protein. To probe the sensitivity of these conformations to changes in surfactant properties, we have studied how the surfactant denaturation of the all α-helix protein Acyl-coenzyme A-binding protein (ACBP) is affected by alkyl sulfate chain length and by micellar charge. The latter is altered by including different proportions of non-ionic surfactant with SDS. We find that ACBP can be denatured by monomeric alkyl sulfates at all chain lengths tested (8-16 carbon atoms), although longer chains lead to significantly faster denaturation kinetics. We also have indirect evidence that the denatured states populated by the different alkyl sulfates are significantly different. Furthermore, a reduction in chain length has the same effect as a reduction in micellar charge; both lead to slower and more complex unfolding kinetics. Part of this behavior may be rationalized by micellar structural changes, in particular the transition from spherical to more elongated micelles which also lead to inhibition of unfolding kinetics. In addition, we propose that changing micellar binding sites on globular proteins such as ACBP may lead to non-linear correlations between activation unfolding energies and SDS mole fraction. Mutagenic analysis using a series of hydrophobic truncation mutants did not show any direct correlation between the thermodynamic stability and resistance towards SDS. However, when combined with electrostatic potential, the analysis identified initial site of SDS binding in the vicinity of the ligand binding site, revealing possible overlaps between ligand and surfactant binding.

Introduction:

Protein-surfactant interactions have been studied ever since the since the 1940`s [1]. Protein-surfactant interactions are today of great value for the detergency industry and from a fundamental point of view, these types of interactions also provide a fascinating glimpse into the many different types of protein conformations that can be induced by surfactant monomers and micelles. These effects are rooted in two properties: Firstly, ionic surfactants' high affinity for protein surfaces, derived from a combination of electrostatic and hydrophobic binding interactions. Secondly, a high denaturing potency due to their head groups' high charge density, that leads to strong electrostatic repulsion and consequent expansion and denaturation when sufficient numbers of surfactant have accumulated on the protein surface [2]. All this means that anionic surfactants such as sodium dodecyl sulfate are active at low millimolar concentrations, in contrast to the molar concentration range required for chemical denaturants such as guanidinium chloride. Further, the mechanism of denaturation by surfactants is fundamentally different from chemical denaturants; it proceeds much more rapidly, shows complex concentration dependence and has identifiable initial binding sites [3].

Most studies have focused on only single component systems such as the anionic surfactant SDS, however the surfactants used in industry are polydisperse and are a mixture of different chain lengths. Insight into the interactions of proteins and surfactants with different chain lengths is thus important. In addition, most detergent products include both ionic and nonionic surfactants. Nonionic surfactants have significantly lower critical micelle concentrations (cmc) than ionic surfactants of the same chain length, due to the lack of repulsive head group charges. Therefore, besides reducing charge density, mixtures of nonionic and ionic surfactants have significantly lower cmc values than pure ionic surfactants. This effectively removes the concentration range window in which ionic surfactants can act as monomers on proteins and makes micelles the

only major surfactant component. Nevertheless, to our knowledge, only few studies have been dedicated to the interactions of such mixed micelles with proteins. In this paper we therefore investigate the effect of chain length and the mixing of ionic and nonionic surfactants on denaturation potency against proteins.

As model system we use the 4-helical bundle protein ACBP, an 89-residue protein without disulfides or co-factors. By virtue of its small size and simple composition, ACBP has already been used for numerous folding studies [4-6]. We have previously studied the surfactant-induced denaturation of proteins with different secondary structure composition, including all-β [7], mixed α-β [3, 8, 9] and all-α with prosthetic co-factors [10]. This was motivated by the observation that β-rich proteins generally show increased resistance to surfactants denaturation, while α-rich proteins are more prone to surfactant denaturation [11]. ACBP provides an opportunity to expand these studies to include an α-helix protein without co-factors. Furthermore, the rapid unfolding kinetics of ACBP in SDS and other alkyl sulfates allows us to investigate the interactions with surfactants within a reasonable time window.

We have previously described the interaction of ACBP with SDS using a combination of spectroscopy, calorimetry, capillary electrophoresis and SAXS. This study has given us detailed insight into the stepwise denaturation of ACBP by sub-micellar concentrations of SDS. At low SDS concentrations, ACBP binds a few SDS molecules (between 1 and 3) that do not significantly perturb the native structure. In the next step, 16 SDS molecules are bound pr. ACBP molecule. The SDS forms a decorated micelle which binds two ACBP molecules where half of the polypeptide chain is associated with the decorated micelle and the other half perturbs into the solvent. Further uptake of SDS to a total of 42 leads to a larger decorated micelle that only binds a single ACBP molecule. Finally, at SDS concentrations above the cmc, ACBP associates with bulk micelles to form a complex which it has not been possible to characterize in the same detail.

Here we show that shorter alkyl chains lead to dramatically slower denaturation kinetics in addition to the expected reduction in binding affinity. Interestingly, both a reduction in charge density and shorter chain length lead to more complex unfolding kinetics as well as reducing unfolding rates. This suggests that electrostatics and hydrophobic interactions play similar roles in the denaturation process.

RESULTS AND DISCUSSION

Equilibrium denaturation of ACBP in alkyl sulfates shows similar steps but different denaturation potency

We start our investigation by comparing the denaturing potency of alkyl sulfates of chain length 8-16 towards ACBP, using the intrinsic probe tryptophan and the extrinsic probe pyrene.

As we previously reported for SDS [15], all ACBP titrations with alkyl sulfates start with a short baseline region in which no change in the Trp fluorescence

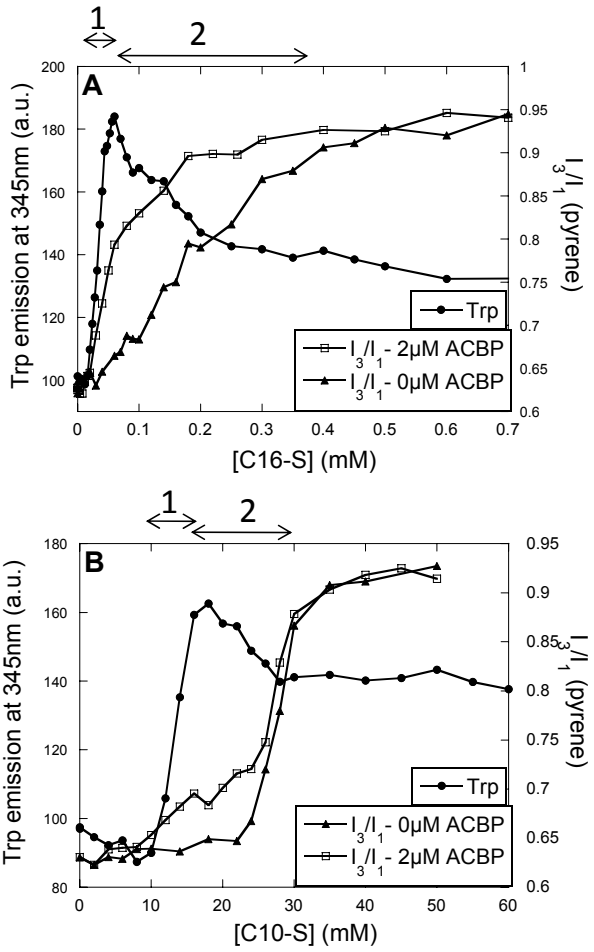

Figure 1. Changes in intrinsic Trp fluorescence emission intensity and extrinsic pyrene emission ratios for ACBP upon titration with (A) C16-sulfate and (B) C10-sulfate. The numbers and arrows refer to transition 1 and 2.

emission takes place. Subsequently, there is a shift in the Trp fluorescence peak maximum (λ_{max}) from ~342 nm to ~346 nm (data not shown), indicating denaturation and increased exposure of the Trp side chain to solvent. This λ_{max} shift is initially accompanied by an increase in fluorescence intensity (representative data for C16-sulfate and C10-sulfate are shown in Fig. 1). We refer to this change in fluorescence as transition 1. We showed for SDS that transition 1 is accompanied by changes in secondary structure and represents the first major denaturation step [15]. Transition 1 is followed by an intensity decrease to an intermediate level (transition 2) without significant changes in λ_{max}. Both transitions are highlighted in Fig. 1.

The change in pyrene's fluorescence emission ratio I_3/I_1 provides two useful pieces of information. Firstly, the critical micelle concentration (cmc) of the different alkyl sulfates under our buffer conditions (10 mM Tris pH 8.0) in the absence of protein (Fig. 1). Cmc is here defined as the alkyl sulfate concentration where the I_3/I_1 ratio reaches its plateau value of 0.95. Results are summarized in Table 1. For SDS, this value (6.0 mM) is identical to the value determined by ITC under the same buffer conditions [15]. Secondly, the formation of hemi-

Table 1. Parameters describing the equilibrium denaturation and kinetics of denaturation of ACBP in alkyl sulfate surfactants at pH 8.0 and 25°C. All errors ~5%.

Chain length	cmc (mM) [a]	Trp denaturation start [b]	$[SXS]^{50\%}$ [c]	*m* [d]	Slope [e]	$k_{max}(s^{-1})$ [f]	log k_{obs} (0mM) [h]
C8	141	60	78.97	0.085	0.0283	12	-2.14
C10	31	10	13.15	0.522	0.157	62	-2.65
C12	6	1.4	1.67	37.021	0.603	175	-1.40
C14	1.06	0.16	0.2	30.753	5.68	- [g]	-0.40
C16	0.38	0.019	0.032	68.038	15.6	- [g]	-1.03

Notes:
[a] The concentration of SXS at which the pyrene I_3/I_1 ratio in the absence of protein reaches 0.95.
[b] The concentration of SXS where initial Trp fluorescence start to increase (onset of transition 1, cfr. Fig. 1).
[c] The concentration of surfactant at which half of the ACBP molecules is denatured. Value obtained by fitting eq. 1 to Trp fluorescence data describing transition 1 in Fig. 1.
[d] The cooperativity parameter *m* obtained using eq. 1 and the same data described in [c].
[e] Slope of the fit in the plot of log k_{obs} vs. SXS concentration in the inserts to Fig. 4.
[f] The highest measured unfolding rate constant (Fig. 4).
[g] Not determined because of limited surfactant solubility.
[h] The unfolding rate of ACBP in the absence of surfactant calculated by extrapolating linear fits in inserts to Fig. 4 to 0 mM surfactant.

micelles on the protein surface, indicated by increases in the I_3/I_1 ratio well below the cmc. The formation of hemi-micelles coincides with an increase in tryptophan fluorescence (Fig. 1), indicating that hemi-micelle formation accompanies or leads to denaturation. The hemi-micelle I_3/I_1 ratio, which is around 0.8 for C12-, C14- and C16-sulfate, decreases to ~0.7 for C10-sulfate and ~0.65 for C8-sulfate, probably because the short-chain hemi-micelles formed are less hydrophobic than the long-chain ones or simply cannot accommodate pyrene to the same extent.

In order to compare the denaturing potency of the alkyl sulfates, we have analyzed transition 1 using a two-state model typically used to analyze denaturation of proteins in chemical denaturants like guanidinium chloride and urea [14]. We emphasize that we do not imply that the surfactants denature ACBP by the same mechanism as chemical denaturants. Nevertheless, the analysis provides two empirical parameters that describe the denaturing potency of the individual surfactants. The first parameter is the midpoint of denaturation $[SXS]^{50\%}$, *i.e.* the surfactant concentration where half of the protein has lost its native conformation. The second parameter is the cooperativity (*m*) which reflects the concentration range over which the protein goes from the native state to the denatured state (the larger the *m*-value, the narrower the concentration range over which this occurs) and thus refers to the efficiency with which each additional surfactant molecule contributes to the denaturation of ACBP. These values are summarized in Table 1.

A log plot of and cmc versus chain length (Fig. 2A) demonstrates that the $[SXS]^{50\%}$ is consistently below cmc and the gap between the two values widens with higher chain length. This may also be demonstrated by normalizing alkyl sulfate concentration with cmc and plotting Trp titration values for C8-C16-sulfate in one plot (Fig. 2B). Thus, the longer the alkyl chain, the more

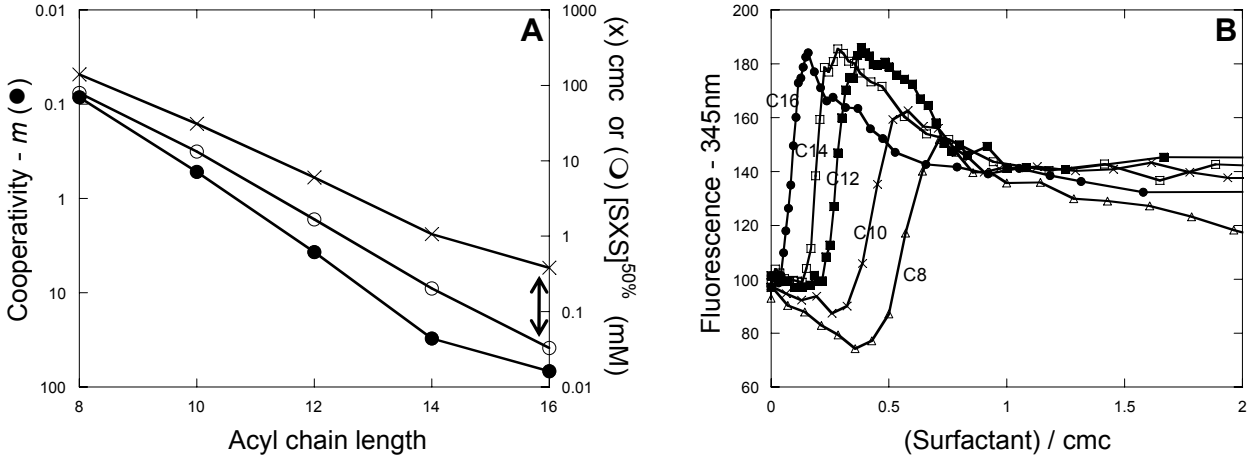

Figure 2. (A) Log plots of cmc and midpoint alkyl sulfate denaturation concentrations $[SXS]^{50\%}$ as function of chain length. The cooperativity of unfolding (*m*) is also included. Data from Table 1. (B) Trp fluorescence emission intensity of ACBP for C8-C16 alkyl sulfates, where surfactant concentration is normalized to cmc. Numbers refer to chain lengths.

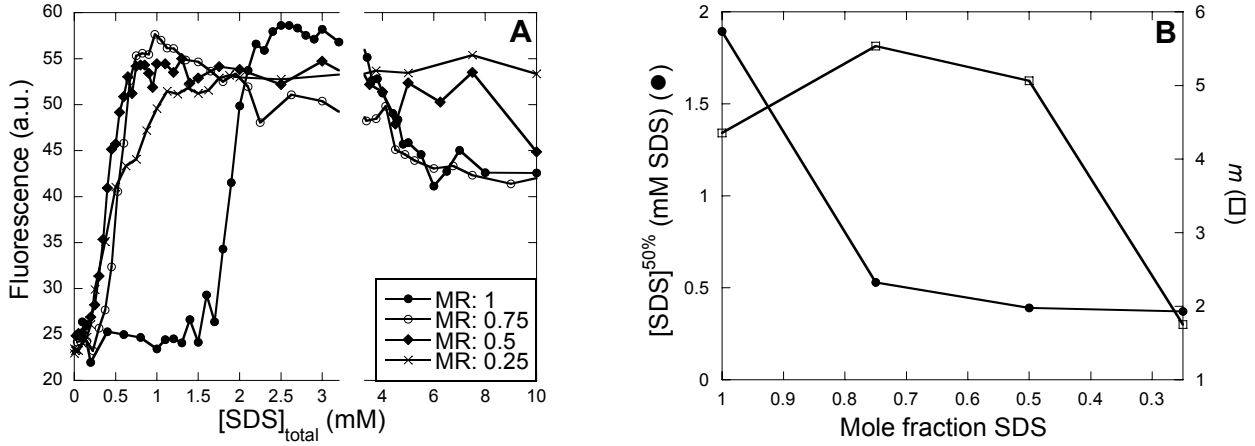

Figure 3. (A) Changes in intrinsic Trp fluorescence emission intensity for ACBP upon titration with mixed micells. (B) The midpoint of SDS denaturation $[SDS]^{50\%}$ and the cooperativity (*m*) plotted as a function of the SDS molar ratio.

potent the denaturation. Our data reveal that denaturation potency (*i.e.* the ability to bind to and induce structural changes in the protein) increases more steeply with chain length than the cmc (which reflects the ability of surfactant monomers to associate and form micelles). In other words, the alkyl sulfate chains have slightly higher affinity for the protein than for each other. Consistent with this, the *m*-values also increase more steeply with chain length than cmc and $[SXS]^{50\%}$ (Fig. 2A), indicating that the surfactants' denaturing efficiency increases faster than the self-association ability. For α-lactalbumin we also observe denaturation below cmc and with increasing divergence from cmc as we increase the chain length [16].

Equilibrium denaturation in mixed micelles show strong dependency on charge density

Data in the previous section and in our previous work [15] indicates that ACBP denaturation by alkyl sulfates is complete by the time the cmc is reached. Thus our data so far only shed light on surfactant monomer (or sub-micellar) activity towards ACBP. In order to focus on the action of micellar species on ACBP under conditions in which monomers are not expected to play a prominent role, we prepared mixed micelles consisting of SDS and the nonionic surfactant dodecyl maltoside (DDM). DDM (cmc 0.17 mM) was chosen due to its prevalence as a model non-ionic detergent and because the acyl-chain has the same length as SDS. Hence the two surfactants differ only in the properties of the head group. The cmc of mixed SDS-DDM micelles remain around 0.2 mM between 0.75 and 0.25 mole fractions [17], so we never have more than 0.2 mM monomeric SDS. Given that monomeric SDS only starts to denature ACBP around 1.3 mM SDS [15], we do not expect monomeric SDS to affect ACBP denaturation which will be wholly induced by micelles. DDM alone has no effect on ACBP (data not shown), due to the general preference of non-ionic surfactants to self-associate rather than bind to proteins. However, Trp fluorescence titration with mixed micelles containing 0.25-0.75 mole fractions SDS showed a double-transition denaturation profile similar to that of neat SDS, with a base line followed by a steep rise in fluorescence and a subsequent decline (Fig. 3A). Just as observed for neat SDS [15], only the first transition gives rise to a change in the far-UV circular dichroism spectrum (data not shown). We conclude that the first transition is initial denaturation, while no change on secondary structure is observed for the second transition. Thus, micelles and monomers appear to denature ACBP by the same two-state mechanism. *A priori*, we cannot rule out that the micellar species rearrange and form hemi-micellar structures on the surface of ACBP in view of the strong affinity of sub-micellar alkyl sulfates for the protein surface. Nevertheless, the mechanism of unfolding must be different since the midpoint of denaturation (expressed in terms of SDS concentration and analyzed according to eq. 1) shifts to significantly lower values for 0.75, 0.5 and 0.25 mole fraction SDS (Fig. 3B) Thus micelles with a preponderance of SDS are more efficient denaturants than monomeric SDS. Nevertheless, the cooperativity of unfolding (also expressed in terms of SDS concentration) only increases slightly from a mole fraction of 1 to 0.75, and declines steeply from 0.5 to 0.25. Thus high denaturing efficiency requires at least an equimolar presence of SDS in the mixed micelles; at lower SDS mole fractions, the micelles interact significantly more weakly with ACBP. Our kinetic studies provide a very detailed extension of this view (see below).

Kinetic studies reveal several modes of unfolding which vary with chain length

Studies on the kinetics of protein denaturation by alkyl sulfates provide useful additional information on the denaturation mechanism, as they allow us to identify changes in rate-limiting steps and study changes in denaturation that occur at concentrations well above the cmc [3, 10, 16, 18, 19]. We have therefore analyzed the kinetics of unfolding in alkyl sulfate detergents of different chain lengths as well as mixed micelles. This is carried out by following the time-course of the change in Trp fluorescence emission intensity when ACBP is

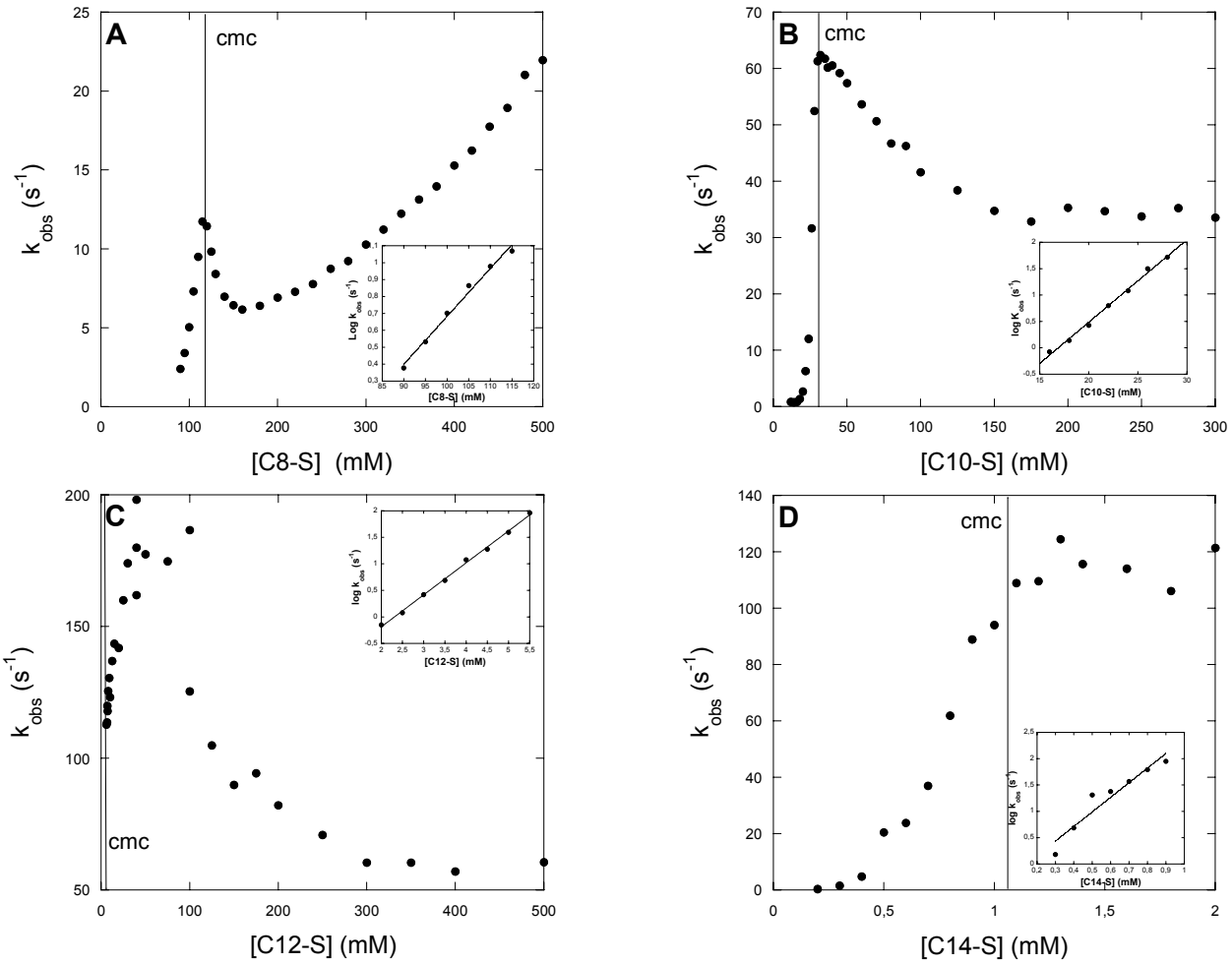

Figure 4. ACBP denaturation kinetics in alkyl sulfates. The unfolding rate constant (k_{obs}) is plotted as function of surfactant and the cmc is indicated with a vertical line. Inserts show the linear dependence on log to the unfolding rate constant vs. surfactant concentration below the cmc. Panels A, B, C and D refer to alkyl chain lengths of 8, 10, 12 and 14 respectively.

mixed with surfactants at different concentrations and fitting the data to single exponential curves to obtain the unfolding rate constant k_{obs}.

Plotting log k_{obs} versus alkyl sulfate concentration reveals several characteristic transitions. The first transition starts at the lowest concentrations where unfolding can be detected, and continues up to a concentration which very precisely coincides with the cmc. In this region we observe a linear rise in log k_{obs} for all alkyl sulfates with slope m_{kin} (Fig. 4A-D inserts). The same type of linear correlation has been observed for chemical denaturants such as GdmCl. log m_{kin} scales linearly with chain length (Fig. 5). The slope of this plot (0.35±0.02) is an indication of how the efficiency of surfactant denaturation capacity grows with the chain length. This value is only very slightly larger than the slope for log cmc versus chain length (0.33±0.01). This indicates that hydrophobic interactions stabilize surfactant-protein contacts and surfactant self-assembly to essentially the same degree, although they are slightly stronger in the former case. The same conclusion was reached from our steady-state measurements (see above).

There are notable differences between denaturation in

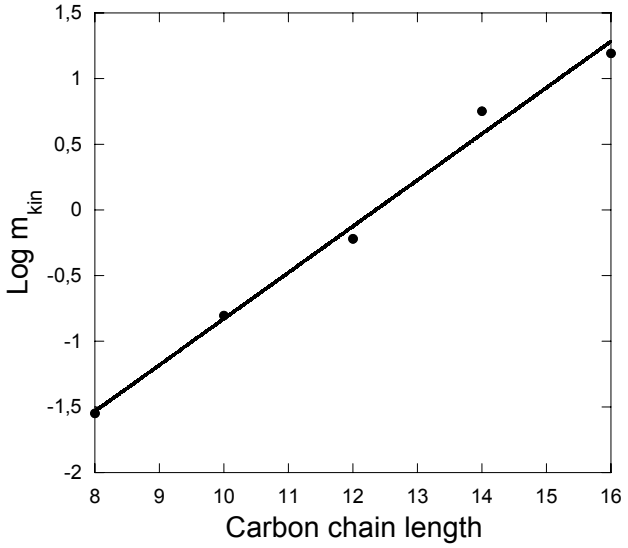

Figure 5. Log of the slope of the fit in Fig. 4 inserts plottet vs. alkyl sulfate chain length. The linear correlation is emphasized by a linear fit.

SDS and GdmCl. Firstly, surfactant denaturation occurs at 50-10.000 fold lower concentrations (depending on the surfactant) than denaturation in GdmCl. Secondly, when we extrapolate log k_{obs} to 0M surfactant, we obtain significantly different values in different surfactants (Table 1), varying by two orders of magnitude. This may reflect subtle differences in the way the surfactants of different chain length bind to ACBP (despite their overall similarity of interactions). Given that binding is very strong and relatively specific at these low concentrations, it is not unreasonable to expect differences at this level. Furthermore, these rate constants are 10^7-10^9 times faster than the rate of unfolding of ACBP in buffer extrapolated from unfolding rate constants in GdmCl [20], which again emphasizes fundamental differences between unfolding mechanisms, and the structure of the denatured state, in GdmCl versus surfactant.

Above the cmc, denaturing kinetics evolve differently depending on the chain length. For SDS, kinetics slowly level off to a plateau value which is reached around 40-60 mM (corresponding to 7-8 x cmc). At higher concentrations of SDS, unfolding kinetics decrease and reach a plateau at around 300 mM. For C8- and C10-sulfates, kinetics do not increase beyond cmc, instead kinetics slows down to a level around 30-50% of the maximal value. For C8-sulfate this is subsequently followed by a rise (Fig. 4A) that is linear in a log-log plot (data not shown). For C14- and C16-sulfate, we cannot measure unfolding kinetics much above cmc due to the surfactants' limited solubility and therefore we do not have data for these transitions.

C8- and C10-sulfate denaturing kinetics differ from SDS-induced unfolding kinetics in that the unfolding kinetics increase above the cmc for SDS while it decreases for C8 and C10 sulfate. This effect may be due to difference in micelle structure/properties. While SDS form spherical micelles at relative low concentrations, a transitions to more elongated micelles takes place at high concentrations [21, 22]. Romani *et al.* [23] have recently determined the transition from spherical to elongated micelles (called cmc_2) to occur at a concentration of 50 mM SDS in the absence of buffer. The very dilute buffer we use (10 mM Tris pH 8.0) only

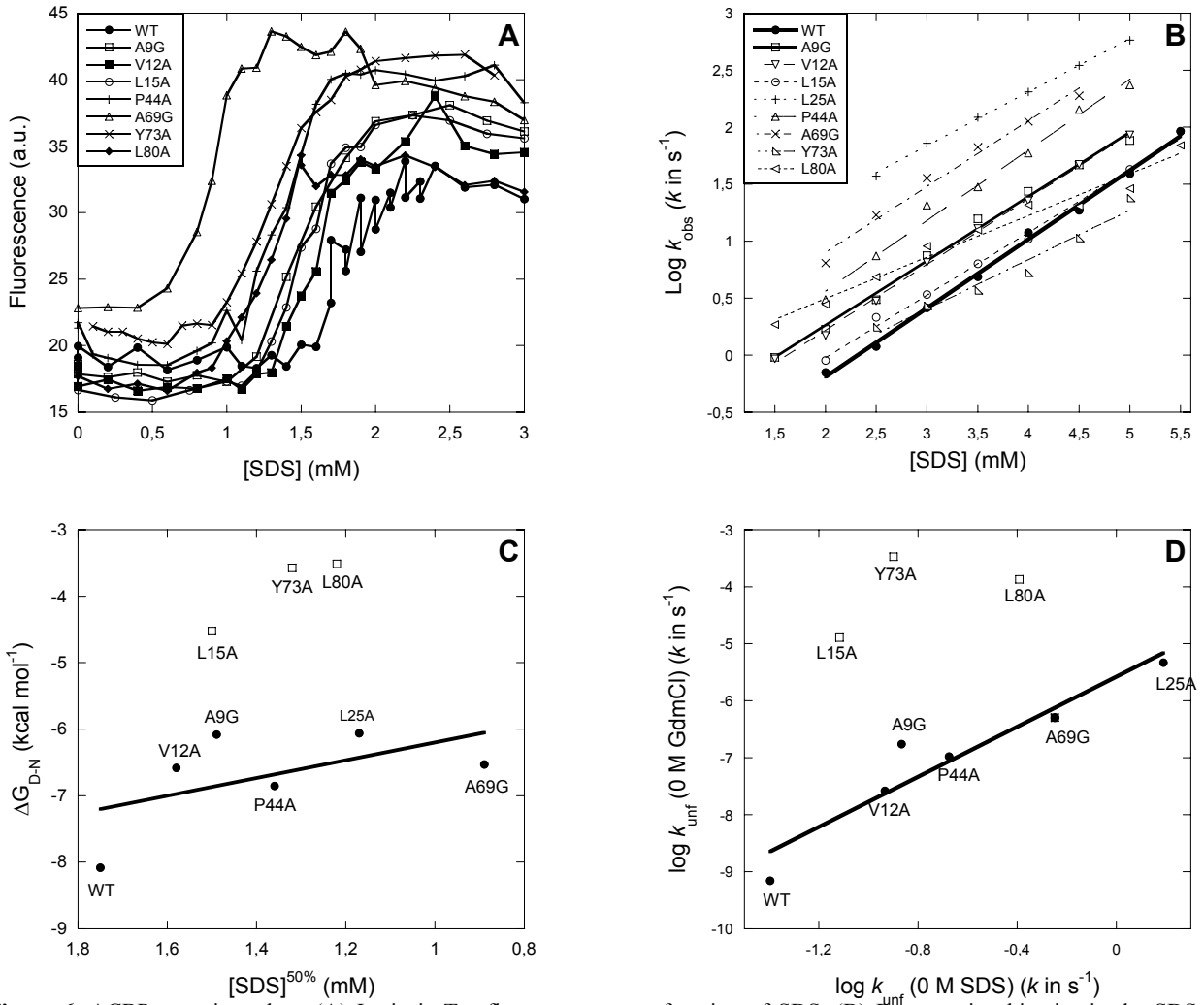

Figure 6. ACBP mutations data. (A) Intrinsic Trp fluorescence as a function of SDS. (B) Denaturation kinetics in the SDS concentration range below the cmc. (C) ΔG_{D-N}values obtained from [31] vs. the $[SDS]^{50\%}$. Mutants are grouped into two populations. WT and the mutants A9G, V12A, L25A, P44A A69G show a linear correlation while L15A Y73A and L80A diverge from this linearity. (D) Unfolding rates constants in 0M GdmCl vs. unfolding rate constants in 0M SDS. As in panel C, mutants can be classified into two groups. WT and the mutants A9G, V12A, L25A, P44A and A69G show a linear correlation while L15A Y73A and L80A diverge from this linearity.

reduces the cmc of SDS from 7 mM in water to 6.0 mM in buffer. Assuming that the buffer reduces cmc_2 to the same extent, we predict a value for cmc_2 around 42 mM in our buffer. This value is quite compatible with our kinetic results, which show that the rate constant for unfolding of ACBP in SDS starts to decline in that concentration range. We have obtained similar results for the unfolding of S6 at low buffer concentrations (Fig. 1A in [18]). This strongly suggests that the appearance of rod-like micelles is responsible for the inhibition of protein unfolding in SDS, simply due to a reduced efficiency of binding and induced conformational changes.

It is unclear whether the power-law rise in k_{obs} observed for C8-sulfate at very high concentrations is related to changes in micellar properties. We have not been able to find any published information about the micellar properties of C8-sulfate at high concentrations. We have observed a similar power-law rise in k_{obs} for the unfolding of several other proteins at concentrations above ~200 mM SDS, namely S6 [18], Tnfn3 and TII27 [19]. However, the transition to power-law rise is delayed to 300-400 mM SDS in the case of CI2 [18] and is completely absent for ACBP in SDS and C10-sulfate. We initially suggested that the power-law rise could be attributed to alterations towards a more elongated micellar structure, but in view of the more recent data presented here and the recent value for cmc_2 provided by Romani *et al.* [23], we have to revise that suggestion. Rather, the power-law rise may reflect the presence of additional weak surfactant-binding sites on the protein surface that only rise to prominence at very high surfactant concentrations. Their effect may be suppressed by the counteracting influence of other binding sites which inhibit protein unfolding. We should emphasize that all these super-cmc phenomena arise as a result of specific interactions between proteins and surfactants which will vary from protein to protein. In dilute Tris buffer, S6 only showed a very modest (ca. 40%) reduction unfolding in SDS (in contrast to the 70% reduction for ACBP), whereas the power-law rise leads to a four-fold increase in k_{obs} between 250 and 500 mM SDS [18]. In the same concentration range, k_{obs} for CI2 only increases by 20% and is constant for ACBP.

Mutant data suggest possible sites of attack by SDS around the ligand binding site

In order to obtain further insight into the role that different side-chains may play in ACBP-SDS interactions, we have analyzed the SDS-induced unfolding of 8 different mutants of ACBP. These mutants, which are based on truncation of hydrophobic side chains distributed randomly within ACBP, have previously been used to study the folding and unfolding of ACBP in denaturants in order to construct a picture of the transition state for folding and unfolding [25]. Given that the unfolding behavior in GdmCl represents the intrinsic unfolding behavior of ACBP, we can in principle identify specific ACBP-SDS interactions by comparing unfolding data in GdmCl and SDS [3]. The SDS parameters we choose to use are the midpoints of unfolding transition 1 (Fig. 6A) and the rate of unfolding at low SDS concentrations where log k_{obs} depends linearly on SDS concentration (Fig. 6B), as summarized in Table 2. These values are then plotted against their GdmCl-based counterparts in Fig. 6C and 6D. For $[SDS]^{50\%}$ the counterpart is the stability of the different mutants (based on equilibrium titration in GdmCl and directly proportional to the midpoint of denaturation in GdmCl); for log k_{obs} (extrapolated to 0 M SDS) the counterpart is the unfolding rate in GdmCl extrapolated to 0 M GdmCl. In both cases we observe a clustering of data. SDS-data for 5 of the mutants (A9G, V12A, L25A, P44A and A69G) correlate well with GdmCl data, whereas 3 other mutants (L15A, Y73A and L80A) form a distinct outlier group. This group shows a much lower unfolding rate constants in SDS – and a much higher SDS midpoint denaturation – than we would predict based on the linear correlations established by the 5 mutants in Fig. 6C and 6D. As we

Table 2. Parameters describing the equilibrium denaturation and kinetics of denaturation of ACBP mutants in SDS. All data at pH 8.0 and 25°C.

Mutant	log $k_{unf}^{0M\ GdmCl}$ [a]	log $k_{unf}^{0\ mM\ SDS}$ [b]	ΔG_{D-N} (kcal mol^{-1}) [a]	$[SDS]^{50\%}$ (mM) [c]	Slope [d]
WT	-9.16	-1.40	-8.08	1.75	0.60
A9G	-6.76	-0.87	-6.08	1.49	0.56
V12A	-7.58	-0.93	-6.58	1.58	0.58
L15A	-4.89	-1.12	-4.52	1.50	0.55
L80A	-3.87	-0.39	-3.51	1.22	0.43
L25A	-5.33	0.19	-6.06	1.17	0.53
P44A	-6.98	-0.68	-6.85	1.36	0.62
A969G	-6.3	-0.25	-6.53	0.89	0.58
Y73A	-3.47	-0.90	-3.57	1.32	0.43

Notes:

[a] Data from [31]

[b] The unfolding rate in the absence of SDS calculated by extrapolating linear fits in Fig. 6B to 0 mM SDS.

[c] The concentration of surfactant at which half of the mutant molecules are denatured. Value obtained by fitting eq. 1 to the Trp fluorescence data describing transition 1 in Fig. 6A.

[d] Slope of fits in Fig. 6B.

have proposed earlier for S6 [3], we would expect that a region of the protein, which is "softened" through initial attack by SDS prior to overall unfolding, would be less sensitive to mutations than regions not bound to SDS before unfolding. This is because such a dynamic region of the protein will not be stabilized by well-defined side-chain interactions.

The two β-sandwich structured protein TnfN3 and TII27 showed that although very similar in protein fold, TII27 could be denatured by SDS monomers while TnfN3 showed very little interaction with monomer SDS and was only denatured in the presence of SDS micelles. We correlated the difference in SDS resistance to the difference in electrostatic potential [19]. In the case of ACBP, there is not a distinct separation of the two classes of mutants identified by our kinetic analysis when mapped onto the protein's structure (Fig. 7). Nevertheless, the three outlier mutants (L15A, Y73A and L80A) are all situated fairly closely in space around the ligand binding site. This region shows a positive electrostatic potential, primarily due to the location of five lysines (13,18, 32, 50 and 54). The side opposite the binding site show large areas of negative electrostatic potential. We have previously suggested that the ligand binding site, due to the positive electrostatic potential, could be the initial site for SDS binding on ACBP and our present kinetic observations are consistent with this [15]. Truncation of side chains in the area which SDS interacts may lead to a more susceptible protein for SDS denaturation. The five other mutants are to a less degree located around the ligand binding site, particularly L25A, P44A and A69G. Though close to the ligand binding site, A9G and V12A are situated in a different area compared to L15A, Y73A and L80A. Thus it is not unreasonable to expect that the five mutations exert their effect on SDS-induced denaturation by a more general effect on protein stability rather than specifically altering initial SDS binding. In contrast, the 3 outlier residues may represent the initial site of attack which is close to the ligand binding site.

The significant differences in unfolding kinetics between the different mutants primarily manifest themselves in the linear plot regions. There is a much smaller variation in the extent to which SDS inhibits unfolding kinetics above the cmc (data not shown). This indicates that the protein conformations induced by SDS at this stage are much less sensitive to specific side chain interactions.

Mixed micelles show similar unfolding kinetics as sub-micellar SDS and highlight the impact of changing micellar compositions

We now describe how mixed micelles of SDS and DDM affect ACBP's unfolding kinetics. Mixed micelles show the same general profile as neat SDS, namely a reasonably linear rise to a plateau level followed by a decrease to another plateau level (Fig. 8A). Thus monomeric SDS is not a prerequisite for the rapid unfolding process that occurs at low surfactant concentrations. However, the SDS concentrations at which the different transitions occur, and the unfolding

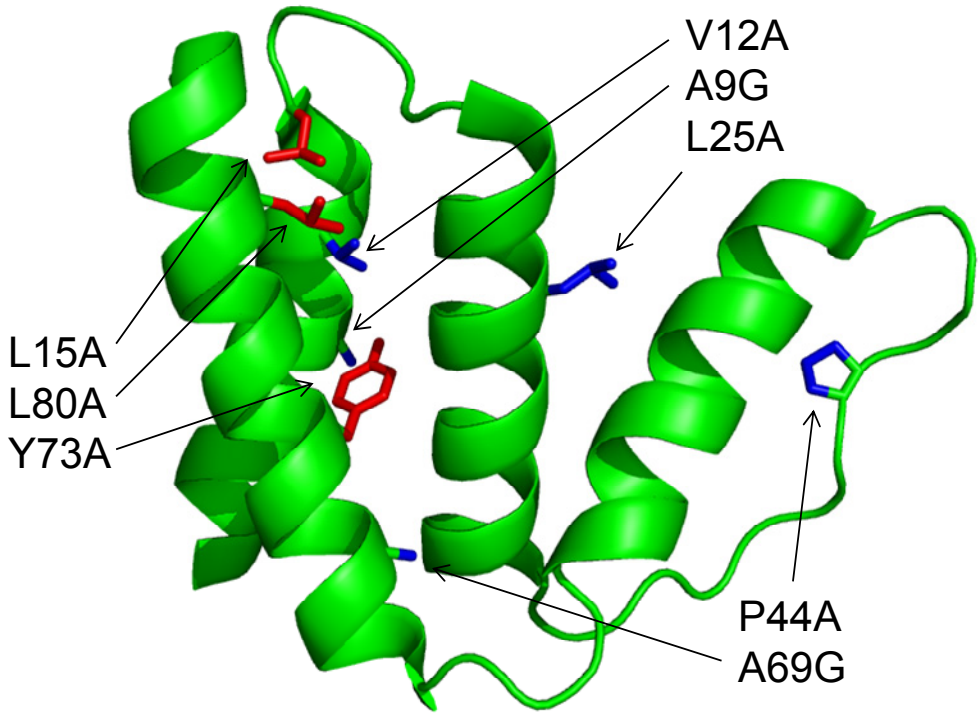

Figure 7. Cartoon representation of ACBP. A9G, V12A, L25A, P44A and A69G mutations are highlighted with blue stick sidechains and L15A Y73A and L80A are highlighted with red stick sidechains. The pdb file 1HB6 was used and presented in Pymol.

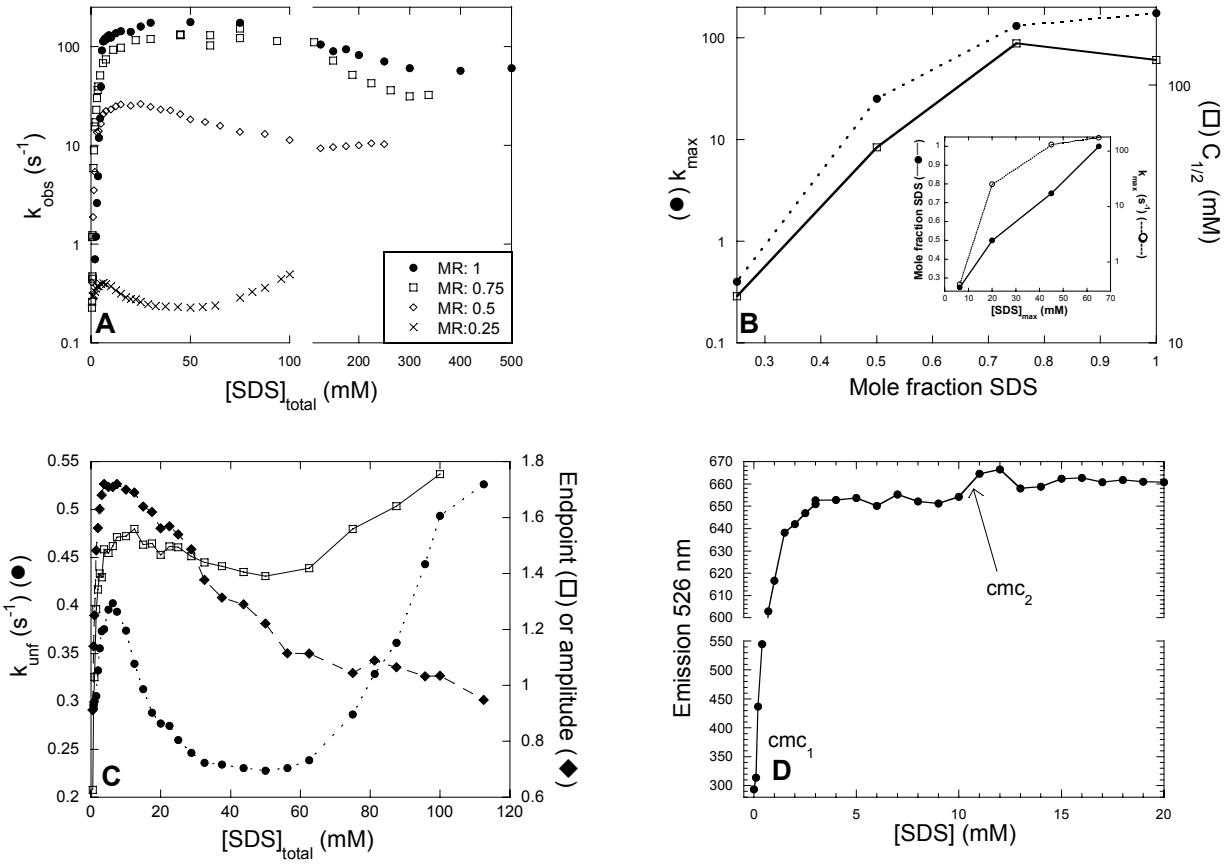

Figure 8. ACBP denaturation kinetics in mixed micelles. (A) Unfolding kinetics at SDS mole ratios of 1(●), 0.75(□), 0.5 (◊) and 0.25 (x). Note that k_{obs} is plotted against the total SDS concentration and not the total surfactant concentration. (B) k_{max}, and $C_{½}$ vs. SDS mole ratio. k_{max} is the unfolding rate constant at which kobs is at its highest and $C_{½}$ is the surfactant concentration where kobs is halfway between k_{max} and the plateau level reached at higher concentrations. Values have been deducted from data presented in Fig. 8A. Insert: the SDS concentration where unfolding is fastest (determined from data in panel A) plotted versus mole fraction of SDS. (C) Unfolding kinetics and the associated amplitude and endpointat a SDS mole ratio of 0.25. (D) Change in acridine orange fluorescence emission as a function of SDS concentration in mixed micelles with an SDS mole ratio of 0.25.

rate constants, vary significantly. Both the maximal rate constant of unfolding (k_{max}) and the midpoint of the second transition ($C_{1/2}$) are reasonably constant for SDS mole fractions 1 and 0.75 but decline at lower mole fractions (Fig. 8B), in the case of k_{max} by more than two orders of magnitude. A similar correlation is obtained (data not shown) if we use the plateau unfolding rate constant (the value of k_{obs} reached at high SDS concentrations after k_{max} starts to decline). Further, the SDS concentration at which k_{max} occurs increases linearly with SDS mole fraction and also increases with log k_{max} (insert to Fig. 8B). Put simply, as we increase the mole fraction of SDS, we also increase the concentration range over which the unfolding rate constant can increase, and consequently we can reach a higher k_{max}.

Although there are only data points for 4 different mole fractions of SDS in Fig. 8B, the individual points are determined with great reliability based on an extensive series of measurements in Fig. 8A. It is clear that the correlation between SDS mole fraction and log k_{max} is not linear, but rather hyperbolic. It is interesting to speculate about the basis of this type of correlation. Pioneering work by Bowie and co-workers on the equilibrium denaturation of membrane proteins such as diacyl glycerate kinase [26] and bacteriorhodopsin [27] in mixed micelles of SDS and DDM suggest a simple linear correlation between SDS mole fraction and the free energy of unfolding. This correlation can be transferred to the analysis of the kinetics of unfolding (where the activation energy of unfolding is proportional to log k of unfolding), as has been shown by ourselves [28, 29] and Booth and co-workers [30]. Such a correlation may be rationalized by the fact that membrane proteins have well-defined binding sites for surfactant micelles, defined by the hydrophobic belt of amino acids that is inserted into the membrane. Therefore mixed micelles can be expected to bind to the native state in much the same way irrespective of their composition, justifying a straightforward comparison between micelles with different SDS compositions. Any change in stability or unfolding kinetics will reflect the impact of an altered amount of SDS "seen" by the protein within the micelle, without having to invoke any micellar rearrangements. In contrast, there are no intrinsic pre-defined micellar binding sites on globular proteins such as ACBP and therefore it is likely that as we alter the micellar composition we will also alter the

relative micelle-binding affinities of different regions of ACBP. This will affect the whole denaturation process and is the most likely reason for the deviation from a simple linear relationship that we observe in Fig. 8B. Micelles containing only DDM do not interact at all with ACBP, and therefore increases in SDS contents at low SDS mole fractions will lead to a series of micelles with a steeply increasing affinity for ACBP and with an opportunity to sample many different binding sites. Above a certain mole fraction SDS, however, we suggest that the impact of changing SDS contents will not lead to significantly altered binding sites. This will lead to a more modest increase in unfolding rate with increasing SDS mole fraction. Although we predict that the same hyperbolic relationship seen in Fig. 8B will be observed for other globular proteins, it is very likely that the sequence and structure of the protein in question, and thus the potential binding sites for micelles, will affect the specific shape of the hyperbolic curve.

Note that these reflections base themselves solely on our kinetic measurements. Our equilibrium measurements for the first transition of unfolding in mixed micelles (Fig. 3) do not show such a dramatic variation in denaturation properties with changing mole fractions (data for neat SDS cannot be included as SDS does not form micelles during the first denaturation transition), indicating that differences between mixed micelles are mainly a question of how they initially "attack" and denature ACBP. As well as highlighting the usefulness of kinetic data for differentiating micelle effects, this also re-emphasizes the difference between globular proteins and membrane proteins, since equilibrium denaturation is a highly informative analytical approach for the latter [27].

The power-law rise may be based on weak protein-surfactant interactions

Interestingly, data at a molar ratio of 0.25 SDS show the same power-law rise at higher surfactant concentrations as we observe for C8-alkyl sulfate. In both cases, the unfolding rate constant, from which the power-law rise starts out, is very low. This suggests a very high activation barrier which can be reduced by micellar changes occurring at high surfactant concentrations. It is remarkable that these kinetic phenomena are induced by micelles which reduce affinity towards ACBP by two very different means, namely by weakening either hydrophobic or electrostatic interactions. In both cases we see that when an attractive interaction is weakened (as indicated by a low unfolding rate constant), other modes of binding can more easily manifest themselves at higher surfactant concentrations. This indicates that both hydrophobicity and electrostatics are central for interactions between micelles and proteins.

More insight into these processes can be obtained by co-plotting k_{obs}, the amplitude and the end-point of the unfolding reaction versus surfactant concentration for the 25% SDS data (Fig. 8C). The amplitude is the difference in fluorescence between the start- and end-point of the reaction we monitor in our stopped-flow apparatus and thus provides an indirect measure of the degree of structural change associated with unfolding, as well as the degree to which this reaction goes to completion. At low concentrations of SDS (up to 5 mM) the amplitude and end-point increase to a plateau level in parallel with k_{obs}, reflecting the fact that more and more of the protein unfolds as we increase SDS concentration (cfr. Fig. 3A). As we increase the SDS concentration from 5 to ~50 mM, both k_{obs} and the amplitude decrease while the end-point remains relatively constant. This can be rationalized as the gradual accumulation of a different type of micelle over this concentration range, which binds to ACBP in a different manner at the beginning of the unfolding reaction, although the end state is relatively unaffected. We have used the acridine orange fluorescence assay reported by Romani *et al.* [23] to determine the concentration cmc_2 at which elongated micelles appear in these mixed micelles (Fig. 8D). This occurs around 10-12 mM SDS which corresponds nicely to the decline in unfolding rate constants, and suggests that the elongated micelles are also responsible for decreasing rate constants even when the proportion of SDS has decreased to a very modest level. It is only as we increase the concentration of SDS_{total} above ~60 mM, and the k_{obs} values start to rise, that the end-species starts to change in fluorescence, while the amplitude now remains relatively constant. This indicates that it is now the end species, rather than the starting species, that is changed by the altered surfactant concentration.

Similar correlations between unfolding rate constants, amplitudes and endpoint values can be observed for unfolding of ACBP in C8-sulfate (data not shown). These data provide an indication of the many subtle changes that occur in protein-detergent interactions with increasing surfactant concentration.

SUMMARY

We undertook this study to explore the correlation between alkyl chain length, micellar charge and denaturation potency towards the protein ACBP. As expected, alkyl sulfates with longer chain lengths and lower cmc values denature ACBP at lower concentrations than the shorter chains; in addition, they also generally give rise to faster denaturation kinetics. However, below cmc all surfactants show the same linear correlation between log k_{unf} and surfactant concentration with slopes that correlate with chain length, indicating a fundamentally similar denaturation mechanism in this range. This linear increase in unfolding rates by monomeric surfactants is halted by the formation of micelles which lead to a marked decrease in folding rates. For SDS, the decline only occurs at concentrations well above cmc and may be attributed to the formation of rod-like micelles with weaker binding affinity as well as the ability to bind to ACBP in multiple modes, some of which can slow down unfolding. We observe that the decline already starts at the cmc in the case of shorter chain length micelles, suggesting that these micelles have a weaker

binding affinity from the beginning. Diluting out SDS with non-ionic surfactants makes the transition to rod-like micelles occur at lower concentrations and also brings on an earlier decline in the unfolding rate constant. For both short-chain surfactants and mixed micelles with reduced charge, the very low unfolding rates give way to a power-law increase in unfolding rates at higher surfactant concentrations which we attribute to the existence of high activation barriers that allow alternative binding sites on the protein surface to emerge. Furthermore, the non-linear response of unfolding rate constants to SDS mole fractions suggests the existence of a range of different binding regions on the ACBP surface, depending on the SDS mole fraction. Thus, a clear conclusion we can draw from these studies is that the overall hydrophobic and electrostatic attraction of micelles for ACBP has a very strong effect on the denaturation mechanism.

MATERIALS AND METHODS

Materials: Tris(hydroxymethyl)aminomethane (Tris) and sodium dodecyl sulfate (SDS) were from AppliChem (Darmstadt, Germany). Pyrene was from Sigma-Aldrich (St. Louis, MO). N-dodecyl-β-D-maltoside was from Calbiochem (San Diego, CA). Sodium n-Octyl-, decyl-, hexadecyl- and tetradecyl-sulfate were from Lancaster synthesis. All chemicals were of molecular biology grade. Native ACBP was prepared as described [12], and ACBP mutants were a kind gift from Flemming M Poulsen.

Spectroscopic measurements: All experiments were conducted in 10 mM Tris pH 8.0 at 25 ^{o}C using 2 μM ACBP unless otherwise stated. Solutions were left to equilibrate in surfactant at 25 °C for at least 30 min before recording spectra. All spectra were recorded as the average of three emission scans in a 10 mm quartz cuvette (Hellma) with a slit width of 10 nm and a scanning speed of 200 nm/min.

Tryptophan fluorescence: ACBP's two tryptophan residues (Trp55 and Trp58) in helix 3 are good intrinsic probes of the tertiary structure. Steady-state fluorescence measurements were performed on a LS-55 Luminescence spectrometer (Perkin-Elmer Instruments, UK), using slit with of 10 nm, an excitation wavelength of 295 nm and measuring the emission between 310-400 nm.

Pyrene interactions: Pyrene is a very hydrophobic molecule, whose very low solubility in water (2-3 μM) drives it to partition into available hydrophobic phases such as micelles or surfactant molecule clusters on the protein surface. The fluorescence emission spectrum of pyrene is sensitive to the polarity of the microenvironment [13]. Thus the ratio between pyrene emission at 372.5 and 383.5 nm (I_3/I_1) makes it possible to determine whether pyrene is in a hydrophilic environment (I_3/I_1 ratio ~0.65) or a hydrophobic environment such as the interior of a micelle (I_3/I_1 ratio ~0.95) or clusters of surfactant on the protein surface (I_3/I_1 values between 0.65 and 0.95). A stock solution of 200 μM pyrene in ethanol was made and added to the surfactant samples to a final concentration of 1 μM. Pyrene was excited at 335 nm and emission between 350-440 nm was monitored. Excitation/emission slit withs of 5/3.5nm were used.

Acridine orange fluorescence: A stock solution of 5 mM acridine orange in ethanol was diluted to 20 μM in the presence of different total concentrations of 1SDS:3 DDM (mole:mole). Excitation was at 420 nm and emission at 526 nm.

Stopped-flow unfolding kinetics: Unfolding kinetics were studied on a SX18MV stopped-flow microanalyzer (Applied Photophysics, Leatherhead, UK) in a thermostatically controlled sample-handling unit. ACBP and surfactant were mixed 1:10 to a final protein concentration of 2 μM, samples were excited at 280 nm, and the emission above 320 nm was monitored using a cut-off filter. The observed kinetics were satisfactorily fitted to single exponential functions. In a few instances an only at low surfactant concentrations, inclusion of a second exponential improved the quality of the fit; however, this relaxation phase did not appear consistently and only constituted up to 10% of the total amplitude.

Two-state unfolding: Sub-micellar denaturation by alkyl sulfates and mixed micelles was analyzed empirically according to a two-state model for unfolding from the native to the denatured state [14]:

$$F = \frac{F_{end} + F_{start} * 10^{(-m([\mathrm{surf}]-[\mathrm{surf}]^{50\%})}}{1+10^{(-m([\mathrm{surf}]-[\mathrm{surf}]^{50\%})}} \qquad (1)$$

where F is fluorescence emission intensity, F_{start} and F_{end} are the start and end levels of fluorescence, $[\mathrm{surf}]^{50\%}$ is the midpoint concentration of denaturation and m is a parameter describing the general sensitivity of unfolding to SDS concentration. This equation is based on the unfolding of proteins in chemical denaturants and the assumptions underlying the equation are not necessarily valid for unfolding in surfactant. Eq. 1 is only used to obtain values of $[\mathrm{surf}]^{50\%}$ and m for comparative purposes.

AKCNOWLEDGEMENTS

K.K.A. is supported by Aalborg University and by a stipend provided by the innovation consortium BIOPRO, financed by the Danish Ministry of Science, Innovation and Technology. We thank Professor Peter Westh, Professor Jan Skov Pedersen and Dr. Cristiano Oliveiro as well as Dr. Torben Madsen for general discussions about protein-detergent interactions and Professor Flemming M. Poulsen for very generously providing purified ACBP mutants.

REFERENCES

[1] Putnam, F. W., *The Interactions of Proteins and Synthetic Detergents.* . Advan. Protein Chem 1948. 4: p. 79-122.

[2] Randolph, T. W. and Jones, L. S., *Surfactant-protein interactions.* Pharm. Biotechnol., 2002. 13: p. 159-175.
[3] Otzen, D. E. and Oliveberg, M., *Burst-phase expansion of native protein prior to global unfolding in SDS.* J. Mol. Biol., 2002. 315(2096): p. 1231-40.
[4] Cunningham, E. L., Jaswal, S. S., Sohl, J. L., and Agard, D. A., *Kinetic stability as a mechanism for protease longevity.* Proc Natl Acad Sci U S A, 1999. 96(20): p. 11008-14.
[5] Kragelund, B. B*., et al.*, *Conserved residues and their role in the structure, function, and stability of acyl-coenzyme A binding protein.* Biochemistry, 1999. 38(8): p. 2386-94.
[6] Kragelund, B. B., Robinson, C. V., Knudsen, J., Dobson, C. M., and Poulsen, F. M., *Folding of a four-helix bundle: studies of acyl-coenzyme A binding protein.* Biochemistry, 1995. 34(21): p. 7217-24.
[7] Nielsen, M. M., Andersen, K. K., Westh, P., and Otzen, D. E., *Unfolding of beta-sheet proteins in SDS.* Biophys J, 2007. 92(10): p. 3674-85.
[8] Otzen, D. E., *Protein unfolding in detergents: effect of micelle structure, ionic strength, pH, and temperature.* Biophys J, 2002. 83(4): p. 2219-30.
[9] Otzen, D. E., Nesgaard, L., Andersen, K. K., Hansen, J. H., Christiansen, G., Doe, H., and Sehgal, P., *Aggregation of S6 in a quasi-native state by monomeric SDS.* Biochim Biophys Acta, 2008. 1784: p. 400-414.
[10] Andersen, K., Westh, P., and Otzen, D. E., *A global study of myoglobin-surfactant interactions.* Langmuir, 2008. 15(4078): p. 399-407.
[11] Manning, M. and Colón, W., *Structural basis of protein kinetic stability: resistance to sodium dodecyl sulfate suggests a central role for rigidity and a bias toward beta-sheet structure.* Biochemistry, 2004. 43(3612): p. 11248-11254.
[12] Mandrup, S., Hojrup, P., Kristiansen, K., and Knudsen, J., *Gene synthesis, expression in Escherichia coli, purification and characterization of the recombinant bovine acyl-CoA-binding protein.* Biochem J, 1991. 276 (Pt 3): p. 817-23.
[13] Kalyanasundaram, K. and Thomas, J. K., *Environmental Effects on Vibronic Band Intensitiesin Pyrene Monomer Fluorescence and Their Application in Studies of Micellar Systems.* Journal of the American Chemical Society, 1976. 99:7: p. 2039-2044.
[14] Pace, C. N., *Determination and analysis of urea and guanidine hydrochloride denaturation curves.* Methods Enzymol., 1986. 131(874): p. 266-279.
[15] Andersen, K. K., Larsen, K. L., Poulsen, F. M., Callisen, T. H., Westh, P., Oliveira, C. L. P., Pedersen, J. S., and Otzen, D. E., *The role of decorated micelles in sub-cmc protein denturation and association.* 2008. Submitted.
[16] Otzen, D. E., Sehgal, P., and Westh, P., *a-lactalbumin is unfolded by all classes of detergents but with different mechanisms.* J. Coll. Int. Sci., 2008. In press.
[17] Sehgal, P., Mogensen, J. E., and Otzen, D. E., *Using micellar mole fractions to assess membrane protein stability in mixed micelles.* Biochim Biophys Acta, 2005. 1716: p. 59-68.
[18] Otzen, D. E., *Protein unfolding in detergents: Effect of micelle structure, ionic strength, pH, and temperature.* Biophys. J., 2002. 83(2097): p. 2219-2230.
[19] Nielsen, M. M., Andersen, K. K., Westh, P., and Otzen, D. E., *Unfolding of b-sheet proteins in SDS.* Biophys. J., 2007. 92(4613): p. 3674–3685.
[20] Kragelund, B. B., Robinson, C. V., Knudsen, V., Dobson, C. M., and Poulsen, F. M., *Folding of a four-helix bundle: Studies of acyl-coenzyme A binding protein.* Biochemistry, 1995. 34(801): p. 7217-7224.
[21] Croonen, Y., Geladé, E., Van der Zegel, M., Van der Auweraer, M., Vandendriessche, H., De Schryver, F. C., and Almgren, M., *Influence of salt, detergent concentration and temperature on the fluorescence quenching of 1-methylpyrene in sodium dodecyl sulfate with m-dicyanobenzene.* J. Phys. Chem., 1983. 87(2226): p. 1426-1431.
[22] Clint, J. H., *Surfactant aggregation*. 1992, New York: Chapman & Hall.
[23] Romani, A. P., da Hora Machado, A. E., Hioka, N., Severino, D., Baptista, M. S., Codognoto, L., Rodrigues, M. R., and de Oliveira, H. P., *Spectrofluorimetric Determination of Second Critical Micellar Concentration of SDS and SDS/Brij 30 Systems.* J Fluoresc, 2008.
[24] Stoner, M. R., Dale, D. A., Gualfetti, P. J., Becker, T., and Randolph, T. W., *Surfactant-induced unfolding of cellulase: kinetic studies.* Biotechnol Prog, 2006. 22(1): p. 225-32.
[25] Kragelund, B. B., Osmark, P., Neergaard, T. B., Schiødt, J., Kristensen, K., Knudsen, J., and Poulsen, F. M., *The formation of a native-like structure containing eight conserved hydrophobic residues is rate-limiting in two-state protein folding of ACBP.* Nature Struct. Biol., 1999. 6(2227): p. 594-601.
[26] Lau, F. W. and Bowie, J. U., *A method for assessing the stability of a membrane protein.* Biochemistry, 1997. 36(2153): p. 5884-5892.
[27] Faham, S., Yang, D., Bare, E., Yohannan, S., Whitelegge, J. P., and Bowie, J. U., *Side-chain contributions to membrane protein structure and stability.* J. Mol. Biol., 2004. 335(3416): p. 297-305.
[28] Otzen, D. E., *Folding of DsbB in mixed micelles: A kinetic analysis of the stability of a bacterial membrane protein.* J. Mol. Biol., 2003. 330(3113): p. 641-649.
[29] Sehgal, P. and Otzen, D. E., *Thermodynamics of unfolding of an integral membrane protein in mixed micelles.* Prot. Sci., 2006. 15: p. 890-9.

[30] Curnow, P. and Booth, P. J., *Combined kinetic and thermodynamic analysis of a-helical membrane protein unfolding.* Proc. Natl. Acad. Sci. U.S.A., 2007. 104(4576): p. 18970-18975.

[31] Kragelund, B. B., Osmark, P., Neergaard, T. B., Schiodt, J., Kristiansen, K., Knudsen, J., and Poulsen, F. M., *The formation of a native-like structure containing eight conserved hydrophobic residues is rate limiting in two-state protein folding of ACBP.* Nat Struct Biol, 1999. 6(6): p. 594-601.

Paper VI

Thermomyces lanuginosus Lipase is a kinetically stable enzyme

Thermomyces lanuginosus Lipase is a kinetically stable enzyme

Andersen K.K.[1,2], Sehgal P.[2,3], Callisen, T.[4] Westh P.[5], Otzen D.E.[1,2*].

[1] Interdisciplinary Nanoscience Centre, University of Aarhus, Gustav Wieds Vej 10C, DK – 8000 Aarhus C.
[2] Department of Life Sciences, Aalborg University, Sohngaardsholmsvej 49, DK-9000 Aalborg, Denmark
[3] Present address: Department of Biochemistry and Biomedical Sciences. McMaster University, Room 4H41 Health Sciences Centre, 1200 Main Street West, Hamilton, ON, Canada,L8N 3Z5.
[4]Novozymes A/S, DK-2880 Bagsværd, Denmark
[5] NSM Functional Biomaterials, Roskilde University, P.O. Box 260, DK-4000 Roskilde, Denmark

* To whom correspondence should be addressed. Tel. + 45 89425946, fax +4586123178, e-mail dao@inano.dk.

Work in progress

ABSTRACT

***Thermomyces lanuginosus* Lipase (TlL) is a commercially available enzyme that catalyzes the hydrolysis of triglycerides. The enzyme is able to work under harsh chemical conditions which denature most other proteins. In this study we describe TlL resistance towards denaturation by both the ionic surfactant sodium dodecyl sulfate (SDS) and the nonionic surfactant decyl maltoside (DM). TlL is a kinetically stable protein that shows pronounced hysteresis in its folding behavior. It remains folded (albeit destabilized in the case of SDS) and enzymatically active in the presence of 10 mM surfactant and higher; however, sub-mM concentrations of the same surfactants are sufficient to prevent refolding and regain of enzymatic activity from the low pH urea-denatured state. Despite their inability to denature native lipolase, both SDS and DM bind to this state, leading to subtle changes in tertiary structure. However, isothermal titration calorimetry indicates an unusually low degree of SDS binding to lipolase. Only 23 molecules are found to bind to one TlL molecule, equivalent to 0.23 gram SDS pr gram TlL. This is significantly less than the reported 1.4 gram SDS pr gram protein normally observed. In combination with the extremely low unfolding rate (84 days in water, comparable to other kinetically stable proteins), this demonstrates that TlL retains kinetic stability over a range of different denaturant conditions.**

Keywords: surfactant binding, SDS, decyl maltoside, folding, hysteresis, enzyme activity.

INTRODUCTION

Most proteins are able to unfold and refold reversibly on the time scale of seconds to minutes. Within transition state theory, this is interpreted to mean that the activation barrier separating the folded and denatured state is relatively low, allowing the protein to rapidly access the state that is thermodynamically most stable under the given conditions. However, in some cases, proteins are able to retain their native structure and activity under denaturing conditions (*e.g.* high concentrations of denaturant or charged surfactant), despite an inability to fold from the denatured to the native state under these same conditions. This phenomenon, which is termed kinetic stability, entails a high transition barrier from the folded state to the unfolded state. Such a high energy barrier is reflected in a very slow conversion from the native state to the denatured/inactive state. At sufficiently slow conversion rates the protein is to all intents and purposes completely trapped in the native state [1, 2].

There is nothing intrinsically mysterious about kinetic stability, since it simply involves a very high activation barrier between the folded and unfolded states, *i.e.* a highly unstable transition state for the rate-limiting step in folding and unfolding. Nevertheless the structural factors that determine kinetic stability are not well known. There are several indications that long range interactions as well as rigidity play an important role [1]. Thus no all α-helix proteins have reported to be kinetically stable; rather, all kinetically stable proteins reported so far have a high content of β-sheet structure. α-helix interactions tend to be local, *i.e.* close in the primary sequence and α-helical structure can be retained for isolated regions of a protein despite a loss of tertiary interactions. In contrast β-sheet interactions are more global and tend to form only late in the folding process; conversely their unraveling requires extensive unfolding. All this may play a role for the way in which denaturants are able to bind and denature the proteins. For example, proteins denatured in surfactants such as SDS tend to adopt α-helical structures [3] and individual α-helices have been identified as the initial site of attack in a protein engineering study of the denaturation of the mixed α/β protein S6 [4]. There are also reports of oligomeric (usually β-sheet rich) structures that are kinetically stable, although the individual proteins are not [5]. This again suggests that long range interactions are important for kinetic stability, as well as rigidity (or a network of cooperative and mutually stabilizing

interactions), which will be increased in oligomeric assemblies.

Although the kinetically stable proteins found to date usually have a high degree of β structure it does not mean that all proteins with β structure are kinetically stable, as illustrated by our own studies of the two β sandwich protein TII27 and TnfN3 [6]. Despite sharing the same fold, the two proteins show different properties towards SDS denaturation. TII27 could be denatured by SDS monomers while Tnfn3 was only denatured in the presence of SDS micelles. The underlying effect of β structure was however evident in that the unfolding kinetics were significantly slower than the α-helix-containing proteins we have studied, namely the mixed α/β proteins S6 and CI2 [4, 7] and the all-α-helix myoglobin [8].

In this study we investigate the kinetic stability of the 269-residue lipase (triacylglycerol acylhydrolase) from *Thermomyces langinosus*. TlL finds widespread use in the detergent industry due to its resistance to inactivation under harsh washing conditions. Its ability to remain active at surfactant concentration that normally denature most other proteins, suggested to us that TlL might be kinetically stable. We have previously shown that it can be activated as well as inhibited by surfactants [9], reflecting the presence of a helix forming a flexible lid over the active site. The lid needs to be opened to allow substrate access and this opening, which is triggered by adsorption onto an interface or substrate, clearly alters the overall flexibility of the protein and thus susceptibility to surfactants. TlL has a mixed α/β fold and a catalytic triad composed of Ser, Asp, and His, similar to what is found in serine proteases. It also contains three disulfide bridges that stabilize the tertiary structure and four tryptophans which are useful probes of changes in tertiary structure.

Here we show that TlL is a kinetic stable protein that resists SDS denaturation. While TlL interacts with both ionic and nonionic surfactants the enzyme does not undergo denaturation. The unfolding rate in water is very slow with a half rate of ~80 days, indicating very high activation barrier associated with unfolding. As a consequence TlL is trapped in the native state. This indicates a high activation barrier to unfolding which is supported by folding experiments:

Full activity is obtained when refolding the protein in the absence of surfactants; however, low concentrations of surfactant are sufficient to block refolding from the denatured state.

RESULTS

In this study we attempt to elucidate the properties that enable the *Thermomyces lanuginosus* Lipase (TlL) to remain active in the presence of surfactants that normally denature most proteins. We focus predominantly on the stability of TlL in surfactants, since these are most relevant for the protein's functional environment as a detergent enzyme. Further, its biological activity towards triglycerides generates carboxylic acids which also have surfactant properties.

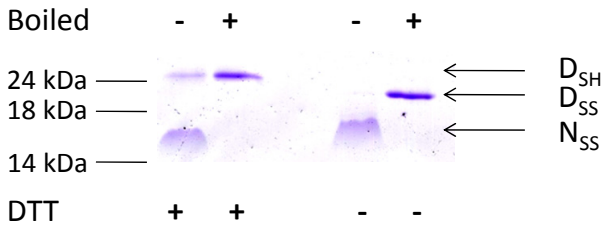

Figure 1. SDS-PAGE assay of kinetic stability. Native TlL with intact disulphide bridges are denoted Nss. Denatured TlL with intact or DTT reduced disulphide bridges are denoted D_{SS} and D_{SH} respectively. B or U indicates boiled or unboiled samples.

Migration patterns in SDS-PAGE suggest kinetic stability

SDS/PAGE provides a rapid way to screen for kinetic stability [1, 2]. The SDS (2%) present in the sample buffer will denature kinetically unstable proteins, whereas kinetically stable proteins will not denature unless boiled prior to loading. (A few proteins are sufficiently stable to resist even SDS boiling; however, such proteins tend to be involved in higher order structures such as functional amyloid [12] and will therefore typically not even enter the separation gel). Unfolding will lead to a band shift on the gel, since the unfolded state will be able to bind more SDS and also have an altered hydrodynamic radious compared to the native state. We performed these experiments with and without 100 mM (final concentration) of the reducing agent DTT. As shown in Fig. 1, the boiled but non-reduced sample migrates differently than the non-boiled sample, providing the first indication that TlL is a

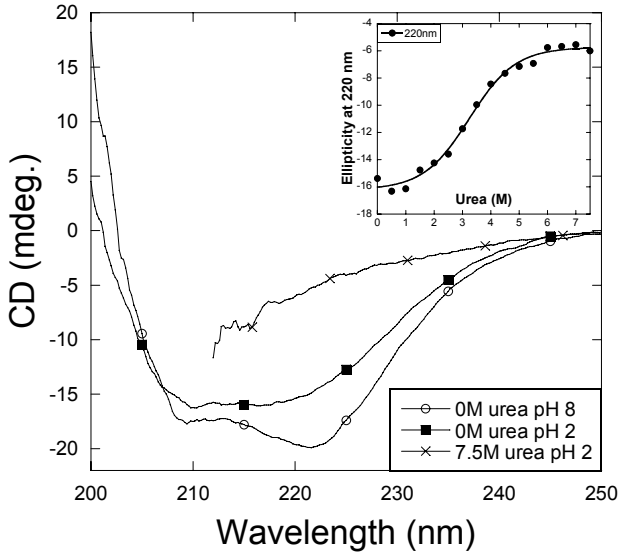

Figure 2. pH and urea unfolding of TlL. Far-UV CD spectra of TlL at pH 8 (O), pH 2 (■) and 7.5 M urea pH 2 (x). Spectra at pH 8 show native secondary structure while some structure has been lost at pH 2. Addition of 7.5 M urea at pH 2 results is random coils secondary structure. The transition to random coil is illustrated in the insert where the ellipticity at 220 nm is plotted as a function of urea.

kinetically stable protein. Reduction of the three disulfide bonds by DTT decreases the mobility of the boiled sample, because reduced TlL can be denatured to a higher degree due to the loss of its three disulfide bonds, and thus attain a greater hydrodynamic radius, restricting its mobility on the gel. In addition to the band corresponding to native TlL, the non-boiled reduced TlL sample also contained a small amount of denatured TlL, indicating that a small proportion of reduced TlL can be denatured without boiling. This highlights the importance of disulphide bonds for TlL's kinetic stability.

TlL is trapped in different conformations in the presence of surfactants, depending on starting conditions

A more systematic analysis of the kinetic stability of TlL and the presence of a very high activation barrier requires us to demonstrate that the protein is not subject to the principle of microscopic reversibility, that is, the protein does not reach the same structural/functional state independent of the starting conditions. Thus we need to compare the structure and activity of TlL at a range of surfactant concentrations, starting out from conditions where the protein is initially either in the native state or in the denatured state. As surfactants we use both SDS (already tested qualitatively on SDS-PAGE in the previous section) and the non-ionic surfactant decyl maltoside (DecM). Denaturation of TlL cannot be accomplished by high concentrations of urea at neutral pH or by lowering the pH (data not shown); however, a combination of the two (namely urea in 10 mM Glycine pH 2.0) leads to the formation of a random coil structure with a midpoint of 3.24 M urea (Fig. 2). We therefore use a combination of 10 mM Gly pH 2 and 6 M urea to unfold TlL.

We start our equilibrium experiments by titrating native TlL with SDS and DecM in 10 mM Tris pH 8 and monitoring the reaction using Trp fluorescence (Fig. 3A and B). These titrations indicate that TlL interacts with SDS and DecM monomers as well as micelles. For SDS there is a small but significant increase in tryptophan fluorescence in the monomer range 0 ~ 0.5 mM which then levels out around 4 mM SDS, after which we observe a major decrease in fluorescence (Fig. 3B). This decrease correlates very well with the formation of SDS micelles as shown by pyrene fluorescence. In the absence of TlL, the pyrene I_3/I_1 ratio changes from ~0.65 to ~0.93 when pyrene partitions into SDS micelles, indicating micelle formation in the concentration range 4-6 mM SDS. The close correlation between the decrease in tryptophan fluorescence and the change in the pyrene I_3/I_1 ratio allows us to conclude that TlL interacts with SDS micelles, while the interaction with monomeric SDS is less significant. For DecM (cmc around 2 mM [9]) an increase in tryptophan fluorescence is observed in the monomer range 0~1mM followed by a plateau, and then a rise starting at ~2 mM DecM due to the interaction of TlL with DecM micelles (Fig. 3B). The fact that SDS micelles give rise to a decrease in fluorescence whereas DecM micelles lead to an increase is most likely to reflect changes in the way Trp fluorescence in the native state of TlL is affected by the two classes of micelles, rather than significant structural changes. This is further substantiated by far-UV CD spectra, which are not affected by surfactant micelles (in contrast to other proteins such as α-lactalbumin where binding is accompanied by denaturation [13]), indicating that no significant change in the secondary content takes place in either SDS or DecM (Fig. 4A and B). The most likely explanation to the change in tryptophan fluorescence is that the lid region where Trp89 is located interacts with micelles. Interactions with micelles probably lead to a change from the closed to the open conformation without significant change in the secondary structure.

We now turn our focus to the refolding of TlL in the

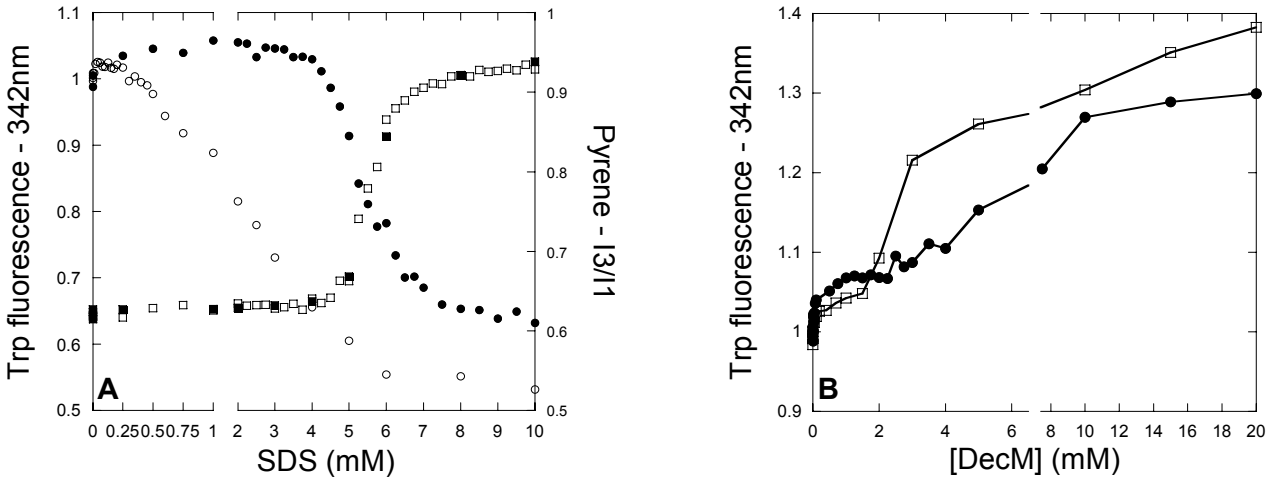

Figure 3. TlL-SDS and DecM interactions measured with fluorescence (A) Trp fluorescence as a function of SDS. (●) indicate samples where SDS has been added to native TlL while (○) indicate samples where TlL is refolded in the presence of SDS. The pyrene I3/I1 ratio report on the formation of micelles in the absence (□) and presence (■) of 1μM TlL. Formation of SDS micelles occurs in the concentration range 4-6 mM. (B) Trp fluorescence as a function of DecM. (●) indicate samples where DecM has been added to native TlL while (○) indicate samples where TlL is refolded in the presence of DecM.

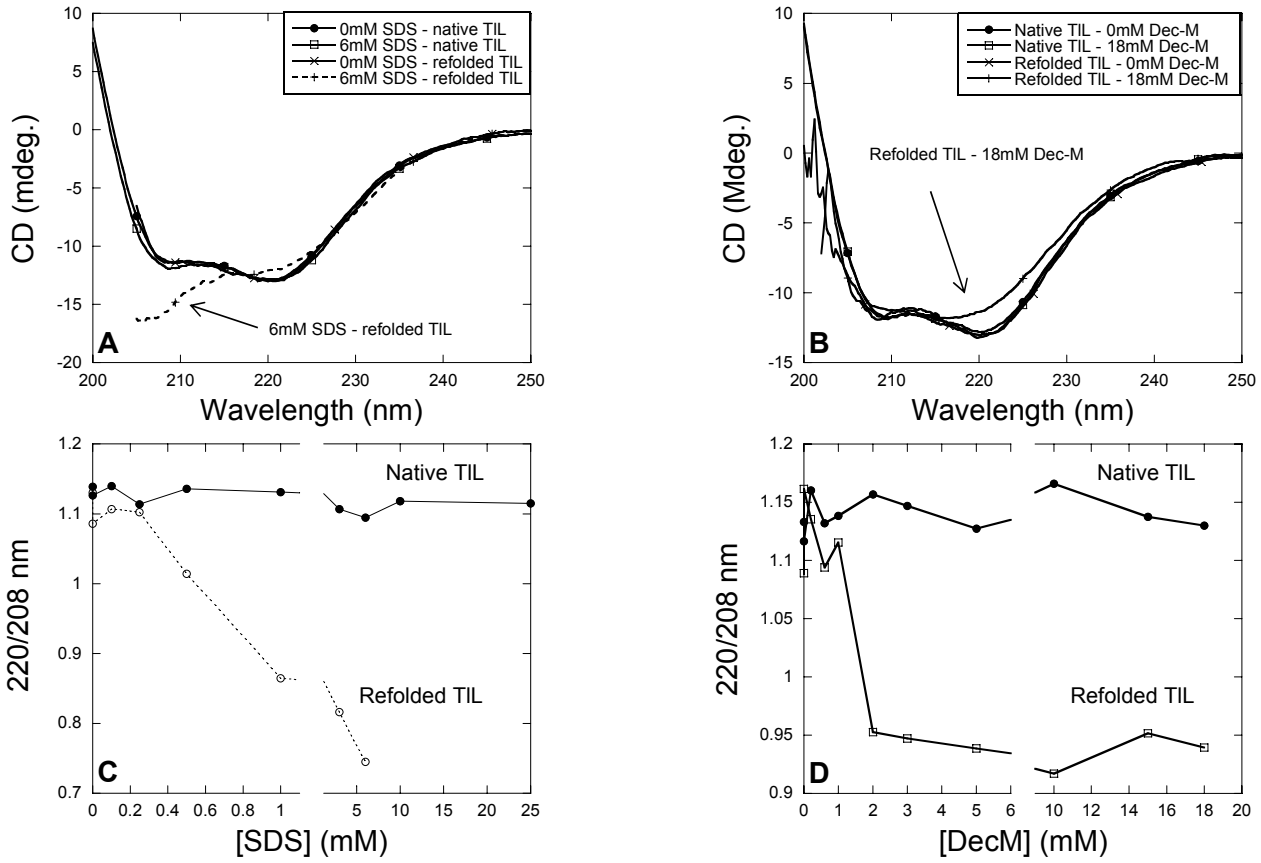

Figure 4. TIL-SDS and DecM interactions measured with far-UV CD. (A) Spectra of native TIL (●) and native TIL to which 6 mM SDS has been added (□). TIL refolded in the absence of SDS (x) and TIL refolded in the presence of 6 mM SDS (+). (B) Spectra of native TIL (●) and native TIL to which 18 mM DecM has been added. TIL refolded in the absence of SDS (x) and TIL refolded in the presence of 6 mM SDS (+). The 220nm/208 ratio report on the interference of SDS (C) and DecM (D) in the refolding process.

presence of surfactants. In the absence of surfactant, fluorescence and CD spectra of refolded and native are identical (Fig. 4), showing that it is possible to refold TIL. Furthermore full activity is restored (Fig. 5). However, in the presence of SDS, refolding efficiency diminishes markedly. This effect is most dramatic in activity measurements where a steady decrease in activity of the refolded protein is observed as the surfactant concentration increases from 0 to 0.5 mM SDS, where after no activity can be detected (Fig. 5). We also observe clear deviations between the fluorescence and CD spectra of native versus refolded TIL from ~0.2 mM SDS onwards. CD spectra of TIL refolded in the presence of higher concentrations of SDS (*e.g.* 6 mM in Fig. 4A) are typical of SDS-denatured proteins, where a shift in the relative intensities at the two minima (220 and 208 nm) is often observed [13, 14]. This makes the 220/208 nm ratio a good indicator of the degree of denaturation (Fig. 4C and D).

When refolding takes place in the presence of DecM, the change in fluorescence and CD spectra is most profound at concentrations above the cmc (~2 mM) (Fig. 3B and 4D). The fluorescence intensity of refolded TIL is generally higher than native TIL, while CD spectra again show a decrease in CD at the minima at 222nm.

TIL refolding was also observed with the use of stopped flow, which can follow the kinetics. In the time window of 500 seconds three phases could be detected; 2 relatively fast phases subsequently followed by a slow phase. The refolding rate constants did not change very much as a function of either SDS or DecM (data not shown), however the associated amplitudes of the three phases decreased in parallel with increasing surfactant concentration (Fig. 6). This was more pronounced for SDS than for DecM as we could not fit data due to the small amplitudes above concentrations of 0.35 mM for SDS and 1.25 mM for DecM. This decrease in amplitude indicate that the surfactants interact with the unfolded state of TIL within the dead time of the experiment (typically ~5 ms), preventing TIL from refolding. As the amplitudes decrease in parallel it also indicates that once the folding nucleus has been formed, the following folding events are unaffected by the presence of surfactant. In other words surfactant interferes with the refolding process by binding to parts of TIL that are vital in the initial folding reaction. However if the first step in the folding process allowed to form, surfactants do not interfere with the remaining folding steps, and native like structure is allow to form. This should however be correlated with activity data in the region 0-0.25 mM SDS that suggests that even

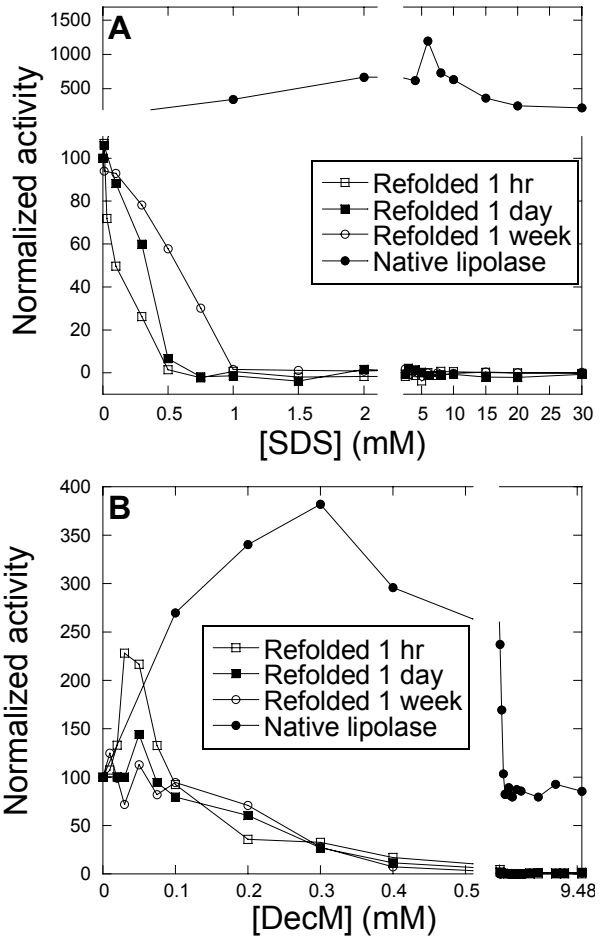

Figure 5. Activity of TlL when refolded in the presence of surfactant. (A) Full activity is achieved when TlL is refolded in the absence of SDS. The activity declines with the addition of SDS and no activity is observed above 1mM SDS. (B) Refolding in the presence of DecM also leads de decreased activity.

though native like structure is formed in this concentration range, activity declines sharply. Thus, although both activity and spectroscopic assays show a disjunction between refolded and native TlL, it is clear that the activity affects are manifested at even lower concentrations than the spectroscopic changes. Activity is more sensitive to subtle structural changes than spectroscopy; furthermore, it is possible that the surfactants are able to bind to the active site at sufficiently low concentrations to inhibit restoration of activity while still allowing the protein to fold. This indicates that several layers of hysteresis are involved in TlL refolding.

ITC shows an unusually low degree of SDS binding to TlL

Stoichiometric and thermodynamic information on the interactions between TlL and SDS are provided by Isothermal Titration Calorimetry (ITC). Since essentially all interactions involving binding and/or conformational changes lead to a heat flow, we can obtain a very comprehensive picture of the different

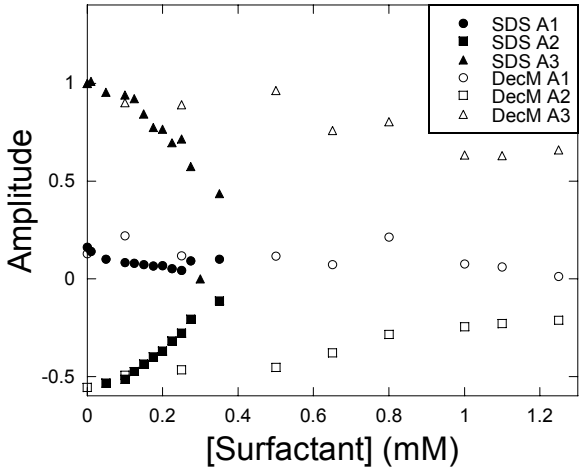

Figure 6. Refolding amplitudes as a function of surfactant concentration. Three amplitudes could be detected in the time range 0-500 seconds. The amplitudes decrease as a function of surfactant indicating decreased amount of TlL refolding. The effect is most pronounced for SDS (filled) where refolding cannot be monitored at concentrations above 0.4mM. Refolding in DecM (open) can be monitored up till 1.25mM where after amplitudes are too small to fit.

transitions involved, including spectroscopically steps, as we have demonstrated for other proteins [6, 8].

Different concentrations of TlL were titrated with SDS, leading to the enthalpograms shown in figure 7. The titrations give rise to a systematic developmement as a function of TlL concentration, and we have selected several inflexion point that give valuable information of the interactions between TlL and SDS. In general the enthalpy values obtained in theses experiment are lower than the values from our previous studies [6, 8] indicating a smaller number of binding sites. The enthalpograms can be described by an exothermic process at low SDS concentrations peaking at point 1 (see figure 7 insert). A second exothermic process, although smaller than the first one, sets in at higher SDS concentrations (peak 2), after which the signal merges with that of SDS titrated into buffer. From this point onwards, the concentration of monomeric SDS does not increase further and no further interaction between TlL and SDS are registered. Previously we have described the stoichiometry between SDS and proteins at different points in the enthanpogram using a mass balance approach.

$$[SDS]_{tot} = [SDS]_{free} + N[ACBP] \quad (1)$$

where N is the number of SDS molecules bound to ACBP at specific points in the enthalpogram. At each point, the total SDS concentration $[SDS]_{tot}$ is the sum of SDS bound to ACBP and SDS free in solution ($[SDS]_{free}$) [15]. Point I in the enthalpogram however diverges from this approach as the point moves towards lower SDS concentrations when the TlL concentrating is increased. The enthalpy of the peak I does thus not

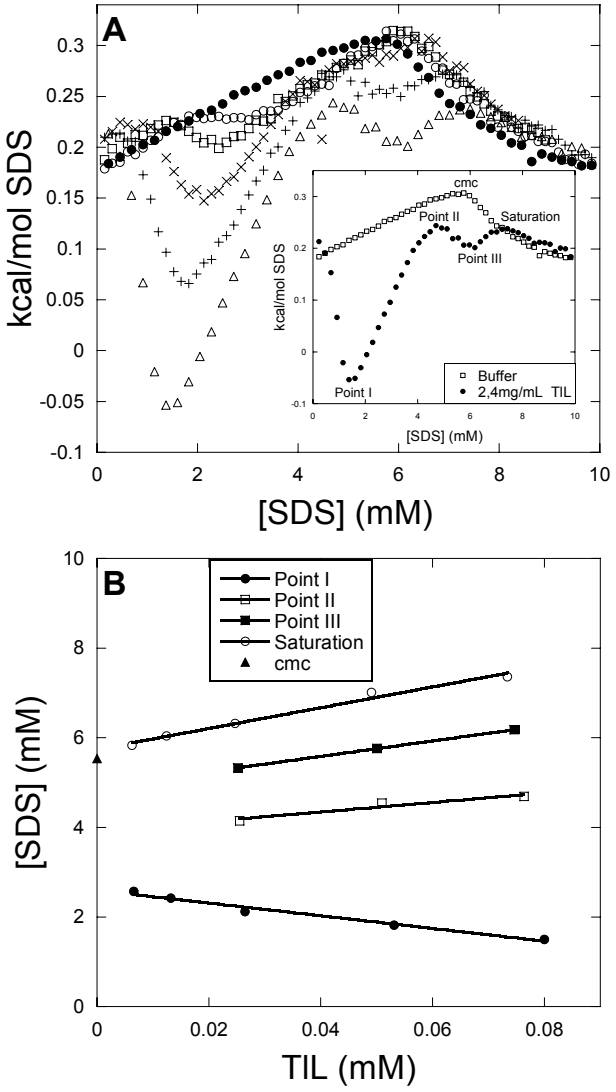

Figure 7. ITC enthalpograms of TlL upon SDS titration with SDS. (A) SDS is titrated into Buffer (●) 0.2 (○) 0.4 (□) 0.8 (x) 1.6 (+) and 2.4 (Δ) mg/mL TlL. Insert show discussed transition points. (B) Total concentrations of SDS, at the different transition points indicated in figure A, plotted as a function of TlL concentration. Binding numbers and free SDS concentrations are derived from eq 1, and summarized

only reflect a simple binding process but must somehow be the sum of different processes that overlap. TlL has previously been shown to oligomerize in the presence of isopropanol, an alcohol that can induce the open conformation of TlL [16]. Upon interaction with SDS TlL may also adopt the open conformation and in parallel form oligomeric structures. Such a process will occur more readily at higher protein concentrations, which could rationalize the shift in point I to lower SDS concentrations at increasing TlL concentrations. However, eq. 1 provides the expected positive values of N for the other inflexion points in the enthalpogram, allowing us to determine both binding numbers and $[SDS]_{free}$ at the different transition points (see table 1). Thus at the points that we have defines as II, III and saturation TlL binds ~10, 17 and 23 SDS molecules respectively. At point II just prior to the second

Table 1. Binding Parameters for SDS-TlL[a].

Inflexion point[b]	Binding number[c]	$[SDS]_{free}$ (mM)[c]
I	-14.17±1.23	2.59±0.06
II	10.61±2.71	3.92±0.15
III	17.20±0.05	4.90±0.01
Saturation	23.18±1.71	5,74±0.07

Notes:
[a] All experiments in 10mM Tris pH 8.0 at 25 °C.
[b] Transition points indicated in Fig. 6B
[c]Parameters defined in eq. 1.

exothermic peak the free concentration is 3.92mM. This is equivalent to the point in the Trp fluorescence titration just before tryptophan fluorescence decreases and pyrene report on SDS micelle formation. This means that the second exothermic peak is due to the interactions of TlL with SDS micelles.

Another important information we can extract from the ITC data is that we do not observe any endothermic processes. Our previous studies all concur in showing that SDS induced denaturation is an endothermic process. As we do not observed such a process we must conclude that TlL does not denature under our titration conditions, in full agreement with our other observations.

TlL unfolds very slowly in chemical denaturants

In order to ascertain whether TlL's kinetic stability is a phenomenon that is strictly related to interactions with ionic and nonionic surfactants or reflects a more general property of the protein, we measured unfolding kinetics in GdmCl. Given that GdmCl reacts only weakly and unspecifically with proteins, the stability of TlL obtained using different GdmCl concentrations will

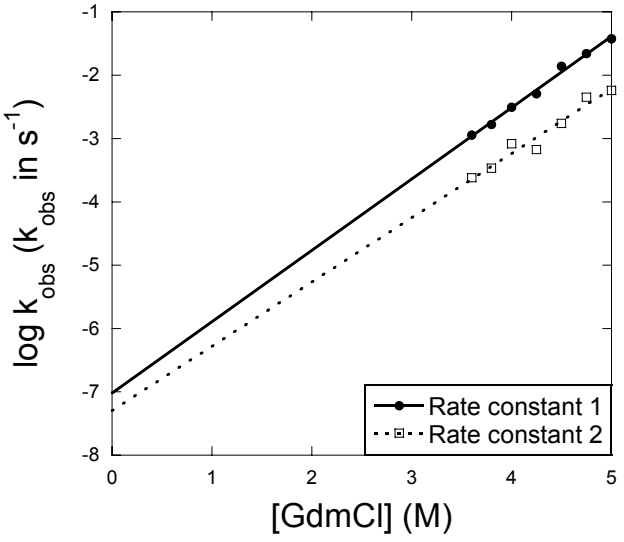

Figure 8. TlL unfolding rate constants as a function of GdmCl. Linear fits extrapolated to 0M GdmCl indicate the unfolding rate constants in buffer (10 mM Tris pH 8). The unfolding half-rate of TlL is 84 days, indicating that is unfolds very slowly and thus can be defined as a kinetic stable protein.

reflect intrinsic protein properties rather than the presence of specific binding sites. Unfolding rate constants scale logarithmically with GdmHCl concentration (Fig. 8), and the unfolding rate constant in 0M GdmHCl is extrapolated to 0.008 day^{-1} equivalent to a half life of 84 days. This shows that the unfolding rate is very slow and fully compatible with the slow rates obtained for other kinetically stable proteins [1, 17]. For example, Serum amyloid P has a half life of 79 days [1] and the extracellular bacterial proteases, *Streptomyces griseus* protease B (SGPB) has half life of 11 days [17]. These values are many orders of magnitude slower than those for proteins not classified as kinetically stable [1].

DISCUSSION

Possible reasons for TlL kinetic stability

In the present study we focus on a subject of growing interest, namely kinetically stable proteins. Kinetically stable proteins have limited access to partially and globally unfolded conformations under both native and denaturing conditions. In both industrial and physiological conditions, kinetic stability can be a more useful parameter than thermodynamic stability, since the former value will be the actual determinant of the amount of active protein under given conditions. Enhancing kinetic stability is thus considered a viably strategy to inhibit amyloidogenesis which typically requires access to flexible and partially unfolded conformations [18-20].

The most well-characterized kinetically stable protein is α-lytic protease (αLP) [17, 21-27]. In its native and active state it is actually thermodynamically unstable. The native structure is obtained due to a folding catalyst the so-called pro-region. This region is cleaved upon activation of the protease, leaving it trapped in a conformation that is thermodynamically unfavorable. The energy barrier associated with unfolding however prevents the protein from unfolding. Furthermore αLP also has rigidity well beyond that of traditionally thermodynamically stabilized proteins [22]. Hydrogen-deuterium exchange monitored by NMR showed very slow exchange over the entire protein, confirming high rigidity not only for the core but throughout the protein [22].

While TlL is synthesized with a signal sequence to export it outside the cell, TlL does not have a folding catalyst similar to the pro-region found in αLP. Unlike αLP the native state of TlL must thus be thermodynamically favored over the denatured state. This is confirmed by our studies on the regain of TlL activity from the low pH-urea denatured state (D), which show that the native state is readily accessible in the absence of surfactant, while unfolding extremely slowly back to D. Thus, under native conditions the native structure of TlL (N) is both kinetically and thermodynamically favored over the unfolded state, indicating a small barrier between D and the transition state (TS) but a large barrier between TS and N. However, even small amounts of surfactant dramatically increase the D-TS barrier and keep the N-TS barrier high. This increased D-TS barrier, which we have also seen for refolding of the lipolytic enzyme cutinase [28], could be caused by a dramatic stabilization of D (possibly in the form of a partially folded intermediate state) or just as dramatic destabilization of TS. At present it is difficult to distinguish the two possibilities, though the steady decrease in the amplitudes of the refolding phases (while leaving the refolding rates only slightly affected) suggests that we gradually titrate out the population of molecules that can fold directly to the native state and instead trap the TlL molecules in a stably unfolded state. This is currently being investigated by following the more complex long-term refolding signals as a function of SDS concentration.

TlL structure and stability

A central element in kinetic stability is β-sheet structure. TlL has mixed α/β structure, like many other kinetically stable protein proteins [2]. The dominant β structure in TlL consists of a central β-sheet spanning 8 individual β-strands oriented in both parallel and antiparallel direction. As previously described rigidity is an important element for kinetic stability, we speculate that the β-sheet in TlL is the key element in the structure which keeps TlL from unfolding. More generally, the decreased rate of local and global unfolding of kinetically stable proteins may account for their resistance to SDS-induced denaturation. The rest of the TlL structure, especially the α-helical lid region, is probably somewhat more flexible. Other elements proposed to be important for rigidity include tight turns which prevent flexibility provided by a high content of glycines which facilitates tight packing in the short turns and loops [22]. The glycine content in TlL is however only ~10% as opposed to 18% in α-lytic protease, however this is still more than any other amino acid in TlL.

In addition to the large β-sheet three disulphide bridges also seems to play an important role for rigidity. The two samples in sample buffer without a reducing agent showed different degrees of migration. However in the presence DTT, a small proportion of TlL showed the same migration as the boiled sample. This indicates loss of kinetic stability. Reduced disulphide bridges increases the conformational freedom of TlL, providing easier access for SDS to bind and denature TlL. Essentially this suggests that TlL is not kinetically stable under reducing conditions. Furthermore, as the α-helix parts of TlL probably are more flexible than the β-sheet, disulphide brudges may provide rigidity to parts of the protein where β-structure is unfeasible. Two disulphide bridges are located in loop regions (Cys36-Cys41) and (Cys104-Cys107) and the third (Cys22-Cys268) is associated to the C-terminal. This again indicates that rigidity in loops and flexible regions are important for kinetic stability. Reduction of the disulfide bonds thus appears to reduce the activation barrier sufficiently to allow reasonably rapid equilibration between the different states. We have ongoing

experiments to test reversibility of folding under reducing conditions.

It is possible that other changes in solvent conditions such as pH can play a role too. Preliminary data indicate that reversibility of unfolding in both surfactants and denaturants is much more readily attained when pH is lowered below 7 (H. Wang, K.K.A. and D.E.O., unpublished data). These pH changes can also affect protein rigidity by titrating out salt bridges and thus lowering the activation barrier for unfolding. It remains to be seen whether the very strong sensitivity to refolding in anionic and non-ionic surfactants is a quirk of lipolytically active enzymes or is a general phenomenon.

MATERIALS AND METHODS

Chemicals

Tris(hydroxymethyl)aminomethane (Tris), sodium dodecyl sulfate (SDS) and glycine were from AppliChem (Darmstadt, Germany). Pyrene and urea was from Sigma-Aldrich (St. Louis, MO). Decyl maltoside was from Anatrace. All chemicals were of the highest grade available. Experimants were performed at 25º C.

TlL preparation

TlL was provided by Novozymes A/S as a liquid formulation at a concentration of 16,7 mg/mL, diluted with water to a concentration of ~5 mg/mL and dialyzed against water at 5 ºC for 24 hours. Dialysis tubing with MWCO of 12000-14000 dalton was used and water was changed 4 times. After dialysis small amounts of precipitate was removed by centrifugation and protein concentration was determined to be 5.1 mg/ml or 174 µM (using a molar extinction coefficient of 37275 M^{-1} cm^{-1}).

SDS-PAGE

SDS-PAGE was performed with a standard 12% resolving gel. Prior to loading TlL was mixed 1:1 with sample buffer containing 4% SDS. Reduced samples included a final concentration of 100 mM DTT. Gels were stained with 0.1% Comassie.

Unfolding kinetics in GdmHCl

TlL unfolding kinetics were investigated using a Cary Eclipse Fluorescence spectrophotometer (Varian, CA, USA). Appropriate amounts of 8 M GdmHCl in 10 mM Tris pH 8 and buffer (10 mM Tris pH8) was mixed in a 1.5 mL cuvette with magnet stirring (Hellma) to a final volume of 950 µL. Tryptophan excitation was performed at 295 nm and TlL unfolding was followed at 338 nm by injecting 50 µL of 20 µM TlL in 10 mM Tris pH 8 into the cuvette. Slit widths of 5 nm were used. Final TlL concentration was 1 µM and temperature was held constant at 25 ºC. Rate constants were obtained by fitting the data to a double exponential decay.

Native TlL interaction with surfactants

TlL was equilibrated with varying concentrations of SDS and DecM in 10mM Tris pH 8.0. Fluorescence spectra were recorded on a LS-55 Luminescence spectrometer (Perkin-Elmer Instruments, UK) using 1.0 µM TlL with excitation at 295 nm and slit widths 10 nm. CD spectra were recorded on a JASCO J-715 spectropolarimeter (Jasco Spectroscopic Co. Ltd., Japan) with 5.0 µM TlL using a data pitch of 0.2 nm, 50 nm/min scan speed, 2 s response time, 1 nm bandwidth and 3 accumulations.

Refolding of TlL in surfactant

For refolding experiments TlL was initially unfolded in 10 mM glycine pH 2 and 6 M urea. 10 and 50 µM were unfolded for fluorescence and CD experiments respectively. Refolding was initiated by a ten times dilution with 10 mM Tris pH 8.

Pyrene

Pyrene is a highly hydrophobic molecule with low solubility in water (2-3 µM). The ratio of the emission peaks at 372.5 (I_1) and 383.5 nm (I_3) can be used to evaluate the polarity of its environment [10]. 1 µM TlL was mixed with appropriate amounts of SDS and buffer (10 mM Tris pH 8). After equilibration for 30 min pyrene was added from a 200 µM stock in ethanol to a final concentration of 1 µM. Scans were performed from 360 – 410 nm using an excitation wavelength of 335 nm and excitation/emission slits of 5/3.5 nm.

Stopped-flow refolding kinetics:

Refolding kinetics in the presence of SDS were studied on a SX18MV stopped-flow microanalyzer (Applied Photophysics, Leatherhead, UK) in a thermostatically controlled sample-handling unit. Unfolded TlL (in 6 M urea and 10 mM glycine pH 2) and surfactant were mixed 1:10 to a final protein concentration of 3 µM. Samples were excited at 280 nm, and the emission above 320 nm was monitored using a cut-off filter. The observed kinetics were fitted to triple exponential functions.

Isothermal titration calorimetry: Calorimetric measurements were conducted on an ITC(MicroCal Inc., Northampton, MA, USA). The reference cell was filled with water and in a typical experiment, the sample cell was loaded with a solution of 0.2-2.4mg/mL TlL. The cell solution was titrated with aliquots of 4µl of 70 mM SDS in 10mM Tris, pH 8. All experiments were done at 25°C, where the enthalpic contribution from SDS demicellization is very small [11]. Therefore the enthalpic contribution from demicellization of SDS upon injection can be neglected in data analysis. The obtained heat signals from the ITC were integrated using the Origin software supplied by MicroCal Inc.

Activity: assays

Activity assays were performed using a concentration of 30 nM TlL in 10 mM Tris pH 8.0 and 370 µM p-nitrophenyl butyrate (diluted from a 150 mM stock in ethanol). Immediately after mixing TlL and substrate,

the mixture was transferred to a cuvette and the absorption at 400 nm measured over several minutes, giving rise to linear plots over this time period. The activity was obtained as the slope of these plots. For refolding experiments, TlL was first denatured in 6M urea and 10 mM glycine pH 2.0, equilibrated for one hour and then diluted 100-fold in the presence of different concentrations of surfactant, after which activity was measured as described previously.

ACKNOWLEDGEMENTS
K.K.A., P.S. and D.E.O. are supported by the innovation consortium BIOPRO.

REFERENCES

[1] Manning, M. and Colon, W., *Structural basis of protein kinetic stability: resistance to sodium dodecyl sulfate suggests a central role for rigidity and a bias toward beta-sheet structure.* Biochemistry, 2004. 43(35): p. 11248-54.

[2] Xia, K., Manning, M., Hesham, H., Lin, Q., Bystroff, C., and Colon, W., *Identifying the subproteome of kinetically stable proteins via diagonal 2D SDS/PAGE.* Proc Natl Acad Sci U S A, 2007. 104(44): p. 17329-34.

[3] Jirgensons, B., *Effect of detergents on the conformation of proteins. I. An abnormal increase of the optical rotatory dispersion constant.* Arch Biochem Biophys., 1961. 94: p. 59-67.

[4] Otzen, D. E. and Oliveberg, M., *Conformational plasticity in folding of the split b-a-b protein S6: evidence for burst-phase disruption of the native state.* J. Mol. Biol., 2002. 317(2099): p. 613-27.

[5] Houry, W. A., Frishman, D., Eckerskorn, C., Lottspeich, F., and Hartl, F. U., *Identification of in vivo substrates of the chaperonin GroEL.* Nature, 1999. 402(6758): p. 147-54.

[6] Nielsen, M. M., Andersen, K. K., Westh, P., and Otzen, D. E., *Unfolding of beta-sheet proteins in SDS.* Biophys J, 2007. 92(10): p. 3674-85.

[7] Otzen, D. E., *Protein unfolding in detergents: Effect of micelle structure, ionic strength, pH, and temperature.* Biophys. J., 2002. 83(2097): p. 2219-2230.

[8] Andersen, K. K., Westh, P., and Otzen, D. E., *Global Study of Myoglobin-Surfactant Interactions.* Langmuir, 2007.

[9] Mogensen, J. E., Sehgal, P., and Otzen, D. E., *Activation, inhibition, and destabilization of Thermomyces lanuginosus lipase by detergents.* Biochemistry, 2005. 44(5): p. 1719-30.

[10] Kalyanasundaram, K. and Thomas, J. K., *Environmental Effects on Vibronic Band Intensitiesin Pyrene Monomer Fluorescence and Their Application in Studies of Micellar Systems.* Journal of the American Chemical Society, 1976. 99:7: p. 2039-2044.

[11] Nielsen, A. D., Arleth, L., and Westh, P., *Interactions of Humicola insolens cutinase with an anionic surfactant studied by small-angle neutron scattering and isothermal titration calorimetry.* Langmuir, 2005. 21(10): p. 4299-307.

[12] Chapman, M. R., Robinson, L. S., Pinkner, J. S., Roth, R., Heuser, J., Hammar, M., Normark, S., and Hultgren, S. J., *Role of Escherichia coli curli operons in directing amyloid fiber formation.* Science, 2002. 295(3736): p. 851-855.

[13] Otzen, D. E., Sehgal, P., and Westh, P., *a-lactalbumin is unfolded by all classes of detergents but with different mechanisms.* J. Coll. Int. Sci., 2009. 329: p. 273-283.

[14] Otzen, D. E., *Folding of DsbB in mixed micelles: A kinetic analysis of the stability of a bacterial membrane protein.* J. Mol. Biol., 2003. 330(3113): p. 641-649.

[15] Nielsen, A. D., Arleth, L., and Westh, P., *Analysis of protein-surfactant interactions--a titration calorimetric and fluorescence spectroscopic investigation of interactions between Humicola insolens cutinase and an anionic surfactant.* Biochim Biophys Acta, 2005. 1752(2): p. 124-32.

[16] Zhu, K., Jutila, A., Tuominen, E. K., and Kinnunen, P. K., *Effects of i-propanol on the structural dynamics of Thermomyces lanuginosa lipase revealed by tryptophan fluorescence.* Protein Sci, 2001. 10(2): p. 339-51.

[17] Truhlar, S. M., Cunningham, E. L., and Agard, D. A., *The folding landscape of Streptomyces griseus protease B reveals the energetic costs and benefits associated with evolving kinetic stability.* Protein Sci, 2004. 13(2): p. 381-90.

[18] Hammarstrom, P., Wiseman, R. L., Powers, E. T., and Kelly, J. W., *Prevention of transthyretin amyloid disease by changing protein misfolding energetics.* Science, 2003. 299(5607): p. 713-6.

[19] Petrassi, H. M., Johnson, S. M., Purkey, H. E., Chiang, K. P., Walkup, T., Jiang, X., Powers, E. T., and Kelly, J. W., *Potent and selective structure-based dibenzofuran inhibitors of transthyretin amyloidogenesis: kinetic stabilization of the native state.* J Am Chem Soc, 2005. 127(18): p. 6662-71.

[20] Wiseman, R. L., Johnson, S. M., Kelker, M. S., Foss, T., Wilson, I. A., and Kelly, J. W., *Kinetic stabilization of an oligomeric protein by a single ligand binding event.* J Am Chem Soc, 2005. 127(15): p. 5540-51.

[21] Cunningham, E. L., Jaswal, S. S., Sohl, J. L., and Agard, D. A., *Kinetic stability as a mechanism for protease longevity.* Proc Natl Acad Sci U S A, 1999. 96(20): p. 11008-14.

[22] Jaswal, S. S., Sohl, J. L., Davis, J. H., and Agard, D. A., *Energetic landscape of alpha-lytic protease optimizes longevity through kinetic stability.* Nature, 2002. 415(6869): p. 343-6.

[23] Cunningham, E. L. and Agard, D. A., *Disabling the folding catalyst is the last critical step in alpha-lytic protease folding.* Protein Sci, 2004. 13(2): p. 325-31.

[24] Kelch, B. A. and Agard, D. A., *Mesophile versus thermophile: insights into the structural mechanisms of kinetic stability.* J Mol Biol, 2007. 370(4): p. 784-95.
[25] Kelch, B. A., Eagen, K. P., Erciyas, F. P., Humphris, E. L., Thomason, A. R., Mitsuiki, S., and Agard, D. A., *Structural and mechanistic exploration of acid resistance: kinetic stability facilitates evolution of extremophilic behavior.* J Mol Biol, 2007. 368(3): p. 870-83.
[26] Truhlar, S. M. and Agard, D. A., *The folding landscape of an alpha-lytic protease variant reveals the role of a conserved beta-hairpin in the development of kinetic stability.* Proteins, 2005. 61(1): p. 105-14.
[27] Fuhrmann, C. N., Kelch, B. A., Ota, N., and Agard, D. A., *The 0.83 A resolution crystal structure of alpha-lytic protease reveals the detailed structure of the active site and identifies a source of conformational strain.* J Mol Biol, 2004. 338(5): p. 999-1013.
[28] Sehgal, P., Nielsen, S. B., Pedersen, S., Wimmer, R., and Otzen, D. E., *Modulation of cutinase structure and stability by phospholipid detergents.* Biochim. Biophys. Acta, 2007. 1774: p. 1544-1554.

Chapter VI: Discussion and Perspectives

In this thesis six papers are presented that study how proteins and surfactants interact. The interactions have been investigated using an array of different biophysical techniques which give insight into the mechanisms of interaction. The purpose of this chapter is to summarize and discuss important results from the papers. Focus will primarily be on the anionic surfactants and especially SDS because it is used in all of the papers. The chapter starts out by describing the proteins which are easily denatured by SDS. The chapter will then move towards the more SDS resistant proteins here among the β-structured proteins and the enzyme TlL. Lastly micelle structures/properties will be discussed in relation to denaturation potency. Throughout the chapter a perspective view includes possible ways to follow up on the results and questions which this thesis provides.

SDS susceptible proteins

Three of the six proteins studied in this thesis are easily denatured by SDS, i.e. they all loose native structure at relatively low SDS concentrations and also unfold fast. These are ACBP, myoglobin and αLA. ACBP and myoglobin are primarily α-structured, while αLA has mixed α/β structure. Because these three proteins easily denature they provide good models for comparison purposes with other well studied proteins such as BSA and lysozyme.

Structural investigations on ACBP-SDS complexes

Most structural studies on protein-surfactant complexes have focused on proteins saturated with SDS at concentrations above the cmc. There is thus a lack of structural information on how proteins interact with surfactants below the cmc. Our structural studies, using SAXS, tries to close the gap up till the cmc by studying the gradual binding of SDS to ACBP. Using fluorescence, CD, CE and ITC we identified two interesting stages in the denaturation process and used SAXS to characterize the structure of the protein/surfactant complex at these stages. At the first stage the complex is a central decorated micelle consisting of ~33 SDS molecules which binds two ACBP polypeptide chains. In this stage only half of the protein is associated with the decorated micelle while the second half protrudes into the solvent. Although a dimeric complex between SDS and cutinase has been reported previously no structural model was provided [91]. In the next stage of the denaturation process, additional SDS binds and monomeric ACBP is at associated with a decorated micelle of ~42.5 SDS molecules. In general, very little literature is available on complexes formed between proteins and surfactants at sub-cmc concentrations. Rare studies like the crystallographic structure of lysozyme in complex with SDS have been performed at low SDS concentrations [84]. The complex formed in these experiments was the result of first denaturing lysozyme at high SDS concentrations and then refolding the protein by dialysis. This procedure did not remove all SDS and four SDS molecules were identified in the crystal structure. The SDS molecules obstructed lysozyme from reaching the native state and kept lysozyme in a “open-winged” conformation [84]. Importantly this kind of study describes

locations where SDS can bind from the denatured state. This does not necessarily describe the locations where SDS initially will bind when SDS is added to the native protein. In contrast to the study on lysozyme, our structural studies on ACBP-SDS complexes do not involve complete SDS saturation of the protein. Instead we focus on the stepwise binding of SDS and characterize the structural arrangement of the polypeptide chain and SDS molecules at certain stages in the denaturation process.

While we have presented structural information on two import stages in the denaturing process, there is still room for expansion. Firstly, although mutant investigations indicate that SDS binding occur around the ACBP ligand binding site, with the present data, we are unable to identify the amino acids residues that are involved in initial binding of SDS. The initial binding site may be identified with the use of isotopically labeled ACBP and NMR. Outside x-ray crystallography, NMR is the only spectroscopic method that can provide precise 3-D structural detail about where and how ligands bind to proteins [139]. The complex between ACBP and palmitoyl-Coenzyme A has already been studied using multidimentional ^{1}H, ^{13}C and ^{15}N NMR [140].The initial binding site of SDS could possibly be identified using SDS instead of palmitoyl-Coenzyme, in a similar approach. A drawback of this method is however that it requires labeled protein/SDS, is expensive and time consuming.

Another method which could be used to identify the initial binding site is Molecular Dynamic (MD) simulations. MD simulations have already been used to study protein-surfactant complexes especially on membrane proteins or membrane associated proteins [141-145]. This method is like our mutant studies an indirect method of identifying the initial binding site. However, if MD simulations identify residues around the ligand binding site of ACBP as the initial SDS binding site this will strengthen the evidence that this part of the protein is involved in initial binding of SDS. Another benefit of using MD simulations is to test if it is possible to reproduce the two structures that we have modeled using SAXS data. The structural information provided in this thesis could be used as verification whether or not the parameters used in MD simulations to a satisfactory degree describe the interactions between surfactants and globular proteins.

The last part of the denaturing mechanism that we are missing structural information about is the saturated complex where ACBP associates with bulk SDS micelles. Several models at this stage of the denaturing process have been proposed (see introduction) here among the “bead and necklace” model, which has received most acknowledgement. Our anisotropy data clearly indicate that ACBP tumbling is reduced upon formation of bulk SDS micelles. It is thus most likely that the complex formed between SDS and ACBP at this stage in the denaturation process is different from the two other structures which we have modeled. We have discussed the use of SAXS to study the complex at SDS concentrations where bulk SDS micelles are formed. This approach is however not without drawbacks. Scattering data under such conditions will not only involve contributions from the ACBP/SDS complex but also from free bulk SDS micelles. Scattering data would thus be the sum of the ACBP/SDS complex and free SDS micelles. Isolating the ACBP/SDS data from the free SDS micelles

may be a very difficult task (personal communication, Jan Skov Pedersen, Århus University). One possibility to overcome this problem is to do the experiment at SDS concentrations only slightly above the cmc where the concentration of free SDS micelles is very small compared to the concentration of the ACBP/SDS complex. In this way the contribution from free SDS micelles will be very small and possibly insignificant compared to the contribution from the ACBP/SDS complex. The scattering data could thus be used to model the complex formed between ACBP and bulk SDS micelles. This would enable us to do direct comparative studies with other SDS/protein complexes.

Co-factor binding proteins

To date, the proteins which have undergone most studies with regards to protein-surfactant interaction do not have co-factors. This has to be set in contrast to the number of proteins which bind co-factors; over 30 % of proteins in living cells require co-factors to perform biological activity [146]. Myoglobin provided an opportunity to investigate how surfactants interact with this large class of proteins.

The myoglobin denaturing mechanism is very complex compared to many of the other proteins we have studied. This is probably most pronounced in the enthalpograms, where we do not observe a distinct endothermic peak, which we often associate with initial unfolding of the protein. We believe that the absence of this endothermic peak is directly correlated with the presence of the heme co-factor. In order to understand why the presence of a heme co-factor leads to a complex denaturing mechanism, it is first of all important to know how heme interacts with myoglobin. In principle, co-factors can bind to proteins in three ways : (1) before folding (2) during folding and (3) after folding [147]. *In vivo* studies indicate that heme binding takes place after folding of the apo-protein, however heme is also found to have high affinity for the unfolded polypeptide chain [147]. Furthermore a general feature of co-factors is that they stabilize the native conformation [148]. The high affinity of heme may result in a more complicated denaturation mechanism because heme prevents SDS binding to specific parts of myoglobin. Smulevich and co-workers have previously shown that heme does not dissociate at SDS concentrations below the cmc [149]. This means that heme is associated to the myoglobin polypeptide chain throughout the concentration region which we have studied. It is thus most likely heme binding is the reason why the denaturation mechanism is so complex compared to many of the other proteins which we have studied.

Heme is a relatively large co-factor compared to the Ca co-factor in αLA, which is the second protein in this thesis that can bind a co-factor. Although αLA can bind Ca, it has been removed in the studies presented in this thesis. It is thus difficult to do a direct comparison between the two proteins based solely on the studies presented in this thesis. The interactions between surfactants and αLA has however recently been thoroughly studied by Otzen D.E., Sehgal P. and Westh P. [128]. This study primarily focuses on the apo-protein; however a few experiments are conducted in the presence of Ca. In general, the study show very similar results as those observed for ACBP, i.e. the enthalpogram is dominated by two endothermic

peaks and tryptophan fluorescence first increases and is followed by a decrease to an intermediate level. This indicates that in the absence of a co-factor the denaturing mechanism is similar to that of ACBP and simpler than the mechanism observed for myoglobin. This raises the question of why the myoglobin denaturation mechanism is so complex. We know that the heme co-factor binds tightly to the myoglobin polypeptide and only dissociates at surfactant concentrations above the cmc [149]. There is however no report on when the Ca co-factor dissociates from the αLA during the denaturation process. If Ca dissociates early in the unfolding process the denaturing mechanism may be less complicated as compared to a co-factor which has high affinity for the unfolded polypeptide chain. Furthermore the Ca co-factor is significantly smaller compared to heme, and it is possible that heme has more interaction sites with the polypeptide chain thus preventing SDS binding to these regions. This could lead to a series of events in the denaturing mechanism that are different from those observed for proteins that do not contain co-factors. In order to clarify these issues, it would be interesting to study the interaction of SDS with the apo-form of myoglobin. Comparing the results of the apo-form with the holo-form would shed more light on the role of the co-factor in the denaturation mechanism.

Myoglobin and αLA are example of a protein that binds a co-factor non-covalently. Some proteins bind co-factors covalently; e.g heme is covalently attached to *c*-type cytochromes [150]. In order to understand how surfactants interact with co-factor binding proteins, it would be interesting to also include proteins that have covalently bound co-factors. Such a study lead to an even better understanding of the importance of co-factor in regards to protein-surfactant interactions.

Protein-surfactants complexes and alkyl-sulfates

In paper V we investigate the denaturation potency of alkyl-sulfates with chain lengths both shorter and longer than SDS (C12). These studies showed that denaturation potency increase with increasing chain length, stressing the importance of the hydrophobic part of the surfactant. The denaturation potency of alkyl-sulfates is primarily based on two parameters; 1) The concentration which is required to disrupt the native state of ACBP and 2) the rate of unfolding. From these parameters important information can be deducted but it does not provide structural insight in the same degree as our SAXS studies with SDS. SAXS studies are demanding in regards of both amount of protein and the resources required to collect and handle data. We have thus limited our structural studies to involve only SDS. Therefore we can only speculate if the denaturing mechanism which we have characterized with SDS is similar for other alkyl-sulfates.

Several indications speak for the same denaturation mechanism. E.g. when comparing tryptophan fluorescence as a function of alkyl-sulfate concentration, it is apparent that they all have the same profile. An initial lag phase is followed by an increase in fluorescence which then decreases to an intermediate level. The fact that this profile is the same for all alkyl-sulfates no matter chain length indicate similarities in the denaturation mechanism.

Other data speak against the same denaturing mechanism. The decorated SDS micelles, characterized using SAXS, have aggregation numbers of 33 and 42, respectively. These numbers are lower than the aggregation number of bulk SDS micelles which is 64 (see introduction). In paper IV, we suggest that a minimum number of SDS molecules is required to form a decorated micelle. Hence, a minimum of ~33 molecules is required to form decorated SDS micelles. Using this number to compare with alkyl-sulfate properties a number of observations can be made. E.g. the aggregation number of bulk micelles increases with increasing chain length and for C8-sulfate it is 27. This number is only ~1/3 of the SDS aggregation number and smaller than the number of SDS molecules required to form a decorated SDS micelle. Bulk C8-sulfate micelles are thus significantly smaller than the SDS decorated micelles. The complex formed between ACBP and short chain alkyl-sulfates may thus be quite different than the complex formed with SDS, as bulk micelles are smaller and less hydrophobic than the SDS decorated micelles. It is however possible that upon interaction with ACBP, C8-sulfate decorated micelles have larger aggregation numbers than free bulk micelles. The facts that there is much difference in the aggregation number of alkyl-sulfates indicate that the denaturing mechanism may be different between different alkyl-sulfates. This means that the complexes formed between ACBP and alkyl-sulfates may be different dependent on the length of the alkyl chain.

In relation to industrial surfactants which are poly-disperse it would be interesting to mix alkyl-sulfates with different chain lengths and study how this influences the denaturation mechanism. Such a study could also contain higher concentrations of buffer such that the ionic strength reflects more practical used conditions.

Denaturation-resistant proteins

In this thesis we have studied a number of proteins with varying degree of resistance towards surfactant denaturation. E.g. the two β-structured proteins can both be denatured by SDS; however the unfolding rates are significantly slower than the rates observed for the α-structured proteins ACBP and myoglobin. The resistance is in this case mostly of kinetic nature. Furthermore, although the proteins are homologous there are individual differences. TII27 can be denatured by SDS monomers, while Tnfn3 is only denatured in the presence of SDS micelles. The last protein in this thesis which shows SDS resistance is TlL. This enzyme clearly interacts with surfactants however it is not denatured at pH 8. In all, these three proteins have been good models as they give in insight into the different degrees of resistance towards surfactant denaturation.

Importance of size and fold for SDS resistance

Paper I deals with the importance of β-structure in regards of resistance towards SDS denaturation. As described above the two β-sandwich proteins TII27 and Tnfn3 showed varying degree of SDS resistance however both proteins unfolded relatively slowly in SDS. The two proteins share the same type of fold and show the importance of β-structure in regards to resistance towards surfactant denaturation. The conclusion that we have deducted

from this study are based on two homologous proteins with similar β-structure. The fact that these two proteins are very similar and not different raises the question whether the knowledge obtained in thus study can be transferred to other proteins with large content of β-structure. Other factors which could be important in relation to SDS resistance and β-structure could be type of fold and also size of the protein. Different type of fold and size could in theory lead to more long distance interactions, which have been found to be important for SDS resistance [123].

Although not presented in this thesis, during the thesis period, studies have been performed on outer membrane protein A (OmpA) from *E.coli* [151-158]. This two-domain protein consists of a membrane embedded domain and a periplasmic domain. The focus of this work has been on the membrane embedded part which consists of an 8-stranded β-barrel [159, 160]. Proper folding this protein requires a hydrophobic environment, which we have provided by the means of nonionic surfactants. Upon folding OmpA is very stable; it cannot be denatured by the addition of large amounts of SDS, and we observe bandshift when using the SDS-PAGE assay for identification of kinetic stability. This indicates that OmpA does not undergo local or global unfolding and it can thus be regarded as more SDS resistant compared to the two β-proteins TII27 and Tnfn3. Although a membrane proteins, the size and β-structure content of OmpA is comparable to that of TII27 and Tnfn3. One of the main differences is found in the fold. The OmpA fold is a β-barrel and each strand interacts with two neighboring strands. In contrast, the sandwich fold consists of two individual β-sheets. The sandwich fold may be more flexible compared to the barrel fold and thus also explain why TII27 and Tnfn3 are susceptible to SDS denaturation and why OmpA is not.

There are also soluble β-barrel proteins. Avidin is a soluble protein, which like OmpA, has a β-barrel fold that consists of 8-antiparallel β-strands [161]. In addition avidin also has a singe cystine bridge between Cys4 and Cys83, which most likely restricts N-terminal mobility. As described in the introduction avidin has been shown to be SDS resistant and is not denatured unless heated/boiled. This resistance was correlated with a half rate of unfolding in water of 270 years [123]. This means that avidin is a highly rigid protein that does not undergo local or global unfolding. The fact that these two β-barrel proteins are resistant to SDS denaturation indicate that not only β-structure but also type of fold (and possibly size) are important parameters for kinetic stability and thus also resistance towards SDS denaturation.

In order to clarify the properties of β-structure in relation to resistance towards surfactant denaturation a study of proteins with different β-domain folds could be undertaken. This study could include folds such as β-barrels, β-sandwiches, β-prisms [162], β-propellers [163, 164] and β-helices (both left- and right handed) [165]. In addition the study should include proteins of different sizes. Finally the study should also include proteins that have parallel as well as anti-parallel β-sheets, to address the importance of this parameter. Such a study is not a minor task but it could possibly identify parameters in β-structure that are important for protein resistance towards surfactant denaturation.

TlL thermophilic properties in relation to kinetic stability

The first five papers presented in this thesis involve proteins that are susceptible to SDS denaturation, i.e. they can all be denatured by either SDS monomers or micelles. Paper VI is devoted to the enzyme TlL which provided the opportunity to study the interactions of surfactants with an enzyme that is completely resistant to surfactant denaturation (at pH 8). Although TlL clearly interacts with surfactants, here among SDS, the enzyme is by no means denatured. We attribute this to the very slow rate of unfolding in water, and the enzyme can be characterized as kinetically stable.

At pH 8 and 25 ºC it is apparent that TlL unfolding is very slow. In contrast, we found that activity could be regained quite fast when TlL was refolded from the pH and urea denatured state. Put together this indicates a high energy barrier between the folded state and the transition state, while the energy barrier between the unfolded state and the transition state is small. This leads us to believe that TlL is thermodynamically very stable. However, at the present time we cannot provide thermodynamic values due to lack of kinetic refolding data (work in progress).

The organism from which TlL originates may provide clues to the thermodynamic properties of this enzyme. TlL is expressed in *Thermomyces lanuginosus* which is a thermophile fungi that grows optimally at 48-52 ºC, but can be cultured between 30 and 55 ºC [166, 167]. The fact that TlL originates from a thermophilic organism and not a mesophilic organism may be a vital clue in the understanding of why TlL is a kinetically stable enzyme that resists SDS denaturation

Raziv and Scholtz [168] collected data from 26 proteins that originated from thermophilic organisms (growth temperatures 45-75 ºC) and compared them with mesophilic counterparts. They found and average 30.5 ºC increases in T_m from the mesophilic proteins to the thermophilic homologues. The T_m of TlL is 74 ºC at pH 8 [22, 23]. In addition to the increase in T_m an average of 8.7 kcal/mol increase in thermodynamic stability was observed for the thermophilic proteins. This indicates a direct correlation between the thermo stability of proteins from thermophilic organisms and thermodynamic stability. Hence TlL may also be significantly more thermodynamically stable at 25 ºC as compared to mesophilic counterparts. The correlation between thermo stability and increased thermodynamic stability (at room temperature) has not only been made for mesophilic and thermophilic homologues but also mesophilic and hyperthermophilic proteins (growth temperatures >75 ºC) [169].

Proteins from thermophilic and hyperthermophilic organisms require high T_m in order to maintain native structure at elevated temperatures. In general increasing thermo stability can be obtained by a combination of different structural parameters such as: increased number of ionic interactions, increased extent of hydrophobic-surface burial, increased number of prolines, decreased number of glutamines, improved core packing, greater rigidity, extended secondary structure, shorter surface loops, and higher states of oligomerization ([169] and references therein). Futhermore Szilagyi and Zavodszky proposed that hyperthermostable proteins have stronger ion pairing, fewer cavities, and higher β-sheet contents as compared to

thermostable proteins [169]. Interestingly many of these parameters are the same as the ones that Manning and Còlon describe that are important for kinetic stability and resistance to SDS denaturation [123]. All these possible ways of increasing thermo stability can be divided into three approaches/thermodynamic models. They have all been depictured in figure 27.

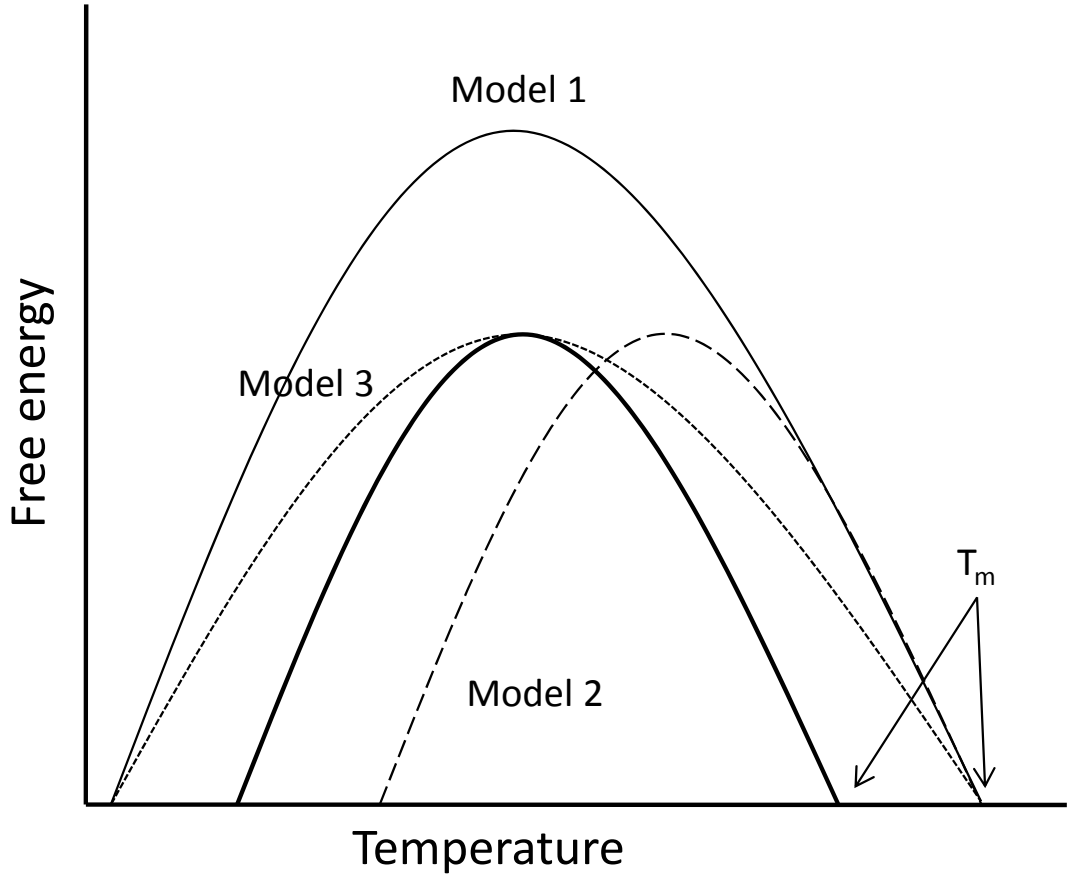

Figure 27. Stability curves showing methods for achieving higher thermo stability. The thermo stability of a hypothetical mesophilic protein (fat solid line) can be increased by shifting the stability curve up (solid line – model 1), by shifting the curve to the right (stippled – model 2) or by flattening the curve (stippled – model 3). Adapted from [169] and [168].

Model 1 describes a protein that has been stabilized over the entire temperature range. In model 2 the stability profile is shifted horizontally to the right and model 3, higher thermo stability is achieved by flattening of the profile. While these are all theoretical methods for achieving higher thermo stability, they have all been found in practice and often in combination [168]. Model 1, is the single most used approach in nature to achieve higher thermo stability, followed by model 3 and 2 [169]. Model 1 is interesting because the proteins in this category are thermodynamic very stable around room temperature, where most biophysical studies are conducted, including our own studies on TlL. Under normal conditions hyperthermophilic organisms thrive at higher temperatures and here the proteins are only marginally thermodynamically stable. However, at room temperature they are thermodynamically very stable. Hence when studying proteins from thermophilic organisms,

one should note that the proteins are not optimized to function at room temperatures. An interesting feature of proteins which have been stabilized according to model 1 is the folding kinetics. While refolding rates for homologous thermophilic and mesophilic proteins are very similar, thermophilic protein show a dramatic decrease in unfolding rates [169, 170]. This is interesting in that our studies show that TlL unfolds very slowly. It is thus possible that TlL has been thermo stabilized according to model 1. Slow unfolding kinetics and high thermodynamic stability may both be vital clues to why TlL is resistant to SDS denaturation. Because the native state is thermodynamically highly favored over the denatured state, TlL may be "trapped" in the native state and practically never undergo local or globe unfolding. Because SDS denaturation is directly linked with SDS binding to the unfolded state of proteins, TlL is resistant to SDS denaturation.

In order to verify whether or not TlL can be considered as a protein that is stabilized according to model 1, the thermodynamic stability of TlL will have to be determined as a function of temperature, such that a plot similar to that presented in fig. 27 can be made. This can be achieved using either equilibrium or kinetic approaches using denaturants such as urea or GdmCl. Due to the very slow unfolding rate at room temperature an equilibrium approach is unfeasible as the time required to reach equilibrium will be very time consuming. This approach was attempted for ribonuclease HII from *Thermococcus kodakaraensis*, however after 1 month at 20 ºC equilibrium was not reached. Equilibrium could be achieved after two weeks at 50 ºC [170]. Determining refolding- and unfolding rate constants as a function of denaturant at different temperatures thus seem to be the more feasible approach, especially around room temperature.

An interesting feature about theromostable proteins is that they are not confined to thermophilic or hyperthermophilic organisms, but proteins with high thermo stability are also found in mesophilic organisms. In particular *Bacillus* species are able to populate moderately thermophilic habitats [171]. This is interesting because many of the enzymes that are used in detergents originate from *Bacillus* species.

Kinetic stability = resistance to SDS denaturation?

Many proteins from thermophilic organisms are thermodynamically very stable at room temperature and unfold slowly (described above). The slow unfolding can be viewed upon as kinetic stability, but how does this relate to resistance towards surfactant denaturation? The proteins identified to date which are resistant towards surfactant denaturation are all kinetically stable. However does this also mean that all kinetically stable proteins are resistant towards surfactant denaturation? In order to clarify this, it would be interesting to select a number of well characterized proteins that unfold slowly and perform the simple SDS-PAGE assay that can reveal whether or not the proteins are also resistant to SDS denaturation. This could shed light on whether SDS resistance can be gained by increasing the thermodynamic stability and not least decreasing unfolding kinetics.

Micelle structure and modeling of unfolding kinetics

Our studies on the denaturing properties of SDS revealed that not only surfactant concentration, but also micelle structure is an important parameter when considering protein unfolding in surfactants. Micelle structure is influenced by several parameters (see introduction) including surfactant and salt concentration. When studying protein unfolding rates as a function of surfactant concentration we found a profound correlation between micelles structure and the rate of unfolding. This was evident for both α- and β-structured proteins, although the unfolding kinetics was influenced in different ways. E.g. in the transition range from spherical to "rod-like" micelles, we see a decrease in the ACBP unfolding rates. For the β-structured proteins TII27 and Tnfn3 the unfolding rates showed dual characteristics. For Tnfn3 the unfolding rates decreased significantly while the decrease less dramatic for TII27. It is thus clear that the effect of micelle structure is protein dependent. This difference indicate that proteins are denatures in different ways, i.e. "rod-like" micelles may bind to different sites on proteins compared to "spherical" micelles. This may in turn give rise to a different denaturing mechanism which is reflected in the unfolding rates. In all, this means that interpretation of denaturing kinetics using surfactants are much more complicated as compared to chemical denaturants such as urea and GdmCl which do not show similar effects. For correct modeling of unfolding kinetics, micelle structure has to be accounted for. At the present time this can be a very difficult task due to the lack of structural data at different concentrations of SDS. In general structural data on anionic surfactants (and mixed micelles) is still in its infancy [34], while more data is available on cationic surfactants. A natural follow up on the kinetic studies is thus to investigate SDS micelle structure in more detail. This could be done with the same techniques which have been used to study cationic surfactant structures. Such studies could possibly be used to describe protein-surfactant interactions in more detail, especially at high surfactant concentrations.

Co-solvents and micelle structure

Co-solvents are used in liquid detergents to stabilize proteins and avoid phase separation. Co-solvents may also interact with surfactants, thereby changing their denaturation properties. E.g. a recent study describes the unusual effect of mono- and di-alcohol osmolytes that can modulate the protein denaturation properties of SDS [172, 173]. These studies showed that the denaturation potency of SDS could be dramatically reduced by addition of the co-solvent 2,4-methyl-2-pentanediol (MPD). MPD was in several cases able to drive the transition from the SDS-denatured to the fully functional native state. When looking at table 4 which shows typical formulations of a liquid detergent, one cannot avoid to notice the co-solvent 1,2-propanediol. Although 1,2-propanediol was is not included in the studies described above both 1- and 2-propanol acted as protection agents, similar MPD. The mechanism by which MPD and other small organic molecule alter SDS denaturing properties is not fully explained in these studies, however organic molecules like alcohols with moderate to long hydrocarbon

chains are known to be adsorbed in to outer region of the micelle forming a palisade ("fence-like") structure with the surfactant molecules [35]. This can decrease the cmc due to reduced repulsion as well as change the micelle shape [35]. It is thus likely that 1,2-propanediol, like the organic molecules described above act in a similar fashion on surfactants in liquid formulations. The modulation of surfactant denaturing potency during storage could prevent enzymes from being denatured. Enzymes in solid detergents do not interact with surfactants or other possible denaturing compounds during storage as the enzymes are prepared in small granules separated from other components in the formulation. Enzymes in solid formulations thus only encounter surfactants during the washing process.

It would be very interestingly to study the effects of 1,2-propanediol on SDS micelle structure in more detail, though this is outside the scope of the present thesis. E.g. the structure of SDS micelles could be studied with increasing concentrations using scattering techniques. In parallel the denaturing potency of SDS in presence of 1,2-propanediol could be performed in parallel, such that eventually change in micelle structure be correlated with denaturation potency.

Chapter VII: References

[1] Showell, M. S., *Handbook of detergents - Part D : Formulation*. Surfactant science series Vol. 128. 2006: Taylor and Francis.

[2] Callisen, T. H. and Damhus, T., *Frustrerede molekyler i centrum af vaskeprocessen.* Dansk Kemi, 2006. 87(1): p. 17-20.

[3] Ròhm, O., *Patent #283923*. 1913: Germany.

[4] Schàfer, T., Kirk, O., Borchert, T. V., Fuglsang, C. C., Pedersen, S., Salmon, S., Olsen, H. S., and Deinhammer, R. L., H., *Polyamides and Complex Proteinaceous Materials I*. Biopolymers. Vol. 7. 2002: Wiley-VCH. 377-437.

[5] Damhus, T., *Vaskemidler anno 2005 - dagligprodukter, hvor stofkemi mødes med overfladevidenskab og bioteknologi II.* Dansk Kemi, 2005. 86(9): p. 5-8.

[6] Callisen, T. H., Damhus, T., Nielsen, V. S., and Skagerlind, S., *Enzymer til vaskemidler.* Dansk Kemi, 2006. 87(3): p. 25-28.

[7] Schäfer, T*., et al.*, *Advances in Biochemical Engineering/Biotechnology - Industrial Enzymes* Vol. 105. 2007 Springer Berlin / Heidelberg. 59-131.

[8] Kirk, O., Borchert, T. V., and Fuglsang, C. C., *Industrial enzyme applications.* Curr Opin Biotechnol, 2002. 13(4): p. 345-51.

[9] Dhawan, S. and Kaur, J., *Microbial mannanases: an overview of production and applications.* Crit Rev Biotechnol, 2007. 27(4): p. 197-216.

[10] Tobin, M. B., Gustafsson, C., and Huisman, G. W., *Directed evolution: the 'rational' basis for 'irrational' design.* Curr Opin Struct Biol, 2000. 10(4): p. 421-7.

[11] Damhus, T., *Vaskemidler anno 2005 - dagligprodukter, hvor stofkemi mødes med overfladevidenskab og bioteknologi I* Dansk Kemi, 2005. 86(8): p. 1-4.

[12] Shaw, B. F., Schneider, G. F., Bilgicer, B., Kaufman, G. K., Neveu, J. M., Lane, W. S., Whitelegge, J. P., and Whitesides, G. M., *Lysine acetylation can generate highly charged enzymes with increased resistance toward irreversible inactivation.* Protein Sci, 2008. 17(8): p. 1446-55.

[13] Connell, D. W., *Basic Concepts of Environmental Chemistry*. Second Edition ed. 2005: CRC.

[14] Schick, M. J., *Nonionic Surfactants* 1987, CRC.

[15] Bergstrom, L. M., Bastardo, L. A., and Garamus, V. M., *A small-angle neutron and static light scattering study of micelles formed in aqueous mixtures of a nonionic alkylglucoside and an anionic surfactant.* J Phys Chem B, 2005. 109(25): p. 12387-93.

[16] Broze, G., *Handbook of Detergents*. Surfactants Science Series. Vol. 82. 1999: Taylor & Francis, Inc.

[17] Maurer, K. H., *Detergent proteases.* Curr Opin Biotechnol, 2004. 15(4): p. 330-4.

[18] Olsen, H. S. and Falholt, P., *The Role of Enzymes in Modern Detergency.* Journal of Surfactants and Detergents, 1998. 1: p. 555-567.

[19] Sonesson, A. W., Elofsson, U. M., Brismar, H., and Callisen, T. H., *Adsorption and mobility of a lipase at a hydrophobic surface in the presence of surfactants.* Langmuir, 2006. 22(13): p. 5810-7.

[20] Sonesson, A. W., Callisen, T. H., Brismar, H., and Elofsson, U. M., *Lipase surface diffusion studied by fluorescence recovery after photobleaching.* Langmuir, 2005. 21(25): p. 11949-56.

[21] Svendsen, A., *Lipase protein engineering.* Biochim Biophys Acta, 2000. 1543(2): p. 223-238.

[22] Mogensen, J. E., Sehgal, P., and Otzen, D. E., *Activation, inhibition, and destabilization of Thermomyces lanuginosus lipase by detergents.* Biochemistry, 2005. 44(5): p. 1719-30.
[23] Zhu, K., Jutila, A., Tuominen, E. K., and Kinnunen, P. K., *Effects of i-propanol on the structural dynamics of Thermomyces lanuginosa lipase revealed by tryptophan fluorescence.* Protein Sci, 2001. 10(2): p. 339-51.
[24] Schülein, M., *Enzymatic properties of cellulases from Humicola insolens.* J. Biotechnol., 1997. 57(1804): p. 71-81.
[25] Skagerlind, S. and Damhus, D., *Builderne – vaskemidlernes basisingredienser.* Dansk Kemi, 2005. 86(12): p. 13-16.
[26] Rosen, J. R. and Dahanayake, M., *Industrial utilization of surfactants - Principles and practice.* AOCS press, 2000.
[27] Shaw, D. J., *Introduction To Colloid And Surface Chemistry.* Butterworrth Heinemann, 1992.
[28] Tanford, C., *The Hydrophobic Effect: Formation of micelles and biological membranes*. 1991: Krieger.
[29] Garg, G., Aswal, V. K., Kulshreshtha, S. K., and Hassan, P. A., *Effect of substitution on aniline in inducing growth of anionic micelles.* PRAMANA - journal of physics, 2004. 63(2): p. 351-355.
[30] Ericsson, C. A., Soderman, O., Garamus, V. M., Bergstrom, M., and Ulvenlund, S., *Effects of temperature, salt, and deuterium oxide on the self-aggregation of alkylglycosides in dilute solution. 2. n-Tetradecyl-beta-D-maltoside.* Langmuir, 2005. 21(4): p. 1507-15.
[31] Bergstrom, M. and Pedersen, J. S., *Structure of pure SDS and DTAB micelles in brine determined by small-angle neutron scattering (SANS).* Phys. Chem. Chem. Phys., 1999. 1: p. 4437-4446.
[32] Rharbi, Y., Chen, L., and Winnik, M. A., *Exchange mechanisms for sodium dodecyl sulfate micelles: high salt concentration.* J Am Chem Soc, 2004. 126(19): p. 6025-34.
[33] Joshi, J. V., Aswal, V. K., Bahadur, P., and Goyal, P. S., *Role of counterion of the surfactant molecule on the micellar structure in aqueous solution.* CURRENT SCIENCE, 2002. 83(1): p. 47-49.
[34] Dreiss, C. A., *Wormlike micelles: where do we stand? Recent developments, linear rheology and scattering techniques.* Soft Matter, 2007. 3: p. 956-970.
[35] Hunter, R. J., *Foundations of Colloid Science: Volume I.* Oxford Science Publications, 1990.
[36] Ranganathan, R., Tran, L., and Bales, B. S., *Surfactant- and Salt-Induced Growth of Normal Sodium Alkyl Sulfate Micelles Well above Their Critical Micelle Concentrations.* J. Phys. Chem. B, 2000. 104: p. 2260-2264.
[37] Quina, F. H., Nassar, P. M., Bonilha, J. B. S., and Bales, B. S., *Growth of Sodium Dodecyl Sulfate Micelles with Detergent Concentration.* J. Phys. Chem., 1995. 99: p. 17028-17031.
[38] Kim, H. and Lim, K., *Sizes and Structures of Micelles of Cationic Octadecyl Trimethyl Ammonium Chloride and Anionic Ammonium Dodecyl Sulfate Surfactants in Aqueous Solutions.* Bull. Korean Chem. Soc., 2004. 25(3): p. 282-288.
[39] Wimmer, R., Andersen, K. K., Vad, B., Davidsen, M., Molgaard, S., Nesgaard, L. W., Kristensen, H. H., and Otzen, D. E., *Versatile interactions of the antimicrobial peptide novispirin with detergents and lipids.* Biochemistry, 2006. 45(2): p. 481-97.
[40] Nielsen, M. M., Andersen, K. K., Westh, P., and Otzen, D. E., *Unfolding of beta-sheet proteins in SDS.* Biophys J, 2007. 92(10): p. 3674-85.

[41] Gudiksen, K. L., Gitlin, I., and Whitesides, G. M., *Differentiation of proteins based on characteristic patterns of association and denaturation in solutions of SDS.* Proc Natl Acad Sci U S A, 2006. 103(21): p. 7968-72.

[42] Kalyanasundaram, K. and Thomas, J. K., *Environmental Effects on Vibronic Band Intensitiesin Pyrene Monomer Fluorescence and Their Application in Studies of Micellar Systems.* Journal of the American Chemical Society, 1976. 99:7: p. 2039-2044.

[43] Liu, Y. and Guo, R., *Interaction between casein and sodium dodecyl sulfate.* J Colloid Interface Sci, 2007. 315(2): p. 685-92.

[44] Hassan, P. A., Fritz, G., and Kaler, E. W., *Small angle neutron scattering study of sodium dodecyl sulfate micellar growth driven by addition of a hydrotropic salt.* J Colloid Interface Sci, 2003. 257(1): p. 154-62.

[45] Couillet, I., Hughes, T., Maitland, G., Candau, F., and Candau, S. J., *Growth and scission energy of wormlike micelles formed by a cationic surfactant with long unsaturated tails.* Langmuir, 2004. 20(22): p. 9541-50.

[46] Singh, M., Ford, C., Agarwal, V., Fritz, G., Bose, A., John, V. T., and McPherson, G. L., *Structural evolution in cationic micelles upon incorporation of a polar organic dopant.* Langmuir, 2004. 20(23): p. 9931-7.

[47] Zhang, R., Marone, P. A., Thiyagarajan, P., and Tiede, D. M., *Structure and Molecular Fluctuations of n-Alkyl-beta-D-glucopyranoside Micelles Determined by X-ray and Neutron Scattering.* Langmuir, 1999. 15: p. 7510-7519.

[48] Dupuy, C., Auvray, X., Petipas, Rico-Lattes, I., and Lattes, A., *Anomeric Effects on the Structure of Micelles of Alkyl Maltosides in Water.* Langmuir, 1997. 12: p. 3965-3967.

[49] Dupuy, C., Auvray, X., and Petipas, C., *Anomeric Effects on the Structure of Micelles of Alkyl Maltosides in Water.* Langmuir, 1997. 13: p. 3965-3967.

[50] Warr, G. G., Drummond, C. J., Grieser, F., Ninham, B. W., and Evans, D. F., *Aqueous Solution Properties of Nonionlc n-Dodecyl beta-D-Maltoside Micelles.* J. Phys. Chem., 1986. 90(19): p. 4581-4586.

[51] Drummond, C. J., Warr, G. G., Grieser, F., Ninham, B. W., and Evans, D. F., *Surface Properties and Micellar Interfacial Microenvironment of n-Dodecyl beta-D-Maltoside.* J. Phys. Chem., 1985. 89(10): p. 2103-2109.

[52] Romani, A. P., da Hora Machado, A. E., Hioka, N., Severino, D., Baptista, M. S., Codognoto, L., Rodrigues, M. R., and de Oliveira, H. P., *Spectrofluorimetric Determination of Second Critical Micellar Concentration of SDS and SDS/Brij 30 Systems.* J Fluoresc, 2008.

[53] Magid, J. L., Li, Z., and Butler, P. D., *Flexibility of Elongated Sodium Dodecyl Sulfate Micelles in Aqueous Sodium Chloride: A Small-Angle Neutron Scattering Study.* Langmuir, 2000. 16: p. 10028-10036.

[54] Shapiro, A. L., Vinuela, E., and Maizel, J. V., Jr., *Molecular weight estimation of polypeptide chains by electrophoresis in SDS-polyacrylamide gels.* Biochem Biophys Res Commun, 1967. 28(5): p. 815-20.

[55] Xiang, J., Fan, J. B., Chen, N., Chen, J., and Liang, Y., *Interaction of cellulase with sodium dodecyl sulfate at critical micelle concentration level.* Colloids Surf B Biointerfaces, 2006. 49(2): p. 175-80.

[56] Lad D, L. V., Briggs B, Green R, Frazier R, *Analysis of the SDS-Lysozyme Binding Isotherm.* Langmuir, 2003. 19: p. 5098-5103.

[57] Narayanan, J., Abdul Rasheed, A. S., and Bellare, J. R., *A small-angle X-ray scattering study of the structure of lysozyme-sodium dodecyl sulfate complexes.* J Colloid Interface Sci, 2008.

[58] Valstar A, B. W., and Almgren M, *The Lysozyme-Sodium Dodecyl Sulfate System Studied by Dynamic and Static Light Scattering.* Langmuir, 1999. 15: p. 2366-2374.
[59] Chatterjee, A., Moulik, S. P., Majhi, P. R., and Sanyal, S. K., *Studies on surfactant-biopolymer interaction. I. Microcalorimetric investigation on the interaction of cetyltrimethylammonium bromide (CTAB) and sodium dodecylsulfate (SDS) with gelatin (Gn), lysozyme (Lz) and deoxyribonucleic acid (DNA).* Biophys Chem, 2002. 98(3): p. 313-27.
[60] Lu, R. C., Cao, A. N., Lai, L. H., Zhu, B. Y., Zhao, G. X., and Xiao, J. X., *Interaction between bovine serum albumin and equimolarly mixed cationic-anionic surfactants decyltriethylammonium bromide-sodium decyl sulfonate.* Colloids Surf B Biointerfaces, 2005. 41(2-3): p. 139-43.
[61] Valstar A, A. M., Brown W, *The Interaction of Bovine Serum Albumin with Surfactants Studied by Light Scattering.* Langmuir, 2000. 16: p. 922-927.
[62] De, S., Girigoswami, A., and Das, S., *Fluorescence probing of albumin-surfactant interaction.* J Colloid Interface Sci, 2005. 285(2): p. 562-73.
[63] Chakraborty, A., Seth, D., Setua, P., and Sarkar, N., *Photoinduced electron transfer in a protein-surfactant complex: probing the interaction of SDS with BSA.* J Phys Chem B, 2006. 110(33): p. 16607-17.
[64] Hazra, P., Chakrabarty, D., Chakraborty, A., and Sarkar, N., *Probing protein-surfactant interaction by steady state and time-resolved fluorescence spectroscopy.* Biochem Biophys Res Commun, 2004. 314(2): p. 543-9.
[65] Nielsen, A. D., Borch, K., and Westh, P., *Thermochemistry of the specific binding of C12 surfactants to bovine serum albumin.* Biochim Biophys Acta, 2000. 1479(1-2): p. 321-31.
[66] Kelley D, M. D., *Interactions of bovine serum albumin with ionic surfactants in aqueous solutions.* Food Hydrocolloids, 2003. 17(1): p. 73-85.
[67] Reynolds, J. A., Gallagher, J. P., and Steinhardt, J., *Effect of pH on the binding of N-alkyl sulfates to bovine serum albumin.* Biochemistry, 1970. 9(5): p. 1232-8.
[68] Pitt-Rivers, R. and Impiombato, F. S., *The binding of sodium dodecyl sulphate to various proteins.* Biochem J, 1968. 109(5): p. 825-30.
[69] Ghosh, S., *Interaction of trypsin with sodium dodecyl sulfate in aqueous medium: a conformational view.* Colloids Surf B Biointerfaces, 2008. 66(2): p. 178-86.
[70] Otzen, D. E. and Oliveberg, M., *Burst-phase expansion of native protein prior to global unfolding in SDS.* J Mol Biol, 2002. 315(5): p. 1231-40.
[71] Otzen, D. E., *Protein unfolding in detergents: effect of micelle structure, ionic strength, pH, and temperature.* Biophys J, 2002. 83(4): p. 2219-30.
[72] Otzen, D. E. and Oliveberg, M., *A simple way to measure protein refolding rates in water.* J Mol Biol, 2001. 313(3): p. 479-83.
[73] Sehgal, P. and Otzen, D. E., *Thermodynamics of unfolding of an integral membrane protein in mixed micelles.* Protein Sci, 2006. 15(4): p. 890-9.
[74] Fersht, A., *Structure and Mechanism in Protein Science: A Guide to Enzyme Catalysis and Protein Folding* 1998: W. H. Freeman. 650.
[75] Ptitsyn, O. B., *How the molten globule became.* Trends Biochem Sci, 1995. 20(9): p. 376-9.
[76] Lau, F. W. and Bowie, J. U., *A method for assessing the stability of a membrane protein.* Biochemistry, 1997. 36(2153): p. 5884-5892.
[77] Sehgal, P., Mogensen, J. E., and Otzen, D. E., *Using micellar mole fractions to assess membrane protein stability in mixed micelles.* Biochim Biophys Acta, 2005. 1716: p. 59-68.

[78] Kragelund, B. B., Robinson, C. V., Knudsen, J., Dobson, C. M., and Poulsen, F. M., *Folding of a four-helix bundle: studies of acyl-coenzyme A binding protein.* Biochemistry, 1995. 34(21): p. 7217-24.

[79] Andersen, K. K., Oliveira, C. L. P., Larsen, K. L., Poulsen, F. M., Callisen, T. H., Westh, P., Pedersen, J. S., and D.E., O., *The role of decorated SDS micelles in sub-cmc protein denaturation and association.* Resbbmitted to Journal of Molecular Biology, 2009.

[80] Jones, M. N., *Surfactant Interactions with Biomembranes and Proteins.* Chem. Soc. Rev., 1992. 21: p. 127-136.

[81] Otzen, D. E., Christiansen, L., and Schulein, M., *A comparative study of the unfolding of the endoglucanase Cel45 from Humicola insolens in denaturant and surfactant.* Protein Sci, 1999. 8(9): p. 1878-87.

[82] Gitlin, I., Gudiksen, K. L., and Whitesides, G. M., *Peracetylated bovine carbonic anhydrase (BCA-Ac18) is kinetically more stable than native BCA to sodium dodecyl sulfate.* J Phys Chem B, 2006. 110(5): p. 2372-7.

[83] Timasheff, S. N., *Protein hydration, thermodynamic binding, and preferential hydration.* Biochemistry, 2002. 41(46): p. 13473-82.

[84] Yonath, A., Podjarny, A., Honig, B., Sielecki, A., and Traub, W., *Crystallographic studies of protein denaturation and renaturation. 2. Sodium dodecyl sulfate induced structural changes in triclinic lysozyme.* Biochemistry, 1977. 16(7): p. 1418-24.

[85] Jones, M. N., *A theoretical approach to the binding of amphipathic molecules to globular proteins.* Biochem J, 1975. 151(1): p. 109-14.

[86] Reynolds, J., Herbert, S., and Steinhardt, J., *The binding of some long-chain fatty acid anions and alcohols by bovine serum albumin.* Biochemistry, 1968. 7(4): p. 1357-61.

[87] Jones, M. N. and Manley, P., *Binding of n-alkyl sulphates to lysozyme in aqueous solution.* J. Chem. Soc., Faraday Trans. 1, 1979. 75: p. 1736 - 1744.

[88] Kaneshina, S., Tanaka, M., Kondo, T., Mizuno, T., and Aoki, K., *Interaction of Bovine Serum Albumin with Detergent Cations.* Bull. Chem. Soc. Jpn, 1973. 46: p. 2735-2738.

[89] Reynolds, J. A. and Tanford, C., *Binding of Dodecyl Sulfate to Proteins at High Binding Ratios. Possible Implications for the State of Proteins in Biological Membranes.* Proc. Natl. Acad. Sci., 1970. 66: p. 1002-1007.

[90] Nielsen, A. D., Arleth, L., and Westh, P., *Analysis of protein-surfactant interactions--a titration calorimetric and fluorescence spectroscopic investigation of interactions between Humicola insolens cutinase and an anionic surfactant.* Biochim Biophys Acta, 2005. 1752(2): p. 124-32.

[91] Nielsen, A. D., Arleth, L., and Westh, P., *Interactions of Humicola insolens cutinase with an anionic surfactant studied by small-angle neutron scattering and isothermal titration calorimetry.* Langmuir, 2005. 21(10): p. 4299-307.

[92] Bagger, H. L., Hoffmann, S. V., Fuglsang, C. C., and Westh, P., *Glycoprotein-surfactant interactions: a calorimetric and spectroscopic investigation of the phytase-SDS system.* Biophys Chem, 2007. 129(2-3): p. 251-8.

[93] Reynolds, J. A. and Tanford, C., *The gross conformation of protein-sodium dodecyl sulfate complexes.* J Biol Chem, 1970. 245(19): p. 5161-5.

[94] Shirahama, K., Tsujii, K., and Takagi, T., *Free-boundary Electrophoresis of Sodium Dodecyl Sulfate-Protein Polypeptide Complexes with Special Reference to SDS-Polyacrylamide Gel Electrophoresis* J. Biochem., 1974. 75: p. 309-319.

[95] Waninge, R., Paulsson, M., Nylander, T., Ninham, B., and Sellers, P., *Binding of Sodium Dodecyl Sulphate and Dodecyl Trimethyl Ammonium Chloride to β-*

Lactoglobulin: A Calorimetric Study International Dairy Journal, 1998. 8(2): p. 141-148.

[96] Berman, H. M., Westbrook, J., Feng, Z., Gilliland, G., Bhat, T. N., Weissig, H., Shindyalov, I. N., and Bourne, P. E., *The Protein Data Bank.* Nucleic Acids Res, 2000. 28(1): p. 235-42.

[97] Kragelund, B. B., Knudsen, J., and Poulsen, F. M., *Acyl-coenzyme A binding protein (ACBP).* Biochim Biophys Acta, 1999. 1441(2-3): p. 150-61.

[98] Kragelund, B. B., Osmark, P., Neergaard, T. B., Schiodt, J., Kristiansen, K., Knudsen, J., and Poulsen, F. M., *The formation of a native-like structure containing eight conserved hydrophobic residues is rate limiting in two-state protein folding of ACBP.* Nat Struct Biol, 1999. 6(6): p. 594-601.

[99] Kragelund, B. B*., et al.*, *Conserved residues and their role in the structure, function, and stability of acyl-coenzyme A binding protein.* Biochemistry, 1999. 38(8): p. 2386-94.

[100] Clarke, J., Cota, E., Fowler, S. B., and Hamill, S. J., *Folding studies of immunoglobulin-like beta-sandwich proteins suggest that they share a common folding pathway.* Structure, 1999. 7(9): p. 1145-53.

[101] Fowler, S. B. and Clarke, J., *Mapping the folding pathway of an immunoglobulin domain: structural detail from Phi value analysis and movement of the transition state.* Structure, 2001. 9(5): p. 355-66.

[102] Peng, Z. Y. and Kim, P. S., *A protein dissection study of a molten globule.* Biochemistry, 1994. 33(8): p. 2136-41.

[103] Kuwajima, K., *The molten globule state of alpha-lactalbumin.* Faseb J, 1996. 10(1): p. 102-9.

[104] Griko, Y. V., *Energetic basis of structural stability in the molten globule state: alpha-lactalbumin.* J Mol Biol, 2000. 297(5): p. 1259-68.

[105] Jennings, P. A. and Wright, P. E., *Formation of a molten globule intermediate early in the kinetic folding pathway of apomyoglobin.* Science, 1993. 262(5135): p. 892-6.

[106] Hughson, F. M., Wright, P. E., and Baldwin, R. L., *Structural characterization of a partly folded apomyoglobin intermediate.* Science, 1990. 249(4976): p. 1544-8.

[107] Eliezer, D., Yao, J., Dyson, H. J., and Wright, P. E., *Structural and dynamic characterization of partially folded states of apomyoglobin and implications for protein folding.* Nat Struct Biol, 1998. 5(2): p. 148-55.

[108] Machida, M*., et al.*, *Genome sequencing and analysis of Aspergillus oryzae.* Nature, 2005. 438(7071): p. 1157-61.

[109] Kobayashi, T., Abe, K., Asai, K., Gomi, K., Juvvadi, P. R., Kato, M., Kitamoto, K., Takeuchi, M., and Machida, M., *Genomics of Aspergillus oryzae.* Biosci Biotechnol Biochem, 2007. 71(3): p. 646-70.

[110] Abe, K., Gomi, K., Hasegawa, F., and Machida, M., *Impact of Aspergillus oryzae genomics on industrial production of metabolites.* Mycopathologia, 2006. 162(3): p. 143-53.

[111] Yaver, D. S., Lamsa, M., Munds, R., Brown, S. H., Otani, S., Franssen, L., Johnstone, J. A., and Brody, H., *Using DNA-tagged mutagenesis to improve heterologous protein production in Aspergillus oryzae.* Fungal Genet Biol, 2000. 29(1): p. 28-37.

[112] DeLano, W. L., *The PyMOL Molecular Graphics System* 2002.

[113] Cunningham, E. L., Jaswal, S. S., Sohl, J. L., and Agard, D. A., *Kinetic stability as a mechanism for protease longevity.* Proc Natl Acad Sci U S A, 1999. 96(20): p. 11008-14.

[114] Jaswal, S. S., Sohl, J. L., Davis, J. H., and Agard, D. A., *Energetic landscape of alpha-lytic protease optimizes longevity through kinetic stability.* Nature, 2002. 415(6869): p. 343-6.
[115] Truhlar, S. M., Cunningham, E. L., and Agard, D. A., *The folding landscape of Streptomyces griseus protease B reveals the energetic costs and benefits associated with evolving kinetic stability.* Protein Sci, 2004. 13(2): p. 381-90.
[116] Cunningham, E. L. and Agard, D. A., *Disabling the folding catalyst is the last critical step in alpha-lytic protease folding.* Protein Sci, 2004. 13(2): p. 325-31.
[117] Kelch, B. A. and Agard, D. A., *Mesophile versus thermophile: insights into the structural mechanisms of kinetic stability.* J Mol Biol, 2007. 370(4): p. 784-95.
[118] Kelch, B. A., Eagen, K. P., Erciyas, F. P., Humphris, E. L., Thomason, A. R., Mitsuiki, S., and Agard, D. A., *Structural and mechanistic exploration of acid resistance: kinetic stability facilitates evolution of extremophilic behavior.* J Mol Biol, 2007. 368(3): p. 870-83.
[119] Truhlar, S. M. and Agard, D. A., *The folding landscape of an alpha-lytic protease variant reveals the role of a conserved beta-hairpin in the development of kinetic stability.* Proteins, 2005. 61(1): p. 105-14.
[120] Jaswal, S. S., Truhlar, S. M., Dill, K. A., and Agard, D. A., *Comprehensive analysis of protein folding activation thermodynamics reveals a universal behavior violated by kinetically stable proteases.* J Mol Biol, 2005. 347(2): p. 355-66.
[121] Fuhrmann, C. N., Kelch, B. A., Ota, N., and Agard, D. A., *The 0.83 A resolution crystal structure of alpha-lytic protease reveals the detailed structure of the active site and identifies a source of conformational strain.* J Mol Biol, 2004. 338(5): p. 999-1013.
[122] Brayer, G. D., Delbaere, L. T., and James, M. N., *Molecular structure of the alpha-lytic protease from Myxobacter 495 at 2.8 Angstroms resolution.* J Mol Biol, 1979. 131(4): p. 743-75.
[123] Manning, M. and Colon, W., *Structural basis of protein kinetic stability: resistance to sodium dodecyl sulfate suggests a central role for rigidity and a bias toward beta-sheet structure.* Biochemistry, 2004. 43(35): p. 11248-54.
[124] Xia, K., Manning, M., Hesham, H., Lin, Q., Bystroff, C., and Colon, W., *Identifying the subproteome of kinetically stable proteins via diagonal 2D SDS/PAGE.* Proc Natl Acad Sci U S A, 2007. 104(44): p. 17329-34.
[125] Rodriguez-Larrea, D., Minning, S., Borchert, T. V., and Sanchez-Ruiz, J. M., *Role of solvation barriers in protein kinetic stability.* J Mol Biol, 2006. 360(3): p. 715-24.
[126] Lakowicz, J. R., *Principles of Fluorescence Spectroscopy* 3rd edition ed. 2006: Springer. 954.
[127] Lund, H., Christensen, B. P., Nielsen, A. D., and Westh, P., *Proton exchange coupled to the specific binding of alkylsulfonates to serum albumins.* Biochim Biophys Acta, 2006. 1764(7): p. 1243-51.
[128] Otzen, D. E., Sehgal, P., and Westh, P., *Alpha-Lactalbumin is unfolded by all classes of surfactants but by different mechanisms.* J Colloid Interface Sci, 2009. 329(2): p. 273-83.
[129] Gudiksen, K. L., Gitlin, I., Yang, J., Urbach, A. R., Moustakas, D. T., and Whitesides, G. M., *Eliminating positively charged lysine epsilon-NH3+ groups on the surface of carbonic anhydrase has no significant influence on its folding from sodium dodecyl sulfate.* J Am Chem Soc, 2005. 127(13): p. 4707-14.
[130] Gudiksen, K. L., Urbach, A. R., Gitlin, I., Yang, J., Vazquez, J. A., Costello, C. E., and Whitesides, G. M., *Influence of the Zn(II) cofactor on the refolding of bovine*

carbonic anhydrase after denaturation with sodium dodecyl sulfate. Anal Chem, 2004. 76(24): p. 7151-61.
[131] Skoog, D. A., Holler, F. J., and Crouch, S. R., *Principles of Instrumental Analysis* 5th Edition ed. 1998: Brooks/Cole.
[132] Creighton, T. E., *Proteins: Structures and Molecular Properties* Second Edition ed. 1992: W. H. Freeman.
[133] Whitmore, L. and Wallace, B. A., *Protein secondary structure analyses from circular dichroism spectroscopy: methods and reference databases.* Biopolymers, 2008. 89(5): p. 392-400.
[134] Miles, A. J. and Wallace, B. A., *Synchrotron radiation circular dichroism spectroscopy of proteins and applications in structural and functional genomics.* Chem Soc Rev, 2006. 35(1): p. 39-51.
[135] Chang, R., *Physical Chemistry for the Chemical and Biological Sciences* 3rd Edition ed. 2000: University Science Books.
[136] Woody, R. J., *in Circular Dichroism and the Conformational Analysis of Biomolecules* ed. G.D. Fasman. 1996: Springer.
[137] *http://www.microcal.com/technology/itc.asp*.
[138] Heiger, D. N., *High Performance Capillary Electrophoresis - An Introduction*. 3rd Edition ed. 1992: Hewlett Packard Company.
[139] Jiskoot. W and Crommelin, D., *Methods for Structural Analysis of Protein Pharmaceuticals* 2005, American Association of Pharmaceuticals Scientists.
[140] Kragelund, B. B., Andersen, K. V., Madsen, J. C., Knudsen, J., and Poulsen, F. M., *Three-dimensional structure of the complex between acyl-coenzyme A binding protein and palmitoyl-coenzyme A.* J Mol Biol, 1993. 230(4): p. 1260-77.
[141] Psachoulia, E., Bond, P. J., and Sansom, M. S. P., *MD simulations of Mistic: Conformational stability in detergent micelles and water.* Biochemistry, 2006. 45(4193): p. 9053-9058.
[142] Bond, P. J., Cuthbertson, J., and Sansom, M. S. P., *Simulation studies of the interactions between membrane proteins and detergents.* Biochem. Soc. Transact., 2005. 33(4645): p. 910-912.
[143] Deol, S. S., Bond, P. J., Domene, C., and Sansom, M. S., *Lipid-protein interactions of integral membrane proteins: a comparative simulation study.* Biophys J, 2004. 87(6): p. 3737-49.
[144] Sansom, M. S., Bond, P. J., Deol, S. S., Grottesi, A., Haider, S., and Sands, Z. A., *Molecular simulations and lipid-protein interactions: potassium channels and other membrane proteins.* Biochem Soc Trans, 2005. 33(Pt 5): p. 916-20.
[145] Lindahl, E. and Sansom, M. S., *Membrane proteins: molecular dynamics simulations.* Curr Opin Struct Biol, 2008. 18(4): p. 425-31.
[146] Higgins, C. L., Muralidhara, B. K., and Wittung-Stafshede, P., *How do cofactors modulate protein folding?* Protein Pept Lett, 2005. 12(2): p. 165-70.
[147] Wilson, C. J., Apiyo, D., and Wittung-Stafshede, P., *Role of cofactors in metalloprotein folding.* Q Rev Biophys, 2004. 37(3-4): p. 285-314.
[148] Wittung-Stafshede, P., *Role of cofactors in protein folding.* Acc Chem Res, 2002. 35(4): p. 201-8.
[149] Tofani, L., Feis, A., Snoke, R. E., Berti, D., Baglioni, P., and Smulevich, G., *Spectroscopic and interfacial properties of myoglobin/surfactant complexes.* Biophys J, 2004. 87(2): p. 1186-95.
[150] Di Matteo, A., Gianni, S., Schinina, M. E., Giorgi, A., Altieri, F., Calosci, N., Brunori, M., and Travaglini-Allocatelli, C., *A strategic protein in cytochrome c*

maturation: three-dimensional structure of CcmH and binding to apocytochrome c. J Biol Chem, 2007. 282(37): p. 27012-9.

[151] Kleinschmidt, J. H. and Tamm, L. K., *Secondary and tertiary structure formation of the beta-barrel membrane protein OmpA is synchronized and depends on membrane thickness.* J Mol Biol, 2002. 324(2): p. 319-30.

[152] Kleinschmidt, J. H., *Folding kinetics of the outer membrane proteins OmpA and FomA into phospholipid bilayers.* Chem Phys Lipids, 2006. 141(1-2): p. 30-47.

[153] Kleinschmidt JH, W. M., Tamm LK, *Outer membrane protein A of E. coli folds into detergent micelles, but not in the presence of monomeric detergent.* Protein Science, 1999. 8: p. 2065–2071.

[154] Kleinschmidt, J. H. and Tamm, L. K., *Folding intermediates of a beta-barrel membrane protein. Kinetic evidence for a multi-step membrane insertion mechanism.* Biochemistry, 1996. 35(40): p. 12993-3000.

[155] Kleinschmidt, J. H. and Tamm, L. K., *Time-resolved distance determination by tryptophan fluorescence quenching: probing intermediates in membrane protein folding.* Biochemistry, 1999. 38(16): p. 4996-5005.

[156] Kleinschmidt, J. H., den Blaauwen, T., Driessen, A. J., and Tamm, L. K., *Outer membrane protein A of Escherichia coli inserts and folds into lipid bilayers by a concerted mechanism.* Biochemistry, 1999. 38(16): p. 5006-16.

[157] Pocanschi, C. L., Patel, G. J., Marsh, D., and Kleinschmidt, J. H., *Curvature elasticity and refolding of OmpA in large unilamellar vesicles.* Biophys J, 2006. 91(8): p. L75-7.

[158] Tamm, L. K., Hong, H., and Liang, B., *Folding and assembly of beta-barrel membrane proteins.* Biochim Biophys Acta, 2004. 1666(1-2): p. 250-63.

[159] Pautsch, A. and Schulz, G. E., *High-resolution structure of the OmpA membrane domain.* J Mol Biol, 2000. 298(2): p. 273-82.

[160] Pautsch, A. and Schulz, G. E., *Structure of the outer membrane protein A transmembrane domain.* Nat Struct Biol, 1998. 5(11): p. 1013-7.

[161] Nardone, E.*, et al.*, *Biochemical characterization and crystal structure of a recombinant hen avidin and its acidic mutant expressed in Escherichia coli.* Eur J Biochem, 1998. 256(2): p. 453-60.

[162] Shimizu, T. and Morikawa, K., *The beta-prism: a new folding motif.* Trends Biochem Sci, 1996. 21(1): p. 3-6.

[163] Paoli, M., *Protein folds propelled by diversity.* Prog Biophys Mol Biol, 2001. 76(1-2): p. 103-30.

[164] Jawad, Z. and Paoli, M., *Novel sequences propel familiar folds.* Structure, 2002. 10(4): p. 447-54.

[165] Branden, C. and Tooze, J., *Introduction to Protein Structure*. 2nd Edition ed. 1999: Garland Science.

[166] Jensen, B., Olsen, J., and Allermann, K., *Effect of media compositionon the production of extracellular amylase from the thermophilic fungus Thermomyces Lanuginosus.* Biotechnology Letters, 1987. 9(5): p. 313-316.

[167] Jensen, B., Nebelong, P., Olsen, J., and Reeslev, M., *Enzyme production in continuous cultivation by the thermophilic fungus, Thermomyces lanuginosus.* Biotechnology Letters, 2002. 24: p. 41–45.

[168] Razvi, A. and Scholtz, J. M., *Lessons in stability from thermophilic proteins.* Protein Sci, 2006. 15(7): p. 1569-78.

[169] Luke, K. A., Higgins, C. L., and Wittung-Stafshede, P., *Thermodynamic stability and folding of proteins from hyperthermophilic organisms.* Febs J, 2007. 274(16): p. 4023-33.

[170] Mukaiyama, A., Takano, K., Haruki, M., Morikawa, M., and Kanaya, S., *Kinetically robust monomeric protein from a hyperthermophile.* Biochemistry, 2004. 43(43): p. 13859-66.
[171] Duy, C. and Fitter, J., *Thermostability of irreversible unfolding alpha-amylases analyzed by unfolding kinetics.* J Biol Chem, 2005. 280(45): p. 37360-5.
[172] Michaux, C., Pomroy, N. C., and Prive, G. G., *Refolding SDS-denatured proteins by the addition of amphipathic cosolvents.* J Mol Biol, 2008. 375(5): p. 1477-88.
[173] Michaux, C., Pouyez, J., Wouters, J., and Prive, G. G., *Protecting role of cosolvents in protein denaturation by SDS: a structural study.* BMC Struct Biol, 2008. 8: p. 29.